Macrophage Immunometabolism in the Host Response to *Mycobacterium tuberculosis* Infection

A Thesis Submitted to the University of Dublin, Trinity College, for the Degree of Doctor of Philosophy in the Faculty of Medicine

by

Dr. Laura E. Gleeson, MB BCh BAO BA

Submitted February 2017

Supervisor: Prof Joe Keane, MD

TB Immunology Lab, Institute of Molecular Medicine

St James's Hospital,

Dublin 8

DECLARATION OF AUTHORSHIP

I, Laura Gleeson, declare that this thesis has not been submitted as an exercise for a degree at this or any other university and it is entirely my own work.

I agree to deposit this thesis in the University's open access institutional repository or allow the library to do so on my behalf, subject to Irish Copyright Legislation and Trinity College Library conditions of use and acknowledgement.

Signed: Date:

_____ _____

Laura Gleeson

SUMMARY

Tuberculosis (TB) is the leading infectious disease killer in the world, alongside HIV. Our understanding of the complex host immune response to *Mycobacterium tuberculosis* (Mtb) remains incomplete, but varied clinical outcomes of infection seen in humans (ranging from death to complete asymptomatic clearance of the bug) suggest that understanding host defence mechanisms may provide new insights and novel approaches to vaccine and treatment development. Integral to the host immune response to infection is the tissue-resident alveolar macrophage (AM), capable of early eradication of the bacillus but, conversely, vulnerable to subversion by the bacillus to be used as a nidus for survival and replication. Specifically, the pro-inflammatory cytokine Interleukin-1β (IL-1β) is essential for its mycobactericidal activity. Recent work in the burgeoning field of immunometabolism has linked TLR-induced changes in intracellular macrophage glucose metabolism – namely, a shift towards aerobic glycolysis, known as the Warburg effect – to production of IL-1β. Thus, in this body of work we investigate the metabolic impact of Mtb infection on human macrophage glucose metabolism and examine downstream functional effects of infection-induced metabolic alterations.

The results presented in this body of work offer new insights into the metabolic characteristics of primary human monocyte-derived macrophages (MDM) and primary human AM. We demonstrate infection-induced glycolytic reprogramming in human and murine macrophages, mediated through TLR2/6 signalling. We find glycolytic reprogramming to be essential for optimal production of *IL1B* mRNA at a transcriptional level, with consequent secretion of mature IL-1β. This glycolysis-driven increase in IL-1β leads to upregulation of the eicosanoid Prostaglandin E2 (PGE2) and suppression of the anti-inflammatory cytokine Interleukin-10 (IL-10), with ultimate enhancement of macrophage mycobactericidal activity in both human and murine macrophages. We further demonstrate a similar requirement for glycolytic reprogramming in *Salmonella typhimurium*-infected murine macrophages. Pharmacological augmentation of glycolysis using meclizine dihydrochloride enhanced early bacillary clearance by human MDM, suggesting this newly delineated pathway of host defence may warrant exploration in the search for host-directed therapies for TB disease. Finally, we demonstrate reduced baseline metabolic activity and reduced metabolic reserves in macrophages exposed to cigarette smoke. Smoke-exposed macrophages had an attenuated metabolic response to Mtb infection, concurrent with impaired production of IL-1β and PGE2.

This work demonstrates for the first time a functional role for glycolytic reprogramming in the context of host defence. This novel mechanism of the anti-mycobacterial macrophage response may be targeted for the development of new therapies and vaccines to combat this global

pathogen, particularly given our observation of pharmacological manipulation of glycolytic metabolism enhancing macrophage mycobactericidal activity. Experiments with *S. typhi* also suggest that this metabolic/immune axis is not specific to mycobacterial infection, thus exploration of this pathway may yield insights that can combat many infectious diseases. Impairments in metabolic responses in smoke-exposed macrophages may partly explain the increased susceptibility to infection observed in the smoking population, and possibly highlighting this group as one which may particularly benefit from metabolism-targeted host-directed therapies in the future.

PUBLICATIONS ARISING FROM THIS THESIS

- **Gleeson LE**, Sheedy FJ. Metabolic reprogramming and inflammation: fuelling the host response to pathogens. Semin Immunol 2016 Oct 22 [epub ahead of print]. PMID:27780657
- O'Connor G, **Gleeson LE**, Fagan-Murphy A, Cryan SA, O'Sullivan MP, Keane J. Sharpening nature's tools for efficient tuberculosis control: A review of the potential role and development of host-directed therapies and development of host-directed therapies and strategies for targeted respiratory delivery. Adv Drug Deliv Rev 2016 Jul 1;102:33-54. PMID:27151307
- **Gleeson LE**, Sheedy FJ, Palsson-McDermott EM, Triglia D, O'Leary SM, O'Sullivan MP, O'Neill LA, Keane J. Cutting Edge: Mycobacterium tuberculosis induces aerobic glycolysis in human alveolar macrophages that is required for control of intracellular bacillary replication. J Immunol 2016 Mar 15;196(6)2444-9. PMID: 26873991
- Ní Cheallaigh C, Sheedy FJ, Harris J, Muñoz-Wolf N, Lee J, West K, McDermott EP, Smyth A, **Gleeson LE**, Coleman M, Martinez N, Hearnden CH, Tynan GA, Carroll EC, Jones SA, Corr SC, Bernard NJ, Hughes MM, Corcoran SE, O'Sullivan M, Fallon CM, Kornfeld H, Golenbock D, Gordon SV, O'Neill LA, Lavelle EC, Keane J. A common variant in the adaptor Mal regulated Interferon gamma signaling. Immunity 2016 Feb 16;44(2):368-79. PMID: 26885859
- **Gleeson LE,** Keane J. First steps in biomarker assessment for reactivation risk in latent TB. Am J Respir Crit Care Med 2015 Sep 1;192(5):534-5. PMID: 26325153
- Palsson-McDermott EM, Curtis AM, Goel G, Lauterbach MA, Sheedy FJ, **Gleeson LE**, van den Bosch MW, Quinn SR, Domingo-Fernandez R, Johnson DG, Jiang JK, Israelsen WJ, Keane J, Thomas C, Clish C, Vanden Heiden M, Xavier RJ, O'Neill LA. Pyruvate kinase M2 regulates Hif-1α activity and IL-1β induction and is a critical determinant of the Warburg effect in LPS-activated macrophages. Cell Metab. 2015 Jan 6;21(1):65-80. PMID: 25565206
- O'Leary S, Coleman M, Chew WM, Morrow C, McLaughlin AM, **Gleeson LE**, O'Sullivan MP, Keane J. Cigarette smoking impairs human pulmonary immunity to *Mycobacterium tuberculosis*. Am J Respir Crit Care Med. 2014 Dec 15;190(12):1430-6. PMID: 25390734

MANUSCRIPTS IN PREPARATION

- **Gleeson LE,** Sheedy FJ, O'Leary S, Keane JK. Cigarette smoking reduces alveolar macrophage metabolic reserves and impairs the glycolytic host response to *Mycobacterium tuberculosis*. [*Manuscript in preparation*]

ACKNOWLEDGEMENTS

Foremost, I would like to thank my supervisor Professor Joe Keane, whose constant enthusiasm, encouragement and support has been a source of inspiration and motivation throughout this work.

I wish also to thank past and present members of the TB Immunology Research Group, Trinity College Dublin, for their expertise, guidance, help and patience over the last few years. I also extend thanks to the many scientists from research groups throughout the Institute of Molecular Medicine and the Trinity Biomedical Sciences Institute who generously offered their advice and insight at various points during this project, a true reflection of the collaborative nature of science. Specifically, I would like to thank Professor Richie Porter, Professor Luke O'Neill and Dr Eva Palsson-McDermott for their invaluable guidance. I would like to acknowledge also the clinical staff in St James's Hospital and research nurses in the Dublin Centre for Clinical Research for their assistance in acquiring bronchoalveolar lavage specimens to facilitate much of this work, and of course the patients attending for bronchoscopy in St James's Hospital who permitted retrieval of these specimens, without whom this work would not have been possible.

Finally, I would like to express my incredible gratitude to Dr Frederick Sheedy and Dr Eimear Gleeson, without whom I am certain I would not have reached this point. Thank you both for your constant support, your enduring friendship, your unfaltering logic and your indisputable brilliance.

TABLE OF CONTENTS

CHAPTER 3: THE MACROPHAGE METABOLIC RESPONSE TO MTB INFECTION

CHAPTER 4: THE FUNCTIONAL IMPACT OF GLYCOLYTIC REPROGRAMMING IN THE MACROPHAGE RESPONSE TO MTB INFECTION

GLOSSARY OF FIGURES

CHAPTER 1: INTRODUCTION AND LITERATURE REVIEW

CHAPTER 2: METHODS AND MATERIALS

CHAPTER 3: THE MACROPHAGE METABOLIC RESPONSE TO MTB INFECTION

CHAPTER 4: THE FUNCTIONAL IMPACT OF GLYCOLYTIC REPROGRAMMING IN THE MACROPHAGE RESPONSE TO MTB INFECTION

CHAPTER 5: THE EFFECT OF CIGARETTE SMOKE EXPOSURE ON MACROPHAGE METABOLIC RESPONSE TO MTB INFECTION

GLOSSARY OF TABLES

CHAPTER 4: THE FUNCTIONAL IMPACT OF GLYCOLYTIC REPROGRAMMING IN THE MACROPHAGE RESPONSE TO MTB INFECTION

GLOSSARY OF ABBREVIATIONS

ΔΨ	Mitochondrial membrane potential
2-DG	2-deoxyglucose
5-LO	5-lipoxygenase
AASS	Asparte-arginosuccinate shunt
ADP	Adenosine diphosphate
AFB	Acid fast bacilli
AM	Alveolar macrophage
AMPK	5'-adenosinemonophosphage activated protein kinase
APC	Antigen presenting cells
Arg1	Arginase-1
ASC	Apoptosis-associated speck-like protein containing a caspase recruitment domain
ATCC	American Type Culture Collection
ATP	Adenosine triphosphate
B[a]P	Benzo(a)pyrene
BAL	Bronchoalveolar lavage
BCA	Bicinchoninic acid
BCG	Bacillus Calmette-Guerin
BMDM	Bone marrow-derived macrophage
BSA	Bovine serum albumin
BSL	Biosafety level
CARKL	Carbohydrate kinase-like protein
CD	Cluster of differentiation
cDNA	Complementary DNA
CFU	Colony forming units
CIC	Mitochondrial citrate carrier
CO_2	Carbon dioxide
COX	Cyclooxygenase
cRPMI	Complete RPMI
CSE	Cigarette smoke extract
Ct	Cycle threshold
CV	Crystal violet
DAMP	Danger-associated molecular pattern
DCF	2',7'-dichlorofluorescin
DCFDA	2',7'-dichlorofluorescin diacetate
DM2	Type 2 diabetes
DMEM	Dulbecco's Modified Eagle's Medium
DMSO	Dimethyl sulfoxide
DNA	Deoxyribonucleic acid
ECAR	Extracellular acidification rate
EDTA	Ethylenediaminetetraacetic acid
ELISA	Enzyme-linked immunosorbent assay
ETC	Electron transport chain
$FADH_2$	Flavin adenine dinucleotide
FBS	Foetal bovine serum
FCCP	Carbonyl cyanide-4-(trifluoromethoxy)phenylhydrazone
FSL-1	Pam2CGDPKHPKSF
G6P	Glucose-6-phosphate
GLUT	Glucose transporter
GR	Glycolytic reserve
H_2SO_4	Sulfuric acid

HDT	Host-directed therapy
HIF-1α	Hypoxia-inducible Factor alpha
HIV	Human Immunodeficiency Virus
HK1	Hexokinase 1
HRE	Hypoxia Response Element
HRP	Horseradish peroxidase
IBTS	Irish Blood Transfusion Service
IDH	Isocitrate Dehydrogenase
IFN	Interferon
Ig	Immunoglobulin
IKK	Inhibitor of NFκB kinase
IL	Interleukin
IL-1R1	IL-1 receptor
IL-1Ra	IL-1R antagonist
IL-1RAcP	IL-1R accessory protein
iNOS	Inducible nitric oxide synthase
IRAK	IL-1R associated kinase
Irg1	Immune responsive gene 1
iRv	γ-irradiated H37Rv
JNK	Jun N-terminal kinase
kDa	Kilodalton
KO	Knock-out
LAM	Lipoarrabinomannan
LB	Luria broth
LDHA	Lactate dehydrogenase A
LPS	Lipopolysaccharide
LT	Leukotriene
LTBI	Latent TB Infection
LXA	Lipoxin
MAPK	Mitogen-activated protein kinase
M-CSF	Macrophage colony-stimulating factor
MDM	Monocyte-derived macrophage
MDR	Multiple drug resistant
MHC	Major histocompatibility complex
MMP	Matrix metalloproteinase
MOI	Multiplicity of infection
mRNA	Messenger RNA
mROS	Mitochondrial ROS
Mtb	*Mycobacterium tuberculosis*
mTOR	Mechanistic target of rapamycin
mTORC1	mTOR complex 1
MyD88	Myeloid differentiation primary response gene 88
NAD	Nicotinamide adenine dinucleotide
NADP	Nicotinamide adenine dinucleotide phosphate
NFκB	Nuclear factor κ-light chain enhancer of activated B cells
NK	Natural killer
NLRP3	NACHT, LRR and PYD domains-containing protein 3
NMR	Nuclear magnetic resonance
NO	Nitric oxide
NOX	NADPH oxidase
NSAID	Non-steroidal anti-inflammatory drug
oATP	Oxidised ATP
OCR	Oxygen consumption rate

OD	Optical density
OXPHOS	Oxidative phosphorylation
P2RX7	PX2 purinergic receptor 7
P3C	Pam3Cys-Ser-(Lys)4
PAMP	Pathogen-associated molecular pattern
PBMC	Peripheral blood mononuclear cell
PBS	Phosphate buffered saline
PCR	Polymerase chain reaction
PCYT2	CTP:phosphoethanolamine cytidylyltransferase
PDK3	Pyruvate dehydrogenase kinase 3
PFA	Paraformaldehyde
PFK2	Phosphofructokinase-2
PG	Prostaglandin
PGE2	Prostaglandin E2
PGE2-ALP	Alkaline phosphatase conjugated PGE2
PHD2	Prolyl hydroxylase 2
PI	Propidium iodide
PI3K	Phosphoinositide 3-kinase
PIM	Phosphatidylinositol mannoside
PKM2	Pyruvate kinase M2
PL	Proton leak
PMA	Phorbyl myrisate acetate
PPAR	Peroxisome proliferator-activated receptor
PPP	Pentose phosphate pathway
PRR	Pattern recognition receptor
RET	Reverse electron transport
RIPA	Radioimmunoprecipitation assay buffer
RNA	Ribonucleic acid
RNS	Reactive nitrogen species
ROS	Reactive oxygen species
RPMI-1640	Roswell Park Memorial Institute-1640 medium
rRNA	Ribosomal RNA
RT-qPCR	Quantitative reverse transcription PCR
SDH	Succinate dehydrogenase
SNP	Single nucleotide polymorphism
SRC	Spare respiratory capacity
TB	Tuberculosis
TBHP	Tert-butyl hydrogen peroxide
TCA	Tricarboxylic acid
TEPP-46	Thieno[3,2-b]pyrrole[3,2-d]pyridazinone-46
TGF-β	Transforming growth factor-β
TIR domain	Toll/IL-1R domain
TLR	Toll-like receptor
TNF-α	Tumour necrosis factor-α
TNFR1	TNF-α receptor 1
TRAF6	TNF receptor associated factor 6
WT	Wild type
YVAD	Z-YVAD-FMK

CHAPTER 1:

Introduction and Literature Review

1.1 The Host Response to *Mycobacterium tuberculosis* Infection

1.1.1 The Tuberculosis Pandemic

Tuberculosis (TB) is the leading infectious disease killer in the world, alongside HIV [1]. Predominantly a disease of the lung (evident in approximately 70% of cases) [2], it is caused by infection with the acid-fast bacillus *Mycobacterium tuberculosis* (Mtb), spread from human-to-human by respiratory transmission. Despite existence of effective chemotherapy since the 1940s [1], and the World Health Organisation's "Stop TB Strategy" setting targets for TB control by 2015 [3], TB killed 1.5 million people in 2014 [1]. A combination of factors is responsible for the limited success of global TB control programmes [1,2,4], including the lack of an effective vaccine [5-7], the emergence of drug-resistant strains [8-10], HIV co-infection [10,11], and the lack of rapid and sensitive diagnostics [12]. Even for drug sensitive strains, treatment regimens are arduous, with the current recommendations advising six months of treatment with four first-line drugs [1].

Interestingly, of the 2 – 3 billion people infected with Mtb worldwide (representing one-third of the world's population), only 5 – 15% will develop active TB disease during their lifetime [1,13]. The remainder have persistent asymptomatic infection, referred to as "latent TB infection" (LTBI) [14]. Furthermore, a proportion of people exposed to Mtb are believed to clear the bacillus completely without treatment and without the development of LTBI [14-16]. Thus, the human immune response to Mtb infection is varied and complex. Enhanced understanding of this intricate orchestration of host defence against the bacillus has been heralded as fundamental to advancing global TB control [4], and recent years have seen gathering interest in the development of host-directed treatments and vaccinations [6,8,9,17]. Adjuvant host-directed therapies (HDTs), either through enhancement of successful host defence strategies or through limitation of tissue-damaging inflammation, have the potential to shorten treatment duration, circumvent drug resistance, reduce infectivity and improve vaccine efficacy [6,8,9,17]. Thus, improved understanding of the host immune mechanisms in Mtb infection is paramount to combatting this global pandemic.

1.1.2 Host Immune Responses to Mtb: the Vital Role of Early Macrophage Response

Mtb is spread by the inhalation of airborne droplets into the airways and alveoli of the host [18]. Here, the bacillus encounters the alveolar macrophage, a mononuclear phagocyte resident in the alveolus, and is internalised via phagocytosis [19,20]. Once internalised, a phagosome forms

around the bacillus, from which mycobacterial material can be delivered to the antigen presentation pathway to allow major histocompatibility complex II (MHC II)-mediated antigen expression, necessary for the activation of T cells [19]. Phagosomes ultimately fuse with lysosomes through the process of phagolysosomal maturation, facilitating lysosomal destruction of the bacillus [21-23]. Virulent Mtb strains, however, preventing phagosome-lysosome fusion and perversely allowing the macrophage to be used as a niche for intracellular survival and replication of the bug [24-27]. Activation of macrophages – for example, following toll-like receptor (TLR) recognition of mycobacterial ligands, or following stimulation by host-derived antimicrobial peptides or cytokines, such as interferon-γ (IFN-γ) – can overcome this phagolysosomal maturation block to promote elimination of Mtb [19,27-29], as well as producing directly toxic reactive oxygen species (ROS), reactive nitrogen species (RNS), and toxic metals [30-35]. Nitric oxide (NO) specifically is fundamental to macrophage mycobactericidal activity in murine macrophages [31,35], though its contribution to Mtb killing in human macrophages is less clear [2,32,33,36-38]. In retaliation, Mtb has evolved a number of strategies to prevent both macrophage activation [39,40] and generation of ROS, RNS and toxic metals [41-44]. Similarly, macrophage cell death plays a role in host defence [2], with apoptotic cell death thought to favour mycobacterial elimination through limiting intracellular replication [45,46] and enhancing antigen presentation [47], but virulent Mtb strains can arrest apoptosis to allow continued bacillary growth and can induce necrotic cell death to facilitate cell-to-cell spread of infection [45,48,49]. Thus, a dynamic battle between macrophage and bacillus will determine the success of the alveolar macrophage in clearing the infection or, conversely, the success of the bacillus in subverting this immune cell into a niche for survival and replication.

Where alveolar macrophages fail to destroy the invading pathogen, ongoing bacillary replication prompts an influx of phagocytic cells to the site of infection [50] – including neutrophils, monocytes, and dendritic cells – which are also capable of phagocytosing the bacillus [51-54] via a diverse array of receptors [20]. Neutrophils are the most abundant immune cell found in the airways of patients with active Mtb infection [55], playing an important role in macrophage activation [56-58] and dendritic cell maturation [59,60], although Mtb subversion of neutrophil function has implicated these cells in increasing susceptibility to infection also [53,61]. Monocytes recruited from the circulation differentiate into macrophages and, similar to alveolar macrophages, can be hijacked by the bacillus to provide a nidus for replication [50]. Resident and recruited immune cells produce proteases [62,63], anti-microbial peptides [64], pro-inflammatory cytokines [54,65-68] and chemokines [69,70]. These products can directly inhibit mycobacterial growth, activate mycobactericidal functions in surrounding cells, and recruit further immune cells to the site of infection, but are also responsible for tissue-damaging excessive inflammation which

can contribute to the pathology observed in TB disease [50,71,72]. Conversely, Mtb-induced production of anti-inflammatory cytokines such as interleukin-10 (IL-10) and transforming growth factor-β (TGF-β) [73,74], though associated with impaired immune responses and increased susceptibility to infection, may help regulate inflammation and prevent tissue damage [50].

Dendritic cells are integral to the orchestration of host defence. In their role as professional antigen presenting cells (APCs) [75], dendritic cells migrate from the site of initial infection within the lung parenchyma to the draining lymph node [76,77]. There, they are responsible for activating T cell responses via MHC-mediated antigen presentation [78,79], in conjunction with costimulatory molecule expression and cytokine production [75], particularly interleukin-12p40 (IL-12p40) [80]. Again, however, Mtb seeks to disrupt this important host defence mechanism, and evidence for infection-induced inhibition of dendritic cell maturation and function also exists [52,81-84]. Activation of adaptive immunity does not occur until 12 days post infection in mice [85], and can be delayed until 5 – 6 weeks post infection in humans [86-88], a phenomenon that has been linked to impaired trafficking of bacilli to the lymph node for antigen presentation [89]. Slow migration of activated T cells to the site of infection can further delay mounting of an efficient adaptive immune response [2], and during this so-called "lag" phase bacilli replicate exponentially and infection can become established within the lung [50,90].

Despite this delayed onset in adaptive immunity, animal studies demonstrate both $CD4^+$ and $CD8^+$ T cell-mediated responses as critical in the host defence against Mtb infection [2,91], with $CD4^+$ Th1 and Th17 cells having the predominant role [2,92]. $CD4^+$ Th1 cells produce IFN-γ, a potent activator of macrophage mycobacteristatic and mycobactericidal activity, and absence of either $CD4^+$ cells or IFN-γ renders mice hypersusceptible to Mtb infection [2,91]. $CD4^+$ Th17 cells produce IL-17 and are implicated in neutrophil recruitment, which can contribute to inflammation and increased pathology [92], but also appears to be crucial in mounting an effective host response to the hyper-virulent strain of Mtb HN878 [93]. Mobilisation of the adaptive immune response also permits cytokine- and chemokine-directed formation of granulomas, the characteristic histopathological lesions of TB disease [90,94]. The granuloma is an inflammatory structure comprising a central mass of infected macrophages, foam cells, Langerhan's multinucleated giant cells and neutrophils, surrounded by lymphocytes and fibroblasts, which create a peripheral fibrotic capsule [2,90,94]. Within this structure, mycobacterial replication and dissemination of infection can be contained [90], and the human host may remain asymptomatic despite persistent chronic infection, so-called "latent TB infection" (LTBI). Bacilli are believed to enter a dormant, non-replicative state [90,95,96], and consequent decreases in the cellularity of the granuloma often mean no clinical signs of disease are evident on chest radiograph either [97]. Conversely, active TB disease is associated with progressive accumulation of caseum within the hypoxic

centres of these structures, leading to necrosis and cavitation of the granuloma centre and to release of replicating bacilli into the airways (facilitating both aerogenous dissemination to other sites within the lung and human-to-human transmission) and the circulation (facilitating haematogenous dissemination to other organs in the body) [90,98]. Progressive caseation and dissemination of the granuloma can occur immediately following primary infection, or may occur many years (even decades) later due to alterations in host immune function, termed "reactivation" of LTBI [99,100].

Thus, the host immune response to Mtb infection is complex and varied, depending on a multitude of factors, including host immunogenetics, Mtb virulence and environmental influences [2,50,71]. Initial infection of the alveolar macrophage can result in complete clearance of the bacillus, with no mobilisation of the adaptive immune system [15,16]. If infection is not cleared in this initial phase, recruitment of other innate immune cells and delayed activation of adaptive immunity occurs, characterised by heterogeneous granuloma development at sites of infection [2,50]. Progressive caseation of the granuloma may then lead to the development of active TB disease [90,98], characterised by continued bacillary replication, excessive inflammation and tissue damage, dissemination within the lung and to other organs, and aerosol transmission to other human hosts. Alternatively, granuloma formation may limit replication, leading to latent infection that can persist asymptomatically for the lifetime of the host [90,101], though reactivation may occur should immune function become compromised [50,90]. A summary of the cellular immune response occurring early after infection with Mtb is depicted in **Figure 1.1**.

Elucidating the fundamental mechanisms underlying these diverse human host immune responses to Mtb infection is vital to understanding susceptibility factors associated with clinical disease, developing therapies to enhance successful immune strategies, and improving vaccine efficacy in order to decrease the global burden of TB. Specifically, an appreciation of early immune events in the alveolar macrophage – which can either facilitate complete clearance of the bug or permit bacillary survival and replication, with consequent progression to either persistent latent infection or active pathological disease – is a crucial step in our fight against this deadly pathogen. In this work, we seek to understand some of the mechanisms governing anti-Mtb functions in the human macrophage.

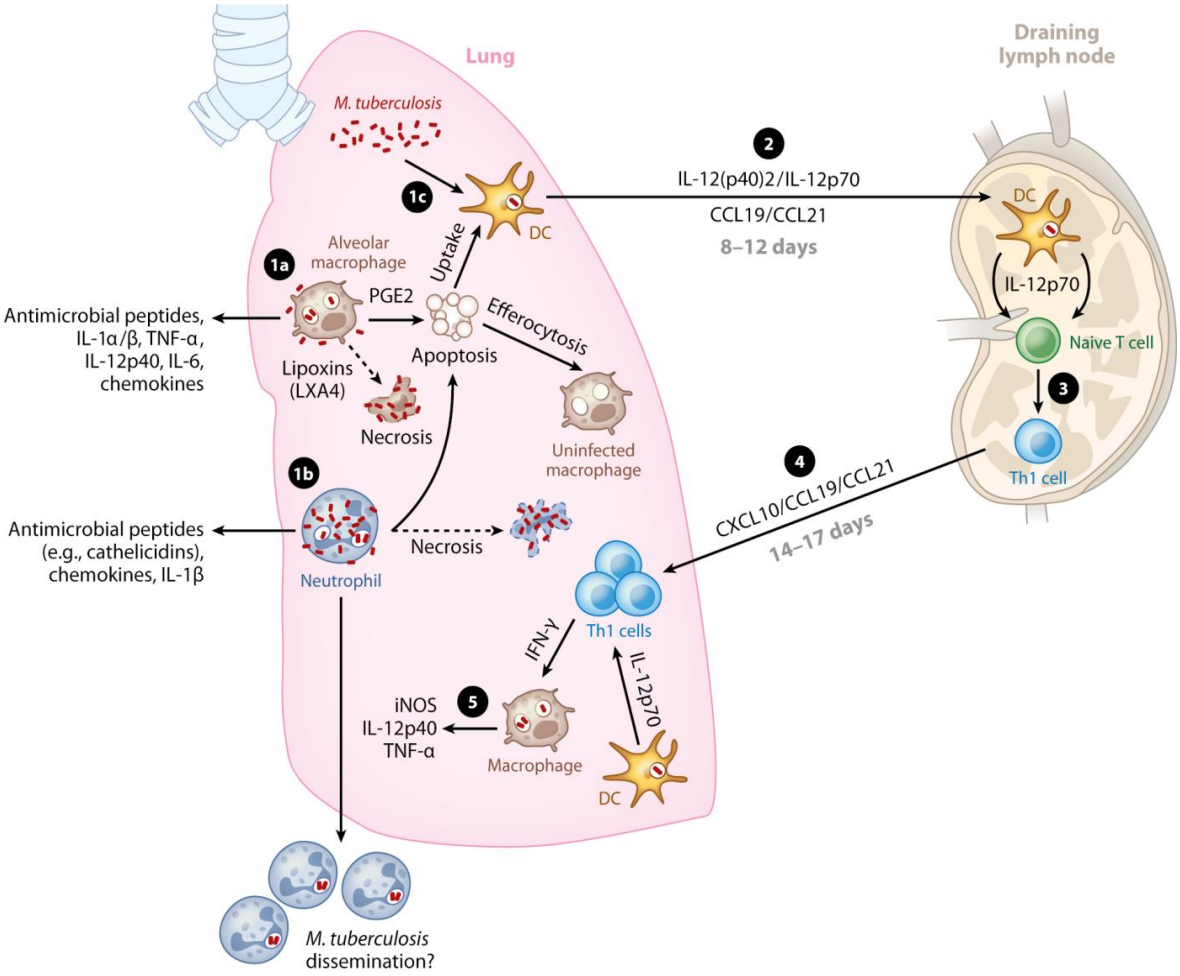

O'Garra A, et al. 2013.
Annu. Rev. Immunol. 31:475–527

FIGURE 1.1: The cellular immune response to *M. tuberculosis*: Following aerosol infection with M. tuberculosis, resident lung alveolar macrophages (1a), neutrophils (1b) and lung DCs (1c) can become infected, leading to the production and secretion of antimicrobial peptides, cytokines, and chemokines. The balance of lipid mediators, such as prostaglandin E2 (proapoptotic) or lipoxin (LX) A4 (pronecrotic), within infected macrophages plays a major role in determining downstream pathways leading to the induction of either apoptosis or necrosis. Infected apoptotic cells can be taken up by resident lung DCs or efferocytosed by uninfected lung macrophages (1c). M. tuberculosis–infected DCs migrate to the local lung-draining lymph nodes by 8–12 days post infection. DCs migrate to the lymph nodes under the influence of IL-12(p40)2 and IL-12p70 and that of the chemokines CCL19 and CCL21 (2), to drive naive T cell differentiation toward a Th1 phenotype (3). Protective antigen-specific Th1 cells migrate back to the lungs in a chemokine-dependent manner 14–17 days after the point of initial infection/exposure (4) and produce IFN-γ, leading to macrophage activation, cytokine production, the induction of microbicidal factors including iNOS (5), and bacterial control. *Reproduced from O'Garra et al, 2013 [2]*.

1.1.3 Polarisation and Plasticity of the Alveolar Macrophage

The divergent pathways of classical M1 or alternative M2 macrophage activation have been recognised since the 1990s [102]. Broadly speaking, classical M1 activation, induced by Th1-derived signals such as IFN-γ, leads to production of pro-inflammatory cytokines (TNF-α, IL-1β, IL-6), inducible nitric oxide synthase (iNOS) and ROS [102,103]. Alternative M2 activation, induced by Th2-type cytokines IL-4 or IL-13, generates anti-inflammatory IL-10 and TGF-β, enhanced phagocytic activity, reduced ROS, and upregulation of Arginase 1 (Arg1) rather than iNOS [102,103]. Accordingly, M1 macrophage activation is vital for inflammatory responses and cellular immunity, whereas M2 activation is linked to resolution of inflammation, humoral immunity and wound healing [102-104]. A pictorial representation of classical and alternative macrophage activation is offered in **Figure 1.2**. This classification is overly simplistic, however, and *in vivo* macrophage phenotype demonstrates significant heterogeneity and overlap and, interestingly, plasticity [103,105-107].

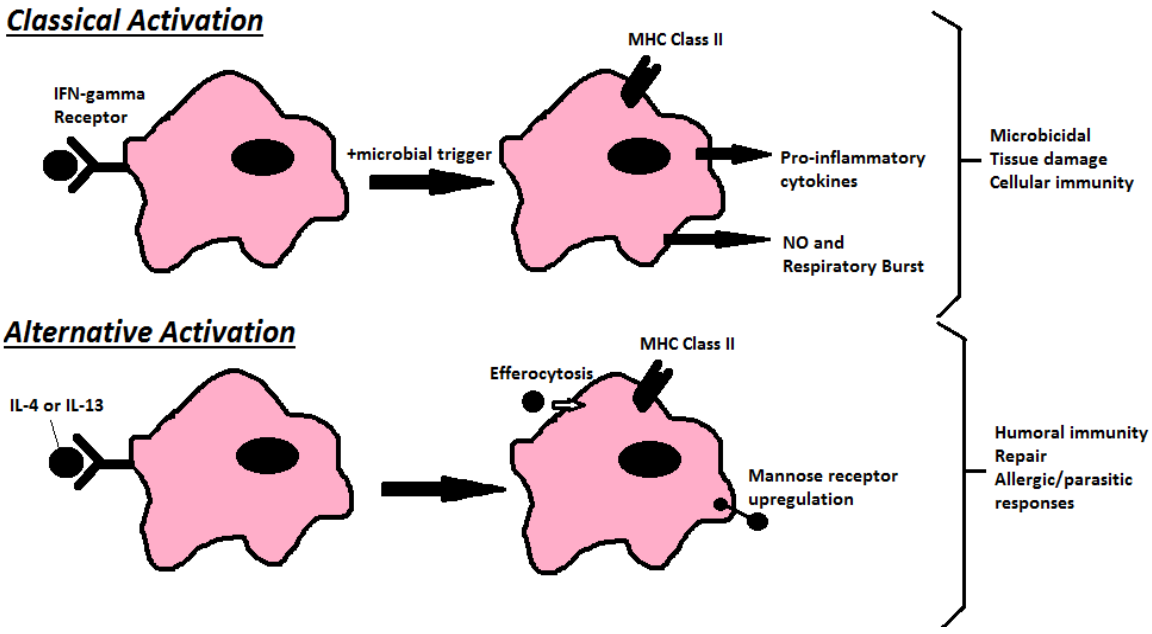

FIGURE 1.2: Classical and alternative activation of macrophages. Classical activation is mediated by the priming stimulus IFN-γ, followed by a microbial trigger (e.g. LPS). Alternative activation is mediated by IL-4 and IL-13, acting through a common receptor chain. *Adapted from Gordon et al, 2003 [102].*

The tissue-resident alveolar macrophage (AM) is considered, amid controversy [104], to be an alternatively activated M2 macrophage [103]. AM express high levels of M2-associated receptors [103], including the mannose receptor (aka CD206) [108] and peroxisome proliferator-activated receptor-γ (PPAR-γ) [109,110], which downregulate inflammatory functions [111,112]. AM demonstrate an attenuated oxidative burst, decreased antigen presentation, increased phagocytic ability, and increased anti-inflammatory cytokines [104,113,114]. They also contribute to the differentiation of regulatory T cells [115]. This M2-like phenotype may reflect the important role of AM in limiting inflammation-mediated lung tissue damage, and possibly represents a necessary mechanism to prevent AM activation in response to airway commensal bacteria [104].

Conversely, M1 macrophage functions are essential for effective AM clearance of Mtb [116]. Polarisation studies of mouse macrophages indicate that alternative activation is associated with delayed and impaired anti-mycobacterial functions [117]. Using a computational granuloma formation model in combination with calculated macrophage polarisation ratios, Marino et al also linked M1 macrophage polarisation early post infection (within 2 – 4 months) to favourable granuloma outcome [118]. AMs retain an inherent phenotypic plasticity that renders them amenable to M1 reprogramming – confirmed by the ability of *ex vivo* AM from healthy non-smokers to transcriptionally upregulate M1-associated genes in response to IFN-γ stimulation [119]. Transcriptional studies of macrophages infected with virulent Mtb also show upregulation of M1-associated genes [120], and AM in bronchoalveolar lavage (BAL) fluid from Mtb-infected mice were predominantly M1 polarised, as were granuloma-associated macrophages [121].

However, Mtb infection can also subvert this essential AM M1 polarisation [116]. Raju et al describe a subset of pulmonary TB patients with upregulated Th2-related genes found on gene expression analysis of BAL fluid cells [122]. Similarly, virulent Mtb strain H37Rv has been shown to induce macrophage PPAR-γ expression, as did the mycobacterial antigen mannose-capped lipomannan, mediated through the mannose receptor [123]. Mtb-mediated induction of anti-inflammatory IL-10 has also been well-described [124-126], as has upregulation of Arg1 [127]. IL-10 downregulates IFN-γ response [128,129] and inhibits phagosome-lysosomal fusion [124] in Mtb infection. This Mtb-induced redirection of AM polarisation results leads to reduced mycobactericidal function [116,130], and it has been suggested that M2 polarisation may facilitate “hijacking” of the macrophage for bacillary survival and replication [116,127].

Thus, AM polarisation plays a central role in the early host response to Mtb, with M1 polarisation likely favouring elimination. As discussed below, the pro-inflammatory cytokine IL-1β, characteristic of M1 polarisation [102], has been demonstrated in human AM infected with Mtb [131], and plays a crucial role in the early host immune response to Mtb.

1.2 IL-1β in the Host Response to Mtb infection

1.2.1 IL-1β Signalling

IL-1β is a potent pro-inflammatory cytokine crucial in the host response to a myriad of pathogens [132-137]. It is primarily a product of monocytes, macrophages and dendritic cells, though low levels are produced by natural killer (NK) cells and B lymphocytes also [138]. Within the lungs of Mtb-infected mice, inflammatory monocytes and dendritic cells were demonstrated to be the predominant source of IL-1 [139].Via the IL-1 receptor (IL-1R1), it activates release of other pro-inflammatory cytokines (such as TNF-α and IL-6), recruits neutrophils, enhances T cell activation and antigen recognition, promotes Th17 differentiation, and induces prostaglandin synthesis and release [135,138,140]. IL-1β is also implicated in systemic features of the acute phase response such as fever and in the chronic inflammation implicated in the pathogenesis of many diseases, including Type 2 Diabetes (DM2) [132,138,141].

The IL-1R1 is an 80kDa membrane-spanning protein that contains an extracellular immunoglobulin-like ligand-binding domain and an intracellular Toll/IL-1R (TIR) domain [142]. Upon activation by IL-1β, which also requires binding of the IL-1R accessory protein (IL-1RAcP), myeloid differentiation primary response gene (MyD88) is recruited to the intracellular TIR domain, leading to downstream activation of IL-1R associated kinases (IRAKs). Subsequent modification and activation of TNF receptor-associated factor 6 (TRAF6) ultimately leads to activation of nuclear transcription factor kappa B (NFκB) (via modification of inhibitor of NFκB kinase (IKK)) and JUN N-terminal kinase (JNK) and p38 kinase [142]. NFκB translocates to the nucleus where it induces transcription of a number of target genes, causing rapid mobilisation of pro-inflammatory responses [142]. Pro-inflammatory IL-1α and anti-inflammatory IL-1R antagonist (IL-1Ra) – a natural inhibitor of IL-1 signalling which blocks binding of IL-1α and IL-1β as well as preventing recruitment of IL-1RAcP – also bind to IL-1R1 [138]. The IL-1 signalling cascade is summarised in **Figure 1.3**.

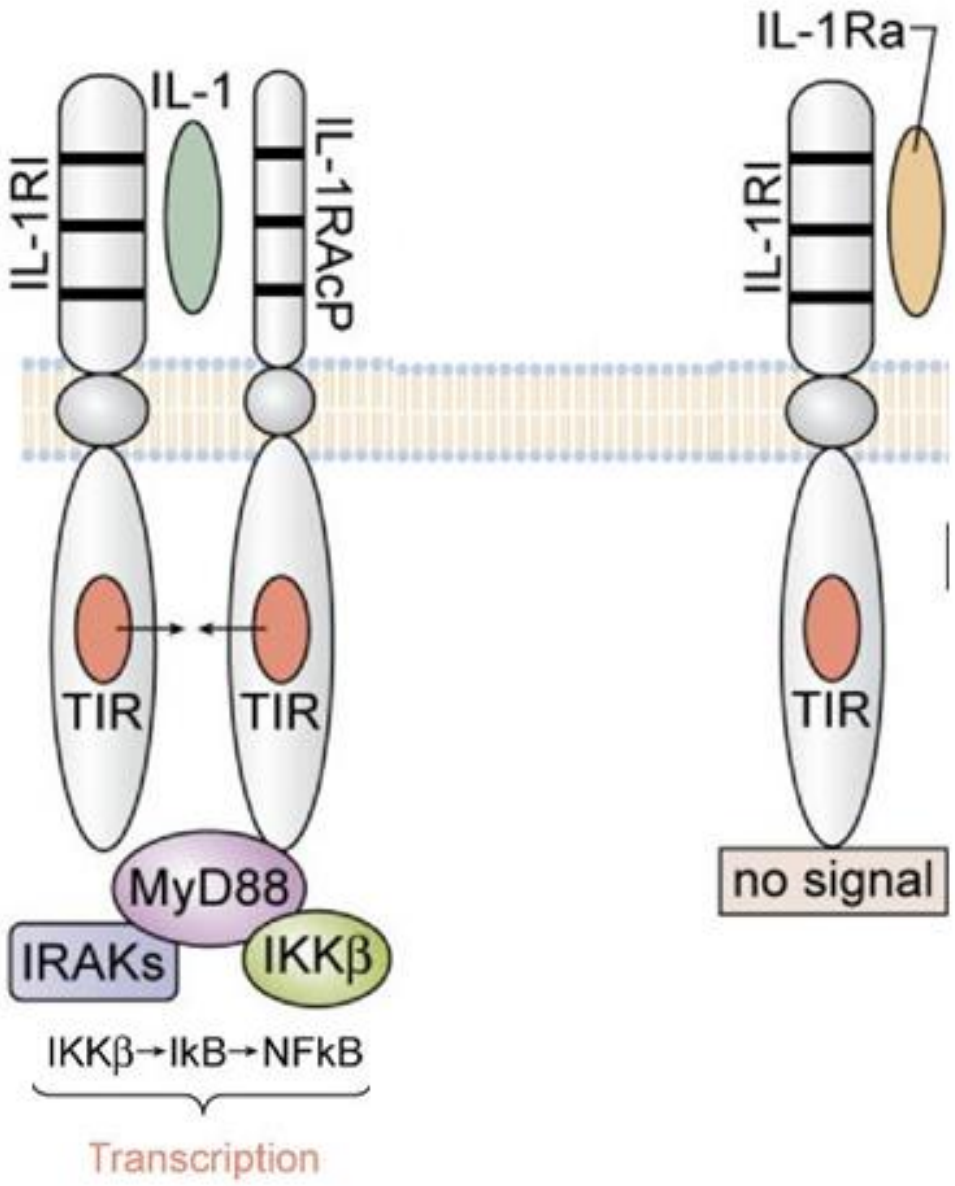

FIGURE 1.3: The IL-1 signalling cascade. IL-1α or mature IL-1β bind to the IL-1R1 and with the IL-1RAcP forms the receptor heterodimeric complex. The TIR domain of each receptor chain approximate recruit MyD88, followed by phosphorylation of IRAKs and IKKβ, resulting in a signal to the nucleus. Conversely, IL-1Ra binds to IL-1R1, but there is no signal because there is failure to form a complex with IL-1RAcP. *Adapted from Dinarello et al, 2011 [141].*

1.2.2 IL-1β and the Host Immune Response to Mtb

IL-1 signalling is crucial in the innate immune response to Mtb infection [133,134,139,143-146]. Using IL-1α/β double-knockout (KO) mice infected with H37Rv via an airborne infection apparatus, Yamada et al reported significantly larger lung granulomas compared to WT animals [144]. The same group subsequently demonstrated increased granuloma size and decreased survival in IL-1R1-KO mice compared to WT following infection with virulent Mtb *Kurono* strain [145]. These findings echoed those of Jufferman et al, who reported defective granuloma formation and increased mortality in IL-1R1-KO mice compared to their WT counterparts [143]. Fremond et al similarly reported rapid-onset necrotizing pneumonia with neutrophilic influx and impaired granuloma formation in IL-1R1-KO mice following intranasal inoculation with low dose H37Rv, with these animals dying approximately 4 weeks post-infection while their WT counterparts survived the duration of the experiment (3 months) [133].

Confirming the essential role of IL-1β specifically, Mayer-Barber et al saw increased lung bacillary load, increased granuloma size, increased lung inflammation and decreased survival in experiments with IL-1β-KO mice, results that were in line with those observed in both IL-1R1-KO and MyD88-KO mice [134]. Importantly, IL-1α levels in BAL fluid from IL-1β-KO mice 4 week post infection were significantly higher than in WT controls [134], possibly indicating that upregulation of this alternative IL-1 mediator in the absence of IL-1β is insufficient to restore immune responses. This agrees with observations that IL-1β, not IL-1α, plays a critical role in early defence against pathogens such as *Streptococcus pneumoniae* [147] and *Leishmania major* infection [148]. Conversely, others have implicated IL-1α as the dominant mediator of IL-1 signalling in a chronic model of Mtb infection [149,150], and Guler et al speculate that antagonism of IL-1α signalling secondary to upregulation of IL-1Ra in IL-1β-KO mice may explain the increased susceptibility of these animals to Mtb [149]. In actuality, a cooperative response involving both IL-1α and IL-1β is probably required, with combined antagonism or absence of both cytokines resulting in increased TB disease severity than that of either cytokine in isolation [139,149]. Within human populations, several polymorphisms in the *IL1B* gene sequence have been linked to TB disease susceptibility [151-153], and a protection-conferring single nucleotide polymorphism (SNP) at position -511 in the *IL1B* promoter region functions to increase IL-1β production in response to TLR stimulation [154], suggesting that IL-1β is important in early host defence.

Prolonged excessive IL-1β production is also implicated in the pathophysiological progression of TB disease, however [155-158]. Functional polymorphisms in the *IL1B* gene predisposing to excessive IL-1β production have also been linked to increased susceptibility to TB disease [155,159]. Elevated serum IL-1β levels correlate to disease severity in multidrug resistant (MDR)

TB patients [160], and inflammasome activation has been linked to tissue destruction caused by matrix metalloproteinases (MMPs) [157]. Furthermore, the IL-1R1 antagonist anakinra, approved for clinical use in a range of inflammatory disorders, has not been associated with increased rates of TB disease to date [161,162], though isolated case reports of reactivation secondary to this drug do exist [163,164]. Thus, though IL-1β is a crucial component of early host responses to Mtb infection, its persistent production can be detrimental to the host.

1.2.3 IL-1β induction by Mtb infection

Production of IL-1β is a two-step process. During the priming step, a 31kDa inactive precursor protein, so-called "pro-IL-1β", is produced in response pathogen associated molecular patterns (PAMPs) or danger associated molecular patterns (DAMPs) binding to pattern recognition receptors (PRRs) on the macrophage [165] – for example, members of the toll-like receptor (TLR) family. Mtb is known to stimulate TLR2, TLR4 and TLR9, leading to MyD88 recruitment to the intracellular TIR domain and activation of downstream signalling cascades [20]. Following PRR stimulation, pro-IL-1β transcription is induced by NFκB, a transcription factor activated in response to pro-inflammatory stimuli [166,167], including IL-1β itself (see above) [142]. TLR stimulation also activates phosphoinositide-3 kinase (PI3K) and its downstream target Akt [168] (which activates mammalian target of rapamycin (mTOR) [169]), and this path has been linked to IL-1β production in murine macrophages [170,171]. Importantly, hypoxia inducible factor-1α (HIF-1α) can also induce pro-IL-1β transcription [172,173], with both human (*IL1B*) and mouse (*Il1b*) gene sequences (located on chromosome 2) containing conserved canonical HIF-1α binding sites [174]. Thus, while NFκB mediates rapid early induction of pro-IL-1β, HIF-1α facilitates its sustained production at later timepoints.

In the context of Mtb infection, Kleinnijenhuis et al used peritoneal macrophages infected with H37Rv to demonstrate that induction of pro-IL-1β expression requires TLR2/TLR6 or nucleotide-binding oligomerization domain 2 (NOD2) [131], with MyD88 and mitogen activated protein kinase (MAPK; an upstream activator of NFκB) playing an essential role. Interestingly, TLR4 and TLR9 signalling was dispensable in this setting [131]. Supporting this observation, a study involving *in vitro* Mtb infection of murine bone marrow derived macrophages (BMDM) highlighted both MyD88 and TLR2/9 signalling as vital for IL-1β production [134]. TLR2 is stimulated by bacterial lipopeptides [175-177], and heterodimerises with both TLR1 and TLR6 to expand its ligand spectrum [177]. A number of mycobacterial cell wall constituents bind TLR2, such as lipoarrabinomannan (LAM), phosphatidylinositol mannoside (PIM), lipoproteins and glycoproteins

[20,178], and mice deficient in TLR2 demonstrate increased susceptibility to Mtb infection [179,180].

The second step of IL-1β production requires cleavage of pro-IL-1β by caspase-1 to form the 17kDa mature protein IL-1β in order to permit secretion [165]. Caspase-1 activation involves its recruitment to a multi-protein complex known as the inflammasome [165,181]. A number of different inflammasomes activated by various stimuli can activate caspase-1 [181], but the NLRP3 inflammasome remains the best characterised to date. This molecular scaffold is made up of NLRP3 (consisting of a PAMP/DAMP-sensing C-terminal leucine rich repeat (LRR), a central nucleotide binding domain, and an N-terminal pyrin domain (PYD)), apoptosis-associated speck-like protein containing a caspase recruitment domain (ASC), and caspase-1 [181]. NLRP3 inflammasome activation is induced by a range of PAMPs and DAMPs, such as the bacterial ligand muramyl dipeptide (present in Mtb peptidoglycans) [182], mitochondrial ROS [183,184], or extracellular adenine triphosphate (ATP) (increased in the setting of cell necrosis) signalling via the PX2 purinergic receptor 7 (P2RX7) [185,186]. Interestingly, cathelicidin LL-37, an antimicrobial peptide upregulated in Mtb-infected cells [64], also signals through P2RX7 to induce IL-1β processing [187].

In murine BMDM infected with Mtb *in vitro*, either caspase-1 or ASC deficiency was associated with striking reduction in mature IL-1β production [134]. Importantly, however, caspase-1 independent cleavage of IL-1β by other proteases – such as neutrophil- or macrophage-derived serine proteases (e.g. proteinase 3) or pathogen-derived proteases – has been described also [138,140]. Mayer-Barber et al proposed a caspase-1-independent pathway for IL-1β cleavage *in vivo* after observing that BAL fluid IL-1β levels from both ASC- and Caspase-1-KO mice were similar to that of WT [134]. Though this could possibly be explained by increased neutrophil-derived IL-1β, and these animals did not display increased mortality early post infection, suggesting caspase-1-independent IL-1β production as an important player in host defence against Mtb *in vivo* [134].

1.2.4 IL-1β and Early Macrophage Responses to Mtb

Early protective effects of IL-1β in Mtb infection have been linked to a number of different mechanisms. Links to T cell activation and antigen presentation are well-established [138,140], and numerous studies have implicated IL-1 signalling in IL-12p40 and IFN-γ production [133,134,143,145], both crucial elements of the host response to Mtb [188-191]. IL-1β is important for recruitment of neutrophils also [135,192,193], which can contribute to both effective [56-60] and detrimental [53,61] aspects of the host response.

IL-1 signalling also plays a role in macrophage mycobacteristatic and mycobactericidal activity early post infection, with BMDM from mice deficient in IL-1 signalling demonstrating increased colony forming units (CFU) following infection *in vitro* [146]. As discussed earlier, the early mycobactericidal function of macrophage is integral to determining outcome of infection with respect to clearance of the bug or mobilisation of adaptive immune functions with consequent development of active disease or containment as latent infection. How IL-1β promotes macrophage killing capabilities is an area of investigation. NO is a fundamental player in terms of macrophage mycobactericidal activity [31,33,35]. However, though early experiments using IL-1-α/β-KO and IL-1R1-KO mice demonstrated decreased AM production of NO and decreased iNOS expression, respectively [144,145], later work in both IL-1R1-KO and IL-1β-KO mice failed to corroborate this [133,134,146]. Interestingly, NO-mediated inhibition of IL-1β production in the setting of Mtb infection has been described, a possible autoregulatory feedback loop [156,194].

The pro-inflammatory cytokine TNF-α, characteristically produced by the M1 activated macrophage, is critical in early host defence against TB [100,195,196], and enhances macrophage-mediated mycobacteristatic effects [195]. Though several *in vivo* studies involving IL-1α/β- or IL-1R1-KO mice suggested no downstream effect on TNF-α production [143-146], addition of recombinant IL-1β or exogenous induction of IL-1β has been shown to augment both TNF-α and TNF-α receptor 1 (TNFR1) expression in Mtb infected macrophages *in vitro* [197]. Di Paulo et al have reported reduced expression of TNFR1 on recruited neutrophils in IL-1R1-KO mice, resulting in reduced ROS and increased necrotic death [150]. Neutrophil necrosis is known to subvert the macrophage and dendritic cell activation that is induced by neutrophil apoptosis [57,59], as well as contributing to tissue damaging inflammation via release of proteases. This supports an interesting model whereby TNF and IL-1 signalling may act synergistically to orchestrate early host responses via neutrophil responses [150], rather than direct enhancement of macrophage mycobactericidal activity, with authors suggesting that this could explain increased susceptibility to infection in mice deficient in IL-1 signalling despite normal or increased levels of TNF-α [143-145].

Recently, a novel mechanism for IL-1β-driven enhancement of macrophage mycobacteristatic and mycobactericidal activity has been proposed, implicating eicosanoid reorganisation and type I interferons (IFN-α and IFN-β – collectively, Type I IFNs) downregulation in this process. Eicosanoids are lipid mediators generated enzymatically via oxygenation of arachidonic acid [198], a phospholipid-derived polyunsaturated omega-6 fatty acid. Arachidonic acid can be directed by the enzyme 5-lipoxygenase (5-LO) to generate lipoxin (LXA) and leukotrienes (LTs), or alternatively, by the enzyme cyclooxygenase (constituively expressed COX1, or inducible COX2) to generate prostaglandins (PGs) [198]. Eicosanoids represent a complex network with a vast array

of functions [198], but broadly speaking, LXA and LTs have been linked to increased susceptibility to Mtb infection [199-201], while prostaglandin E2 (PGE2) is linked to increased resistance [202-204]. Significant roles for PGE2 upregulation in inducing macrophage apoptotic cell death (rather than necrotic death, induced by LTs) [202,203,205,206] and inducing early iNOS expression for control of bacillary growth [207] have been demonstrated. As seen in the context of IL-1β production [155-158], prolonged elevations in PGE2 at later stages of infection have been linked to increased bacillary replication and disease progression [207], and COX2 inhibitors (termed "non-steroidal anti-inflammatory drugs", or NSAIDs) can improve outcome in mouse models of TB [208-210], though others have observed a continued role for PGE2 [146]. However, COX2 inhibition resulted in increased lung CFU in Mtb-infected mice early post infection (up to 45 days p.i.) [207], emphasising the importance of this mediator in early macrophage responses.

An alternative, recently elucidated, PGE2-mediated host defence mechanism involves inhibition of Type I IFN responses. Although demonstrating important antiviral effects, Type I IFN induction by virulent Mtb strains has been linked to hypersusceptibility to infection [211-214], possibly due to suppression of Th1 responses [215] (including IL-1α and IL-1β [139,216]) and induction of anti-inflammatory IL-10 and IL-1Ra [139]. Based on experiments involving mice defective in IL-1 signalling, Mayer-Barber et al have described IL-1β-induced upregulation of COX2-mediated PGE2 production [146], necessary for control of both intracellular and extracellular bacillary growth in macrophages cultured *in vitro*. Add-back of exogenous IL-1α, IL-1β or PGE2 restored control of bacillary growth in IL-1α/β-KO cells [146]. IFN-β (a Type I IFN) antagonised induction of IL-1β and PGE2, and IL-1 or PGE2 antagonised induction of IFN-β, suggesting a system of counter-regulation [146]. IL-1R1/IFNAR1-double KO mice were less susceptible to Mtb infection than IL-1R1-KO mice, revealing suppression of Type 1 IFNs as a major mechanism of IL-1-mediated host resistance. A role for IL-1-induced PGE2 with concomitant downregulation of Type I IFNs was corroborated via *in vivo* mouse studies [146]. Exogenous administration of PGE2 or zileuton (a 5-LO inhibitor used for treatment of asthma) completely protected mice from weight loss and mortality, correlating with increased PGE2, decreased IFN-β, and decreased IL-1Ra (upregulated via IFN-β) [146].

Thus, IL-1 mediated signalling can influence eicosanoid balance to increase macrophage control of Mtb infection. Furthermore, Mayer-Barber et al demonstrate efficacy for host-directed therapy targeting this pathway in early treatment of Mtb infection in mice. Greater understanding of the mechanisms underlying IL-1β regulation, therefore, may highlight novel therapeutic or vaccine targets for future host-directed therapies, as well as identify causes for increased susceptibility to Mtb infection observed in certain populations (e.g. smokers, DM2). Recent discoveries in the burgeoning field of immunometabolism link IL-1β production in murine macrophages to a TLR-induced shift to glycolytic metabolism, warranting its investigation in the context of Mtb infection.

1.3 Metabolic Reprogramming in the Host Response to Mtb infection

1.3.1 Cell Energy Metabolism: OXPHOS, Glycolysis and the Warburg Effect

Cell energy metabolism refers to the process by which biochemicals are used to generate energy (in the form of ATP) [217]. In a normal, quiescent immune cell, energy requirements are met through metabolism of glucose via the glycolytic pathway to the metabolic intermediate pyruvate. Pyruvate then feeds into the tricarboxylic acid (TCA) cycle in the mitochondrion, mobilising the electron transport chain (ETC) to generate large amounts of ATP (approximately 36 – 38 molecules of ATP per glucose molecule) [218]. This process is known as oxidative phosphorylation (OXPHOS) and requires the presence of molecular oxygen. Cells exposed to a hypoxic environment cannot proceed through OXPHOS due to limited oxygen availability. Instead, glucose is metabolised only through the anaerobic glycolytic pathway, which is less efficient at generating energy (2 molecules of ATP per glucose molecule), but does not require oxygen [218]. During anaerobic glycolysis, pyruvate is converted to lactate, which is then exported from the cell via the monocarboxylate transport system.

In brief description of these events, extracellular glucose is taken up by cells via a family of glucose transporters (GLUT 1 – 14) and hexokinase (HK) irreversibly catalyses its conversion to glucose-6-phosphate (G6P) [218]. From here, it proceeds through glycolysis, a series of enzyme-catalysed reactions that occurs in the cytosol and requires NAD^+. The final irreversible step of the glycolytic pathway generates pyruvate via the enzyme pyruvate kinase. Pyruvate enters the mitochondrion and is decarboxylated to acetyl CoA, which in turn feeds into the catabolic TCA cycle (aka Kreb's cycle; aka citric acid cycle) [218]. The TCA cycle comprises a number of metabolic intermediates (including citrate and succinate), generated through a series of enzyme-catalysed reactions that produce reducing equivalents NADH and Flavin adenine dinucleotide ($FADH_2$) [218]. These reducing equivalents act as electron donors for the ETC [218,219], located on the inner mitochondrial membrane. Complex I and Complex II accept electrons from TCA-cycle generated reducing equivalents, and electrons are transferred via redox reactions through the complexes of the ETC, with Complex IV transferring electrons to molecular oxygen to generate water. Energy generated from this transfer of electrons is used to pump protons (H^+) into the mitochondrial inter-membrane space – via Complexes I, III and IV – creating an electrochemical proton gradient across the inner membrane known as the mitochondrial membrane potential ($\Delta\Psi$). ATP synthase (Complex V) then harnesses this electrochemical gradient, using the energetically favourable return of H^+ ions back across the inner membrane to drive synthesis of ATP [218,219]. To varying degrees, cells can also metabolise substrates other than glucose, including glutamine (via

glutaminolysis) or fatty acids (via β-oxidation), in order to replenish TCA intermediates and fuel OXPHOS [218,220].

As alluded to above, in the absence of oxygen, cells utilise anaerobic glycolysis to meet energy requirements, with lactate dehydrogenase (LDH) catalysing the conversion of pyruvate to lactate (a reaction that replenishes NAD^+, required for continued glycolysis) [218]. **Figure 1.4** summarises the process of intracellular glucose metabolism.

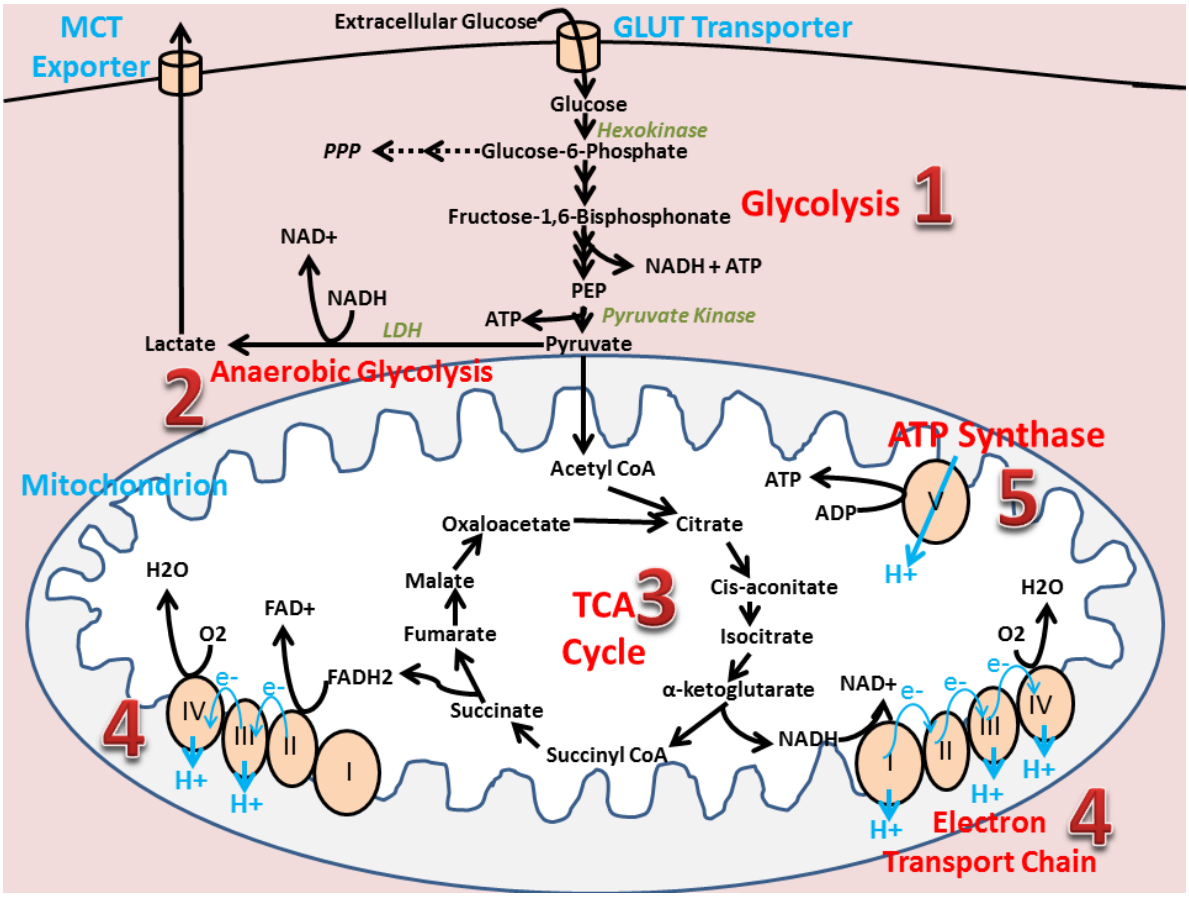

FIGURE 1.4: Intracellular glucose metabolism. [1] Extracellular glucose is taken up via members of the GLUT family of glucose transporters and is catabolised via glycolysis to generate pyruvate, generating a small amount of ATP. [2] In the absence of oxygen, pyruvate is metabolised to lactate which is then exported from the cell, a process known as anaerobic glycolysis. [3] If oxygen is available, pyruvate enters the mitochondrion and is metabolised to acetyl CoA, which feeds into the TCA cycle at citrate. The TCA cycle generates NADH and FADH2 which provide electrons to Complex I and II of the electron transport chain (ETC), respectively. [4] Energy generated via transfer of electrons along the electron transport chain is used to pump hydrogen ions across the inner mitochondrial membrane to the intermembrane space, creating an electrochemical gradient called the mitochondrial membrane potential. [5] ATP synthase harnesses the mitochondrial membrane potential to drive synthesis of a large amount of ATP.

Aerobic glycolysis (aka the Warburg effect), conversely, involves the metabolism of pyruvate to lactate despite adequate availability of oxygen, and is generally associated with downregulation of OXPHOS and diversion of metabolic intermediates such as citrate into biosynthetic pathways [220,221]. First reported in cancer cells in 1923 [222], through the latter half of the 20th century evidence of glycolytic reprogramming in activated immune cells emerged, with elevated rates of glucose utilisation and aerobic glycolysis seen in neutrophils [223-225], monocytes [226], macrophages [227-231] and lymphocytes [232] following stimulation, though the metabolic rewiring observed in immune cells likely differs to the classical Warburg effect of cancer cells. This metabolic shift is understandably necessary in order to meet the energy requirements of rapidly proliferating cells, such as activated T cells, with glycolysis allowing for faster turnover of ATP, while simultaneously providing biosynthetic precursors for required for expansion [233-235].

However, metabolic reprogramming of immune cells plays a functional role far beyond that of simple bioenergetics and biosynthesis [220,221]. The link between glycolytic reprogramming and anti-bacterial functions in neutrophils were postulated as far back as the 1980s – increased flux through the parallel pentose phosphate pathway (PPP) (that occurs in concert with increased flux through the glycolytic pathway and is similarly fed by G6P) was observed to generate the reducing equivalent nicotinamide adenine dinucleotide phosphate (NADPH) and, coupled with increased non-mitochondrial oxygen consumption, allowed formation of ROS important for neutrophil-mediated killing [236,237]. However, it is only in recent years that this fascinating interplay between cellular metabolism and host immune function has been intensively investigated, with pioneering work in dendritic cells carried out by the Pearce laboratory [238-240], as well as seminal work investigating the metabolism of macrophage polarisation by Rodriguez-Prados et al [241], generating renewed interest in the field. The emerging field of immunometabolism examines the interrelationship of immunity and metabolism, and incorporates both impacts of immune processes on metabolic diseases and of metabolic processes (and diseases) on immune functions. Exciting evidence is mounting for immune and metabolic cross-talk at the molecular, cellular, organ and organism level. In line with the work presented in this thesis, the following review centres on the impact of metabolic processes on immune function at the cellular level, with specific focus on macrophages.

1.3.2 Metabolic Reprogramming in Activated Macrophages

Distinct metabolic profiles are associated with M1 and M2 macrophages [221,241,242]. Classically-activated M1 macrophages have increased glycolytic flux, with upregulation of glycolytic enzymes. Following LPS stimulation, mitochondrial OXPHOS is simultaneously

downregulated, similar to observations in cancer cells where the Warburg phenomenon was first observed, though recent work by Lachmandas et al suggests that stimulation with other TLRs may induce increases in OXPHOS in conjunction with increased glycolytic rates, emphasizing the complexity of this intracellular metabolic rewiring [243]. Alternatively-activated M2 macrophages have increased β-oxidation of fatty acids and increased OXPHOS. Crucially, these profound alterations in metabolism instruct respective M1- and M2-macrophage functions, suggesting metabolic reprogramming as a critical determinant of functional phenotype. Considering the important role of M1 macrophages in Mtb infection, this suggests metabolic reprogramming as a potentially critical component of the host response. Furthermore, emerging evidence for plasticity of macrophage metabolic phenotype [244-246] recommends the possibility of therapeutic manipulation to improve early macrophage responses to infection.

Glycolytic reprogramming in classically-activated macrophages and dendritic cells occurs upon stimulation of a range of TLRs, including TLR2 [239,240], TLR3 [239], TLR4 [174,238-240,247], TLR7/8 [239], and TLR9 [239,240]. It has also been described in macrophages infected with *Bordatella pertussis* [174] and (in work conducted as part of this thesis) macrophages infected with *Salmonella typhimurium* [247] or *Mycobacterium tuberculosis* [247,248]. Though the precise mechanism of TLR-induced glycolytic reprogramming has not been fully elucidated, an essential role for Akt has been described [239,240]. Akt can directly increase activity of glycolytic enzymes [249], as well as supporting mTOR complex 1 (mTORC 1) activity, recently implicated in macrophage glycolytic reprogramming [250]. Amongst other functions [251], Akt and mTOR both drive LPS-induced upregulation of HIF-1α [252-255], which induces transcription of glycolytic and glucose transport enzymes [256-258]. TLR-stimulated macrophages express highly active isoforms of glycolytic enzymes, such as u-PFK2 (an isoform of phosphofructokinase-2 with high kinase activity and low bisphosphatase activity, promoting glycolytic flux) which is upregulated at the transcriptional level (*Pfkfb3*) in M1 macrophages [241,242].

Interestingly, glycolytic reprogramming in LPS-stimulated macrophages has also been linked to increased levels of the enzymatically-inactive dimeric form of the glycolytic enzyme PKM2 (pyruvate kinase M2) [247], which can also be induced by HIF-1α [259,260]. Two isoforms of pyruvate kinase exist, PKM1 and PKM2, generated by exclusive alternative splicing of the *Pkm* pre-mRNA [261]. PKM1 is constitutively active, converting phosphoenolpyruvic acid to pyruvate as the final, rate-limiting step of the glycolytic pathway. PKM2, however, can exist in an enzymatically-active tetrameric form or in an enzymatically-inactive dimeric form. In cancer models, it has been demonstrated that dimeric PKM2 translocates to the nucleus where it functions to upregulate glycolysis in a number of ways, including co-activation of HIF-1α activity

[260], as well as redirecting glycolytic intermediates into biosynthetic pathways (e.g. serine and alanine biosysnthesis) as a consequence of reduced conversion to pyruvate [259].

With decreased delivery of pyruvate to the mitochondrion, decreased TCA cycle activity is observed. Additionally, Jha and colleagues have described two functional "breaks" in the TCA cycle, based on an integrated transcriptional-metabolic analysis of macrophage polarisation [244]. Using a novel combined experimental and computational pipeline, termed "concordant metabolomics integration with transcription" (CoMB-T), they characterised the co-ordinated transcriptional (via RNA-seq-based profiling) and metabolic (via mass spectrometry-based profiling) rewiring of murine BMDM following stimulation with LPS/IFN-γ (M1) or IL-4 (M2) for 24 hours, subsequently validating results by isotope labelling experiments using U-^{13}glucose and U-^{13}-glutamine. In this way, two breakpoints in the TCA cycle were identified in M1 macrophages, at the isocitrate-to-α-ketoglutarate conversion step (catalysed by isocitrate dehydrogenase (*Idh*), which was downregulated) and at the succinate-to-malate conversion step (catalysed by succinate dehydrogenase (SDH), possibly functionally inhibited by NO) [244]. These breaks lead to accumulation of TCA intermediates succinate [174,244], citrate [174,244,262] and isocitrate [244], with functional consequences for the macrophage [174,262]. Similarly, using a metabolomics screen and microarray analysis, Tannahill et al observed a 30-fold increase in succinate levels in BMDM stimulated with LPS for 24 hours [174].

Compensatory upregulation of several anapleurotic pathways (i.e. reactions that replenish metabolic intermediates) is also observed in these cells, including increased glutaminolysis [174] (feeding the TCA cycle at α-ketoglutarate) and increased asparte-arginosuccinate shunt (AASS) activity [244] (feeding the TCA cycle at malate and fumarate). Increased AASS activity is proposed be linked to the observed TCA cycle "break" at succinate-to-malate and inhibition of the AASS enzyme aspartate transaminase (Got1) leads to increased OXPHOS and impairs M1 macrophage function [244]. Interestingly, the AASS is also implicated in regeneration of arginine needed for NO generation by iNOS, and mice deficient in aspartate arginosuccinate (Ass1), another AASS enzyme, demonstrate hypersusceptibility to virulent Mtb infection [263]. Concurrent with increased glycolytic flux, M1 macrophages demonstrate elevated PPP activity [244], resulting in increased generation of NADPH. TLR stimulation has been shown to suppress the PPP inhibitor carbohydrate-kinase like protein (CARKL) [264].

Finally, in addition to increased glycolysis, downregulation of OXPHOS has been described in M1 macrophages and dendritic cells following LPS stimulation. This may be a result of NO-mediated nitrosylation of ETC complexes, which can inhibit mitochondrial function and lead to decreased membrane potential [265]. Such NO-mediated progressive inhibition of mitochondrial respiration

has been observed in dendritic cells 6 hours following stimulation with LPS [238]. Increased glycolytic ATP is essential to meet energy requirements of the cell [238,240], therefore, as well as for maintenance of the mitochondrial membrane potential in the absence of a functioning respiratory chain [266,267]. Briefly, impaired function of the proton pump (Complexes I, III and IV) induces a reversal of ATP synthase (Complex V) activity, whereby it delivers protons to the inter-membrane space in order to maintain membrane potential and prevent cell death, consuming ATP in the process [268]. This essential role for glycolytically-derived ATP to facilitate reverse activity of the ETC, known as reverse electron transport (RET), has recently been linked to production of mitochondrial ROS via Complex I [269]. Some of the principal features of macrophage glycolytic reprogramming are summarised in **Figure 1.5**. Conversely, other TLR ligands induce upregulation in OXPHOS, indicating the complexity of metabolic reprogramming observed in activated macrophages [243].

Metabolism is substantially different in alternatively-activated M2 macrophages. IL-4 and IL-13 stimulation inhibits activation of mTOR [270], preventing the glycolytic switch and resulting in reduced HIF-1α levels [271]. M2-polarised macrophages express the less enzymatically-active forms of glycolytic enzymes [241,242] (e.g. the PFKFB1 isoform of phosphofructokinase-2, which demonstrates higher biphosphatase activity than u-PFK), also contributing to decreased glycolytic rate. CARKL expression is increased [264], leading to reduced PPP activity. Alternative activation with IL-4 induces fatty acid oxidation, as opposed to metabolism of glucose, and increased OXPHOS [245], driven by upregulation of the enzyme 5'AMP-activated protein kinase (AMPK) [272,273] and its downstream targets, the peroxisome proliferator-activated receptors (PPARs) [245,274-276]. Combined metabolomic and transcriptomic analysis suggests that glucose is in fact sequestered from central metabolism and instead utilised for the glycosylation of M2 mediators, with UDP-N-acetylglucosamine levels substantially upregulated [244]. Additionally, M2 activation is associated with increased Arg1-mediated metabolism of arginine to generate ornithine and urea, as opposed to iNOS-mediated generation of NO characteristic of M1 macrophages [242,277]. Interestingly, M2 macrophages may be amenable to metabolic retraining in order to boost M1 functions. Inhibition of mitochondrial OXPHOS in IL-4-treated macrophages enabled M1-associated functions following IFNγ/LPS stimulation [245], for example, and glutamine deprivation can inhibit M2 polarisation [244].

Metabolic programmes of M1 and M2 macrophages are substantially different, therefore. A simplified representation of these differences is depicted in **Figure 1.6**. Importantly, the metabolic alterations observed following classical or alternative activation play a vital role in M1 and M2 functions, including mechanisms that are known to be critical in early macrophage responses to Mtb infection.

1.3.3 Metabolic Reprogramming and Macrophage Immune Function

Several macrophage functions, including those playing a role in macrophage response to Mtb infection, are dependent on the metabolic programme of the M1 macrophage. Importantly, evidence is accumulating that the shift towards aerobic glycolysis is essential for both transcription and post-translational modification of IL-1β.

As described above, succinate accumulation is a feature of glycolytic reprogramming in M1 macrophages [244]. Succinate can stabilize the transcription factor HIF-1α through inhibition of the prolyl hydroxylase 2 (PHD2) [278,279], which usually hydroxylates HIF-1α on its two prolyl residues (Pro-402 and Pro-564) in oxygen-dependent manner [280], addressing it to the Von Hippel Lindau complex for ubiquitination and degradation. HIF-1α promotes glycolysis by upregulating many glycolytic enzymes [256-258], in addition to other hypoxia-responsive genes, through binding to the hypoxia response element (HRE) of the promotor sequence of their genes [281]. HIF-1α also induces transcription of IL-1β, with both human (*IL1B*) and murine (*il1b*) gene sequences containing a conserved canonical binding site for HIF-1α [174]. Increased levels of HIF-1α have long been recognised in activated macrophages [282,283], even at normoxia, and are crucial for pro-inflammatory functions [284-287] and for killing of intracellular pathogens such as *Group B streptococcus* [288]. Similarly, HIF-1α has been shown to play an important protective role in murine and zebrafish models mycobacterial infection [289,290]. It was not until 2013, however, that Tannahill et al showed the LPS-induced increase in HIF-1α level to be dependent on glycolytic reprogramming and succinate accumulation in murine BMDM [174]. HIF-1α levels were reduced in the presence of glycolytic inhibitor 2-deoxyglucose (2-DG, a competitive inhibitor of HK) and increased in the presence of diethylsuccinate (a succinate analogue). Authors correlated this to downstream IL-1β transcription, and reduced *Il1b* mRNA and pro-IL-1β were observed in the absence of HIF-1α activity, or when glutamine-dependent anapleurosis was inhibited (glutamine being the primary source of succinate in activated macrophages) [174].

Recently, glycolytic reprogramming has also been implicated in second step of IL-1β production, with mTORC-mediated aerobic glycolysis identified as critical for activation of the NLRP3 inflammasome [250]. Using murine peritoneal macrophages and the murine cell line J774A.1, Moon et al describe mTORC1-mediated HK1 upregulation following ATP treatment of LPS-primed cells [250]. They showed this to be required for glycolysis-dependent NLRP3 inflammasome activation, with decreased IL-1β, IL-18 (another cytokine requiring post-translational modification), and caspase-1 evident in the absence of mTORC activity, HK1 signalling or glycolytic inhibition. Interestingly, these experiments also demonstrated a dose-dependent relationship between extracellular glucose concentration in IL-1β and IL-18 secretion [250]. LPS/ATP-induced

HK1 was observed to co-localise with voltage-dependent ion channel 1 (VDAC1) [250], a mitochondrial outer membrane protein that has previously been implicated in NLRP3 inflammasome activation via induction of mitochondrial ROS (mROS) [291]. Given previous observations of mROS-mediated NLRP3 inflammasome activation [184,291,292], Moon et al examined the impact of both HK1 silencing and glycolytic inhibition on mROS production, finding it to be attenuated in both settings.

Thus, induction of mROS appears to be another metabolism-directed feature of M1-like macrophages. mROS can be generated via Complex I and Complex III when ATP synthesis is downregulated, leading to increased mitochondrial membrane potential due to continued activity of the ETC [293]. Alternatively, mROS generation can occur secondary to a phenomenon known as reverse electron transfer (RET), whereby Complex I receives electrons from Complex II (delivered via Coenzyme Q) and uses them to generate superoxide [293-295]. Interestingly, succinate accumulation also plays a role in mROS generation in this way, as very elevated levels of succinate result in excessive reduction of Complex II (succinate dehydrogenase), which results in reverse electron transfer to Complex I [293,296]. Recent work by Mills et al links glycolysis-enabled reversal in ETC activity and Warburg-driven succinate accumulation, leading to repurposing of mitochondria away from ATP synthesis and towards mROS synthesis [269]. In addition the aforementioned role in inflammasome activation [184,250,291,292], mROS have been shown to induce transcription of Il1b mRNA [297] – possibly a result of HIF-1α stabilisation, also mediated by mROS [255,298] – enhance TNF-α and IL-6 production [299], and downregulate IL-10 [297]. Furthermore, West et al have also demonstrated a TNF receptor associated factor 6 (TRAF6; activated downstream of TLR1/2 or TLR4 stimulation)-mediated delivery of mROS into the phagosome, which enhanced killing of intracellular *Salmonella typhimurium* [300]. It is possible that this co-ordinated delivery of TLR-induced mROS to the phagosome may serve to enhance bactericidal function while limiting the cytotoxic effects of ROS.

Citrate and isocitrate also accumulate as a result of a TCA cycle break at isocitrate dehydrogenase (*Idh*) [244], and accumulated citrate is transported to the cytosol via the mitochondrial citrate carrier (CIC) where it is cleaved by citrate lyase to form acetyl CoA and oxaloacetate [262]. Acetyl CoA is a biosynthetic precursor for *de novo* synthesis of fatty acids [239], including arachidonic acid needed for eicosanoid production [301], and knockdown or inhibition of CIC was associated with decreased PGE2 levels in TNF-α/IFN-γ-stimulated macrophages [262]. Citrate cleavage also contributes to generation of NO and cellular ROS (generating NADPH required for their generation by iNOS and NADPH-oxidase (NOX), respectively [302,303]) and reduced CIC activity was similarly associated with reductions in these biochemical [262]. Interestingly, increased flux through the

PPP also generates NADPH, as well as nucleotides which can be used for mRNA, long non-coding RNA or microRNA synthesis that may be important in directing macrophage responses [221].

Citrate is also a precursor for the nonamino organic acid itaconate [244,304,305], a conversion requiring the enzyme immune-responsive gene 1 (*Irg1*) which is upregulated in both murine and human macrophages following LPS stimulation [304], bacterial infection [304,306,307] and mycobacterial infection [308]. Remarkably, this metabolically-induced compound directly inhibits the bacterial enzyme isocitrate lyase [309,310], a key enzyme in the anabolic glyoxylate shunt that is active in bacteria and fungi, as well as inhibiting methylisocitrate lyase in *Mycobacterium tuberculosis* [304]. Itaconate has been shown to directly decrease growth of a diverse range of pathogens [304,309,310], including *M. tuberculosis* [304]. Silencing of *Irg1* expression in murine macrophages infected with *S. enterica* results in substantially impaired control of intracellular growth [304], providing compelling evidence for metabolically-induced itaconate as an important player in the host innate immune response to intracellular pathogens. Some of the functional consequences of glycolytic reprogramming of M1 macrophages are summarised in **Figure 1.5**.

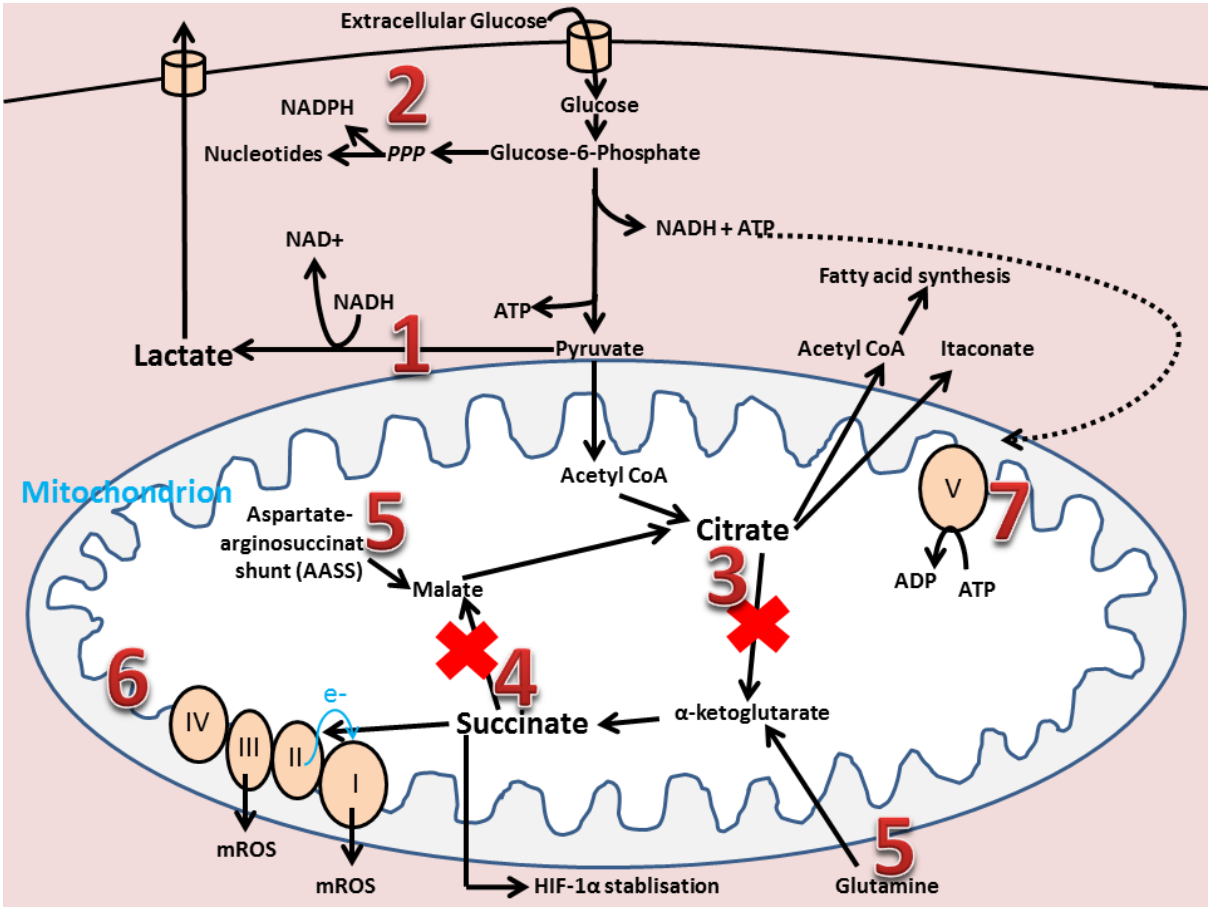

FIGURE 1.5: Macrophage glycolytic reprogramming. [1] In M1 macrophages, glycolytic rate is increased and pyruvate is preferentially metabolised to lactate instead of entering the mitochondrion to feed the TCA cycle, a process termed aerobic glycolysis. [2] Concurrent with increased glycolytic rate is increased PPP flux, generating reducing equivalent NADPH which can be used to make ROS and NO, and also nucleotide precursors which can be used to make mRNA, microRNAs and long non-coding RNAs. [3] Two breaks in the TCA cycle are evident. The first leads to accumulation of citrate, a precursor for fatty acid synthesis, which are needed for eicosanoid synthesis. Citrate can also be used to generate itaconate, which has directly microbicidal functions. [4] The second break in the TCA cycle leads to accumulation of succinate. Succinate accumulation leads to stabilisation of the transcription factor HIF-1α, which has pro-inflammatory and pro-glycolytic functions. Succinate accumulation can also induce reverse flow of electrons from Complex II to Complex I, with consequent mitochondrial ROS generation. [5] Compensatory upregulation of anapleurotic glutaminolysis and AASS activity occur secondary to TCA cycle inactivity. [6] Electron transport chain (ETC) activity is reduced. [7] ATP synthase (Complex V) uses glycolysis-generated ATP to maintain mitochondrial membrane potential. This facilitates cell survival, and has also been suggested to induce reverse flow of electrons through the ETC, generating mitochondrial ROS.

Metabolic features of M2 macrophage activation may play an important role in host defence also. Metabolic regulators AMPK and PPAR-γ downregulate inflammatory function [111,112,245,272,311]. However, a role for this signalling pathway has been identified in the induction of autophagy and the promotion of phagosome-lysosomal fusion [312], which serve to promote mycobacterial clearance. Conversely, PPAR-δ, a related transcription factor that also upregulates fatty acid oxidation downstream of AMPK [276], has been shown to supports persistent *S. typhimurium* infection in macrophages, with PPAR-$\delta^{-/-}$ mice demonstrating enhanced clearance of the pathogen [313]. The invading pathogen was able to fuel replication by sequestering host glucose supplies in the setting of reduced macrophage glucose metabolism. This suggests that M2-associated metabolic changes may in fact facilitate "hijacking" of the macrophage for persistent survival of intracellular pathogens, as is observed in Mtb infection. Furthermore, despite evidence for mutual antagonism of autophagy-inducing AMPK and glycolysis-inducing mTOR [21,314,315], the glycolytic enzyme HK2 and the transcription factor HIF-1α can activate of autophagy in certain situations [316-320], and AMPK has been shown to upregulate glycolysis under conditions of hypoxia or oxidative stress [321,322], suggesting the metabolic regulation of macrophage function is nuanced and complex. Similarly, the characteristic reprogramming of arginine metabolism seen in M2 macrophages may also be important in the context of mycobacterial disease. Diversion of this amino acid away from NO synthesis subverts this killing mechanism, with Arg1-KO mice demonstrating decreased clearance of Mtb and other intracellular pathogens [127]. However, ornithine-derived polyamines and proline also facilitate granuloma formation [323,324], and macrophage Arg1 has been shown to play an important role in limiting Mtb growth within the granuloma [325]. A simple depiction of some of the major differences between M1-polarised and M2-polarised macrophage metabolism is offered in **Figure 1.6**.

Metabolic reprogramming impacts many functions important in the early macrophage response to Mtb infection, therefore. It is likely that many other important responses not discussed here are also governed by metabolic changes. Work with dendritic cells, for example, indicates a vital role for glycolysis and HIF-1α in antigen presentation [239,240,326,327]. Mechanism of cell death, another crucial determinant of outcome in Mtb infection, is tightly linked to cellular ATP levels, mitochondrial function, and ROS production, thus is doubtless influenced by metabolic alterations in the cell also. Despite the complexity of these interdependent pathways, attempts to dissect them may lead to a greater understanding of the host defence against Mtb, possibly identifying new therapeutic or vaccination strategies.

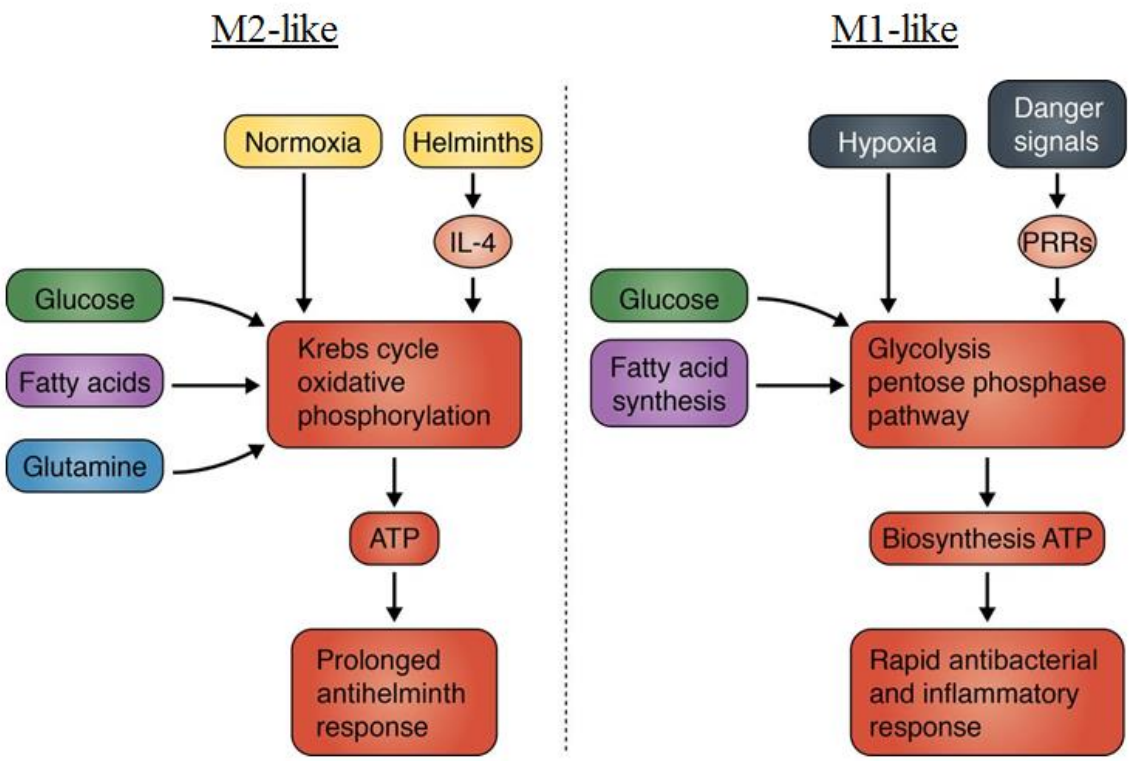

FIGURE 1.6: Immune signals as metabolic reprogrammers in macrophages. Normoxia or hypoxia will reprogram the metabolism of cells, with normoxia promoting the Krebs cycle (aka the TCA cycle) and oxidative phosphorylation and hypoxia promoting glycolysis, both for ATP production. In normoxia, glucose, fatty acids, and glutamine can all feed Krebs cycle, whereas for glycolysis glucose is metabolized. Immune signals can have a similar effect, with helminths driving IL-4 production to promote oxidative phosphorylation and danger signals (e.g., LPS acting via TLR4) promoting glycolysis and fatty acid synthesis. Metabolic reprogramming is therefore not only a consequence of the level of oxygen and nutrients, and instead is being driven by immune signals. The metabolism in IL-4–activated macrophages and DCs allows for long-term responses appropriate for handling parasites, whereas glycolysis is more suited to a rapid response to bacterial infection. *Adapted from O'Neill and Pearce, 2016 [221].*

1.3.4 Evidence for Glycolytic Reprogramming in Early Macrophage Responses to Mtb infection

Several observations support a role for host macrophage metabolism in the immune response to Mtb infection. Firstly, nuclear magnetic resonance (NMR) spectroscopy-based metabolomics analyses of serum or organs from both animals and humans infected with Mtb suggested significant alterations in metabolism, including evidence of increased glycolytic flux [328-333]. Though these studies were performed on animals or patients with established active TB disease, thus are not reflective of early metabolic changes at the cellular level, they suggest altered metabolism to be a characteristic feature of Mtb infection. Similarly, a recent transcriptomic analyses of homogenised lungs from Mtb-infected mice has also demonstrated broad upregulation of glucose transporters, glycolytic enzymes, PPP enzymes, HIF-1α and lactate exporters evident from Day 0 following aerosolised H37Rv infection, and was maintained for the duration of the study (up to Day 30) despite temporal fluctuations [334]. Increased HIF-1α levels were also evident on Day 0 in a macrophage / T cell mixture taken from the animals. In recent weeks, results of a PBMC transcriptional analysis performed in human TB patients before and after treatment likewise demonstrate upregulation of glycolytic genes in the setting of active Mtb infection [335]. These studies provide strong evidence for early glycolytic reprogramming as a feature of the host response to Mtb. However, neither these transcription-based studies nor the NMR metabolomics studies attempt to correlate metabolic alterations to outcome of infection.

Secondly, perturbation of mitochondrial function has been reported in the setting of Mtb infection. Bhargava et al observed reduced mitochondrial DNA: nuclear DNA ratio and reduced activity of mitochondrial Complexes II, III and IV in circulating lymphocytes from patients with extrapulmonary TB compared to uninfected controls [336]. Furthermore, a bioinformatics analysis based on available genomic sequences of several Mtb strains identified 19 Mtb proteins with the potential for targeting host mitochondrial function [337]. In a study involving PMA-differentiated THP-1 cells infected with Mtb for 24 hours, Jamwal et al linked perturbation in mitochondrial function to mycobacterial strain virulence [338]. In this work, they demonstrate early suppression of mitochondrial activity following infection with avirulent strain H37Ra (as indicated by altered mitochondrial ultrastructure, decreased membrane potential, and reduced ATP generation), in contrast to increased mitochondrial activity following infection with virulent H37Rv. This observation supports the hypothesis that Mtb infection impacts upon host macrophage metabolism, and that this interaction has functional consequences in terms of bacillary clearance.

Thirdly, the metabolic disease diabetes is a well-recognised risk factor for TB disease [339-344]. DM2 is characterised by resistance to insulin, a peptide hormone produced by pancreatic β cells, resulting in impaired uptake and utilisation of glucose within cells [345]. Type 1 Diabetes,

conversely, is characterised by decreased insulin production. In both Type 1 and Type 2 Diabetes, hyperglycaemia occurs as a consequence of increased hepatic glucose production and decreased glucose uptake by peripheral cells [346]. Insulin modulates gene transcription in target cells and, amongst a myriad of effects, is known to upregulate expression of glucose transporters and glycolytic enzymes [347]. Impaired host immune responses evident in diabetic patients, therefore, may be a consequence of hyperglycaemia or, alternatively, a consequence of altered glucose uptake and intracellular metabolism due to defective insulin signalling. In terms of the innate immune response to infection, diabetes-associated alterations have been described in neutrophil, macrophage, NK cell and dendritic cell function [348], leading to delayed onset of adaptive immune responses [349]. The impact of diabetes on M1 macrophage function is complex. Despite high basal levels of pro-inflammtory cytokine production, and characteristic M1 macrophage influx causing low-grade inflammation in pancreatic and adipose tissue, infection-induced pro-inflammatory macrophage functions tend to be impaired [348]. Animal studies have suggested phenotypic skewing towards M2 polarisation with attenuated cytokine production in TLR-stimulated macrophages from diabetic rodents [350-352]. Defects in early AM chemokine response to infection have been postulated to result in delayed onset of adaptive immunity and increased bacillary replication, ultimately leading to a late-onset excessive inflammation corresponding to more severe disease pathology [349]. The obvious interrelationship between diabetes (and possibly non-diabetic hyperglycaemia) and macrophage responses to Mtb infection support a role for metabolic reprogramming in influencing host defence. Excitingly, the oral hypoglycaemic agent metformin, used worldwide for the treatment of DM2, has recently been demonstrated to improve macrophage responses to Mtb through activation of the master metabolic regulator AMPK, suggesting a central role for intracellular metabolism in the response to Mtb [353].

In terms of the impact of hyperglycaemia in the absence of diabetes, there is evidence for a direct link between elevated glucose levels and impaired macrophage phagocytic ability [354]. A study examining the effect of varying glucose concentration on H37Rv lysate-induced cytokine production saw no difference in macrophage function in terms of phagocytosis, killing or cytokine production (when correct osmolarity controls were used), aside from a dose-dependent increase in IL-10 production [355]. This is in contrast to observations in LPS/ATP-stimulated macrophages, where glucose concentration-dependent increases in IL-1β and IL-18 production were observed (mediated via NLRP3 inflammasome activiation) [250]. Despite discordant results, both studies demonstrate an interrelationship between glucose availability and macrophage function, supporting the hypothesis that macrophage glucose metabolism plays a role in anti-Mtb responses.

At the time of writing, only one study has examined the link between macrophage glucose metabolism and early host response to Mtb infection. Mehrotra et al used ^{13}C-glucose labelling to metabolically profile PMA-differentiated THP-1 cells (a human macrophage cell line) both uninfected and following infection with different Mtb strains [356]. Using this method, they demonstrate infection-induced increases in surface expression of GLUT1 and GLUT3 glucose transporters, ^{13}C-glucose uptake and glycolytic intermediates, as well as elevated levels of cytosolic citrate leading to upregulation of *de novo* fatty acid synthesis. These metabolic alterations were evident with all infecting strains, but virulent strains induced more substantial increases. Authors go on to suggest that this may facilitate foam cell formation (via infection-induced sequestration of fatty acids to generate lipoid bodies), ultimately leading to necrotic cell death characteristic of virulent Mtb strains, compared to apoptotic cell death induced by avirulent strains such as H37Ra. However, cautious interpretation of cell death assays must be exercised in the context of this work, PMA-stimulated THP-1 cells are highly dependent on glucose metabolism via glycolysis for ATP generation, with uninfected cells cultured in glucose-free pyruvate-supplemented media undergoing apoptosis. Furthermore, addition of the mitochondrial Complex I inhibitor, rotenone, did not affect ATP production in uninfected cells, suggesting redundancy (or possible dysfunction) of mitochondrial OXPHOS at baseline. Thus, PMA-treated THP1 cells likely demonstrate substantial metabolic differences to primary cells, and as such represent an imperfect model for studying the interrelationship of macrophage metabolism and function. However, authors go on to demonstrate reduced colony forming units in Mtb-infected human MDMs 72 hours post-infection in the presence of the glycolytic inhibitor 5-thioglucose, though no viability assays were performed with this inhibitor.

It is clear, therefore, that while substantial evidence exists for the interrelationship of macrophage glucose metabolism and the early host immune response to Mtb infection, so too does equipoise regarding the mechanism, significance and beneficial or harmful effect of this interaction. An enhanced understanding of how this phenomenon applies to the immune response in Mtb infection is imperative if we are to exploit the rapid advancements in this field to improve TB treatments.

1.4 Smoking, Immunometabolism and the Host Response to *Mycobacterium tuberculosis* infection

1.4.1 Colliding Pandemics: Tuberculosis and Tobacco Smoking

There are 996 million tobacco smokers estimated worldwide, smoking 5.8 trillion (5,800,000,000,000) cigarettes in 2014 [357]. This figure continues to rise, particularly in China and sub-Saharan Africa[357], coinciding with high TB incidence [358-360]. Three important meta-analyses published in 2007 confirmed the epidemiological association between cigarette smoking and TB [361-363], with smokers demonstrating a 1.5 – 2.5 relative risk for TB infection, progression to active disease and mortality. Importantly, increased risk was also observed in passive smokers and in those exposed to indoor air pollution through the burning of biomass fuels [361-363]. Smoking also increases the risk of recurrence post treatment [364,365], delays culture conversion [366], prolongs infectivity [367], and is associated with poorer treatment outcomes [368]. Overall, more than 15% of active TB cases each year are believed to be attributable to cigarette smoking [358].

Cigarette smoke, made up of particulate matter and a gaseous phase, comprises more than 4,500 components [369]. Differences in smoking history, genetic susceptibility and environmental variables (such as exercise, nutrition, occupation and ambient air quality) present a challenge in terms of appropriately modelling cigarette exposure *in vitro* or *in vivo* [370]. However, since the 1960s, impacts upon a wide range of host defence mechanisms have been extensively studied and reviewed [370-374]. Smoking inhibits physical respiratory tract defences by inducing mucous hypersecretion [375,376], impairing ciliary function [377-379] and reducing airway clearance [380,381]. Increased numbers of inflammatory cells [382,383] is coupled to defective anti-microbial function of neutrophils [384-387], macrophages [388-398], and dendritic cells [399-401], giving rise to a combination of increased tissue damage and ineffective protective responses. Altered adaptive immunity also exists, with smokers found to have an increased number of $CD8^+$ T cells in BAL fluid and lung biopsies [402-404], and reduced T cell activation and function described [405-407]. Accordingly, cigarette smokers are prone to respiratory infection with a range of bacterial pathogens [408]. In the setting of mycobacterial infection, mouse studies have demonstrated decreased T cell activation and IFN-γ response in cigarette-exposed mice [409,410], and studies with human AM have identified impaired pro-inflammatory cytokine production and reduced intracellular killing [410,411], though surprisingly phagocytosis was unimpaired in human cigarette smoke extract (CSE)-treated human AM infected with BCG [412].

Increased levels of MMPs observed in smokers' lungs [413-415] may also contribute to increased tissue destruction and granuloma breakdown in Mtb infection [62].

1.4.2 Alveolar Macrophage Function in the Smoker

Smoking-related compromise of AM function has been well-described [370-374]. Despite significantly elevated numbers present in the lung [416], AM functions such as efferocytosis [389,398,417], intracellular trafficking [418] and autophagy [392,419] are dramatically impaired. Reduced phagocytic function has been demonstrated in many studies [390,391,393,394,420-423], although this was not observed in a human AM model of BCG infection [412]. Interestingly, a study examining AM phagocytosis of *Streptococcus pneumoniae* suggested that CSE treatment reduced complement-mediated phagocytosis but Fc-mediated phagocytosis or the ingestion of unopsonised bacteria [424]. Cigarette smoke exposure has been variably reported to decrease [425-427] and increase [395,426,428,429] AM apoptosis, another important mediator of host defence in Mtb infection [45-49].

Two independent studies comparing human AM transcriptional profiles of smokers and non-smokers reveal smoking to be associated with suppression of M1-induced gene expression. Shaykhiev et al reported suppression of M1-related and induction of M2-related genes in smokers based on transcriptional analyses of AM from 24 healthy non-smokers and 34 healthy smokers [430]. Graff et al observed decreased expression of M1-induced transcripts and increased expression of M1-repressed transcripts in human AM from smokers compared to non-smokers, though M2-related gene expression was not changed [415]. Functional studies have also suggested an M2-like skewing of macrophages exposed to CSE in vitro [431,432]. Decreased TLR2 expression has been demonstrated in human AM from smokers [396], as well as reduced activity of MAPK family members and impaired downstream NFκB signalling in both smokers' AM [433] and in murine-based smoking models [397,434,435]. This is associated with attenuated pro-inflammatory response following stimulation with TLR agonists [397,435-440], phorbyl myrisate acetate (PMA) [441-443] or infection with intracellular pathogens [440,444,445], including defects in IL-1β production [433,436-438] and PGE2 production [437]. Interestingly, despite reduced pro-inflammatory cytokine (TNF-α, IL-1β, IFN-γ, IL-6 and IL12p40) and NO production seen in these studies, some reports suggest anti-inflammatory IL-10 production to be unimpaired in smokers' AM [436,444], though this finding is not universal [412,440]. This supports the work from Krause[430] and Graff [415] in suggesting reduced M1 polarisation of smokers' AM, rendering early innate immune function defective.

In the context of Mtb infection, we have also demonstrated impaired production of TNF-α, IL-1β and IFN-γ in smokers' AM compared to non-smokers' AM following *ex vivo* infection with avirulent laboratory strain H37Ra [411], and these macrophages are unable to contain bacillary growth [411]. Similarly, BCG-mediated induction of TNF-α and IFN-γ in human MDM and AM was impaired in the presence of CSE [412]. Shang et al demonstrated reduced numbers of IL-12 and TNF-α-producing macrophages and an increased number of IL-10-producing macrophages in an *in vivo* model of Mtb Erdman infection of cigarette smoke-exposed mice compared to controls (infected non-smoke exposed mice), correlating with increased disease burden and bacillary counts at 14 and 30 days post infection [410]. This group also demonstrated impaired bacillary clearance by human AM treated with CSE *in vitro*, evident at Day 2 post-infection [410]. Upregulation of IL-10-producing macrophages has also been described in a mouse model of concurrent Mtb infection and cigarette smoke exposure [410], although this was not seen in human macrophages infected with BCG [412]. Thus, the well-established association between cigarette smoking and TB infection may be mediated in part through defective M1 polarisation of the AM, leading to decreased pro-inflammatory functions such as IL-1β production and impaired bacillary clearance.

1.4.3 Glycolytic Reprogramming in the Smoker's Alveolar Macrophage

Since the 1970s, cigarette smoke-induced mitochondrial alterations have been reported [446,447]. In 1999, Miro et al reported decreased oxygen utilisation, a consequence of reduced Complex IV function, in circulating lymphocytes from smokers compared to non-smokers [448]. More recently, dose-dependent inhibition of Complex I and II with consequent decrease in mitochondrial membrane potential, oxygen consumption and ATP production has been described in lung epithelial cells [449]. A similar effect has been reported in human airway smooth muscle cells treated *ex vivo* with CSE demonstrated reduced mitochondrial function as measured by extracellular flux analyses, with reductions in oxygen consumption rate, spare respiratory capacity and ATP production evident, which authors attributed to imbalances in mitochondrial fission-fusion [450]. Impaired mitochondrial function has been linked to increased mitochondrial ROS generation in response to cigarette smoke [450,451].

Accordingly, cigarette smoke and its components have been shown to inhibit mitochondrial function in murine and rat macrophage cell lines [452,453], in peritoneal macropahges [451,454], and in human alveolar macrophages [395,419]. Monick et al compared mitochondrial function in both CSE-treated and untreated AM, and in smokers' and non-smokers' AM, using JC-1 (a fluorescent cationic dye) staining to measure mitochondrial membrane potential and ATP

bioluminescence to measure mitochondrial function [419]. In both models smoke exposure was associated with decreased mitochondrial membrane potential and CSE-treated AM had decreased ATP production, which they suggest to be partly a consequence of impaired autophagy causing reduced mitochondrial repair.

Less well-defined is the impact of cigarette smoke on AM glycolytic metabolism. Various studies examining the effect of smoking on AM glucose uptake are in disagreement. In 1967, Myrvik et al demonstrated decreased glucose utilisation in unstimulated AM taken from cigarette smoke-exposed rabbits compared to controls [455]. Subsequently, in 1970, Harris et al conducted a small study (including 4 non-smokers and 3 smokers) that demonstrated significantly increased rates of glucose utilisation of "resting" smokers AM using U-^{14}C-labelled glucose [456]. A further study involving 34 smokers and 43 age-matched non-smokers found no difference in glucose utilisation between smokers' and non-smokers' AM, both unstimulated and stimulated with heat-killed *Staphylococcus aureus* or with PMA [457]. Using their smoker v non-smoker AM model, Monick et al reported increased sensitivity of non-smokers' AM to addition of a mitochondrial uncoupler (which functionally inhibits ATP generation via OXPHOS) in terms of ATP production compared to smokers' AM [419]. Authors infer that this is a consequence of increased glycolytic ATP generation in chronically smoke-exposed AM [419], however no direct measurement of glycolysis is performed during this experiment.

Some information on the impact of cigarette smoke on the glycolytic function of other cell types is available, however. In 2001, Zappacosta et al observed potent inhibition of glycolytic activity in neutrophils exposed to aqueous CSE [387]. More recently, differences between smokers and non-smokers in terms of glucose metabolism in Type II alveolar epithelial cells have been investigated by the Cadenas laboratory in California [458,459]. Acrolein, an α,β-unsaturated electrophile, is a component of tobacco smoke as well as an environmental pollutant released into ambient air from diesel exhausts and cooking oil [458]. In concordance with the observations outlined above, Agarwal et al have shown decreased mitochondrial respiration and spare respiratory capacity in acrolein-exposed murine Type II alveolar epithelial cells using extracellular flux analyses [458]. Interestingly, however, this occurred in concert with decreased glycolytic flux, and addition of pyruvate could rescue mitochondrial respiration, leading authors to conclude that decreased OXPHOS was a function of impaired glycolytic function. Acrolein-treated Type II alveolar epithelial cells also preferentially utilised β-oxidation of palmitate to fuel mitochondrial respiration, as opposed to glucose metabolism used by untreated cells [458]. This is reminiscent of M2 macrophage metabolism, which favours β-oxidation of fatty acids to replenish TCA cycle intermediates [221]. Similarly, upregulation of PPAR-γ has been described in smoke-exposed human dendritic cells [400], also an M2-like metabolic feature [109,110,274,275]. However, in

these experiments, acrolein treatment was associated with increased flux through the PPP in Type II alveolar epithelial cells [458], in contrast to PPP downregulation that is observed in M2 macrophages [264]. In a follow-up study, the group proceeded to demonstrate similar impaired glycolysis and increased palmitate oxidation to fuel OXPHOS in Type II alveolar epithelial cells isolated from mice exposed to cigarette smoke for 4 – 8 weeks [459].

These observations are supported by the results of a metabolomic study in human alveolar epithelial adenocarcinoma (A549) published by Vulimiri et al, in which they observed reduced glycolysis and increased β-oxidation of fatty acids in response to *in vitro* exposure to whole smoke [460]. Conversely, chronic CSE exposure increased glycolysis, with upregulation of HIF-1α, in an immortalised human keratinocyte model [461]. Recently, a combined metabolomics and extracellular flux study sought to examine cell-level metabolic effects of another component of cigarette smoke, benzo(a)pyrene (B[a]P). Cells from the human hepatoma cell line SMMC-7721 were co-cultured with B[a]P or DMSO (control) for one month [462]. Using this model, B[a]P-treated cells demonstrated reduced glycolysis, but addition of oligomycin resulted in more pronounced elevation in extracellular acidification rate (ECAR) in B[a]P-treated cells compared to controls. Caution must be exercised in interpreting results of metabolic studies in immortalised cell lines, however, as oncogenic transformation is associated with glycolytic reprogramming and thus these models may not accurately reflect normal cell responses *in vivo*.

Thus, despite evidence for decreased mitochondrial activity [395,419], interrogation of the impact on baseline glycolytic function has been interrogated in an AM model to date. Furthermore, the impact of cigarette smoking on glycolytic reprogramming required for M1 macrophage function has not been explored in any model. In light of the important impairments in macrophage pro-inflammatory cytokine production in Mtb infection, including IL-1β, and evidence for skewing of smokers' cells towards an M2-like metabolic phenotype [400,458], this pathway may be important in the host defence against disease and may contribute to the mechanism by which smokers demonstrate increased susceptibility to TB.

CHAPTER 2:

Methods and Materials

2.1 Cell Culture

2.1.1 Human Alveolar Macrophages

Donors

Human alveolar macrophages (AM) were retrieved at bronchoscopy after written informed consent, as approved by the St James's Hospital / AMNCH Research Ethics Committee. The letter of protocol approval is available on request. All donors were patients undergoing clinically indicated bronchoscopy and consented for additional BAL fluid to be acquired during their procedure. Patients were not remunerated for participation in this study. Exclusion criteria included age under 18 years, inability to provide written informed consent or a known (or probable) diagnosis of malignancy, sarcoidosis, HIV or HCV. Patients undergoing biopsy as part of bronchoscopy were also excluded. All regulations regarding patient confidentiality were adhered to and data is fully anonymised. Pre- and post-bronchoscopy care was not altered by participation in the study. The procedure was prolonged by approximately 5 – 6 minutes.

Donor Smoking Status

Donor current and previous smoking status was confirmed by interview prior to bronchoscopy at the time written informed consent was obtained. For current smokers, number of cigarettes smoked per day and number of years spent smoking were recorded. For ex-smokers, number of cigarettes previously smoked per day, number of years spent smoking, and number of years since cessation were recorded. This data was used to calculate the number of pack-years for all smokers and ex-smokers, using the formula:

No. of pack-years = (No. years smoking x No. cigarettes per day)/20

Based on this information, donors were classified as "smokers", "ex-smokers" or "never-smokers". Due to limited numbers of never-smokers, an alternative classification of "smokers" and "non-smokers" (with non-smokers including both never-smokers and ex-smokers who had ceased smoking more than 2 years prior to sample acquisition) was utilised.

Sample Acquisition

Conscious sedation was achieved using intravenous midazolam and lignocaine gel was administered to the nostril. Flexible video-bronchoscope was inserted through the nostril and advanced to the level of the vocal cords by posterior approach. Further lignocaine spray was administered prior to and subsequent to traversing the vocal cords. Following routine (clinically-indicated) bronchoscopy, the bronchoscope was wedged in the right middle lobe bronchus and 180mL of sterile 0.9% saline administered via a connector inserted into the bronchoscope. Saline was administered as 60mL boluses and aspirated within 5 to 10 seconds under low pressure suction. BAL fluid was transported directly to the laboratory for AM isolation.

AM Isolation and Culture

BAL fluid was filtered through a 100µm nylon strainer (BD Falcon; BD Bioscience, Erembodegem, Belgium) and centrifuged for 15 minutes at 390 x g. Cells were resuspended in RMPI-1640 culture media supplemented with 10% type AB human serum (Sigma-Aldrich) (a.k.a. complete RPMI (cRPMI)), 50µg/mL fungizone and 50µg/mL cefotaxime, and cell count was performed using a haemocytometer. For extracellular flux analysis, cells were immediately plated onto Seahorse Biosciences 24-well plates at 100,000 cells/well. For all other experiments, cells were immediately plated onto Nunc tissue culture-treated 24-well plates (Sigma-Aldrich) at 5 x 10^5 cells/mL. For all experiments involving Mtb infection, cells were also simultaneously plated on 8-well glass Labtek slides at the same density to allow determination of multiplicity of infection (MOI). Cells were incubated for 24 hours at 37°C and 5% CO_2, after which non-adherent cells were removed by multiple washes and fresh antibiotic-supplemented cRPMI medium was applied. Cells were ready for infection or treatment at this point (Day 1).

2.1.2 Human Monocyte-Derived Macrophages

Donors

Human monocyte-derived macrophages (MDM) were isolated from buffy coat whole blood component from anonymous healthy donors using density gradient centrifugation and adherence to plastic. Buffy coats were obtained with permission from the Irish Blood Transfusion Service (IBTS).

MDM Isolation and Culture

The buffy coat was mixed 1:2 with phosphate buffered saline (PBS) and 25mL volumes of this mixture were layered onto 10mL volumes of Lymphoprep (Sigma-Aldrich) in sterile 50mL Falcon tubes. Tubes were centrifuged at 400 x g for 25 minutes at 18°C with no brake, resulting in separation of the blood into a red cell pellet, white cell layer and plasma/platelet layer. The white cell layer was removed and centrifuged at 300 x g for 10 minutes. The resultant pellet was incubated at 37°C for 30 minutes with 3 – 5mL Red Cell Lysis Buffer (Sigma-Aldrich), before again centrifuging at 300 x g for 10 minutes. Cells were then resuspended in cRMPI. Cell count was performed using a haemocytometer and cells were plated at 3 x 10^6 cells/mL on non-treated 12-well plates (Corning Costar). For all experiments involving Mtb infection, cells were also simultaneously plated on 8-well glass Labtek slides at the same density to allow determination of MOI. Cells were incubated for 24 hours at 37°C and 5% CO_2, after which non-adherent cells were removed by multiple washes and fresh cRPMI medium was applied (Day 1). Cells were cultured for 5 days to allow differentiation into macrophages, with further application of fresh media on Day 3 and Day 5. Cells were ready for infection or treatment on Day 6.

For extracellular flux analyses, human MDMs were similarly isolated, plated on 12-well plates, washed at 24 hours and cultured for 5 days to allow differentiation into macrophages. Following application of fresh media on Day 5, macrophages were detached using a cell scraper and centrifuged at 300 x g for 10 minutes. Macrophages were resuspended in cRPMI and cell count performed using a haemocytometer. Cells were plated at 200,000 cells/well on Seahorse Biosciences 24-well plates to form a confluent monolayer. For all experiments involving Mtb infection, cells were also simultaneously plated on 8-well glass Labtek slides at the same density to allow determination of MOI. At 24 hours post-plating (Day 6), cells were washed and fresh media applied. Cells were ready for infection or treatment at this point (Day 6).

2.1.3 Murine Bone Marrow-Derived Macrophages

Animals

Murine bone marrow-derived macrophages (BMDM) were isolated from CS57BL/6 mice purchased from Harlan UK Ltd (Bicester, UK) and from IL-1R knockout mice (CS57BL/6 background, Jackson Laboratories), a kind gift from Professor Kingston Mills, TCD. All mice were bred under specific pathogen-free conditions and maintained according to the regulations and guidelines of the European Union and the Irish Department of Health. All experiments were conducted with prior ethical approval from TCD Animal Research Ethics Committee.

BMDM Isolation and Culture

Mice were culled at 6 – 8 weeks of age, hind-legs removed and cleaned. BMDM were isolated by flushing bone marrow from femurs and tibias. Bone marrow was suspended in DMEM and homogenised by pipetting prior to centrifuging at 300 x g for 15 minutes. Pellets were incubated at 37°C for 15 minutes with Red Cell Lysis Buffer (Sigma-Aldrich), before centrifuging again at 300 x g for 15 minutes. Cells were suspended in DMEM supplemented with 10% foetal bovine serum (FBS) (Sigma-Aldrich), 15% MCSF (conditioned media from L929 cells) and penicillin/streptomycin. Cell count was performed using a haemocytometer and cells were plated in tissue culture-treated dishes at 1 x 10^6 cells/mL. Cells were cultured for 5 days to allow differentiation into macrophages, with application of fresh media on Day 3 and Day 5. Following application of fresh media on Day 5, macrophages were detached using a cell scraper and centrifuged at 300 x g for 10 minutes. Macrophages were resuspended in antibiotic-free MCSF-free DMEM supplemented with 10% FBS, and cell count performed using a haemocytometer. Cells were plated at 1 x 10^6/mL in tissue culture-treated 12-well plates. For all experiments involving Mtb infection, cells were also simultaneously plated on 8-well glass Labtek slides at the same density to allow determination of MOI. At 24 hours post-plating (Day 6), cells were washed and fresh media applied. Cells were ready for infection or treatment at this point (Day 6).

2.2 Infections and Stimulations

2.2.1 Mtb infections

Culture and Preparation of Viable Mtb strains

Mtb strain H37Ra was obtained from the American Type Culture Collection (ATCC 25177) (Manassas, VA), grown to log phase in Middlebrook 7H9 broth (Difco) supplemented with albumin-dextrose-catalase (ADC) (Becton Dickinson) and 0.05% Tween 80 (Difco) made up in endotoxin-free water (Sigma-Aldrich), and aliquots stored at -80°C. Prior to experimentation, aliquots were thawed and propagated in Middlebrook 7H9 broth (supplemented as described) to log phase. All work was performed in a Biosaftey Level 2 (BSL2) facility.

Mtb strain H37Rv also obtained from the American Type Culture Collection (ATCC 25618) (Manassas, VA), was grown to log phase, stored and propagated in the same way. All work was performed in a Biosafety Level 3 (BSL3) facility.

On the day of infection, log phase Mtb were centrifuged at 3800rpm for 10 minutes and the pellet resuspended in serum-free RPMI-1640 culture medium. Mycobacteria were homogenised by aspirating through a 25-gauge needle 10 times and remaining clumps removed by centrifuging at 800rpm for 3 minutes. Supernatant was transferred to a fresh tube and used to determine MOI and to perform infections of macrophages.

Preparation of Non-Viable Mtb

Non-viable Mtb strain H37Rv γ-irradiated whole cells (NR-49098) (BEI Resources, NIAID, NIH) (iRv) were stored in 1mL at -80°C on receipt. Prior to experimentation, aliquots were thawed, resuspended in 5mL endotoxin-free PBS (Sigma-Aldrich) in 15mL tubes and sonicated for 15 minutes in a bath sonicator. Tubes were then centrifuged at 3800rpm for 10 minutes. The pellet was resuspended in 2mL serum-free RPMI 1640 culture medium, sonicated for a further 15 minutes, and the solution aspirated through a 21-gauge (green) needle 10 times. The solution was then diluted 1:5 in serum-free RPMI 1640 culture medium, sonicated for 15 minutes for a third time, and aspirated through a 25-gauge (orange) needle 10 times, and stored at 4°C for up to two weeks.

On the day of infection, 1mL of prepared iRv solution was sonicated for 15 minutes and passed through a 25-gauge (orange) needle 10 times, prior to its use for determination of MOI and infection of macrophages.

Determination of MOI

Because Mtb was prepared fresh from culture on the morning of each infection, variation in concentration was inevitable. Furthermore, inherent variation in phagocytic function can lead to substantial differences in Mtb uptake between different donors. In order to control for variation in mycobacterial concentration and in donor phagocytic ability, MOI was determined for each donor prior to each infection. When preparing and plating macrophages for experimentation, macrophages were simultaneously plated on 8-well glass Labtek slides at the same density. On the day of infection, fresh media was applied to Labtek wells and different volumes of prepared Mtb were added to each well. Cells were incubated for 3 hours at 37°C and 5% CO_2. At 3 hours post-infection, media was removed, cells washed three times with PBS to remove extracellular bacilli and fixed by incubating in 2% paraformaldehyde (PFA) in PBS for 5 minutes. PFA was removed and cells washed twice with water prior to staining.

A TB Modified Auramine O Stain Kit (Becton Dickinson) was used to stain acid-fast bacilli (AFB) by first immersing slides in Modified Auramine O for 1 minute, washing with water, and then immersing slides in Modified Auramine O Decolouriser for 1 minute, and again washing with water. Cell nuclei were subsequently stained by immersing slides in Hoechst 33358 (10µg/mL; Sigma-Aldrich Aldrich) for 5 minutes, and again washing with water. Cover slips were applied to slides using Dako fluorescent embedding medium (Dakocytommation) and slides observed using an inverted fluorescent microscope (Olympus IX51). The ratio of bacilli to cells (i.e. nuclei), the % of infected cells, and the number of bacilli per cell was counted in 5 fields for each unique well, and MOI was expressed as the range of number of bacilli per cell (e.g. MOI 0 – 5 bacilli/cell, MOI 10 – 15 bacilli/cell). Fluorescent microscopy images for varying MOI for 1 representative donor are depicted in **Figure 2.1**. From this, the appropriate volume of prepared mycobacteria required to achieve the desired MOI was calculated with reference to the surface area of wells on plates relevant to the surface area of wells on Labtek. In Results Chapters, “Low MOI” refers to an MOI of 0 – 10 bacilli/cell and “High MOI” refers to an MOI of 5 – 15 bacilli/cell.

Mtb Infection of Macrophages

Following determination of MOI, prepared viable Mtb (H37Ra or H37Rv) were passed through a 25-gauge (orange) needle once and added to macrophages. Prepared iRv was again sonicated for 15 minutes, passed through a 25-gauge (orange) needle 10 times, and added to macrophages. Cells were incubated for 3 hours at 37°C and 5% CO_2. At 3 hours post-infection, media was removed, cells washed three times in sterile PBS to remove extracellular bacilli, and fresh media applied. Uninfected control wells and any wells treated with different ligands (e.g. LPS) were also washed and had fresh media applied at this 3 hour timepoint, to ensure accurate comparison. Any additional treatments (such as inhibitors, antibodies, cytokines or TLR agonists) were reapplied following this 3-hour wash step. Cells were again incubated at 37°C and 5% CO_2 for specified times.

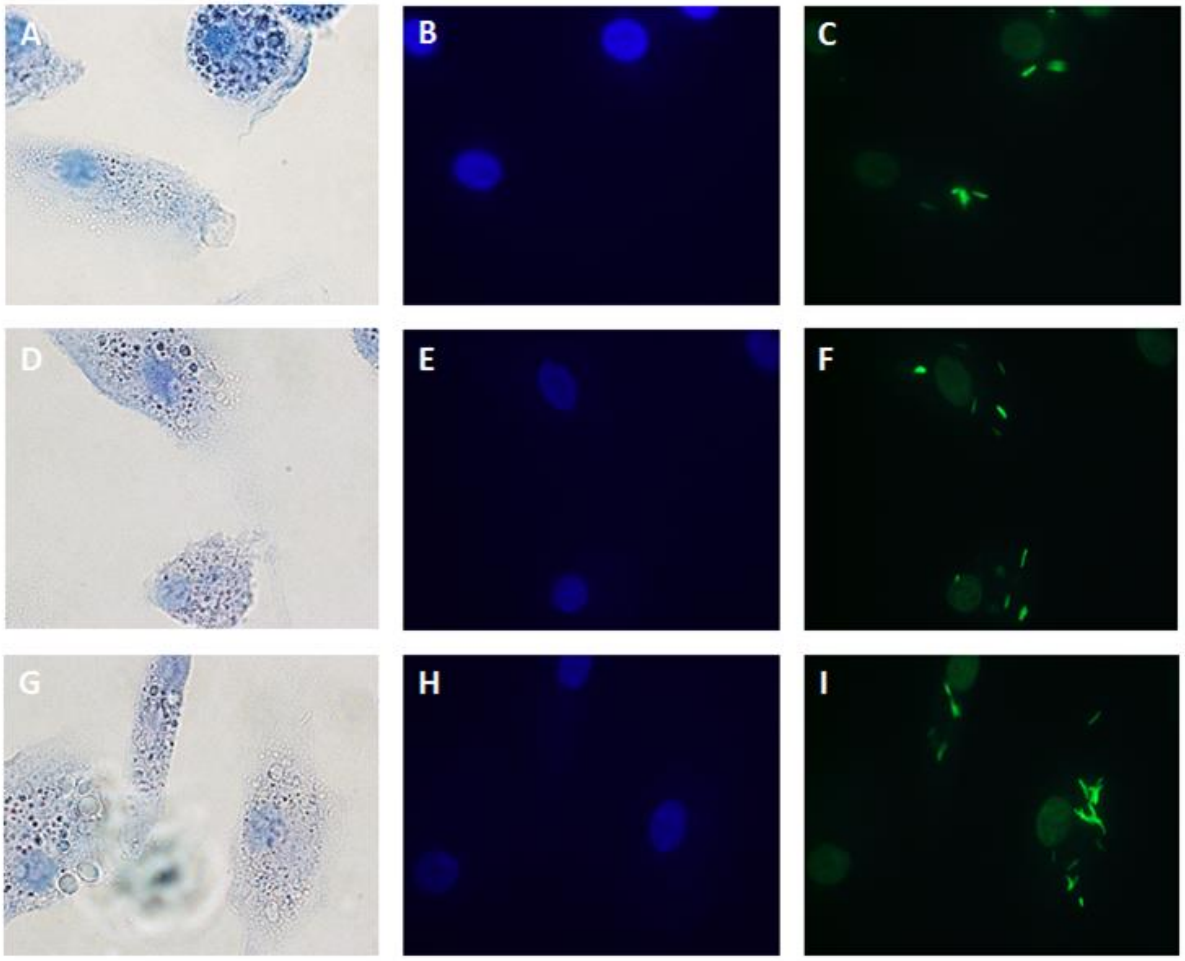

FIGURE 2.1 Determination of multiplicity of infection (MOI). Human MDM isolated from IBTS buffy coats and plated as described were treated with various volumes of prepared H37Ra, washed and fixed with 2% PFA. Cells were stained with the TB Modified Auramine O Stain Kit and with Hoechst 33358 (10µg/mL) and observed using an inverted fluorescent microscope. Figure depicts microscopy images for one representative donor. Panels A – C depict corresponding Brightfield image (A), Hoechst-stained cell nuclei (B) and auramine-stained AFB (C) for cells infected at MOI 0 – 5 bacilli/cell. Panels D – F depict corresponding Brightfield image (D), cell nuclei (E) and AFB (F) for cells infected at MOI 0 – 10 bacilli/cell. Panels G – I depict corresponding Brightfield image (G), cell nuclei (H) and AFB (I) for cells infected at MOI 5 – 15.

2.2.2 *Salmonella typhimurium (S.typhi)* infections

Preparation and Culture of *S. typhi*

S. typhi glycerol stocks were provided by our collaborator Professor Luke O'Neill, TCD. Bacteria from the glycerol stock was streaked onto an agar plate and incubated overnight at 37°C to generate isolated colonies. A single colony was transferred by pipette to 10mL of lysogeny broth (LB) and again incubated overnight at 37°C. 500µL was removed and density measured by spectrophotometry at OD_{600nm}, whereby an absorbance of 1.0 equates to 1 x 10^8 bacteria/mL. Bacteria cultured in LB were centrifuged at 4,000 x g for 10 minutes and the pellet resuspended in antibiotic-free DMEM to obtain the desired concentration of bacteria for the required MOI.

S. typhi Infection of Macrophages

Murine BMDM were isolated, cultured and prepared for experimentation as described in **Section 2.1.3**. On the day of infection, fresh antibiotic-free DMEM was applied and thieno[3,2-b]pyrrole[3,2-d]pyridazinone-46 (TEPP-46) or DMSO treatments applied 1 hour prior to infection as described in **Section 2.5.3**. Bacteria were added to achieve MOI 10, calculated based on spectrophotometry readings and cell count (i.e. MOI 10 = 10 bacteria added per 1 cell). Cells were incubated for 15 minutes at room temperatures. Media was then removed and replaced with media supplemented with gentamicin at 1000µg/mL to kill extracellular bacteria, and again cells were incubated for 15 minutes at room temperature. Gentamicin-supplemented media was then removed and cells washed three times with sterile PBS, and incubated at 37°C for the remainder of the experiment. Designated wells were immediately lysed in ice water and diluted by a factor of 10^8 in PBS. Lysates were then plated on LB agar plates in quadruplicate. The remainder of the cells were incubated for a further 24 hours prior to lysis, dilution and plating as described. 24 hour supernatants were removed and centrifuged, with the bacterial pellet added to cell lysates prior to plating. LB agar plates were incubated for 24 hours prior to enumeration of colony forming units (CFU) by counting.

2.2.3 TLR Stimulations

TLR agonist treatments

The TLR-4 agonist lipopolysaccharide (LPS), the major component of the outer membrane of Gram negative bacteria, was obtained from Sigma-Aldrich, reconstituted in PBS and stored at 4°C prior to experimentation. The TLR-1/2 agonist Pam3Cys-Ser-(Lys)4 (P3C), a synthetic triacylated lipopeptide that mimics the acylated amino terminus of bacterial lipoproteins, was obtained from Invivogen, reconstituted in PBS and stored at -20°C prior to experimentation. The TLR-2/6 agonist Pam2CGDPKHPKSF (FSL-1), a synthetic lipoprotein derived from *Mycoplasma salivarium*, was obtained from Invivogen, reconstituted in sterile water and stored at -20°C prior to experimentation.

Cells were isolated, cultured and prepared as described in **Section 2.1**. On the day of experimentation, working concentration of the TLR agonist was made up in standard culture media. Lipid-soluble LPS was sonicated for 5 minutes in a bath sonicator prior to application. For experiments involving Mtb infection, parallel TLR stimulation was performed at the time of infection and following the 3-hour wash step, the TLR agonist was reapplied to fresh media.

TLR antagonist treatments

Anti-human TLR-2 antibody (anti-hTLR2) (monoclonal human IgA; Invivogen), anti-human TLR-6 antibody (anti-hTLR6) (monoclonal mouse IgG_1; Invivogen), control human IgA (monoclonal human IgA_2; Invivogen) and control mouse IgG (Sigma-Aldrich I5381) were reconstituted in sterile water and stored at -20°C prior to experimentation. Human MDM were isolated, cultured and prepared for experimentation as described in **Section 2.1.2**. For experiments involving inhibition of TLR-2 signalling, cells were treated with anti-hTRL2 (10µg/mL) or with control IgA (10µg/mL) 1 hour prior to infection with Mtb, washed at 3 hours post infection as described in **Section 2.2.1**, and fresh media supplemented with anti-hTLR2 treatment or control IgA reapplied for the duration of the experiment. For experiments involving dual inhibition of TLR-2 and TLR-6 signalling, cells were treated with combined anti-hTLR2 (10µg/mL) and anti-hTLR6 (1µg/mL) or with combined control IgA (10µg/mL) and control IgG (1µg/mL) and a similar protocol followed.

2.3 Metabolic Analyses

2.3.1 Extracellular Flux Analyses

The Seahorse XF^{E}24 Analyzer

Extracellular flux analyses were performed using the Seahorse XF^{e}24 Analyzer (Seahorse Biosciences, Aligent Technologies UK Ltd.). This instrument allows real-time simultaneous measurement of extracellular acidification rate (ECAR) and oxygen consumption rate (OCR) of live cells in a custom-designed multi-well plate. Adherent cells are plated to form a monolayer within the wells of the microplate and Seahorse Assay Cartridge (Seahorse Biosciences, Aligent Technologies UK Ltd.) sensor probes are lowered into each well (to approximately 200µm above the monolayer) to isolate an extremely small (approximately 2µL) volume of media above the monolayer. Probes repeatedly measure the concentration of dissolved oxygen and the concentration of free protons within this "transient microchamber" for 2 – 5 minutes (until the rate of change of both measured values are linear), and the instrument then calculates the OCR and the ECAR. Probes then lift to allow mixing of media within the transient microchamber with the larger volume of media in the well, before lowering again to form another transient microchamber and repeating measurement of OCR and ECAR. Broadly speaking, OCR represents mitochondrial oxidative phosphorylation rate and ECAR represents glycolytic rate within the cells.

The Seahorse XF Cell Mito Stress Test Kit

The Seahorse XF^{e}24 Analyzer also incorporates an integrated drug delivery system, whereby up to four compounds can be added sequentially to all wells at pre-designated intervals. Compounds are prepared prior to experimentation and pre-loaded into ports on the Seahorse Assay Cartridge. Sequence and timing of addition of compounds can be programmed using Seahorse XF Wave Desktop Software. During metabolic interrogation, pre-loaded compounds are then added into all wells at designated intervals, gentle mixing performed, and multiple OCR and ECAR measurements made. In this work, compounds from the Seahorse XF Cell Mito Stress Test Kit (Seahorse Biosciences, Aligent Technologies UK Ltd.) were utilised in experiments where stated. Compounds included in this kit are oligomycin, Carbonyl cyanide-4-(trifluoromethoxy)phenylhydrazone (FCCP) and combined rotenone with antimycin A.

Oligomycin inhibits ATP synthase (Complex V of the electron transport chain (ETC)), preventing ATP synthesis via oxidative phosphorylation. Consequently, cells must increase glycolytic rate in

order to meet demands for ATP synthesis, reflected by increased ECAR on extracellular flux analysis. The difference between baseline ECAR and post-Oligomycin ECAR reflects the Glycolytic Reserve (GR) of the cells i.e. their ability to increase glycolytic rate when stressed.

FCCP is an ionophore that acts as a mitochondrial uncoupler, allowing free passage of protons from the inter-membrane space across the inner mitochondrial membrane to the matrix, bypassing ATP synthase. As a result, Complex I – IV of the ETC must increase their rate of activity in order to maintain mitochondrial membrane potential, with concurrent increase of oxygen consumption at Complex IV (which converts molecular oxygen to water). Thus, OCR increases following addition of FCCP, and the post-FCCP OCR is referred to as the maximal OCR, reflecting the maximal rate of ETC activity that the cells can achieve. Similarly, the difference between baseline OCR and post-FCCP OCR reflects the Spare Respiratory Capacity (SRC) of the cells i.e. their ability to increase mitochondrial respiration when stressed.

Finally, Rotenone and Antimycin A directly inhibit Complex I and Complex III of the ETC, respectively, effectively shutting down all ETC activity and all mitochondrial oxygen consumption. Residual oxygen consumption, therefore, reflects Non-Mitochondrial Oxygen Consumption Rate of the cells.

Interestingly, within a normal cell, a certain amount of mitochondrial oxygen consumption reflects ETC activity that is not coupled to ATP synthesis at ATP synthase (Complex V). A small number of protons leak from the intermembrane space across the inner mitochondrial membrane, bypassing ATP synthase, and the ETC must also pump these protons back into the intermembrane space. Consequently, the difference between the post-Oligomycin OCR (reflecting inhibition of ETC activity linked to ATP synthesis) and the post-Rotenone/Antimycin A OCR (reflecting complete inhibition of the ETC) represents the mitochondrial Proton Leak (PL) within the cells.

A hypothetical example of real-time ECAR and OCR measurements at baseline and following addition of inhibitors, indicating how data can be used to calculate GR, SRC, non-mitochondrial OCR and PL, is depicted in **Figure 2.2**.

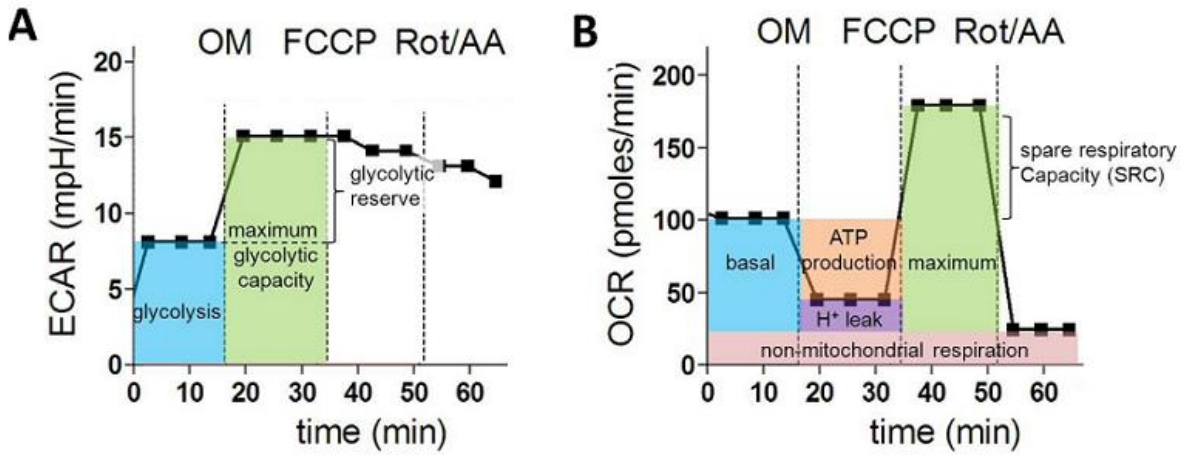

FIGURE 2.2 Metabolic parameters derived from a XF Extracellular flux assay. Panel A depicts ECAR measurements (in mpH/min) at baseline and following sequential addition of mitochondrial inhibitors, illustrating how different glycolytic parameters are calculated. Panel B depicts OCR measurements (in pmol/min) at baseline and following sequential addition of mitochondrial inhibitors, illustrating how different oxygen consumption parameters are calculated. OM = oligomycin A; FCCP = Carbonyl cyanide 4-(trifluoromethoxy)phenylhydrazone; AA = antimycin A; Rot = Rotenone. *Adapted from van den Bossche et al, 2015[463].*

Extracellular Flux Analysis: Protocol

For all extracellular flux analyses, cells were prepared as outlined in **Section 2.1** and plated on Seahorse 24-well microplates in usual culture medium 48 hours prior to interrogation, with 4 designated "blank" wells left free. 24 hours prior to analysis, fresh media was applied and treatments or infections performed. The Seahorse Assay Cartridge was hydrated using Seahorse Calibrant Solution and incubated at 37°C and 0% CO_2 overnight. A non-CO_2 incubator was used to prevent CO_2 present in plastics contributing to acidification of media during analysis.

On the day of interrogation, Seahorse media (bicarbonate-free DMEM) (Seahorse Biosciences, Aligent Technologies UK Ltd.) was supplemented with 2mM glutamine and 10mM glucose (or, where stated, with 10mM galactose), warmed to 37°C and filtered through 0.2µm sterile syringe filters (Corning, NY). Media was removed from all wells of the Searhorse microplate, cells washed once in supplemented Seahorse media, and 500µL of fresh Seahorse media applied to each well (including blank wells) and the microplate was incubated at 37°C and 0% CO_2 prior to interrogation using the Seahorse XF^{e}24 Analyzer. Where indicated, supernatants removed at this point (i.e. 24 hours post-treatment / infection) were retained and stored at -80°C for subsequent measurement of lactate, glucose or cytokines.

Prior to interrogation, compounds from the Seahorse XF Cell Mito Stress Test Kit (Seahorse Biosciences) were prepared in supplemented Seahorse medium under sterile conditions and

loaded into designated ports on the Seahorse Assay Cartridge. Optimal dosing for each compound was determined by optimisation experiments (see below).

Interrogation protocol was designed using Seahorse XF Wave Desktop Software. The Seahorse Assay Cartridge was inserted into the instrument and calibration of probes performed. The Seahorse microplate was then inserted, an equilibration step performed, and three baseline measurements of OCR and ECAR made. Mitochondrial inhibitors were added to all wells in the order oligomycin, then FCCP, then rotenone/antimycin A, with three measurements of OCR and ECAR made following the addition of each compound. Data displayed as real-time graphs of OCR and ECAR using Seahorse XF Wave Desktop Software was then converted to Microsoft Excel format for further analysis. Though three measurements were taken following addition of each mitochondrial inhibitor, only the minimal (oligomycin, rotenone/antimycin A) or maximal (FCCP) OCR measurement, with its corresponding ECAR measurement, was used for analysis.

After completion of interrogation, crystal violet (CV) assay was performed to determine cell viability in each well. Media was removed and 50µL 1% glutaraldehyde (Sigma-Aldrich) was added to each well for 15 minutes. Glutaraldehyde was removed and wells washed twice with PBS. 50µL 0.1% CV (Sigma-Aldrich) was added to each well for 30 minutes. CV was removed, microplate inverted and left to air dry for several hours. 40µL 1% Triton X solution was added to each well and the plate was placed on a shaker for 15 minutes to allow full elution to occur. Contents of each well were transferred to a 96-well plate and absorbance was read at OD_{595nm} using an Epoch™ Microplate Spectrophotometer with Gen 5 Data Analysis software (BioTek Instruments, VT). Results were then used to normalise ECAR and OCR measurements. Normalisation for cell viability reduced inter-donor variability and facilitated pooling of data. CV assay also facilitated interpretation of data by investigating variation in cell viability between treatment conditions that could impact observed results.

Extracellular Flux Analysis: Optimisation of Cell Seeding Density

Cell density optimisation assays were performed for human MDM and human AM. Cells were prepared as described in **Section 2.1.2** and **Section 2.1.1**, respectively. 48 hours prior to interrogation, cells were plated in duplicate at varying densities on Seahorse 24-well microplates in normal media. 24 hours prior to interrogation, fresh media was applied and Seahorse Assay Cartridge hydrated as described above. On the day of interrogation, supplemented Seahorse media was applied to all wells, microplate incubated and interrogation performed as described (save for addition of compounds). CV assay was also performed as described. As per

manufacturer's recommendations, optimal seeding density corresponds to baseline OCR of 50 – 400pmol.min^{-1}. Where OCR falls within this range for two or more seeding densities, the density corresponding to a baseline ECAR of 20 – 120mpH.min^{-1} is recommended. Seeding densities of 200,000 cells/well for human MDM (**Figure 2.3**) and of 100,000 cells/well for human AM (**Figure 2.4**) were determined to be optimal for metabolic interrogation by extracellular flux analysis, and thus were used for all experiments.

Extracellular Flux Analysis: Optimisation of Inhibitor Dose

Dose optimisation was performed for oligomycin and FCCP for both human MDM and human AM. For optimisation of oligomycin dose, cells were prepared as described in **Section 2.1.2** and **Section 2.1.1**, respectively. 48 hours prior to interrogation, cells were plated at 200,000 cells/well (human MDM) or 100,000 cells/well (human AM) in normal media. 24 hours prior to interrogation, fresh media was applied and Seahorse Assay Cartridge hydrated as described. On the day of interrogation, supplemented Seahorse media was applied to all wells and microplate incubated as described. Varying concentrations of oligomycin were made up in supplemented Seahorse medium under sterile conditions and loaded into designated ports on the Seahorse Assay Cartridge, with each concentration present in duplicate. Interrogation was then performed as described and CV assay used to normalise results. Using this method, the optimal final concentration of oligomycin was determined to be 1µM for interrogation of human MDM (**Figure 2.5A**) and 1µM for interrogation of human AM (**Figure 2.6A**). Optimisation of FCCP dose was performed in the same way and the optimal final concentration of FCCP was determined to be 1µM for interrogation of human MDM (**Figure 2.5B**) and 2µM for interrogation of human AM (**Figure 2.6B**). Rotenone and antimycin A are potent inhibitors of Complex I and Complex III, respectively, therefore optimisation experiments were not performed for these compounds and a final concentration of 0.5µM was used for all experiments, both in human MDM and human AM.

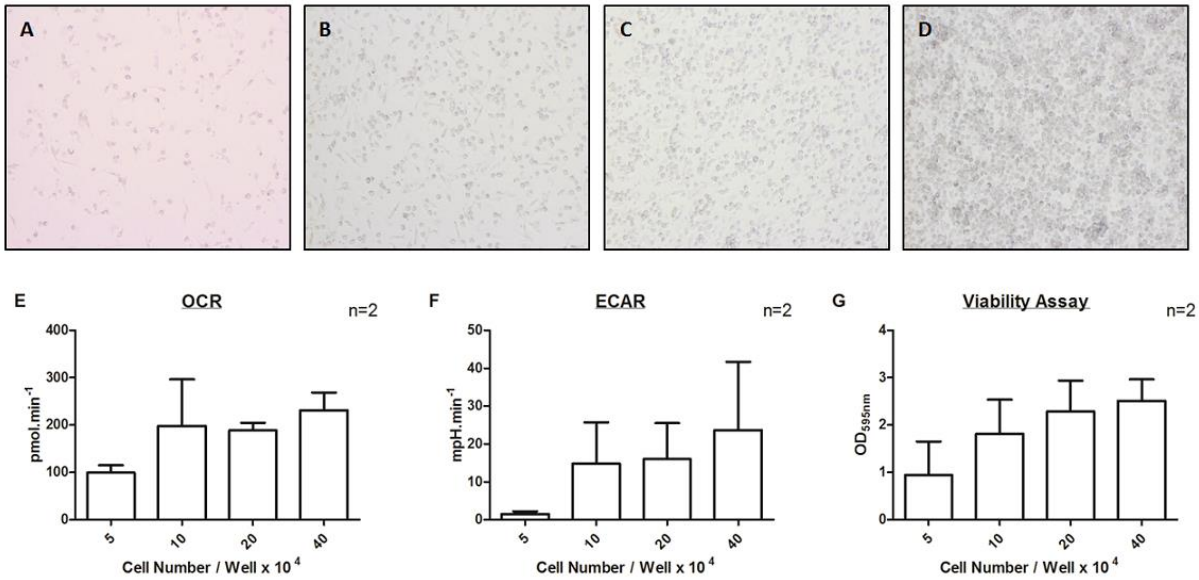

FIGURE 2.3 Optimisation of human MDM seeding density for extracellular flux analysis. MDM were cultured for 5 days, scraped, and plated on Seahorse Biosciences 24-well plates at indicated densities. On Day 7, extracellular flux analyses were performed and data normalised using CV assay. Panel A – D depict light microscopy images of human MDM plated at 50,000 cells/well (A), 100,000 cells/well (B), 200,000 cells/well (C) and 400,000 cells/well (D) for one representative donor. Panel E – F depict mean ± SEM OCR (E) and ECAR (F) of human MDM plated at varying densities for two individual donors. Panel G depicts corresponding absorbance following CV staining of human MDM plated at varying densities for two individual donors.

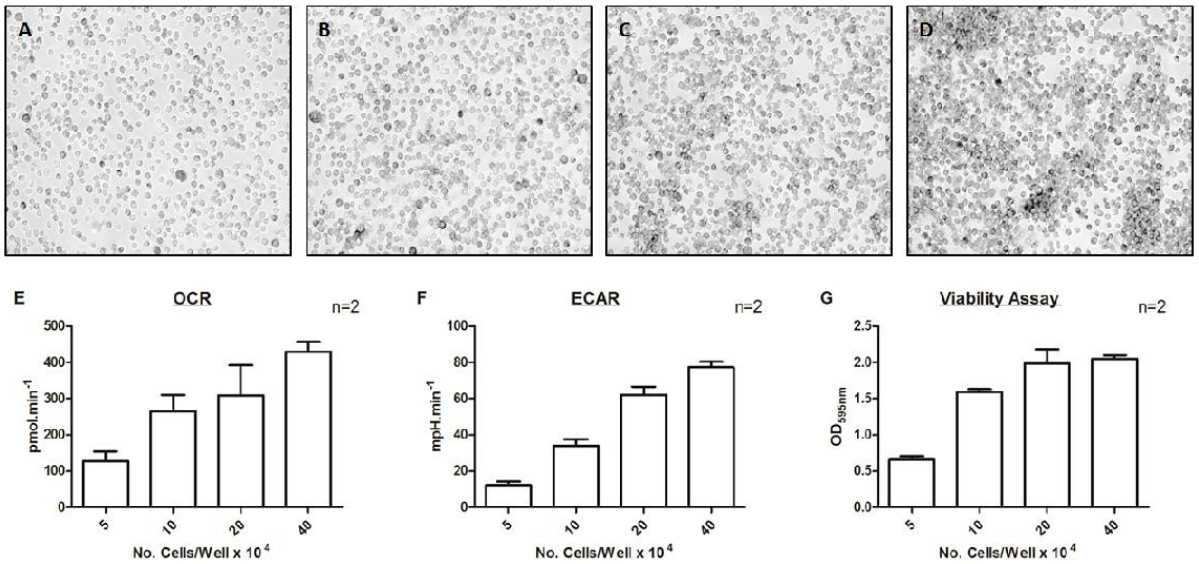

FIGURE 2.4 Optimisation of seeding density of human AM for extracellular flux analysis. Human AM were isolated and plated on Seahorse Biosciences 24-well plates at indicated densities. 48 hours after plating, extracellular flux analyses were performed and data normalised using CV assay. Panel A – D depict light microscopy images of human MDM plated at 50,000 cells/well (A), 100,000 cells/well (B), 200,000 cells/well (C) and 400,000 cells/well (D) for one representative donor. Panel E – F depict mean ± SEM OCR (E) and ECAR (F) of human AM plated at varying densities for two individual donors. Panel G depicts corresponding absorbance following CV staining of human AM plated at varying densities for two individual donors.

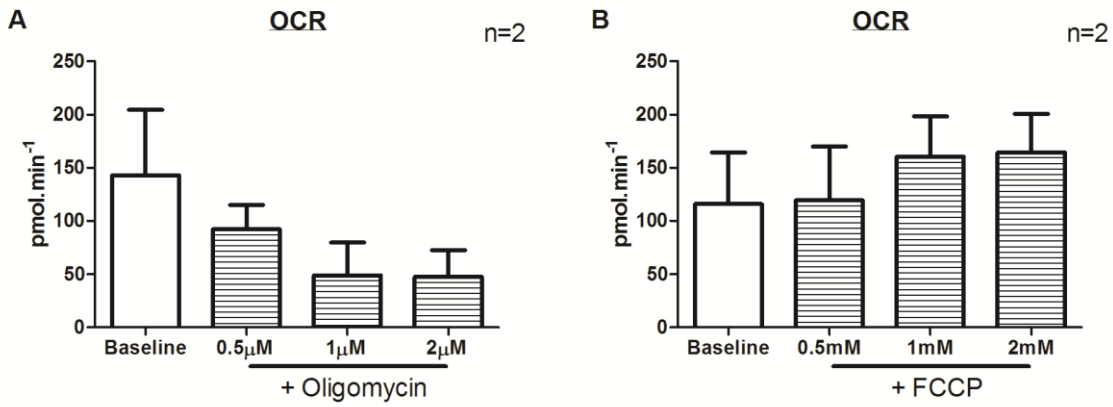

FIGURE 2.5 Optimisation of oligomycin and FCCP dose for human MDM interrogation. MDM were cultured for 5 days, scraped, and plated on Seahorse Biosciences 24-well plates at 200,000 cells/well. On Day 7, extracellular flux analysis was performed. Oligomycin (A) or FCCP (B) was made up in Seahorse media prior to interrogation and added to all wells during the interrogation to achieve the final concentrations indicated. Data were normalised using CV assay. Panel A depicts mean ± SEM minimum measured OCR following addition of oligomycin to achieve a final concentration of 0.5μM, 1μM or 2μM, compared to baseline OCR (control) for two individual donors. Panel B depicts mean ± SEM maximum measured OCR following addition of FCCP to achieve a final concentration of 0.5μM, 1μM or 2μM, compared to baseline OCR (control) for two individual donors.

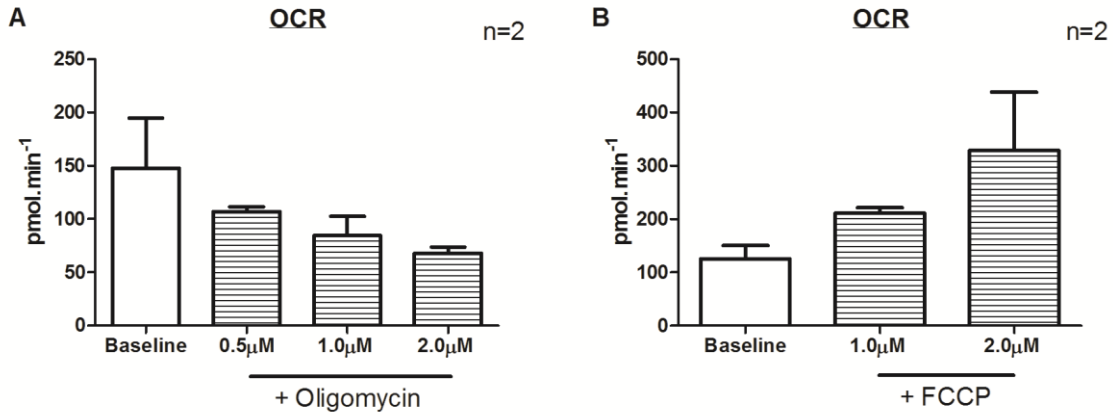

FIGURE 2.6 Optimisation of oligomycin and FCCP dose for human AM interrogation. Human AM were isolated and plated on Seahorse Biosciences 24-well plates at 100,000 cells/well. 48 hours after plating, extracellular flux analysis was performed. Oligomycin (A) or FCCP (B) was made up in Seahorse media prior to interrogation and added to all wells during the interrogation to achieve the final concentrations indicated. Data were normalised using CV assay. Panel A depicts mean ± SEM minimum measured OCR following addition of oligomycin to achieve a final concentration of 0.5μM, 1μM or 2μM, compared to baseline OCR (control) for two individual donors. Panel B depicts mean ± SEM maximum measured OCR following addition of FCCP to achieve a final concentration of 1μM or 2μM, compared to baseline OCR (control) for two individual donors.

2.3.2 Extracellular Glucose Quantification

Glucose concentration in supernatants was measured using the Glucose Assay Kit II (Eton Bioscience). This assay involves addition of enzymes that oxidise glucose to yield a colorimetric product, which can then be measured at OD_{570nm} with colour intensity proportional to glucose concentration. Supernatants were removed from cells at specified timepoints and stored at -80°C for up to one month. Samples were thawed and diluted 1:100 in Assay Buffer provided. Assay was performed as per manufacturer's instructions, with OD_{570nm} measured using the Epoch™ Microplate Spectrophotometer with Gen 5 Data Analysis software. In parallel, a known concentration Glucose Standard provided was used to generate a standard curve of absorbance:glucose concentration (top standard = 200µM), allowing calculation of the glucose concentration in each sample.

2.3.3 Extracellular Lactate Quantification

L(+)-Lactate concentration in supernatants was measured using the Lactate Assay Kit (Sigma-Aldrich Aldrich). This assay involves addition of enzymes that oxidise glucose to yield a colorimetric product, which can then be measured at OD_{570nm} with colour intensity proportional to lactate concentration. Supernatants were removed from cells at specified timepoints and stored at -80°C for up to one month. Samples were thawed and diluted 1:25 (supernatants from 24-well Seahorse plates) or 1:15 (supernatants from 12-well plates) in Assay Buffer provided. Assay was performed as per manufacturer's instructions, with OD_{570nm} measured using the Epoch™ Microplate Spectrophotometer with Gen 5 Data Analysis software. In parallel, a known concentration Lactate Standard was used to generate a standard curve of absorbance: lactate concentration (top standard = 0.2µM = 17.8ng/µL), allowing calculation of the lactate concentration in each sample.

2.3.4 Intracellular ATP Quantification

Intracellular ATP concentration in cell lysates was measured using the ATP Bioluminescence Assay Kit CLS II (Roche). This assay involves the luciferase-catalyzed oxidation of luciferin, a light-emitting reaction that is ATP dependent. Human MDM were prepared and plated at 3 x 10^6/mL on 12-well plates as described in **Section 2.1.2**, and infected on Day 6 as described in **Section 2.2.1**. 24 hours post-infection, supernatants were removed, centrifuged to remove extracellular bacteria and cell debris, and stored at -80°C. Cells were lysed by addition of 50µL

radioimmunoprecipitation assay (RIPA) buffer (Sigma-Aldrich) to each well and scraping cells with an inverted pipette tip over ice. 10µL of each sample lysate was retained for measurement of protein concentration. The remainder of each sample lysate was diluted 1:10 in Assay Buffer, 9 volumes of boiling 100mM Tris + 4mM EDTA (pH7.75) added and incubated at 100°C for 2 minutes. Lysates were then centrifuged and supernatants applied to black microtiter plates over ice, luciferase reagent added and bioluminescence measured using the Fluroskan Ascent™ FL Microplate Fluorometer and Luminometer with Ascent™ Software Version 2.6 (Thermo Fisher Scientific™, MA). In parallel, a stabilised ATP standard was used to generate a standard curve of bioluminescence: ATP concentration (top standard ≈ 16.5M), allowing calculation of the ATP concentration in each sample.

Pierce™ Bicinchoninic acid (BCA) Assay Kit (Thermo Fisher Scientific) was used to quantify protein concentration in each sample lysate, in order to control for variations in cell number between wells. This assay involves the reduction of Cu^{2+} to Cu^{1+} by protein followed by bicinchoninic acid chelation with Cu^{1+} to form a purple product that exhibits absorbance at OD_{562nm}. 10µL of each lysate sample was retained and BCA Assay performed according to manufacturer's instructions, with OD_{562nm} measured using the Epoch™ Microplate Spectrophotometer with Gen 5 Data Analysis software. In parallel, a known concentration Bovine Serum Albumin (BSA) Standard was used to generate a standard curve of absorbance: protein concentration (top standard = 2,000µg/mL), allowing calculation of the protein concentration in each sample.

2.3.5 Glycolytic Gene Expression Analyses

Human MDM were prepared and plated at 3 x 10^6/mL on 12-well plates as described in **Section 2.1.2**, and infected on Day 6 as described in **Section 2.2.1**. Human AM were prepared and plated at 1 x 10^6/mL on 24-well plates as described in **Section 2.1.1**, and infected on Day 1 as described in **Section 2.2.1**. 24 hours post-infection, supernatants were removed and cells were washed once in PBS. Cells were then lysed and homogenised by adding 300µL denaturing Buffer RLT (QIAGEN) to each well to ensure immediate inactivation of RNases while permitting isolation of intact RNA. Lysates were stored at -80°C for up to two weeks prior to isolation of RNA. RNA isolation was performed using the RNeasy Mini Kit (QIAGEN) according to manufacturer's instructions. Lystates were thawed and diluted 1:2 with 70% ethanol before being passed through the RNeasy Spin Column by centrifugation at 14,500rpm for 15 seconds. RNA binds to the membrane of the spin column. Contaminants are then washed away by application of Buffer RW1 (removes biomolecules such as carbohydrates, proteins, fatty acids that are non-specifically bound to the silica membrane while RNA molecules larger than 200 bases remain bound) and Buffer RPE

(removes salts and traces of other buffers) in a series of further centrifugation spins at 14,500rpm. RNA was then eluted in 30µL of RNase-free water (one minute spin at 14,500rpm).

Isolated RNA was used to generate double-stranded cDNA by reverse transcription using the High-Capacity cDNA Archive Kit (Applied Biosystems). First, RNA concentration in each sample was measured using the NanoDrop™ ND-8000n Spectrophotometer with ND-8000 Software Version 1.0 (Thermo Fisher Scientific). The 260nm/280nm absorbance ratio was also noted to assess purity of RNA. For all experiments, a 260/280 ratio of ≥ 1.9 was considered acceptable. Next, 1000ng of RNA was added to each cDNA reaction microtube, along with RT Buffer, RT Random Primers, dNTPs, Reverse Transcriptase and RNase-free water at ratios specified by manufacturer, with a total reaction volume of 20µL per sample. Where RNA yield was too low to allow 1000ng to be added to cDNA reactions microtubes, a lower amount of RNA was used, but equal amounts of each sample were used across the experiment. Reverse transcription was then carried out on a Techne TC-3000 Thermal Cycler (Bibby Scientific Ltd, UK) in accordance with Applied Biosystems™ protocol. Prepared cDNA was stored at -30° for up to one month.

Relative gene expression was then examined by cDNA amplification using real-time quantitative polymerase chain reaction (qPCR). Fluorescent Taqman® probes that bind specific genes of interest anneal to cDNA and are incorporated into new DNA strands, with consequent emission of fluorescence which can be detected by the ABI Prism® 7900HT Sequence Detection System with SDS software Version 2.1 (Applied Biosystems, CT). Increased expression of the target gene results in earlier detection of fluorescence, hence a lower cycle threshold (Ct) at which the fluorescence is detected corresponds to higher expression of the target gene within the sample. For all qPCR experiments in this thesis, 1µL cDNA sample was combined with 0.5µL of the specified Taqman® probe, 5µL Fast Mastermix (containing DNA polymerase) and 3.5µL RNase-free water in a single well of a 384-well PCR plate, in triplicate. 18S rRNA expression was measured in triplicate for each sample, and this was used to normalise for variation in cDNA concentrations between samples by calculating the ΔCt (i.e. Ct value for target gene mRNA for one sample – Ct value for 18S rRNA for corresponding sample). For each gene, infection / treatment-induced expression was then compared to expression in uninfected (control) samples, generating the ΔΔCt (i.e. ΔCt value for infected sample – ΔCt value for control sample). Finally, the fold-change in mRNA expression relative to the control sample was calculated (i.e. $2^{-\Delta\Delta CT}$).

In this way, fold change in relative mRNA expression of glycolytic genes following 24 hours of LPS stimulation or Mtb infection was determined using Taqman® probes specific for glycolytic genes, as indicated.

2.4 Macrophage Functional Analyses

2.4.1 Gene Expression Analyses

RNA expression analysis was carried out as described in **Section 2.3.5**. Human MDM and human AM were isolated and cultured as described in **Section 2.1**, pre-treated with metabolic or immunologic manipulators as described in **Section 2.5** and **Section 2.6**, and infected or treated as described in **Section 2.2**. At indicated timepoints post-infection or treatment, supernatants were removed and cells lysed in RLT buffer to facilitate RNA extraction, cDNA generation and real-time qPCR and analysis as described in **Section 2.3.5**.

2.4.2 Secreted Cytokine Profiling

Secreted cytokine concentrations were measured in supernatants removed from cells using sandwich enzyme-linked immunosorbent assay (ELISA). Briefly, samples were applied to high protein binding plates coated in "capture antibody" (specific for the cytokine being assessed), resulting in immobilisation of the antigen to the surface of the well. A second biotin-conjugated "detection antibody" (also specific for the cytokine being assessed) was added and bound to the immobilised antigen. Horseradish peroxidase (HRP)-conjugated streptavidin (which has a high affinity for biotin) was then applied. Between each step, washes were performed using PBS buffer supplemented with the detergent 0.5% Tween-20. The chromogenic HRP substrate 3,3',5,5'-tetramethylbenzidine (TMB) was then applied, with resultant colorimetric change proportional to the amount of cytokine present in the well. This was then stopped using H_2SO_4 and read OD_{450nm} using the Epoch™ Microplate Spectrophotometer with Gen 5 Data Analysis software. In parallel, a known concentration standard of the cytokine being assessed was used to generate a standard curve of absorbance: cytokine concentration (top standard = 1,000pg/mL), allowing calculation of the cytokine concentration in each sample.

Human IL-1β measurement was performed using the Human IL-1β/IL-1F2 DuoSet ELISA kit (R&D Systems). All reagents were used at concentrations advised by manufacturer. Capture antibody was applied 72 hours prior to experimentation, with plates stored at 4°C for 48 hours and at room temperature for 24 hours prior to application of manufacturer-supplied blocking buffer for one hour, and subsequent application of samples to plate for three hours. Plates were incubated for three hours following application of detection antibody. All other incubations were performed as per the manufacturer's instructions.

Human TNF-α and human IL-10 measurement was performed using the corresponding ELISA Ready-SET-Go kit (eBiosciences). All reagents were used at concentrations advised by manufacturer. Capture antibody was applied 24 hours prior to experimentation and plates stored at 4°C, in line with manufacturer's instructions, prior to application of blocking buffer for one hour and subsequent application of samples to plate. For TNF-α experiments, samples were diluted 1:10 prior to application, samples applied for one hour and subsequently detection antibody applied for one hour, as per manufacturer's instructions. For IL-10 experiments, samples were applied for three hours and subsequently detection antibody applied for two hours. All other incubations were performed as per the manufacturer's instructions.

Murine IL-1β, TNF-α and IL-10 measurement was performed using the corresponding ELISA Ready-SET-Go kit (eBiosciences). All reagents were used at concentrations advised by manufacturer. All incubations were performed as per the manufacturer's instructions. For TNF-α experiments, samples were diluted 1:10 prior to application.

2.4.3 Eicosanoid Measurement

Prostaglandin E_2 (PGE_2) was measured in supernatants using a PGE_2 ELISA Kit (Invitrogen). This assay is based on the competition between PGE_2 in the sample and Alkaline Phosphatase conjugated PGE2 (PGE2-ALP) for a limited amount of PGE_2 monoclonal antibody bound to an Anti-Mouse IgG pre-coated 96-well plate. As the concentration of PGE_2 in the sample increases, the amount of PGE_2-ALP captured by the coating antibody decreases. Bound PGE_2-ALP emits light at 405nm, thus there is an inverse relationship between OD_{405nm} and PGE_2 concentration in the sample. Assay was performed on each sample in duplicate, with samples diluted 1:2 in Assay Buffer provided prior to analysis. OD_{405nm} was measured using the Epoch™ Microplate Spectrophotometer with Gen 5 Data Analysis software. In parallel, a known concentration PGE_2 Standard was used to generate a standard curve of absorbance: PGE_2 concentration (top standard = 0.2µM = 17.8ng/µL), allowing calculation of the PGE_2 concentration in each sample.

2.4.4 ROS Measurement

ROS were measured using a DCFDA Cellular ROS Detection Assay Kit (Abcam). This assay uses the cell permeant reagent 2',7'-dichlorofluorescin diacetate (DCFDA), which is deacetylated by cellular esterases to a non-fluorescent compound upon diffusion into the cell, and is then oxidised by ROS into 2',7'-dichlorofluorescein (DCF). DCF is highly fluorescent, thus endpoint sample fluorescence

is proportional to intracellular ROS activity. Human MDM were isolated and cultured as described in **Section 2.1.2**. On Day 6, cells were treated with Glucose or Galactose as described in **Section 2.5.2**. On Day 7, cells were infected or treatments applied as described in **Section 2.2**. 24 hours post-infection, cells were transferred to a black 96-well clear-bottomed plate in triplicate and allowed to adhere overnight, with Glucose or Galactose treatment continued. Supernatants were then removed, cells stained with DFDCA solution 100µL/well and incubated at 37°C in the dark for 30 minutes, as per manufacturer's instructions. Fluorescence was immediately read with excitation wavelength 485nm and emission wavelength 535nm using the Fluroskan Ascent™ FL Microplate Fluorometer and Luminometer with Ascent™ Software Version 2.6 (Thermo Fisher Scientific™, MA). Tert-butyl hydrogen peroxide (TBHP) 550µM was used as a positive control. No standard curve was utilised, thus results were expressed as relative fluorescence.

2.4.5 Bacterial Uptake Assays

Mtb uptake assay

Human MDM were isolated, cultured and prepared for experimentation as described in **Section 2.1.2**. 24 hours prior to infection, cells were pre-treated with Glucose- or Galactose-supplemented media as described in **Section 2.5.2**, and infections were performed as described in **Section 2.2**. At 3 hours post-infection, cells were washed three times to remove extracellular bacilli, lysed in sterile 0.1% Triton-X, serial dilutions performed in 7H9 Middlebrook Broth and plated on 7H10 Middlebrook Agar in triplicate. Agar plates were incubated at 37°C in a non-CO_2 incubator for 14 – 28 days. CFU were enumerated by counting. CFU count was representative of the number of bacilli phagocytosed by macrophages at 3 hours post-infection.

S. typhi uptake assay

A similar method was used to assess *S. typhi* uptake by murine BMDM. Murine BMDM were isolated, cultured and prepared for experimentation as described in **Section 2.1.3**. *S. typhi* infection was performed as described in **Section 2.2.2**. Following the 30-minute wash step, designated wells were lysed in ice water, serial dilutions to 10^{-8} performed in PBS, and lysates plated on LB agar plates in quadruplicate. LB agar plates were incubated for 24 hours prior to enumeration of CFU by counting. Colony count was representative of the number of bacilli phagocytosed by macrophages at 30 minutes post-infection.

2.4.6 Intracellular Bacterial Killing Assays

Mtb killing assay

An intracellular bacillary killing assay was used to assess macrophage mycobactericidal function. Murine BMDM, human MDM or human AM were isolated as described in **Section 2.1**, pre-treated with metabolic or immunologic mediators as described in **Section 2.5** and **Section 2.6**, and infected as described in **Section 2.2.1**. Following the 3 hour post-infection wash step, designated infected macrophages were lysed in sterile 0.1% Triton-X, serial dilutions performed in 7H9 Middlebrook Broth and plated on 7H10 Middlebrook Agar in triplicate. The remainder of infected cells were incubated following this 3 hour wash step. At 72 hours post-infection, these cells were lysed. Lysates and supernatants were combined and serial dilutions and plating performed. Agar plates were incubated at 37°C in a non-CO_2 incubator for 14 – 28 days. CFU were enumerated by counting. Fold change in CFU number at 72 hours relative to 3 hours (representative of uptake) was reflective of intracellular bacillary killing.

S. typhi killing assay

A similar method was used to assess bactericidal function of murine BMDM infected with *S. typhi*. Murine BMDM were isolated, cultured and prepared for experimentation as described in **Section 2.1.3**. *S. typhi* infection was performed as described in **Section 2.2.2**. Following the 30-minute wash step, designated wells were lysed in ice water, serial dilutions to 10^{-8} performed in PBS, and lysates plated on LB agar plates in quadruplicate. The remainder of the cells were incubated for a further 24 hours prior to lysis, dilution and plating as described. 24 hour supernatants were removed and centrifuged, with the bacterial pellet added to cell lysates prior to plating. LB agar plates were incubated for 24 hours prior to enumeration of CFU by counting. Fold change in colony count at 24 hours relative to 30 minutes (representative of uptake) was reflective of intracellular bacterial killing.

2.5 Metabolic Manipulation of Macrophages

2.5.1 Glycolytic inhibition using 2-deoxyglucose

The compound 2-deoxyglucose (2-DG) is a competitive inhibitor of Hexokinase, the enzyme that catalyses the first step of the glycolytic pathway. Others have used mM concentrations of 2-DG to inhibit the glycolytic shift in LPS-stimulated murine BMDM in order to examine its influence on macrophage function [174].

During initial experiments, 2-DG was similarly used to inhibit glycolysis in murine BMDM. 2-DG powder (Sigma-Aldrich) was reconstituted in PBS to make a stock solution of 1M, which was then filter-sterilised and stored at 4°C. Stock solution was diluted in culture medium on the day of experimentation in order to achieve working concentration. Cells were isolated and cultured as described in **Section 2.1.3**. 3 hours prior to infection with Mtb, cells were treated with culture medium supplemented with 5mM 2-DG or with culture medium alone (control). 3 hours post infection, supernatants were removed, cells washed and fresh media applied, as described in **Section 2.2.1**. 2-DG-supplemented media or control media was reapplied following the 3-hour wash step and cells incubated at 37°C in 5% CO_2 for duration of experiment. Optimisation experiments were performed to ensure equal uptake of Mtb with and without 2-DG.

Glycolytic inhibition using 2-DG was also attempted in human macrophages. However, optimisation studies suggested increased cell death of human MDM following 2-DG treatment (**Figure 2.7**). Thus, 2-DG was not used as a glycolytic inhibitor in human macrophage experiments.

2.5.2 Glycolytic inhibition using Galactose

Galactose is a six-carbon monosaccharide, similar to glucose. In order to enter the glycolytic pathway, galactose must be converted to glucose-6-phosphate via the cumbersome and energy-requiring Leloir pathway. Cells cultured in glucose-free galactose-supplemented media do not, therefore, increase their glycolytic rates as other cells do, but instead rely on oxidative phosphorylation driven by glutamine anapleurosis in order to generate ATP (**Figure 2.8**) [464].

Galactose has been used successfully to inhibit the activation-induced shift towards aerobic glycolysis in human T cells [465]. The potential of galactose to inhibit glycolytic shift in activated macrophages was investigated. Firstly, viability studies were performed to confirm similar levels of cell death in both Glucose- and Galactose-treated cells (**Figure 2.9**).

Human MDM and human AM were isolated and cultured as described in **Section 2.1**. Glucose-free RPMI (Sigma-Aldrich) was supplemented with 10mM Glucose (Sigma-Aldrich) or 10mM Galactose (Sigma-Aldrich), filter-sterilised, and supplemented with 10% Human Serum (Sigma-Aldrich). 24 hours prior to infection with Mtb, cells were treated with Glucose-supplemented or Galactose-supplemented RPMI. 3 hours post infection, supernatants were removed, cells washed and fresh media applied, with Glucose- or Galactose-supplemented cRPMI reapplied. For extracellular flux analyses, Seahorse media was supplemented with 2mM glutamine and either 10mM glucose or 10mM galactose, and the previously described protocol employed (**Section 2.3.1**).

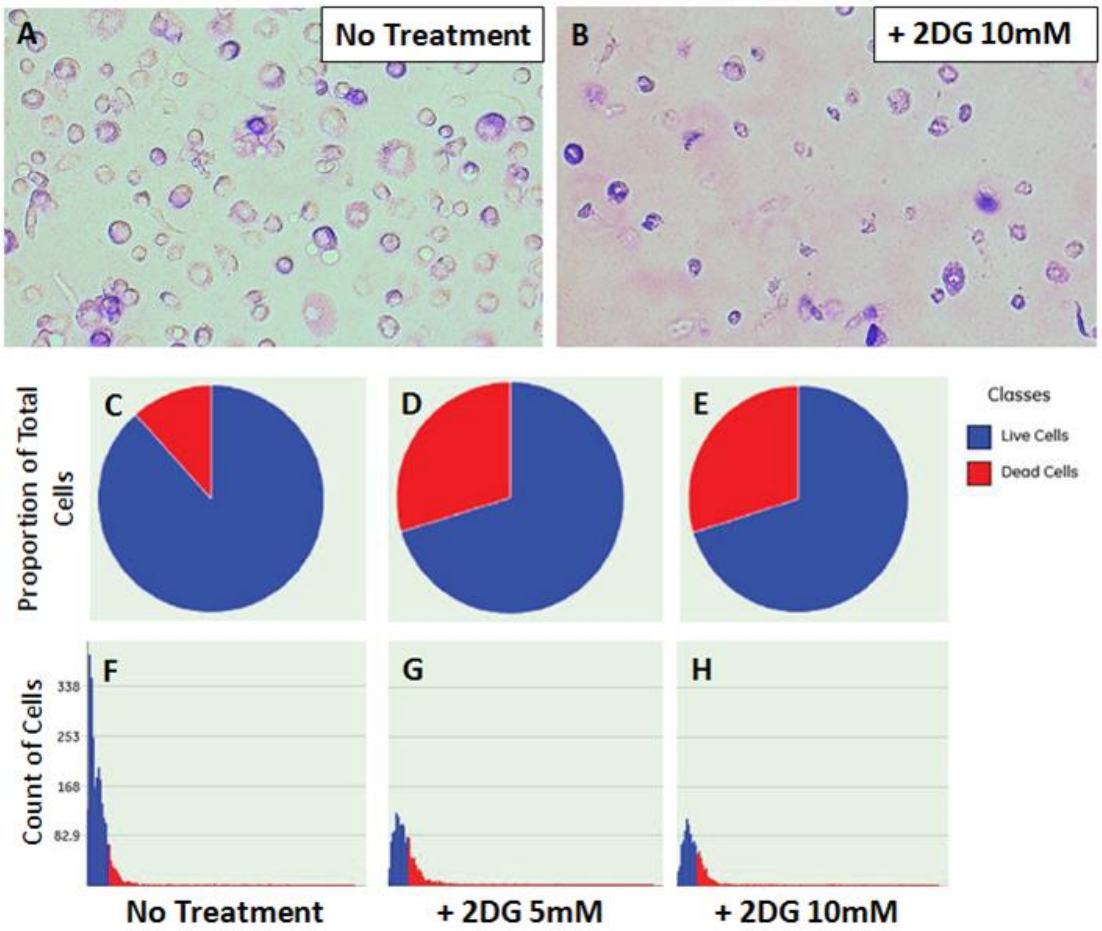

FIGURE 2.7 2-DG treatment reduces human MDM viability. MDM isolated from IBTS buffy coats isolated and cultured as described. On Day 7, supernatants were removed and cells incubated in DMEM with 10% FBS supplemented with 2-DG at 5mM or 10mM or in unsupplemented DMEM with 10% FBS. 48 hours after incubation, cells were stained with propydium iodide (PI) 5µg/mL, Hoechst 33342 20µg/mL and Hoescht 33258 50µg/mL and analysed using the Cytell Imaging System. Panel A and B depict light microscopy images at 10X following 24 hours incubation in cRPMI alone (A) or cRPMI supplemented with 10mM 2-DG (B). Panels C – E depict the proportion of live (blue) and dead (red) cells at 48 hours following incubation with indicated concentrations of 2-DG. Panels F – H depict the count of live (blue) and dead (red) cells at 48 hours following incubation with indicated concentrations of 2-DG. Panels depict data for one representative donor.

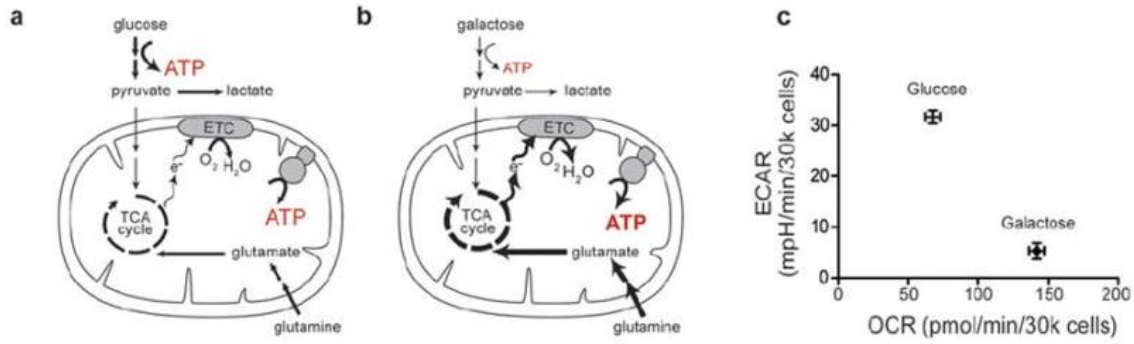

FIGURE 2.8 Metabolic plasticity of human fibroblasts. Panels A and B are schematic representations of cellular energy metabolism pathways, demonstrating cells grown in glucose rich media deriving ATP from both glycolysis and glutamine-driven mitochondrial respiration (A) and cells grown in glucose-deprived galactose-supplemented media generating ATP almost exclusively from glutamine-driven oxidative metabolism (B). Panel C depicts mean ± SD ECAR and OCR of fibroblasts grown in 10 mM glucose or 10 mM galactose containing media for three days, for five individual donors. (TCA = Tricarboxylic Acid; ETC = Electron Transport Chain). *Adapted from Gohil et al, 2010 [464].*

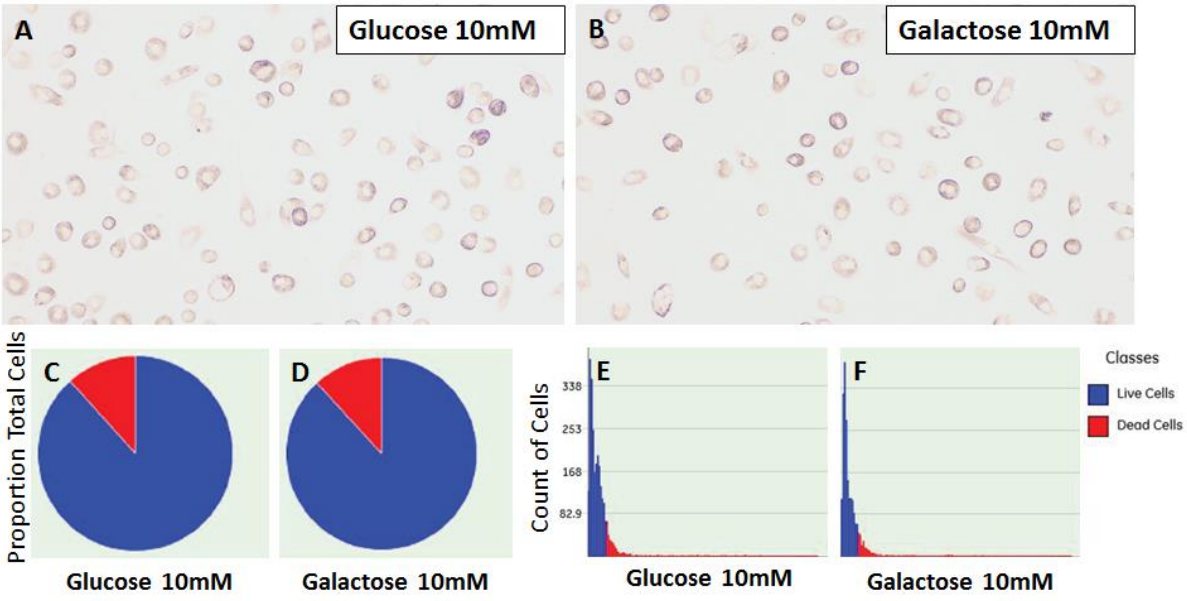

FIGURE 2.9 Galactose does not reduce human MDM viability. MDM isolated from IBTS buffy coats isolated and cultured as described. On Day 7, supernatants were removed and cells incubated in Glucose-free RPMI supplemented with 10mM Galactose and 10% FBS or with 10mM Glucose and 10% FBS (control). 48 hours after incubation, cells were stained with PI 5µg/mL, Hoechst 33342 20µg/mL and Hoescht 33258 50µg/mL and analysed using the Cytell Imaging System. Panel A and B depict light microscopy images at 10X following 24 hours incubation in Glucose-supplemented (A) or Galactose-supplemented (B) RPMI. Panels C and D depict the proportion of live (blue) and dead (red) cells at 48 hours following incubation with Glucose or Galactose. Panels E and F depict the count of live (blue) and dead (red) cells at 48 hours following incubation with Glucose or Galactose. Panels depict data for one representative donor.

2.5.3 PKM2 activation using TEPP-46

The thieno[3,2-b]pyrrole[3,2-d]pyridazinone TEPP-46 has been shown to bind the enzyme PKM2 to promote formation of stable, enzymatically-active tetramers, which have been linked to decreased glycolytic flux in cancer cells [466]. TEPP-46 (stock concentration at 0.5mM, in DMSO) was acquired from our collaborator Professor Luke O'Neill, TCD, following synthesis in accordance with published methods [247,467], and was stored at -80°C for up to one month prior to experimentation. On the day of experimentation, stock solution was diluted in culture medium in order to achieve working concentration of 25µM or 50µM, as indicated. Vehicle control medium was prepared by diluting an equal volume of DMSO in culture medium. Where varying TEPP-46 concentrations were utilised, vehicle control medium was prepared using a volume of DMSO equal to volume of TEPP-46 stock solution used to reach a working concentration of 25µM.

Murine BMDM were isolated and cultured as described in **Section 2.1.3**. 1 hour prior to infection with Mtb, cells were treated with TEPP-46-supplemented medium or with vehicle control medium. 3 hours post infection, supernatants were removed, cells washed and fresh media applied, as described in **Section 2.2**. TEPP-46-supplemented medium or vehicle control medium was reapplied following this 3 hour wash step and cells incubated at 37°C in 5% CO_2 for duration of experiment.

2.5.4 Glycolytic activation using Meclizine Dihydrochloride

The anticholinergic and H1 receptor antagonist meclizine has been demonstrated to induce a shift in cellular energy metabolism from oxidative phosphorylation to glycolysis via inhibition of the cytosolic enzyme CTP:phosphoethanolamine cytidylyltransferase (PCYT2) [464,468]. Meclizine dihydrochloride powder (Sigma-Aldrich) was reconstituted in DMSO (stock concentration 5mg/mL) and stored at -80°C for up to one month prior to experimentation. Gohil et al demonstrated induction of glycolysis without significant toxicity in human skin fibroblasts with meclizine concentration ranging from 10µM to 50µM [464], thus working concentrations of 10µM, 25µM and 50µM were utilised in these experiments. On the day of experimentation, stock solution was diluted in culture medium in order to achieve working concentration as indicated. Vehicle control medium was prepared by diluting an equal volume of DMSO in culture medium. Where varying meclizine concentrations were utilised, vehicle control medium was prepared using a volume of DMSO equal to volume of meclizine stock solution used to reach a working concentration of 25µM.

Human MDM were isolated, cultured and prepared for experimentation as described in **Section 2.1.2**. 1 hour prior to infection with Mtb, cells were treated with meclizine-supplemented medium or with vehicle control medium. 3 hours post infection, supernatants were removed, cells washed and fresh media applied, as described in **Section 2.2.1**. Meclizine-supplemented medium or vehicle control medium was reapplied following this 3 hour wash step and cells incubated at 37°C in 5% CO_2 for duration of experiment .

2.6 Manipulation of IL-1β Signalling

2.6.1 Addition of Exogenous IL-1β

Recombinant human IL-1β from the Human IL-1β ELISA Ready-SET-Go kit (eBiosciences) and recombinant mouse IL-1β from the Mouse IL-1β ELISA Ready-SET-Go kit (eBiosciences) were stored at -80°C. Human MDM and murine BMDM were isolated, cultured and prepared for experimentation as described in **Section 2.1.2** and **Section 2.1.3**, respectively. Infections were performed and 3 hours post infection, supernatants were removed, cells washed and fresh media applied. Following this 3 hour wash step, recombinant IL-1β at 100pg/mL or with PBS control treatments were reapplied.

2.6.2 Inhibition of IL-1β signalling in human MDM

Recombinant anti-human IL-1β/IL-1F2 antibody (anti-hIL-1β) (monoclonal mouse IgG_1 clone; R&D Systems) was reconstituted in sterile endotoxin-free PBS to form a stock solution at 0.5mg/mL and stored at 4°C prior to experimentation. Control mouse IgG (Sigma-Aldrich I5381) was reconstituted to 1mg/mL in 150M saline and stored at 4°C prior to experimentation. Human MDM were isolated, cultured and prepared for experimentation as described in **Section 2.1**, with metabolic inhibition with Galactose (human MDM experiments) performed at 24 hours prior to infection as described in **Section 2.5**. 1 hour prior to infection with Mtb, cells were treated with anti-hIL-1β (0.1µg/mL) or with control IgG (0.1µg/mL). 3 hours post infection, supernatants were removed, cells washed and fresh media applied, as described in **Section 2.2.1**. Anti-IL-1 treatment, metabolic inhibitor treatment and controls were reapplied following this 3 hour wash step.

2.6.3 IL-1R-KO Murine Macrophage Experiments

Murine BMDM were isolated from wild-type (WT) CS57BL/6 mice and from IL-1R-KO mice (CS57BL/6 background), cultured and prepared for experimentation as described in **Section 2.1.3**. Side-by-side infections were performed as described in **Section 2.2.1**.

2.6.4 Inflammasome Interrogation

Oxidised ATP (oATP), an irreversible inhibitor of P2RX7, was used to assess the contribution of ATP-driven inflammasome activation in Mtb-induced IL-1β production. Z-YVAD-FMK (YVAD), an irreversible caspase-1 inhibitor, was used as a positive control. Human MDM were isolated, cultured and prepared for experimentation as previously described. At the time of infection, cells were treated with oATP (300μM), YVAD (100μM) or left untreated (control). At 3 hours post infection, supernatants were removed, cells washed and fresh media applied, as described in **Section 2.2.1**. Following this 3 hour wash step, oATP and YVAD treatments were reapplied and cells incubated at 37°C in 5% CO_2 for 24 hours. Supernatants were removed and centrifuged to remove extracellular bacilli and cell debris and IL-1β quantified by ELISA, as described in **Section 2.4.2**.

2.7 Cigarette Smoke Extract Treatment

2.7.1 Generation of CSE

Cigarette Smoke Extract (CSE) was a kind gift from Dr Jacintha O'Sullivan, TCD. Generation of CSE is based on a validated in vitro pump system whereby water-soluble cigarette smoke constituents are passed from gaseous to aqueous phase [469]. Four Marlboro Red Class A cigarettes (rated as tar 10mg, nicotine 0.8mg and carbon monoxide 10mg) were smoked through 30 mL of RPMI 1640. Each cigarette was smoked for 10 puffs at 30 second intervals, with each puff generating 35 mL of smoke, burning approximately 75% of the cigarette. Thus 1400mL of smoke was generated from four cigarettes and passed through 30mL of RPMI, to create "100% CSE". Apparatus used for generation of 100% CSE is depicted in **Figure 2.9**. Bernhard's volumetric equations are based on the assumption that a human has 6L of blood and one cigarette smoked generates 350mL of smoke [469]. Thus, for a person smoking 20 cigarettes per day (1 standard pack), each 300mL of blood will contain the equivalent smoke from one cigarette (6L ÷ 20 cigarettes). Our 100% CSE contains a 40 times greater concentration of cigarette smoke than this (30mL containing equivalent smoke from 4 cigarettes). Hence, 2.5% CSE is representative of a smoker of 20 cigarettes/day, 5% CSE representative of 40 cigarettes/day and 10% representative of 80 cigarettes/day.

Following preparation, 100% CSE was sterile filtered through a 0.2µm filter, pH adjusted to 7.4 and stored at -20˚C. Dilutions in standard culture media were performed prior to experimentation to achieve stated working concentrations.

2.7.2 CSE treatment of human MDM

Human MDM were isolated, cultured and prepared for experimentation as described in **Section 2.1.2**. 24 hours prior to infection, media was replaced with CSE at varying concentrations or left untreated (control). Infections were performed as described in **Section 2.2.1**. 3 hours post infection, supernatants were removed, cells washed and fresh media applied. CSE or standard culture media (control) was reapplied following this 3 hour wash step and cells incubated at 37°C in 5% CO_2 for duration of experiment.

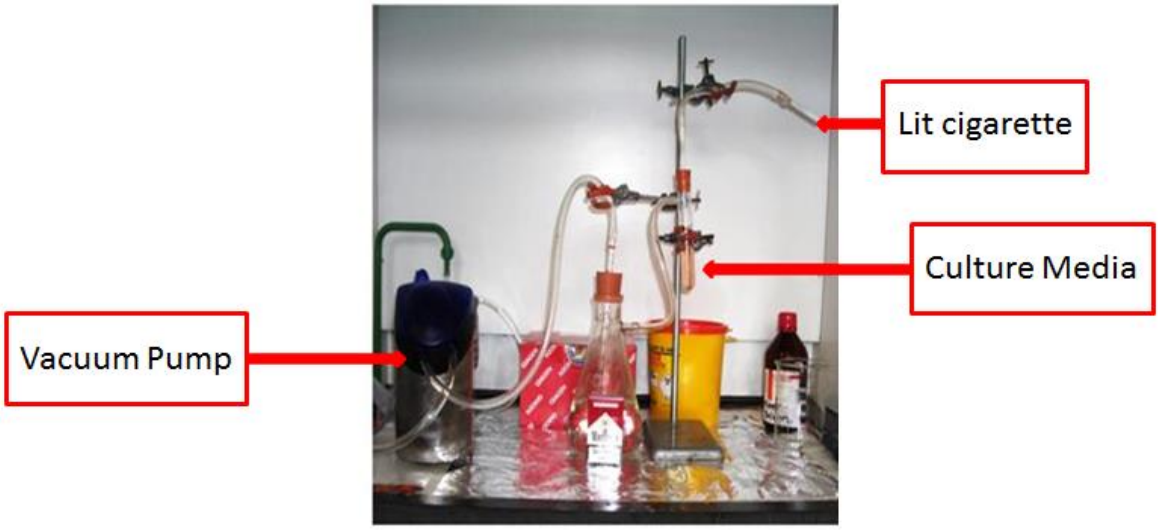

FIGURE 2.10 Generation of CSE. Four Marlboro Red Class A cigarettes were smoked through 30 mL of RPMI 1640 for 10 puffs at 30 second intervals to generate 1400mL of smoke in total.

CHAPTER 3:

The Macrophage Metabolic Response to Mtb Infection

3.1 Introduction

3.1.1 Hypothesis: Mtb infection induces glycolytic reprogramming in human AM

AM responses represent a crucial component of host defence against Mtb infection, capable of completely clearing the bacillus or of initiating mobilisation of robust innate and adaptive immune responses that lead to active disease or latent infection [15,16]. However, the role of metabolic reprogramming in AM response to Mtb is unknown. Despite significant advances in our understanding of macrophage metabolic reprogramming in recent years, most experimentation has involved murine macrophages [174,241,244,245,247,250,270,334,470,471], and investigation of human macrophage metabolism has generally been limited to immortalised cell lines [300,356] which are likely to exhibit significantly altered metabolic profiles in comparison to primary cells. **Chapter 3** aims to describe for the first time the impact of Mtb infection on human AM metabolic profile. Due to limited availability and low yield of human AM retrieved at bronchoscopy, the impact of Mtb infection on primary human MDM metabolic profile is also investigated. Thus, this work demonstrates the novel impact of LPS treatment and Mtb infection on primary human macrophage metabolic profile.

3.2 Results

3.2.1 Baseline metabolic profile of human MDM

First, baseline metabolic profile of human MDM was determined. Human MDM were isolated from IBTS buffy coats and prepared for experimentation as described in **Chapter 2**. An optimal seeding density of 200,000 cells/well was determined through optimisation experiments (**Figure 2.2**). 48 hours after plating, cRPMI was replaced with Seahorse media (DMEM supplemented with 2mM glutamine and 10mM glucose), cells were incubated for 30 minutes in a non-CO_2 incubator and interrogation of OCR and ECAR, broadly representative of oxidative phosphorylation rate and glycolytic rate, respectively, was performed using the Seahorse XF Flux Analyzer. This method is described in detail in **Chapter 2 (Section 2.3.1)**. Using this method, baseline OCR (**Figure 3.1A**) and baseline ECAR (**Figure 3.1B**) were established for seven individual donors. Median OCR and ECAR were 109.7 $pmol.min^{-1}$ and 10.6 $mpH.min^{-1}$, respectively. ECAR/OCR ratio (**Figure 3.1C**) was also calculated and a plot of ECAR relative to OCR (**Figure 3.1D**) was generated, in order to establish the relative utilisation of glycolysis and oxidative phosphorylation in human MDM at baseline.

Next, metabolic reserves of human MDM were interrogated. Mitochondrial inhibitors from the Seahorse XF Cell Mito Stress Test Kit were used to metabolically "stress" cells, allowing examination of metabolic potential, as described in detail in **Chapter 2 (Section 2.3.1)**. Briefly, sequential addition of oligomycin (an ATP synthase inhibitor), FCCP (a mitochondrial uncoupler), and combined rotenone/antimycin A (Complex I and Complex III inhibitors, respectively) at pre-designated intervals during extracellular flux analysis was used to determine GR, SRC, Non-Mitochondrial OCR and PL of macrophages (**Figure 3.2**). Three sequential measurements of simultaneous ECAR and OCR were obtained at baseline, following addition of oligomycin, following addition of FCCP, and following addition of rotenone/antimycin A, generating real-time plots of metabolic activity within the cell for each donor (**Figure 3.2A – B**). Analysis of pooled data from seven individual donors was used to calculate characteristic GR, SRC, Non-Mitochondrial OCR and PL for human MDM (**Figure 3.2C – H**). Using this approach, a median SRC and GR of 16.7 $pmol.min^{-1}$ and 3.6 $mpH.min^{-1}$, respectively, were observed.

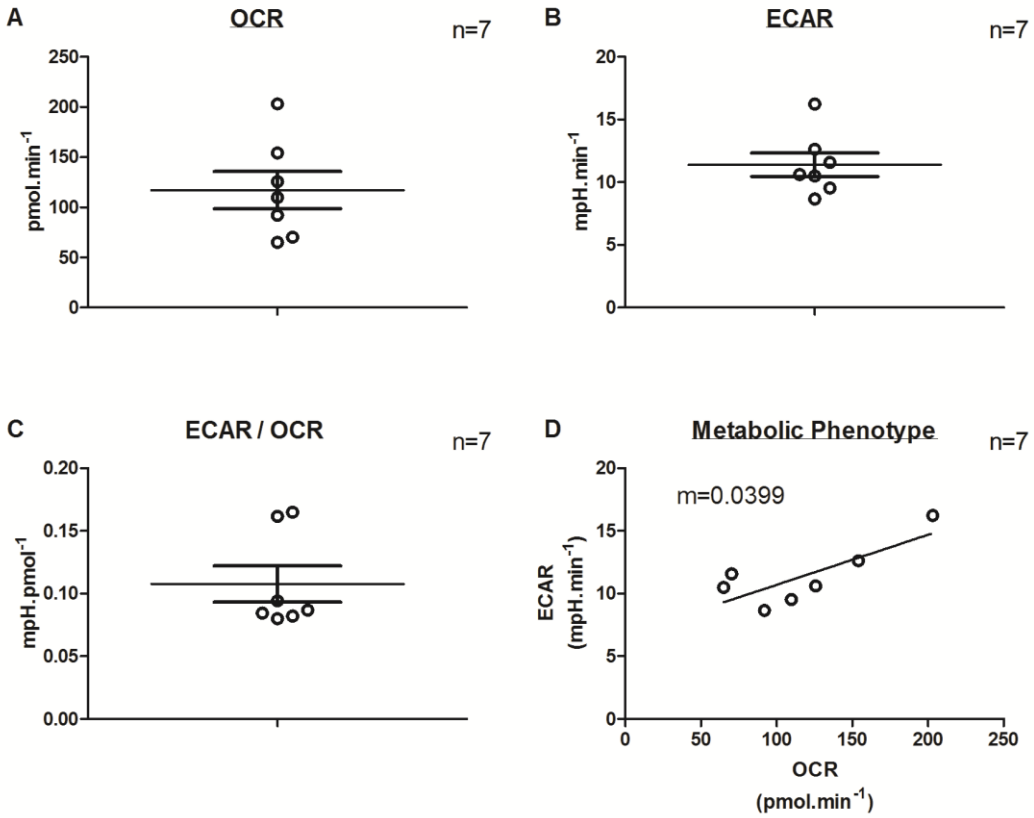

FIGURE 3.1 Baseline metabolic phenotype of human MDM. MDM isolated from IBTS buffy coats were cultured for 5 days, scraped, and plated on Seahorse Biosciences 24-well plates at 200,000 cells/well in cRPMI. On Day 7, extracellular flux analysis was performed and data normalised using CV assay. Panels A – C depict baseline mean ± SEM OCR (A), ECAR (B) and ratio of ECAR/OCR (C) for seven individual donors. Panel D depicts baseline ECAR (y-axis) relative to OCR (x-axis) for seven individual donors, also indicative of the relative utilisation of these two energy pathways.

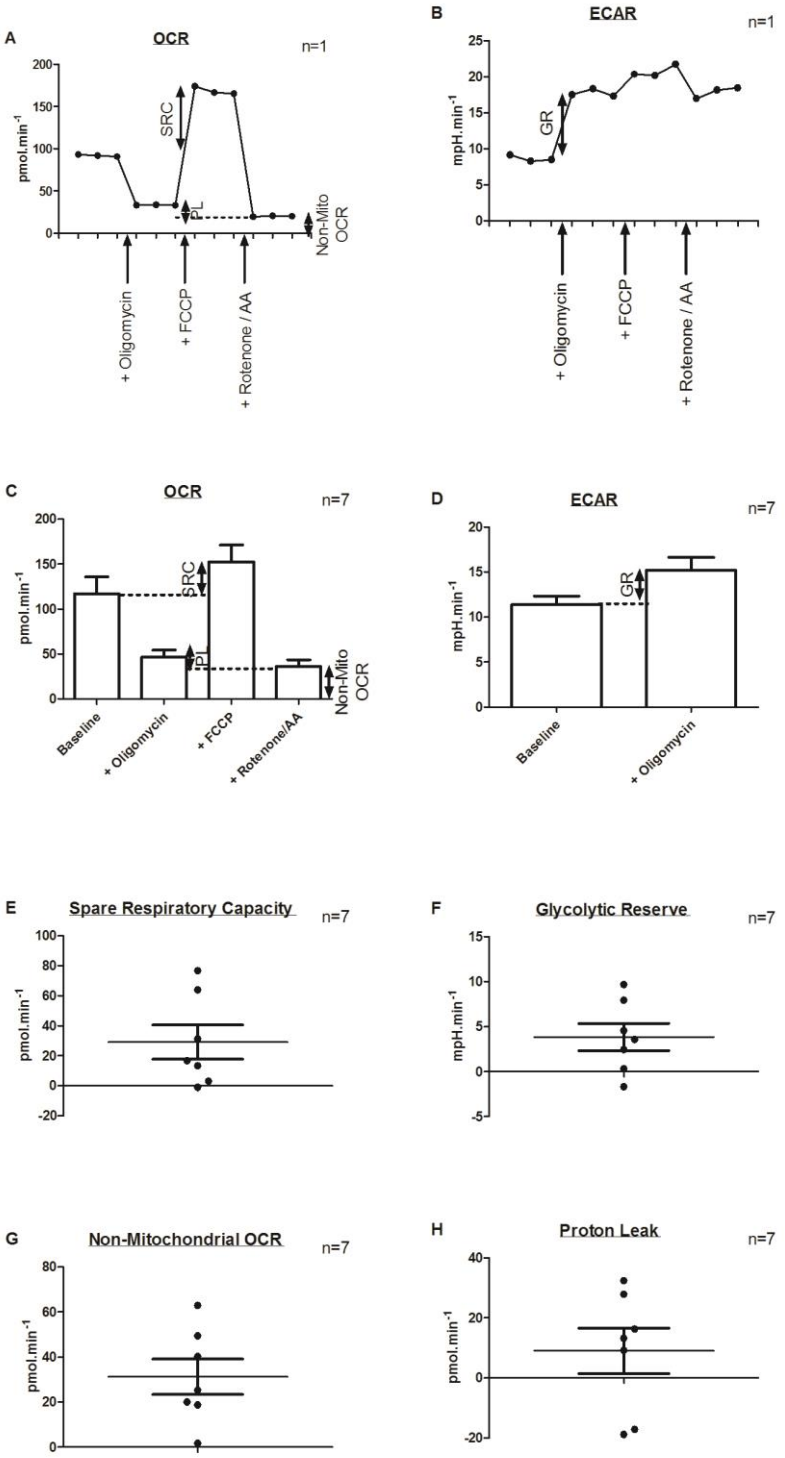

FIGURE 3.2 Baseline metabolic reserves of human MDM. Extracellular flux analysis was performed on human MDM and data normalised using CV assay. Mitochondrial inhibitors were added sequentially to achieve final concentrations of 1µM (oligomycin), 2µM (FCCP) and 0.5µM (rotenone/antimycin A). Panels A and B depict real-time OCR (A) and ECAR (B) for one representative donor. Panels C and D depict normalised mean ± SEM OCR (C) and ECAR (D) for seven individual donors. Panels E – H depict normalised mean ± SEM calculated SRC (E), GR (F), Non-Mitochondrial OCR (G), and PL (H) for seven individual donors.

3.2.2 LPS and IL-4 alter the metabolic profile of human MDM

LPS has been shown to induce glycolytic reprogramming in murine BMDM and murine dendritic cells [174,240]. In order to investigate the impact of LPS on human MDM metabolism, extracellular flux analyses was performed on cells following 24 hours of stimulation with 100ng/mL LPS. Again, MDM were isolated and prepared as described in **Chapter 2 (Section 2.1.2)**. 24 hours after plating on Seahorse Biosciences 24-well plates, MDM were treated with LPS (final concentration 100ng/mL) or left untreated (control). At 24 hours post-treatment, extracellular flux analyses were performed as described in **Chapter 2 (Section 2.3.1)**. LPS treatment did not alter OCR in human MDM (**Figure 3.3A**) but a trend towards increased ECAR was observed (**Figure 3.3B**), and ECAR/OCR ratio was significantly increased (**Figure 3.3C**), confirming an LPS-induced shift towards glycolysis as expected.

Supernatants removed 30 minutes prior to extracellular flux analyses (i.e. 24 hours post-LPS stimulation) and retained. Lactate, the end-product of the glycolytic pathway, is exported from cell via the monocarboxylate transport system, therefore increases in extracellular lactate reflect increased glycolytic activity within the cells. Following LPS treatment, lactate concentration was increased in supernatants (**Figure 3.3D**), supporting the hypothesis of an LPS-induced shift towards glycolysis. Elevated TNF-α concentration confirmed LPS induced activation of human MDM (**Figure 3.3E**) and CV assay results demonstrated no significant differences in cell viability between treated and untreated cells (**Figure 3.3F**). Interrogation of metabolic reserves in the presence of LPS was also performed, as described above. Concurrent with a shift towards glycolysis, LPS treatment reduced GR of human MDM (**Figure 3.4**). Human MDM SRC, Non-Mitochondrial OCR and PL were largely unchanged following LPS stimulation (**Figure 3.4**).

Substantial metabolic differences are observed in M2-polarised macrophages – specifically increased rates of OXPHOS and decreased rates of glycolysis, with cells relying on metabolism of other nutrients (usually fatty acids) to feed the TCA cycle. To investigate this in the human MDM model, cells were treated with IL-4 (final concentration 20ng/mL), a cytokine that induces M2 differentiation in macrophages, using the same protocol as that described for LPS treatment above. IL-4 treatment reduced the ECAR/OCR ratio in human MDM (**Figure 3.5**), suggesting a skewing away from glycolysis and towards mitochondrial oxidative phosphorylation. Further supporting this observation, measured lactate production was reduced in human MDM following IL-4 treatment (**Figure 3.5D**).

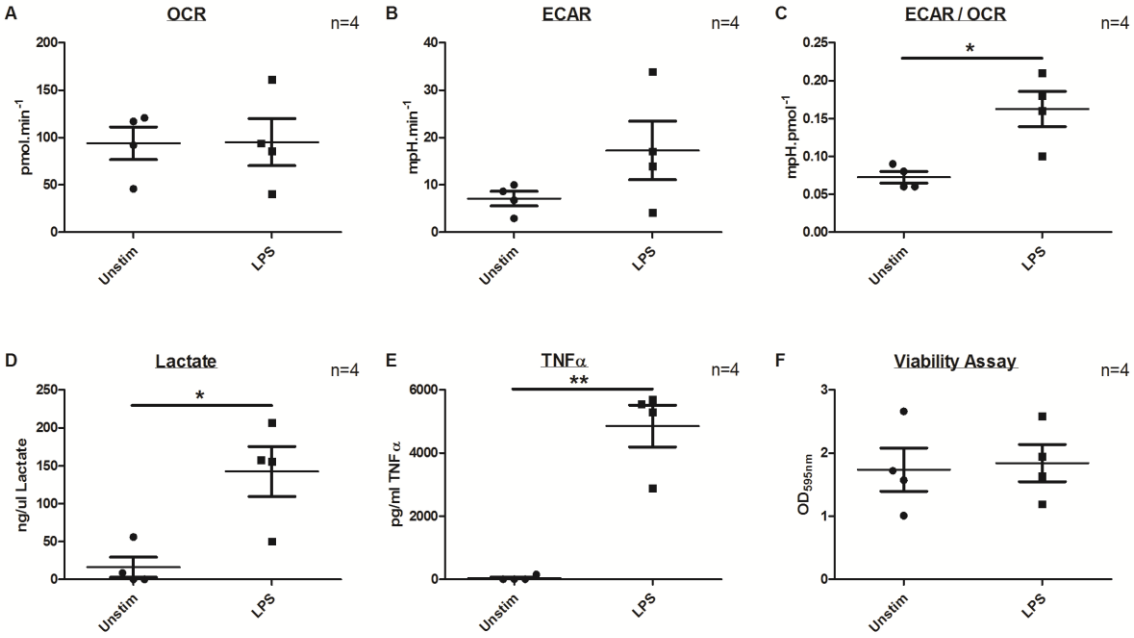

FIGURE 3.3 LPS stimulation induces glycolytic reprogramming in human MDM. Human MDM were plated on Seahorse Biosciences 24-well plates at 200,000 cells/well. 24 hours after plating, cells were treated with LPS (final concentration 100ng/mL) or untreated (control). At 24 hours post-treatment, extracellular flux analysis was performed and data normalised using CV assay. Lactate and TNF-α were measured in retained supernatants. Panels A – C depict mean ± SEM OCR (A), ECAR (B) and calculated ECAR/OCR ratio (C) for four individual donors. Panel D – E depict corresponding mean ± SEM lactate (D) and TNF-α (E) concentration as measured in supernatants for four individual donors. Panel F depicts corresponding absorbance following CV staining, indicative of cell viability, for four individual donors. Statistical analyses were performed using the paired Student's t-test; *$p<0.05$.

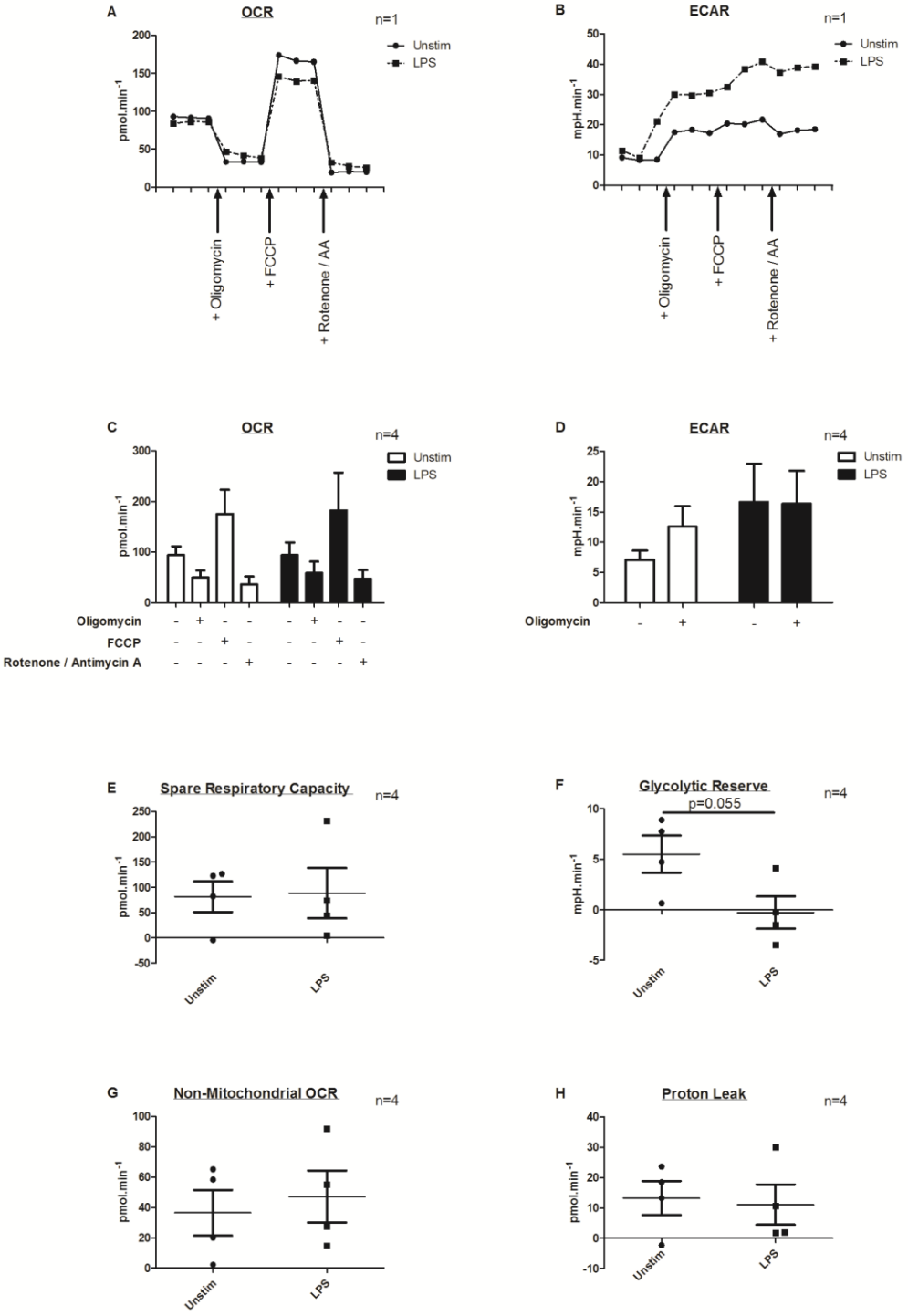

FIGURE 3.4 LPS stimulation reduces Glycolytic Reserve of human MDM. Human MDM were treated with LPS (100ng/mL) or untreated (control). At 24 hours post-treatment, extracellular flux analysis was performed with sequential addition of oligomycin (1µM), FCCP (2µM) and rotenone/antimycin A (0.5µM) and data normalised using CV assay. Lactate and TNF-α were measured in retained supernatants. Panels A and B depict normalised real-time OCR (A) and ECAR (B) for one representative donor. Panels C and D depict normalised mean ± SEM OCR (C) and ECAR (D) for four individual donors. Panels E – H depict normalised mean ± SEM SRC (E), GR (F), Non-Mitochondrial OCR (G) and PL (H) for four individual donors. Statistical analyses were performed using the Student's t-test; statistical significance was set at $p<0.05$.

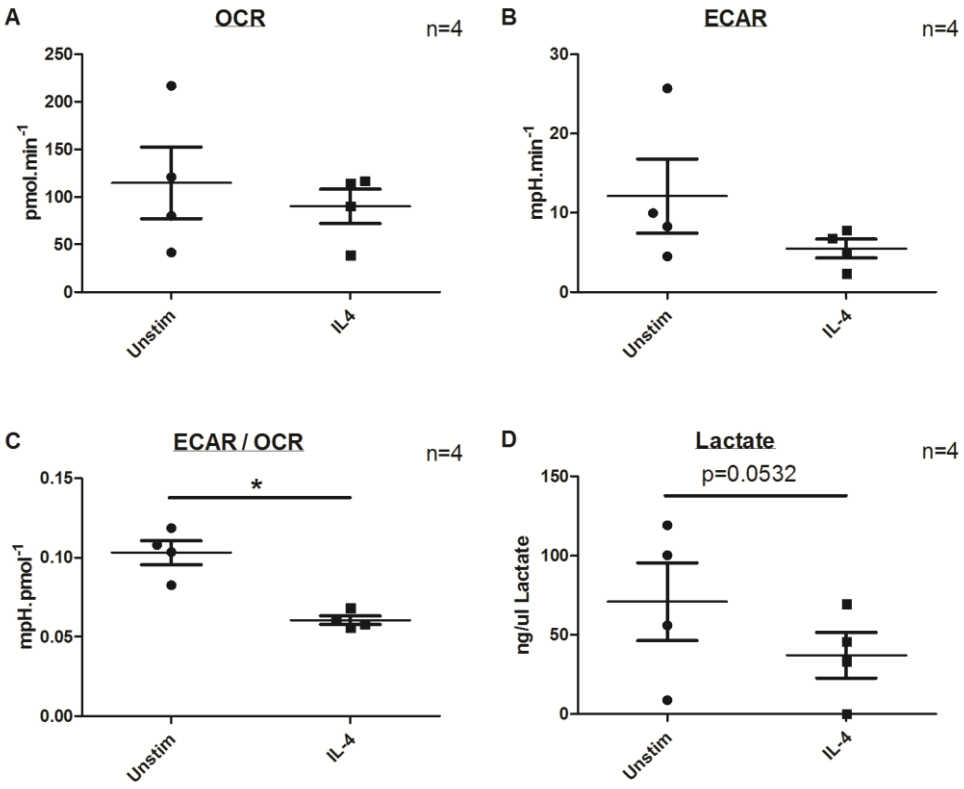

FIGURE 3.5 IL-4 stimulation induces a shift away from glycolysis in human MDM. Human MDM were plated on Seahorse Biosciences 24-well plates at 200,000 cells/well in cRPMI. 24 hours after plating, cells were treated with IL-4 (final concentration 20ng/mL) or untreated (control). At 24 hours post-treatment, extracellular flux analysis was performed and data normalised using CV assay. Lactate was measured in retained supernatants. Panels A – C depict normalised mean ± SEM OCR (A), ECAR (B) and calculated ECAR/OCR ratio (C) for four individual donors. Panel D depicts corresponding lactate concentration as measured in supernatants for four individual donors. Statistical analyses were performed using the paired Student's t-test; *p<0.05.

3.2.3 Mtb infection induces glycolysis in human MDM

Previous reports that LPS induces glycolysis in murine BMDM [174] gave rise to the hypothesis that Mtb infection would have a similar effect. Murine BMDM were isolated and prepared for experimentation as described in **Chapter 2 (Section 2.1.3)**. 24 hours after plating, Mtb infections were performed as previously described, with supernatants removed and centrifuged (γ-irradiation killed iH37Rv and avirulent H37Ra infections) or filtered (virulent H37Rv infections) at 24 hours post-infection. Infection with γ-irradiation killed iH37Rv (**Figure 3.6A**), avirulent H37Ra (**Figure 3.6B**) or virulent H37Rv (**Figure 3.6C**) Mtb strains increased lactate production by murine BMDM, suggesting induction of glycolysis similar to that observed with LPS treatment.

Next, the impact of Mtb infection on human MDM metabolic profile was investigated using extracellular flux analyses. 24 hours after plating on Seahorse Biosciences 24-well plates, MDM were infected with iH37Rv at low MOI or left uninfected (control), as described in **Chapter 2 (Section 2.2.1)**. At 24 hours post-infection, supernatants were removed, extracellular bacilli washed away, and extracellular flux analyses were performed in the presence of supplemented Seahorse media. Mtb infection increased ECAR (**Figure 3.7B**), increased ECAR/OCR ratio (**Figure 3.7C**) and increased extracellular lactate (**Figure 3.7D**) compared to uninfected controls, indicating induction of glycolysis, as predicted. Interestingly, however, OCR was not observed to change (**Figure 3.7A**). Again, increased TNF-α confirmed successful infection (**Figure 3.7E**) and CV assay confirmed similar viability of uninfected and infected cells at the time of interrogation (**Figure 3.7F**). Plotting baseline ECAR relative to OCR for uninfected (**Figure 3.8A**) and iH37Rv-infected (**Figure 3.8B**) human MDM also supported a shift towards glycolytic metabolism following infection. Glucose uptake has also been reported to increase following glycolytic reprogramming of macrophages. Glucose concentration was also measured in supernatants harvested 24 hours post-infection, and was significantly reduced following infection with iH37Rv (**Figure 3.9**), further supporting the hypothesis of an Mtb-induced glycolytic shift.

Interrogation with metabolic inhibitors was also performed during extracellular flux analyses of iH37Rv-infected and uninfected MDM (**Figure 3.10**). Similar to LPS-treated cells, GR was significantly reduced following infection (**Figure 3.10F**). A non-significant trend towards increased PL (**Figure 3.10H**) was also observed in infected cells, possibly indicative of evolving mitochondrial dysfunction or of increased sequestration of oxygen for generation of mitochondrial ROS by Complex I and III of the ETC.

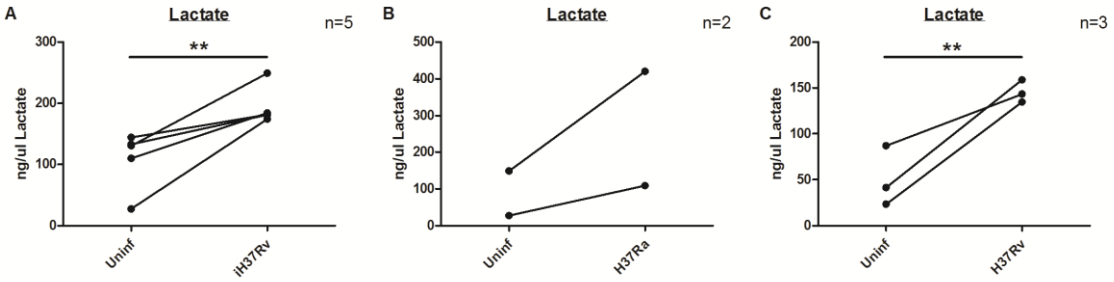

FIGURE 3.6 Mtb infection induces glycolysis in murine BMDM. BMDM were isolated by flushing hind-leg femur and tibia of CS57BL/6 mice and cultured in DMEM supplemented with 10% FBS and 15% MCSF for 5 days. On Day 5, cells were scraped and plated on tissue culture-treated 12-well plates and on labtek slides (for determination of MOI, described in Methods). On Day 6, MCSF supplementation was discontinued, cells were infected with Mtb at low MOI or left uninfected (control), and all cells were washed at 3 hours post-infection to remove extracellular bacilli. At 24 hours post-infection, supernatants were removed and extracellular bacilli and cell debris removed by centrifugation (killed and avirulent strains) or filtration (virulent strains). Lactate concentration in supernatants was quantified using colorimetric assay (Sigma). Panels A – C depict secreted lactate concentration from BMDM following infection with γ-irradiation killed iH37Rv (A), live avirulent H37Ra (B) and live virulent H37Rv (C). Data depict results of four (A), two (B) and three (C) individual experiments. Statistical analyses were performed using the unpaired Student's t-test; **$p<0.01$.

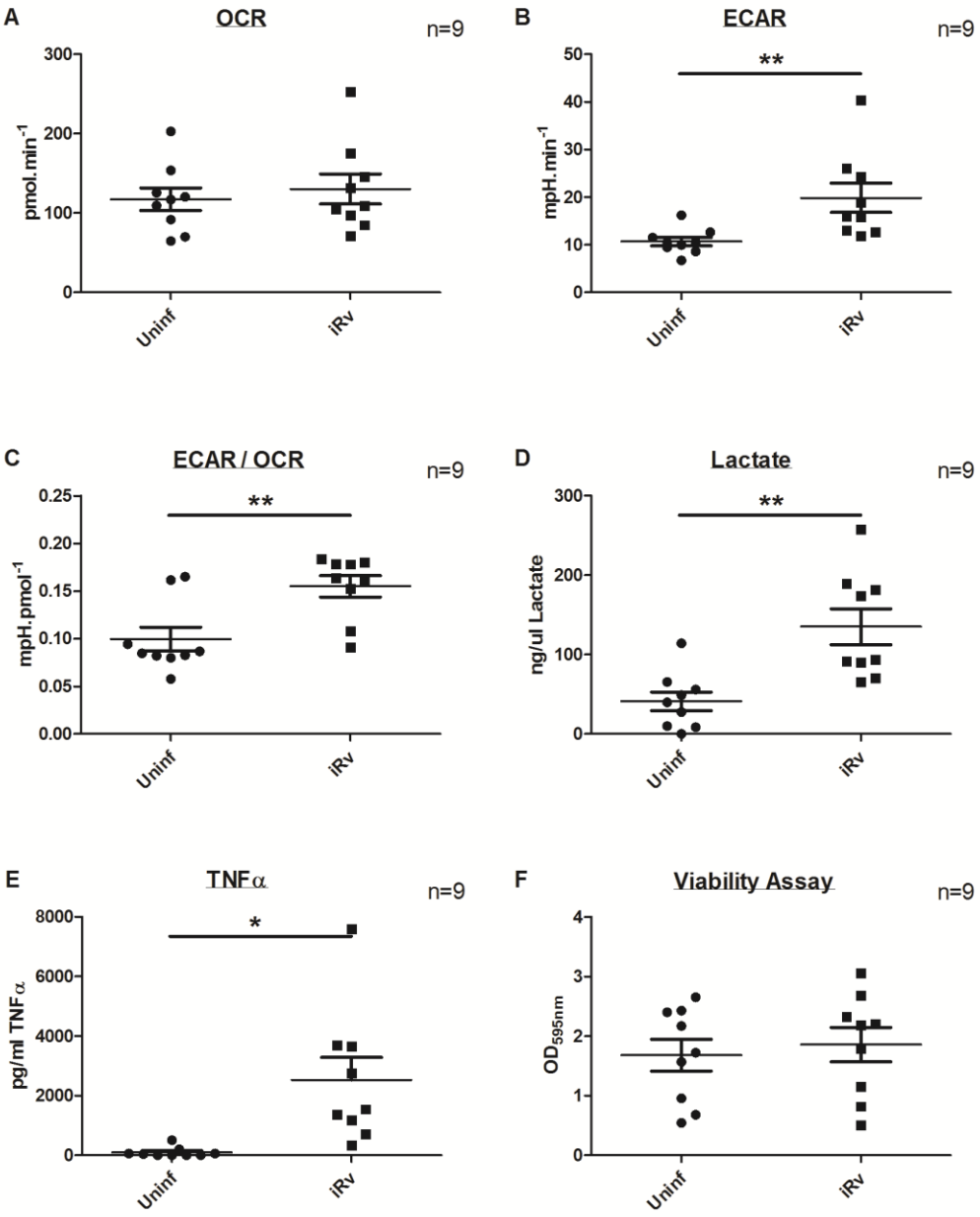

FIGURE 3.7 iMtb infection induces glycolysis in human MDM. MDM were plated on Seahorse Biosciences 24-well plates at 200,000 cells/well. On Day 6, cells were infected with iH37Rv at low MOI or left uninfected (control). At 24 hours post-infection, supernatants were removed and retained for lactate and TNF-α quantification, and extracellular flux analyses were performed with data normalised using CV assay. Panels A – C depict normalised mean ± SEM OCR (A), ECAR (B) and calculated ECAR/OCR ratio (C) for nine individual donors. Panels D – E depict corresponding mean ± SEM lactate (D) and TNF-α (E) concentration as measured in supernatants for nine individual donors. Panel F depicts corresponding absorbance following CV staining, indicative of cell viability, for nine individual donors. Statistical analyses were performed using the paired Student's t-test; *p<0.05, **p<0.01.

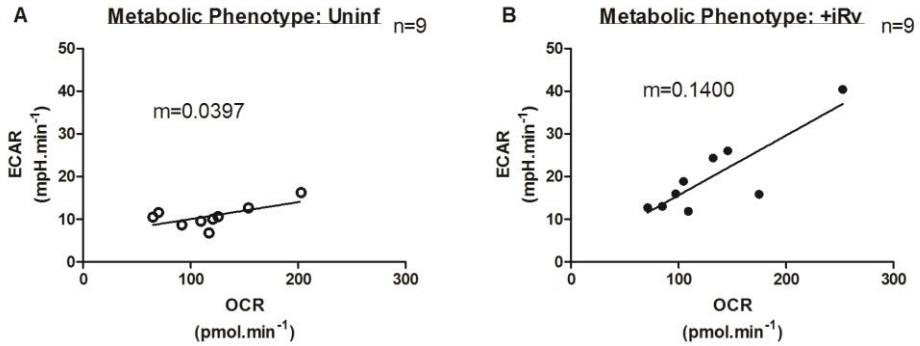

FIGURE 3.8 iMtb infection skews human MDM towards a more glycolytic phenotype. MDM were plated on Seahorse Biosciences 24-well plates at 200,000 cells/well. On Day 6, cells were infected with iH37Rv at low MOI or left uninfected (control). At 24 hours post-infection, extracellular flux analyses were performed using CV assay to normalise results. Panels depict ECAR (y-axis; representative of glycolytic activity) relative to OCR (x-axis; representative of mitochondrial respiration) in uninfected (A) and infected (B) MDM for nine individual donors.

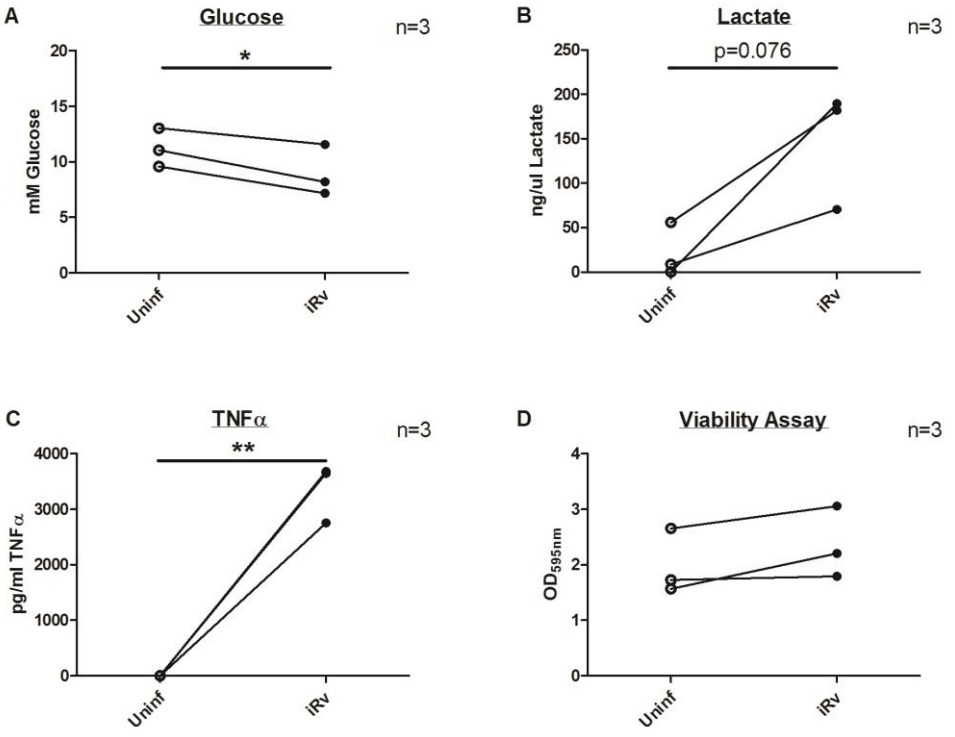

FIGURE 3.9 iMtb infection induces increased glucose utilisation by human MDM. MDM were plated on Seahorse Biosciences 24-well plates at 200,000 cells/well. On Day 6, cells were infected with iH37Rv at low MOI or left uninfected (control). At 24 hours post-infection, supernatants were removed and glucose, lactate and TNF-α concentration quantified. CV assay was performed to determine cell viability. Panels A – C depict measured supernatant glucose (A), lactate (B) and TNF-α (C) concentration for three individual donors. Panel D depicts corresponding absorbance following CV staining for three individual donors. Statistical analyses were performed using the paired Student's t-test; *p<0.05, **p<0.01.

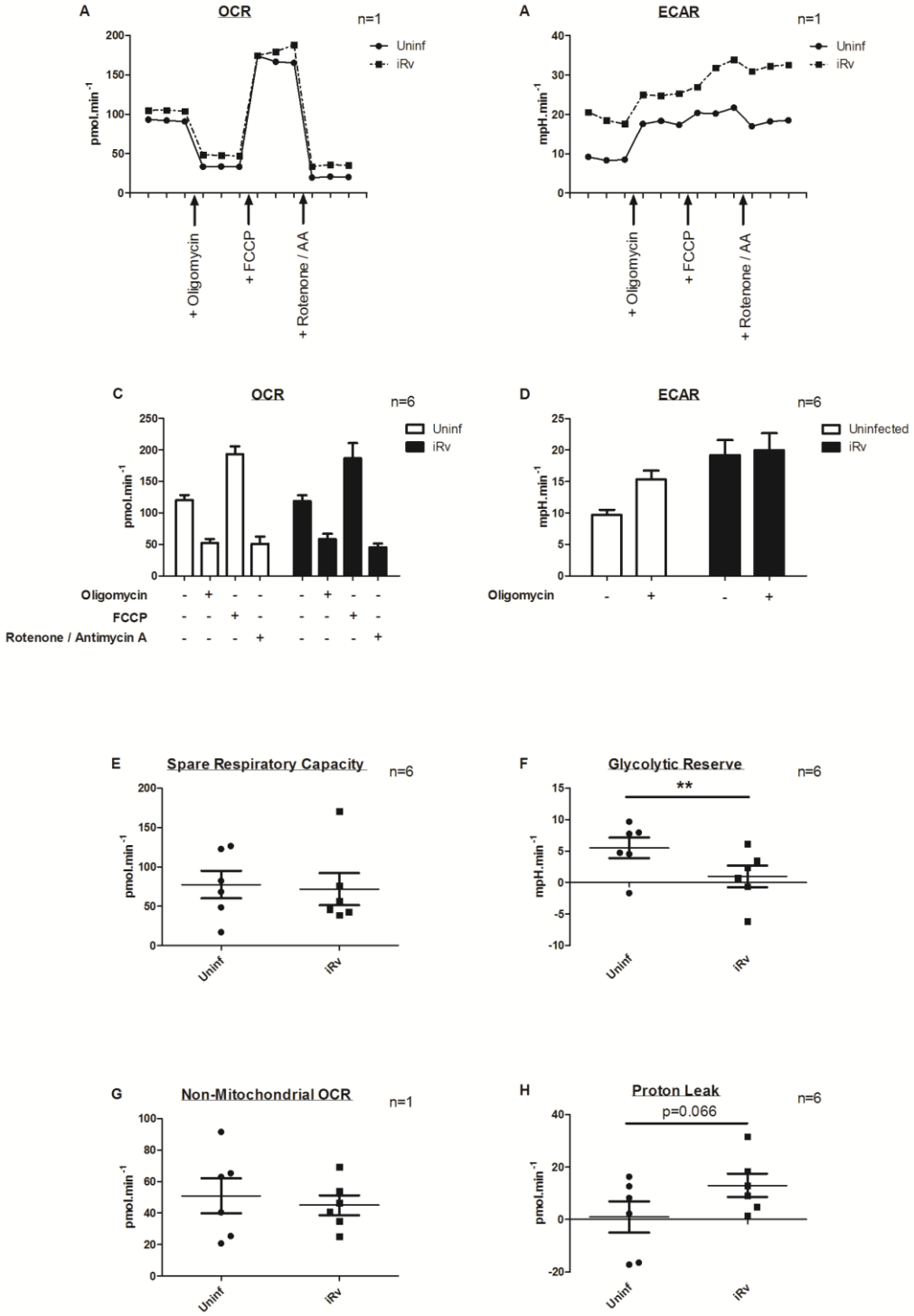

FIGURE 3.10 iMtb infection reduces the glycolytic reserve of human MDM. Human MDM were infected with iH37Rv at low MOI or left uninfected (control). At 24 hours post-infection, extracellular flux analysis was performed with sequential addition of oligomycin (1µM), FCCP (2µM) and rotenone/antimycin A (0.5µM) and data normalised using CV assay. Panels A and B depict normalised real-time OCR (A) and ECAR (B) for one representative donor. Panels C and D depict normalised mean ± SEM OCR (C) and ECAR (D) for six individual donors. Panels E – H depict normalised mean ± SEM SRC (E), GR (F), Non-Mitochondrial OCR (G) and PL (H) for six individual donors. Statistical analyses were performed using the Student's t-test; **p<0.01.

Having demonstrated glycolytic reprogramming of human MDM following infection with iH37Rv, the temporal evolution of these metabolic changes following infection were next investigated. Human MDM were isolated, prepared and infected as before. However, infections were performed in two stages, the first 24 hours prior to interrogation (i.e. 24 hours after plating on Seahorse Biosciences plates) and the second 6 hours prior to interrogation (i.e. 42 hours after plating on Seahorse Biosciences plates). Uninfected control wells were designated for both the 24 hour and 6 hour timepoints. Again, supernatants removed from each well prior to extracellular flux analysis were retained to allow quantification of extracellular lactate. Interestingly, extracellular flux analyses suggested that while increased OCR and ECAR are simultaneously observed at 6 hours post-infection, elevations in OCR begin to dwindle at 24 hours post-infection while ECAR continues to rise (**Figure 3.11A – B**). Consequently, substantial increase in ECAR/OCR ratio was not evident until 24 hours post-infection (**Figure 3.11C**). Increases in lactate concentration were also not evident until 24 hours post-infection (**Figure 3.11D**), possibly reflecting the lower sensitivity of this assay as the 24 hour measurement reflects cumulative lactate production over the previous 24 hours rather than real-time glycolytic rate measured using extracellular flux analysis.

Next the dependence of the observed induction of glycolysis in human MDM on the multiplicity of infection (MOI) used was investigated. It was hypothesised that increased MOI would provide increased PAMPs for stimulation of TLRs and thereby result in a more dramatic induction of glycolysis. Using a similar protocol to that described above, extracellular flux analyses were used to compare human MDM infected with iH37Rv at low MOI, infected with iH37Rv at high MOI and uninfected. Again, iH37Rv infection was observed to increase ECAR, ECAR/OCR ratio and lactate production at both low and high MOI (**Figure 3.12B – D**), confirming previous observations of glycolytic reprogramming in response to infection. However, no significant differences in extracellular flux readouts or in lactate production were detected between low MOI and high MOI-infected cells (**Figure 3.12A – D**). Increased TNF-α concentration in high MOI-infected wells compared to low MOI-infected wells confirmed that MOIs used were significantly different (**Figure 3.12E**), and CV assay demonstrated similar cell viability across all three conditions (**Figure 3.12F**). These observations suggested that iH37Rv-induced glycolytic reprogramming of human MDM is not MOI-dependent. However, subsequent measurement of glucose in retained supernatants suggested MOI-dependent increase in glucose utilisation (**Figure 3.13**). It is possible therefore that the low MOI used induces maximal rates of glycolysis within our human MDM model, rendering further increases negligible. This hypothesis is supported by observations of abrogated GR in human MDM following iH37Rv infection (**Figure 3.10**).

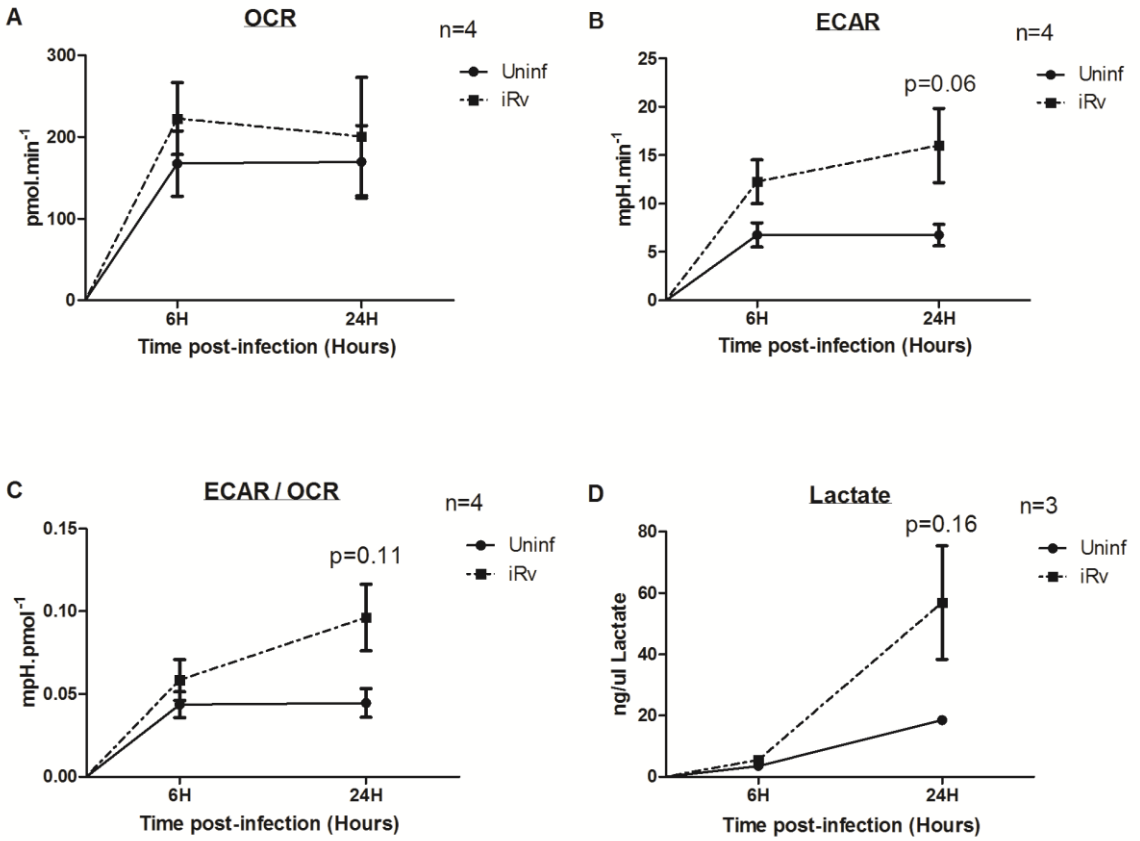

FIGURE 3.11 Glycolytic reprogramming in human MDM is evident 24 hours post infection. Human MDM were infected in duplicate with iH37Rv at low MOI or left uninfected (control) (24 hour condition), and cells washed at 3 hours post-infection to remove extracellular bacilli. 18 hours later, further duplicate wells were infected with iH37Rv at low MOI or left uninfected (control) (6 hour condition), and washed at 3 hours post-infection to remove extracellular bacilli (24 hour condition infected and control wells were not washed at this time). 6 hours later, supernatants were removed and retained for lactate quantification, and extracellular flux analyses were performed with CV assay used to normalise data. Panels A – C depict normalised mean ± SEM OCR (A), ECAR (B) and calculated ECAR/OCR ratio (C) at 6 hours and 24 hours post-infection for four individual donors. Panel D depicts corresponding mean ± SEM lactate concentration as measured in supernatants for four individual donors. Statistical analyses were performed using the paired Student's t-test; statistical significance was set at $p<0.05$.

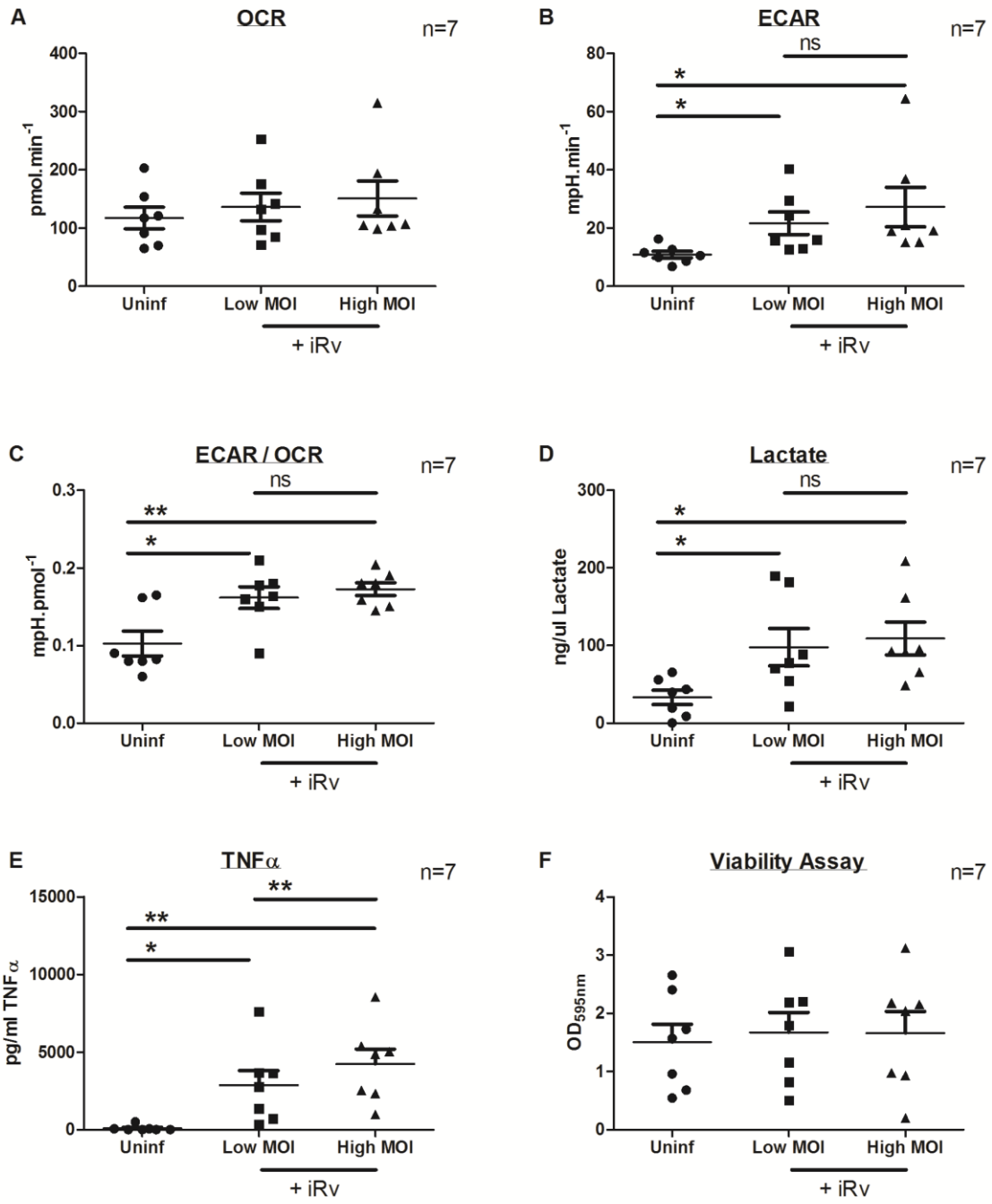

FIGURE 3.12 iMtb-induced glycolytic shift in human MDM is not significantly MOI-dependent. Human MDM were infected with iH37Rv at low MOI, iH37Rv at high MOI or left uninfected (control). At 24 hours post-infection, supernatants were removed and retained, and extracellular flux analysis was performed with data normalised using CV assay. Lactate and TNF-α were measured in retained supernatants. Panels A – C depict normalised mean ± SEM OCR (A), ECAR (B) and calculated ECAR/OCR ratio (C) for seven individual donors. Panel D – E depict corresponding mean ± SEM lactate (D) and TNF-α (E) concentration as measured in supernatants for seven individual donors. Panel F depicts corresponding absorbance following CV staining for seven individual donors. Statistical analyses were performed using the paired Student's t-test; *p<0.05, **p<0.01.

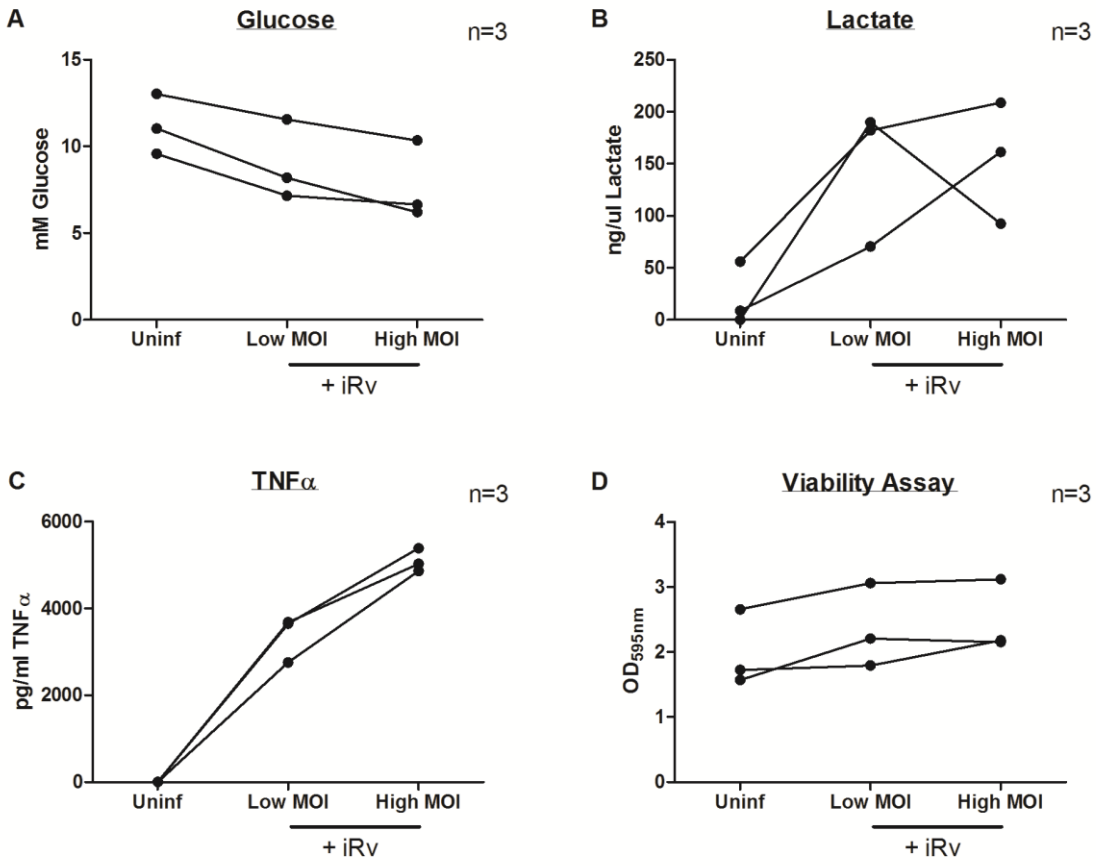

FIGURE 3.13 iMtb-induced increased glucose consumption by human MDM is MOI-dependent. Human MDM were infected with iH37Rv at low MOI, iH37Rv at high MOI or left uninfected (control). At 24 hours post-infection, supernatants glucose, lactate and TNF-α were quantified. Cell viability was determined using CV assay. Panels A – C depict measured supernatant glucose (A), lactate (B) and TNF-α (C) concentration for three individual donors. Panel D depicts corresponding absorbance following CV staining for three individual donors. Statistical analyses were performed using the paired Student's t-test; statistical significance was set at $p<0.05$.

As the primary role of central energy metabolism within the cell is the generation of ATP, correlation between the observed alterations in human MDM glucose metabolism and ATP synthesis within the cell was next investigated. Cells were isolated, prepared and infected as previously described. At 24 hours post-infection, cells were lysed and intracellular ATP quantified using a bioluminescence assay. This method is described in detail in **Chapter 2 (Section 2.3.4)**. In this way, an increase in intracellular ATP levels following infection with iH37Rv at low MOI was demonstrated (**Figure 3.14A**), possibly reflecting increased energy requirements of these activated cells. Again, TNF-α measurement confirmed successful infection (**Figure 3.14B**). BCA assay was used to confirm that variation in cell number was not responsible for observed differences between conditions (**Figure 3.14C**).

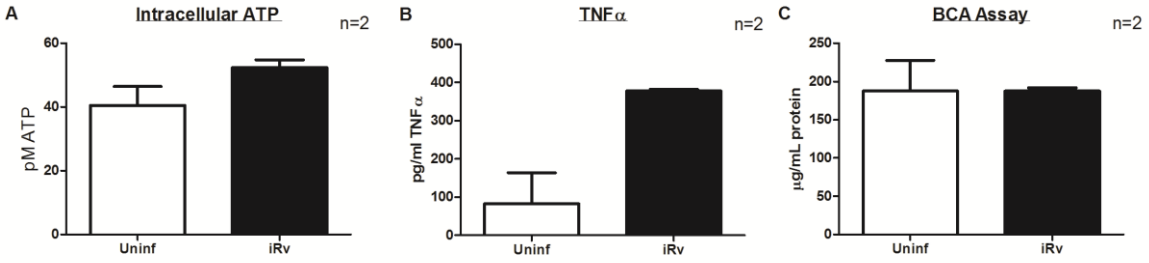

FIGURE 3.14 iMtb infection is associated with increased intracellular ATP in human MDM. MDM were infected with iH37Rv at low MOI, or left uninfected (control). At 24 hours post-infection, cells were lysed and intracellular ATP concentration measured by ATP bioluminescence assay. Panel A depicts measured intracellular ATP concentration for two individual donors. Panel B depicts corresponding TNF-α concentration detected in supernatants by ELISA for two individual donors. Panel C depicts corresponding protein concentration measured in lysates by BCA assay for two individual donors.

Thus far, all human MDM infections had been performed using γ-irradiation killed iH37Rv, as the Seahorse XF Flux Analyzer is not housed in a Biosafety Level 2 or 3 facility (required for live Mtb experiments). In addition, both extracellular flux analysis and lactate quantification rely on interrogating changes in extracellular environment in order to infer information regarding intracellular metabolism. Infection with live Mtb would introduce into the system a live organism with its own independent metabolic activity, rendering the data difficult to interpret and limiting the scope of investigations.

However, live infection may not affect human MDM metabolism in the same way as iH37Rv. To investigate the impact of live infection, human MDM were infected with live avirulent Mtb strain H37Ra as described in **Chapter 2 (Section 2.2.1)**, and both lactate and glucose were measured in supernatants removed at 24 hours post-infection. As seen with iH37Rv, H37Ra infection significantly increased lactate concentration (**Figure 3.15A**) and a non-significant trend towards reduced glucose consumption was also detected (**Figure 3.15B**), demonstrating glycolytic reprogramming of human MDM following live infection. The effect of live Mtb is similar to that seen in murine BMDMs infected with H37Ra or H37Rv (**Figure 3.6**).

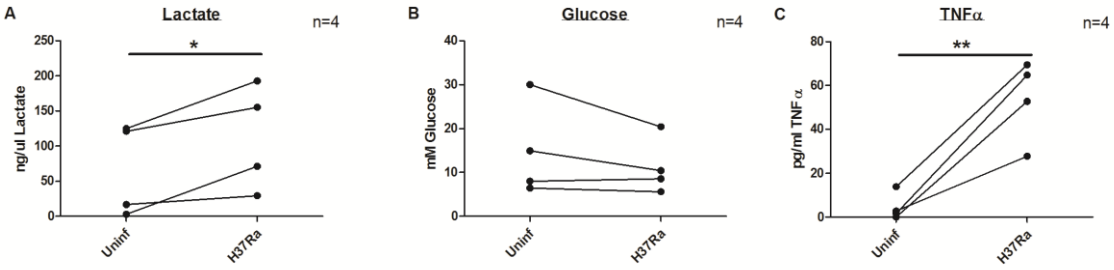

FIGURE 3.15 Live Mtb infection induces glycolysis in human MDM. MDM were infected with live H37Ra at low MOI or left uninfected (control). At 24 hours post-infection, supernatants were removed, extracellular bacilli and cell debris removed by centrifugation, and lactate, glucose and TNF-α concentration quantified using. Panels A – C depict measured lactate (A), glucose (B) and TNF-α (C) concentration for four individual donors. Statistical analyses were performed using the paired Student's t-test; *p<0.05, **p<0.01.

Glycolytic reprogramming in macrophages is associated with upregulation of glycolytic genes. In order to investigate this in the setting of Mtb infection, human MDM were isolated and prepared as previously described. Side-by-side infections with iH37Rv and H37Ra were performed as described in **Chapter 2 (Section 2.2.1)**. At 24 hours post infection, cells were lysed, RNA extracted and used to generate cDNA, and real-time PCR was performed in triplicate using Taqman probes, with normalisation of data to *18S* rRNA. This method is described in detail in **Chapter 2 (Section 2.3.5)**. Infection with either iH37Rv or H37Ra induced expression of several glycolytic genes including *SCL2A1* (coding for the glucose transporter GLUT1), *LDHA* (coding for lactate dehydrogenase, the enzyme responsible for conversion of pyruvate to lactate, deviating it away from entering the mitochondrion to feed the TCA cycle), *PDK3* (pyruvate dehydrogenase kinase 3, an enzyme that inhibits the conversion of pyruvate to acetyl CoA, thus preventing it from feeding into the TCA cycle) and *HK1* (hexokinase 1, the enzyme responsible for converting glucose to glucose-6-phosphate as the first irreversible step of both the glycolytic and the pentose phosphate pathways) (**Figure 3.16**). A trend towards Mtb-induced induction of glycolytic enzyme transcription was observed, though this failed to reach statistical significance.

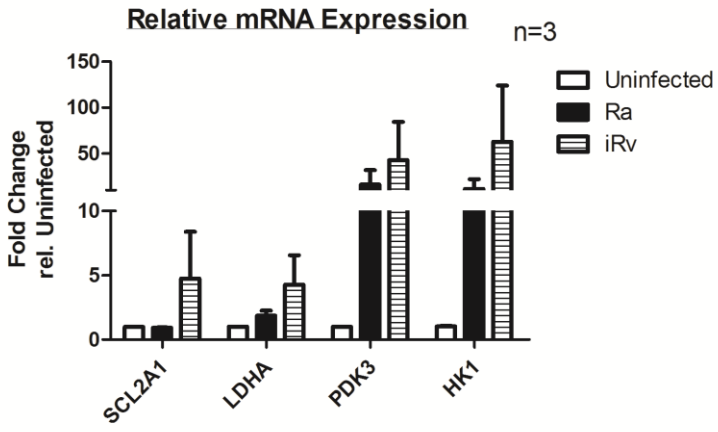

FIGURE 3.16 Mtb infection induces upregulation of glycolytic gene expression in human MDM. MDM isolated from IBTS buffy coats were cultured for 6 days on untreated 12-well plates and on labtek slides (for determination of MOI, described in Methods). On Day 6, cells were infected with live H37Ra at low MOI, γ-irradiation killed iH37Rv at low MOI, or left uninfected (control), and all cells were washed at 3 hours post-infection to remove extracellular bacilli. At 24 hours post-infection, cells were lysed in RLT lysis buffer, RNA extracted and cDNA generated. Real-time PCR was performed in triplicate using Taqman primers and data were normalised to 18S rRNA. Data depicts mRNA expression fold-change relative to uninfected cells for indicated genes, as calculated by the $2^{-\Delta\Delta Ct}$ method. Statistical analyses were performed using the paired Student's t-test; statistical significance was set at $p<0.05$.

3.2.4 Human AM are similar to IL-4-treated MDM at baseline, but they retain substantial metabolic reserves

In order to investigate whether Mtb infection would also induce glycolytic reprogramming in alveolar macrophages, human AM were isolated from BAL fluid obtained with consent from patients attending for bronchoscopy, as described in **Chapter 2 (Section 2.1.1)**. On the day of isolation, AM were plated directly onto Seahorse Bioscience 24-well plates at 100,000 cells per well, established as the optimal density for interrogation via preliminary optimisation experiments (**Figure 2.4**). Cells were washed at 24 hours to remove non-adherent cells and extracellular flux analysis performed 48 hours after plating. In this way, baseline OCR (**Figure 3.17A**) and ECAR (**Figure 3.17B**) were measured for four individual donors. Median OCR and ECAR were 135.4 $pmol.min^{-1}$ and 8.645 $mpH.min^{-1}$, respectively, suggesting higher baseline metabolic activity compared to that observed in our human MDM model (**Figure 3.1**). This data was used to calculate baseline ECAR/OCR ratio (**Figure 3.17C**) and to generate a plot of ECAR relative to OCR (**Figure 3.17D**), in order to establish the relative utilisation of glycolysis and oxidative phosphorylation in human AM at baseline.

Baseline AM metabolic reserves were investigated by sequential addition of mitochondrial inhibitors, as previously described, following optimisation of dosing via preliminary experiments (**Figure 2.6**). Real-time plots of OCR and ECAR were generated for individual donors (**Figure 3.18A – B**) and pooled data from four individual donors was used calculate characteristic GR, SRC, non-Mitochondrial OCR and PL (**Figure 3.18C – H**). Median SRC and GR of 147.2 $pmol.min^{-1}$ and 7.725 $mpH.min^{-1}$, respectively, were calculated in this way, again suggesting higher metabolic reserves compared to our human MDM model (**Figure 3.2**).

Human AM are suggested, amid controversy, to behave as M2-polarised macrophages. To investigate the metabolic phenotype of these cells, extracellular flux analyses was performed on human AM alongside both untreated human MDM and IL-4-treated human MDM. 24 hours after plating on Seahorse Biosciences 24-well plates, MDM were treated with IL-4 (final concentration 20ng/mL) or left untreated (control). Human AM were isolated and plated directly onto Seahorse Biosciences 24-well plates, alongside plated MDMs, and washed 24 hours after plating to remove non-adherent cells as previously described. 48 hours after plating of both human MDM and human AM, extracellular flux analyses were performed. Human AM demonstrated higher baseline OCR and ECAR than either untreated MDM or IL-4-treated MDM (**Figure 3.19A – B**), suggesting these cells are more metabolically active. However, baseline ECAR/OCR ratio in human AM was significantly lower than that of untreated MDM, and was equitable to that of IL-4-treated MDM

(**Figure 3.19C**), suggesting that similar to M2-polarised macrophages, human AM are metabolically skewed away from glycolysis and towards OXPHOS at baseline.

Next, metabolic reserves of human AM were compared to those of untreated MDM and IL-4-treated MDM using mitochondrial inhibitors, as described above. Both SRC (**Figure 3.20E**) and GR (**Figure 3.20F**) were substantially higher in human AM compared to IL-4-treated MDM, though this did not achieve statistical significance.

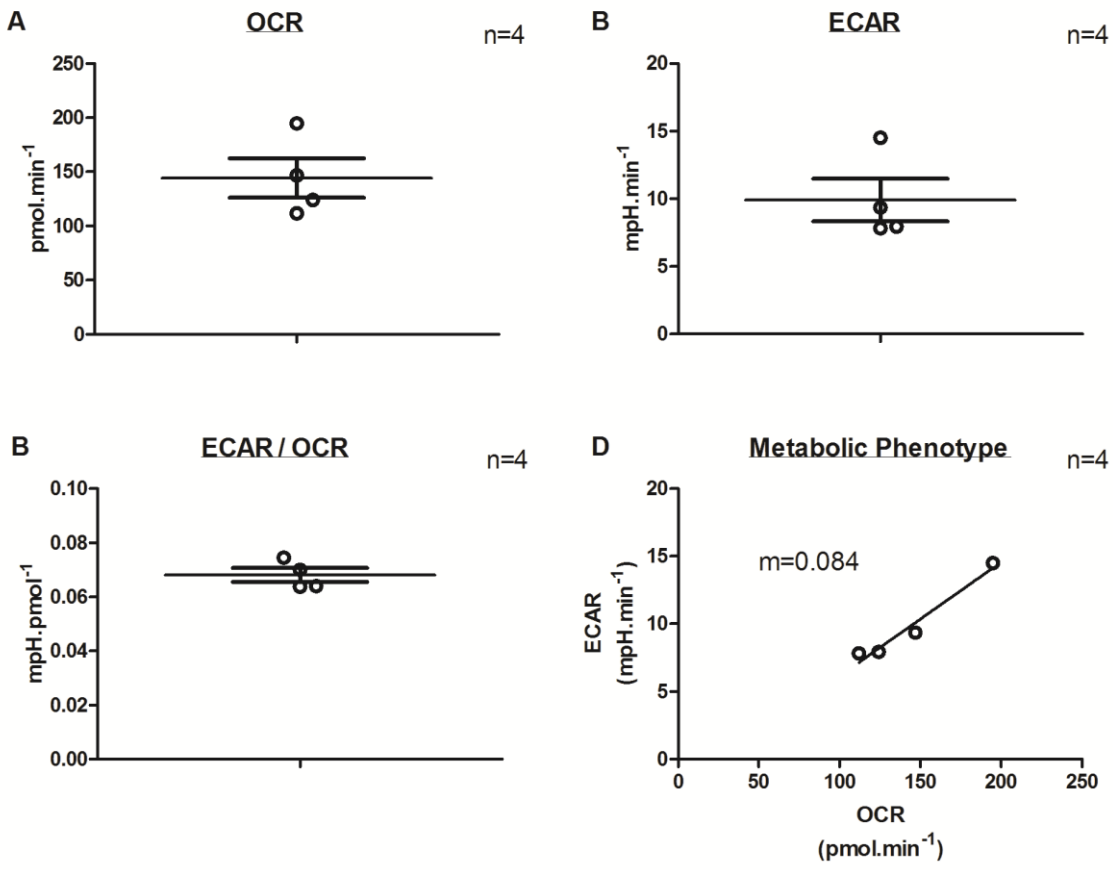

FIGURE 3.17 Baseline metabolic phenotype of human AM. Human AM were plated on Seahorse Biosciences 24-well plates at 100,000 cells/well in cRPMI supplemented with cefotaxime (50µg/mL) and fungizone (50U/mL). On Day 1, non-adherent cells were removed by washing. On Day 2, extracellular flux analyses were performed with CV assay used to normalise data. Panels A – C depict baseline mean ± SEM OCR (A), ECAR (B) and ratio of ECAR/OCR (C) for four individual donors. Panel D depicts baseline ECAR (y-axis) relative to OCR (x-axis) for four individual donors, also indicative of the relative utilisation of these two energy pathways.

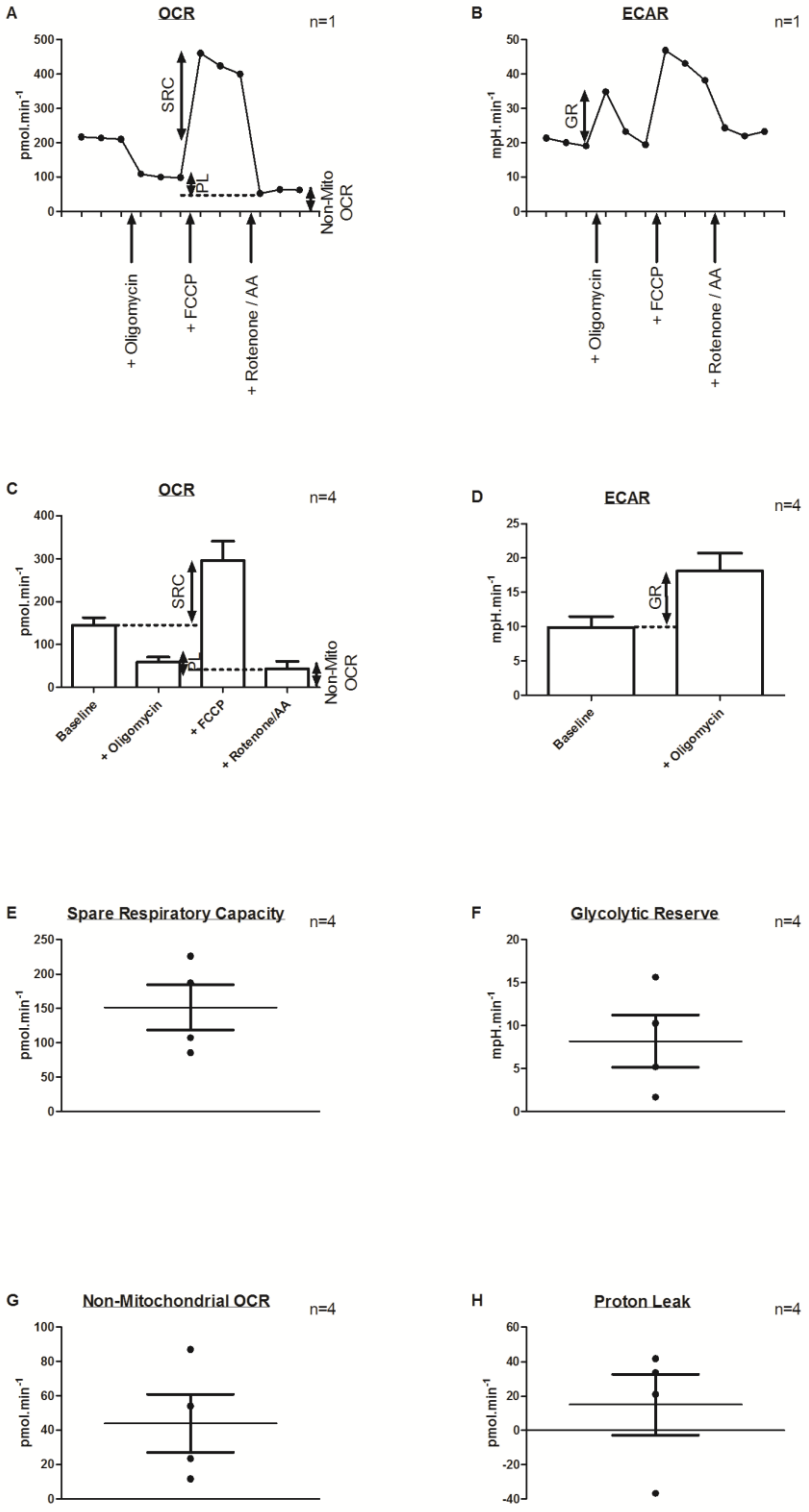

FIGURE 3.18 Baseline metabolic reserves of human AM. Extracellular flux analysis was performed on human AM and data normalised using CV assay. Mitochondrial inhibitors were added sequentially to achieve final concentrations of 1µM (oligomycin), 2µM (FCCP) and 0.5µM (rotenone/antimycin A). Panels A and B depict real-time OCR (A) and ECAR (B) for one representative donor. Panels C and D depict normalised mean ± SEM OCR (C) and ECAR (D) for four individual donors. Panels E – H depict normalised mean ± SEM calculated SRC (E), GR (F), Non-Mitochondrial OCR (G), and PL (H) for four individual donors.

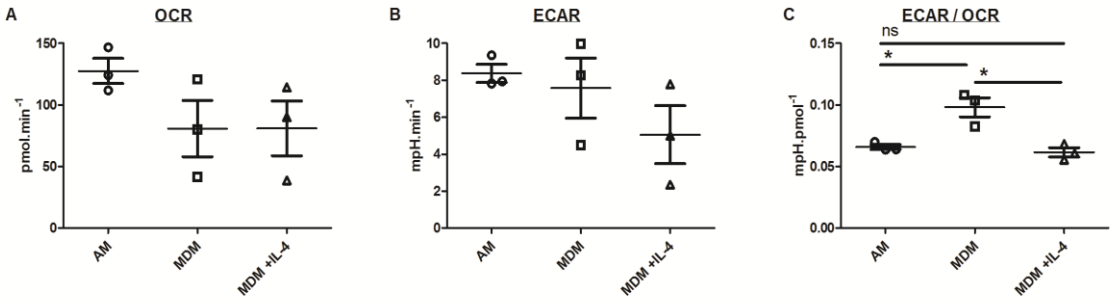

FIGURE 3.19 At baseline, human AM are metabolically skewed towards mitochondrial respiration, similar to IL-4 treated MDM. MDM were cultured for 5 days, scraped, and plated at 200,000 cells/well on Seahorse Biosciences 24-well plates. 24 hours after plating, MDM were treated with IL-4 (final concentration 20ng/mL) or left untreated. Human AM isolated from bronchoalveolar lavage fluid (BALF), plated at 100,000 cells/well on Seahorse Biosciences 24-well plates in cRPMI supplemented with cefotaxime (50µg/mL) and fungizone (50U/mL), and non-adherent cells removed by washing. 48 hours after plating of AM and MDM, extracellular flux analyses were performed with CV assay used to normalise results. Panels A – C depict baseline OCR (A), ECAR (B) and ECAR/OCR ratio (C) for three individual AM donors and three individual MDM donors. Statistical analyses were performed using the unpaired Student's t-test; *$p<0.05$.

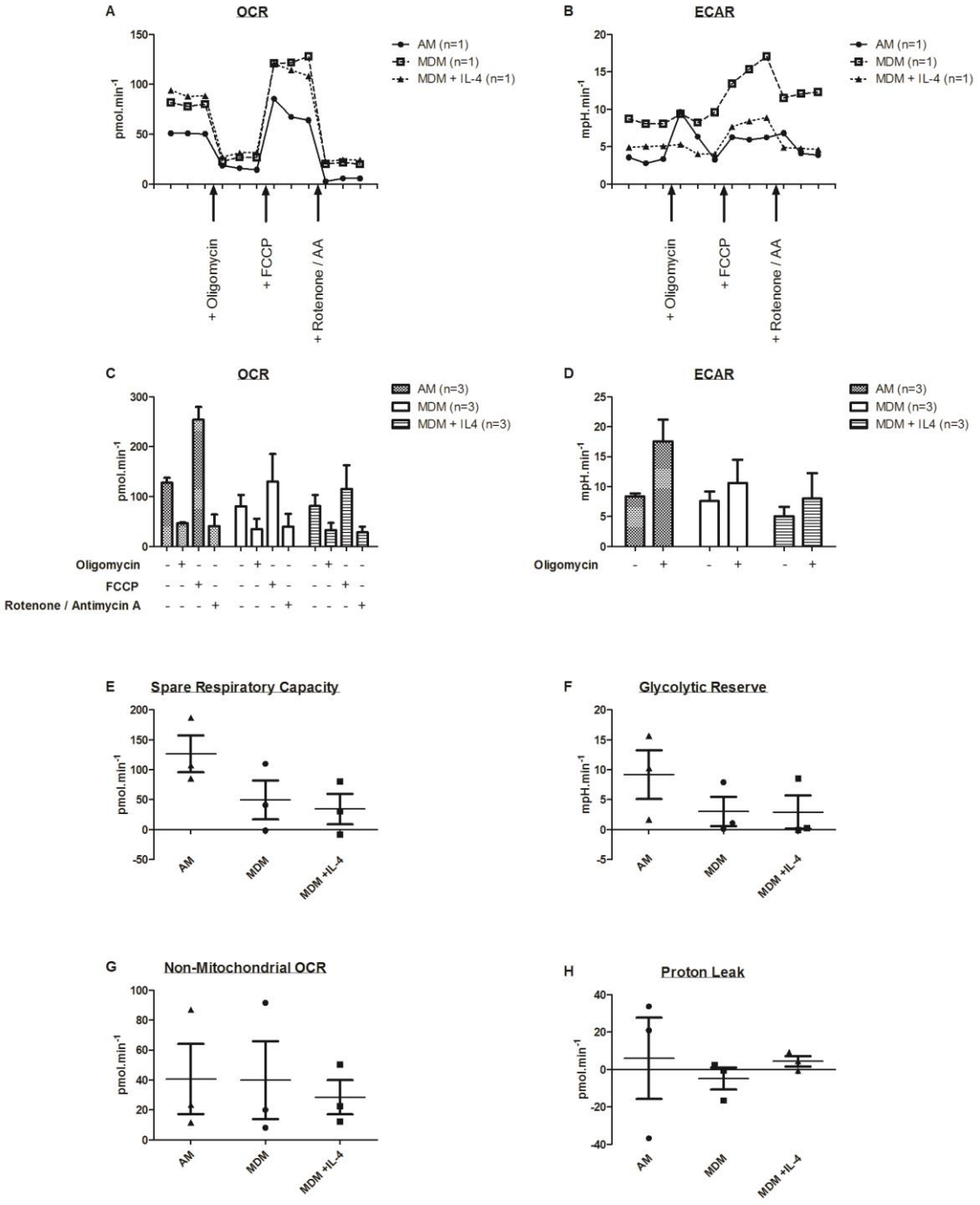

FIGURE 3.20 Human AM demonstrate greater metabolic reserves than human MDM. MDM were plated on Seahorse Bioscience plates at 200,000 cells/well and, 24 hours after plating, treated with IL-4 (final concentration 20ng/mL) or left untreated. Human AM were plated at 100,000 cells/well on Seahorse Biosciences plates. 48 hours after plating of AM and MDM, extracellular flux analyses were performed with sequential addition of mitochondrial inhibitors, and data was normalised using CV assay. Panels A and B depict real-time OCR (A) and ECAR (B) for one representative AM donor and one representative MDM donor. Panels C and D depict mean ± SEM OCR (C) and ECAR (D) for three individual AM donors and three individual MDM donors. Panels E – H depict normalised mean ± SEM SRC (E), GR (F), Non-Mitochondrial OCR (G) and PL (H) for three individual AM donors and three individual MDM donors. Statistical analyses were performed using the unpaired Student's t-test; statistical significance was set at $p<0.05$.

3.2.5 LPS treatment induces glycolysis in human AM

Next, the impact of LPS stimulation of human AM metabolism was investigated. Human AM were isolated, plated and washed as previously described. Immediately after washing, cells were treated with LPS (final concentration 100ng/mL) or left untreated (control). At 24 hours post-treatment, extracellular flux analysis and lactate measurement was performed. Similar to that observed in MDM experiments, LPS treatment significantly increased ECAR (**Figure 3.21B**) and ECAR/OCR ratio (**Figure 3.21C**), and a non-significant increase in lactate production was also detected (**Figure 3.21D**). Interestingly, a non-significant trend towards increased OCR was also observed (**Figure 3.21A**).

Next, utilising a similar approach to that outlined in MDM experiments, AM glycolytic gene expression was also assessed. LPS treatment induced expression of *SCL2A1*, *LDHA*, *PDK3* and *HK1* in human AM (**Figure 3.22**), indicating a switch towards glycolytic metabolism following stimulation.

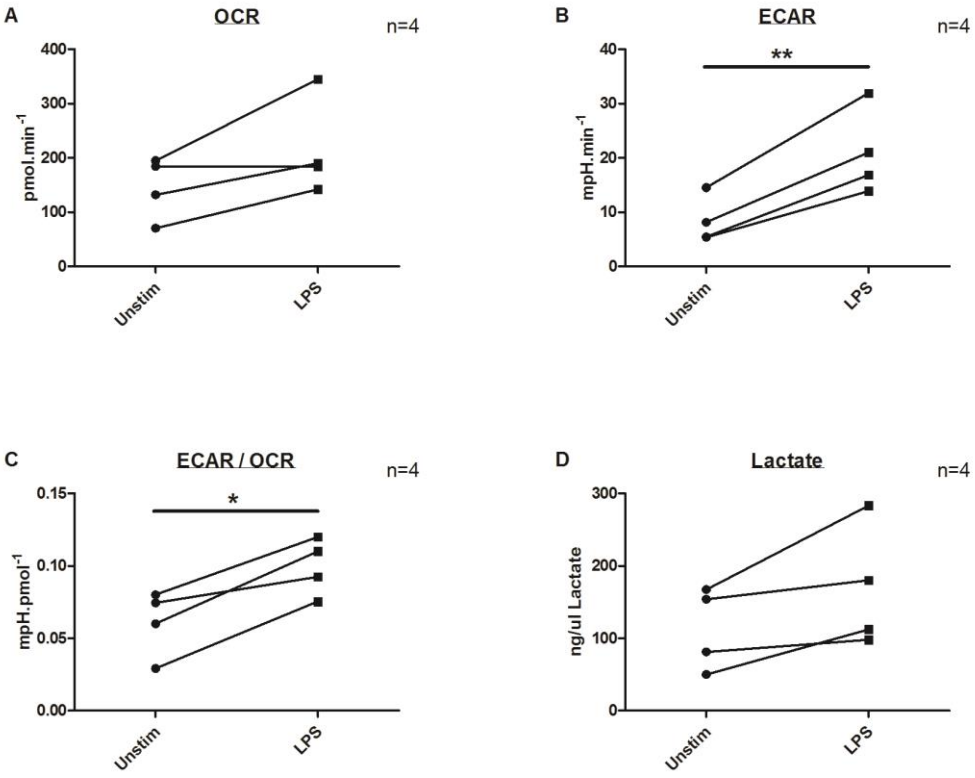

FIGURE 3.21 LPS stimulation induces glycolytic reprogramming in human AM. Human AM were treated with LPS (final concentration 100ng/mL) or left untreated (control). At 24 hours post-treatment, supernatants were removed and retained for quantification of lactate, and extracellular flux analyses were performed with CV assay used to normalise data. Panels A – C depict OCR (A), ECAR (B) and calculated ECAR/OCR ratio (C) for four individual donors. Panel D depicts corresponding lactate concentration as measured in supernatants for four individual donors. Statistical analyses were performed using the paired Student's t-test; *p<0.05, **p<0.01.

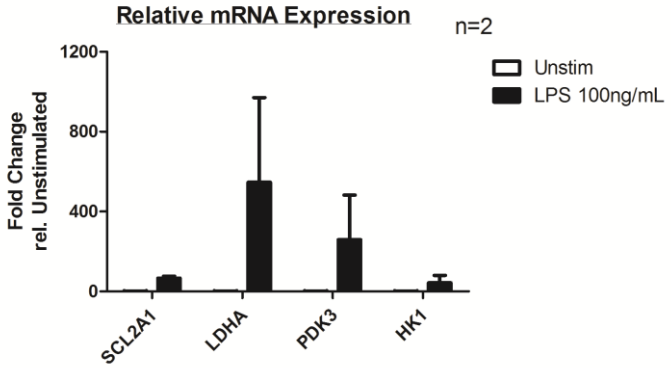

FIGURE 3.22 LPS stimulation induces upregulation of glycolytic gene expression in human AM. Human AM were treated with LPS (final concentration 100ng/mL) or left untreated (control). At 24 hours post-treatment, cells were lysed in RLT lysis buffer, RNA extracted and cDNA generated. Real-time PCR was performed in triplicate using Taqman primers and data were normalised to 18S rRNA. Data depicts mRNA expression fold-change relative to uninfected cells for indicated genes, as calculated by the $2^{-\Delta\Delta Ct}$ method.

3.2.6 Mtb infection induces glycolysis in human AM

Next, the impact of Mtb infection on human AM metabolism was investigated. Human AM were infected with iH37Rv at low MOI or left untreated (control) as before. At 24 hours post-infection, extracellular flux analysis and lactate measurement were performed as previously described. Infected cells demonstrated a significant increase in ECAR/OCR ratio (**Figure 3.23C**) and lactate production (**Figure 3.23D**), as well as a trend towards increased ECAR (**Figure 3.23B**), suggesting a shift towards glycolytic metabolism. Plotting baseline ECAR relative to OCR for uninfected (**Figure 3.24A**) and iH37Rv-infected (**Figure 3.24B**) human AM confirmed overall increases in metabolic activity following infection, with infection-induced skewing towards glycolytic metabolism evident.

Interrogation with inhibitors suggested reduced AM GR following iH37Rv infection (**Figure 3.25F**), similar to that observed in human AM. Similar to LPS-treated AM, however, and in contrast to that observed in MDM experiments, infected AM also demonstrated a non-significant trend towards increased OCR (**Figure 3.23A**). Following interrogation with inhibitors, a trend towards increased Non-Mitochondrial OCR was evident in infected human AM (**Figure 3.25G**).

In order to examine Mitochondrial OCR in isolation (truly representative of oxidative phosphorylation), Non-Mitochondrial OCR was subtracted from measured OCR (**Figure 3.26**). Interestingly, Mitochondrial OCR was not substantially altered following iH37Rv infection (**Figure 3.26C**), suggesting that increased OCR observed following infection may be a result of oxygen consumption via non-mitochondrial pathways, outlined in the Discussion below (**Section 3.3.3**).

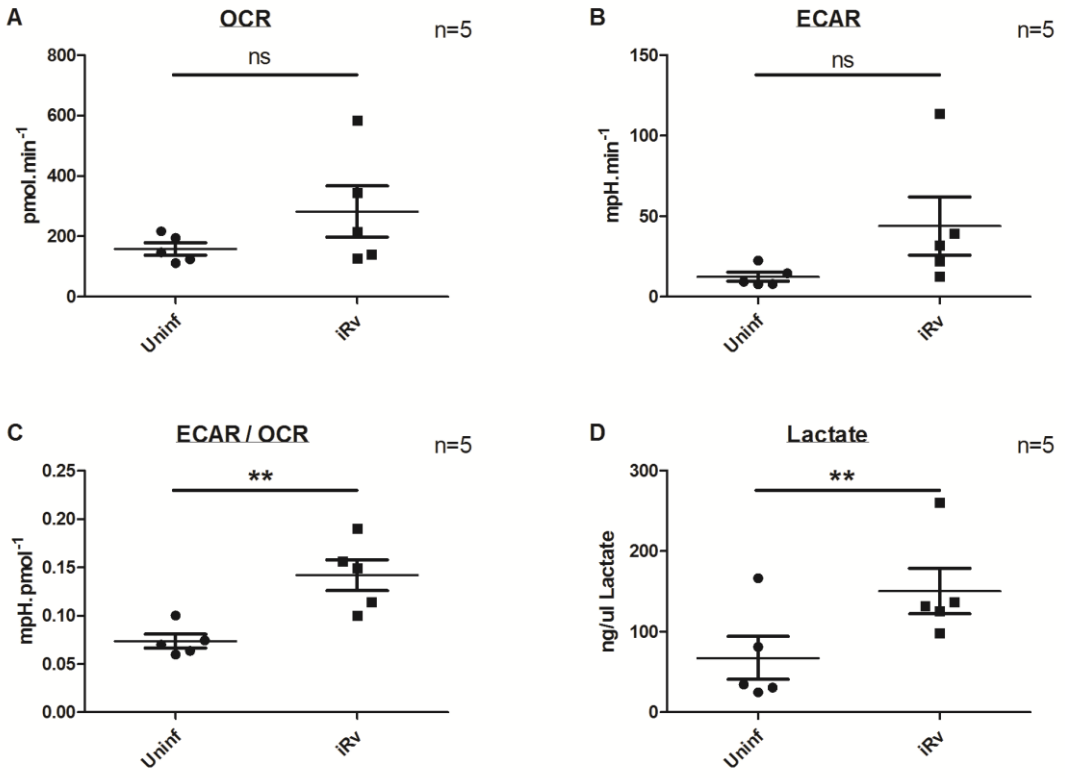

FIGURE 3.23 iMtb infection induces glycolytic reprogramming in human AM. Human AM were infected with iH37Rv at low MOI or left uninfected (control). At 24 hours post-infection, supernatants were removed and retained for lactate measurement, and extracellular flux analyses were performed using CV assay to normalise data. Panels A – C depict normalised mean ± SEM OCR (A), ECAR (B) and calculated ECAR/OCR ratio (C) for five individual donors. Panel D depicts corresponding mean ± SEM lactate concentration as measured in supernatants for five individual donors. Statistical analyses were performed using the paired Student's t-test; *p<0.05.

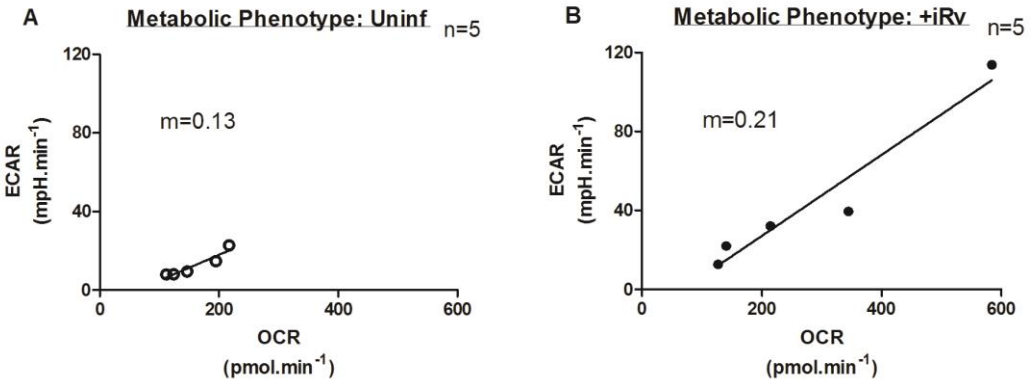

FIGURE 3.24 iMtb infection skews human AM towards a more glycolytic phenotype. Human AM were infected with iH37Rv at low MOI or left uninfected (control). At 24 hours post-infection, extracellular flux analyses were performed using CV assay to normalise data. Panels depict normalised ECAR (y-axis; representative of glycolytic activity) relative to OCR (x-axis; representative of mitochondrial respiration) in uninfected (A) and infected (B) MDM for five individual donors.

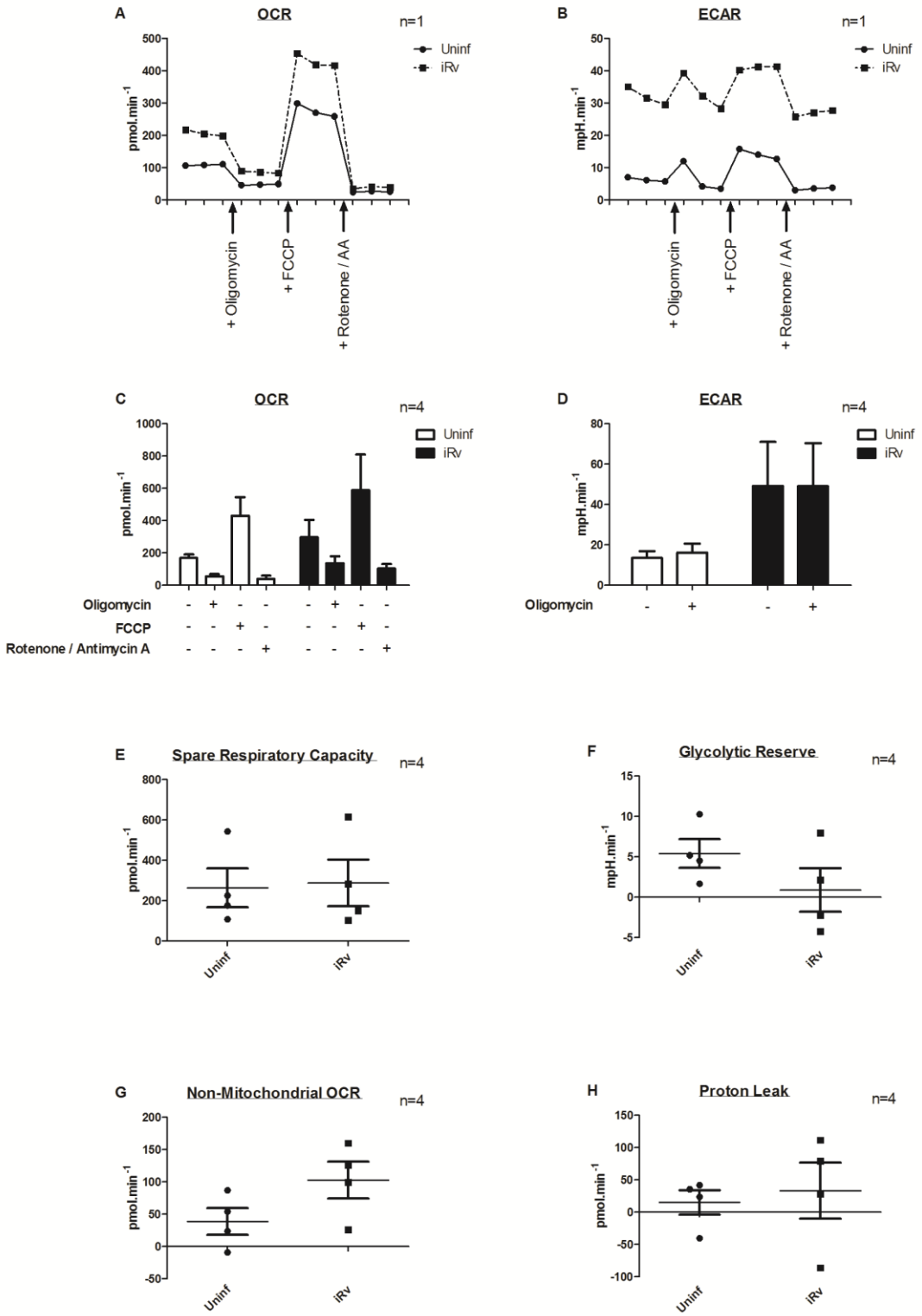

FIGURE 3.25 iMtb infection reduces glycolytic reserve of human AM. Human AM were infected with iH37Rv at low MOI or left uninfected (control). At 24 hours post-infection, extracellular flux analyses were performed with sequential addition of mitochondrial inhibitors and CV assay used to normalise data. Panels A and B depict real-time OCR (A) and ECAR (B) for one representative donor. Panels C and D depict mean ± SEM OCR (C) and ECAR (D) for four individual donors. Panels E – H depict mean ± SEM SRC (E), GR (F), Non-Mitochondrial OCR (G) and PL (H) for four individual donors. Statistical analyses were performed using the Student's t-test; statistical significance was set at $p<0.05$.

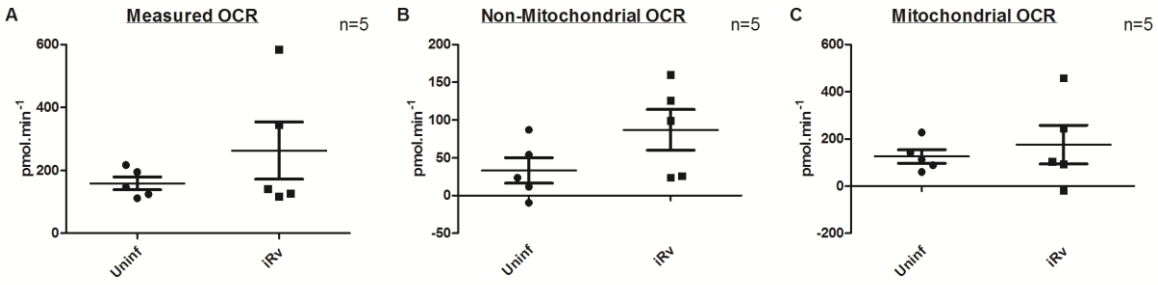

FIGURE 3.26 iMtb infection increases non-mitochondrial OCR. Human AM were infected with iH37Rv at low MOI or left uninfected (control). At 24 hours post-infection, extracellular flux analyses were performed with addition of rotenone/antimycin A (0.5µM) following baseline interrogation, and CV assay used to normalise data. Panel A depicts baseline OCR measured for five individual donors. Panel B depicts post-rotenone/antimycin A OCR (representative of Non-Mitochondrial OCR) measured for five individual donors. Panel C depicts Mitochondrial OCR, calculated by subtracting post-rotenone/antimycin A OCR from baseline OCR (i.e. subtracting Non-Mitochondrial OCR from Total OCR) for five individual donors. Statistical analyses were performed using the Student's t-test; statistical significance was set at $p<0.05$.

Using a similar approach as that employed in MDM experiments (**Figure 3.11**), early metabolic responses in iH37Rv-infected human AM were interrogated. As seen with MDM, infection induced an elevation in both OCR and ECAR at 6 hours post-infection (**Figure 3.27A – B**). Interestingly, ECAR elevation appeared to be more pronounced at 6 hours in comparison to that observed in MDM experiments, with increased ECAR/OCR ratio and increased lactate production both evident at the earlier timepoint (**Figure 3.27C – D**). This may reflect increased sensitivity of human AM to stimulation due to baseline skewing towards oxidative phosphorylation, as previously demonstrated (**Figure 3.19C**). As in MDM experiments, ECAR (**Figure 3.27B**), ECAR/OCR ratio (**Figure 3.27C**) and lactate production (**Figure 3.27D**) continued to increase following up to 24 hours post-infection. However, in contrast to MDM experiments, and in concordance with previous observations in human AM infections, OCR was also elevated at 24 hours post-infection (**Figure 3.27A**). As discussed above, this may reflect increases in non-mitochondrial oxygen consumption induced by iH37Rv infection.

Next, the impact of increasing MOI on human AM metabolic responses to infection was investigated. Interestingly, increasing MOI was associated with a trend towards increased ECAR (**Figure 3.28B**) and increased ECAR/OCR ratio (**Figure 3.28C**), while OCR was unchanged (**Figure 3.28A**). CV assay confirmed cell viability to be similar across conditions (**Figure 3.28D**). The discrepancy in apparent MOI-dependency of metabolic changes observed between human AM and human MDM may be a result of human MDM having a reduced GR compared to human AM (**Figure 3.20F**), meaning that glycolytic activity cannot be further increased in response to increasing MOI.

Finally, in order to confirm the ability of live Mtb infection to induce glycolytic reprogramming in human AM, infections with γ-irradiation killed iH37Rv and with live virulent H37Rv were performed in parallel. Both killed and live Mtb strains induced lactate production in human AM (**Figure 3.29**).

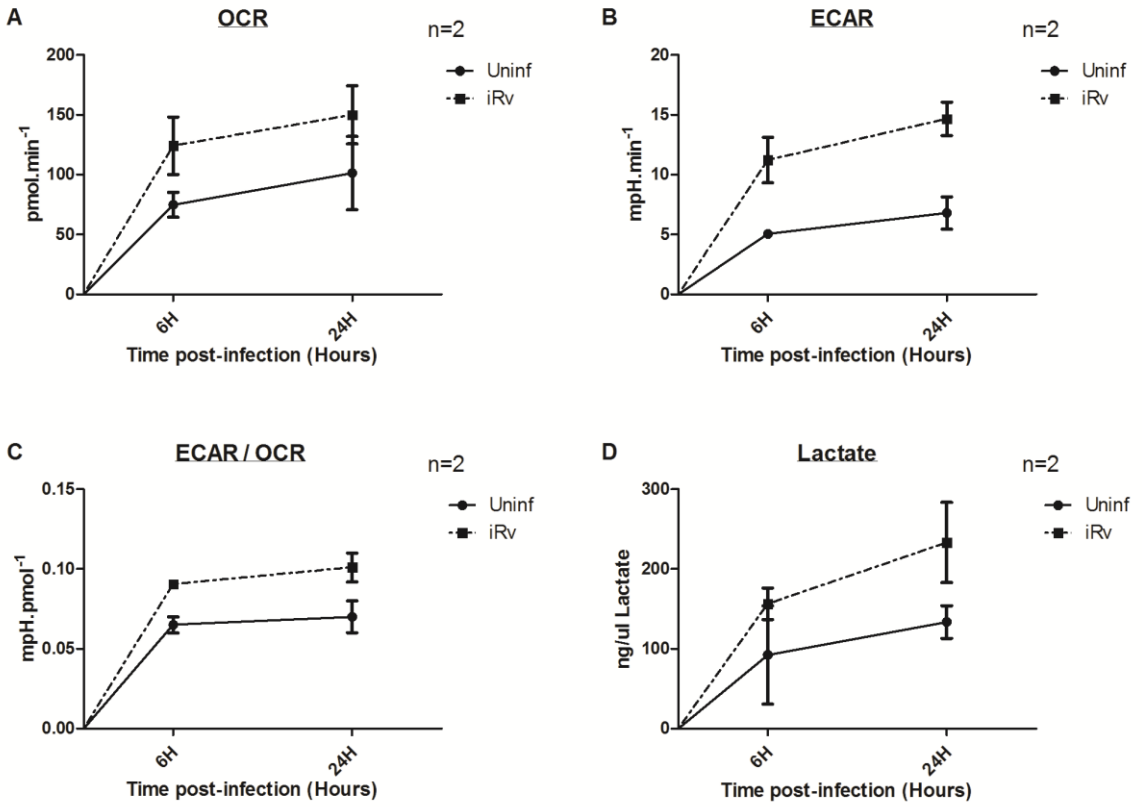

FIGURE 3.27 Glycolytic reprogramming in human AM is evident 24 hours post infection. Human AM were infected in duplicate with iH37Rv at low MOI or left uninfected (control) (24 hour condition), and cells washed at 3 hours post-infection to remove extracellular bacilli. 18 hours later, further duplicate wells were infected with iH37Rv at low MOI or left uninfected (control) (6 hour condition), and washed at 3 hours post-infection to remove extracellular bacilli (24 hour condition infected and control wells were not washed at this time). 6 hours later, supernatants were removed and retained for lactate quantification, and extracellular flux analyses were performed with CV assay used to normalise data. Panels A – C depict normalised mean ± SEM OCR (A), ECAR (B) and calculated ECAR/OCR ratio (C) at 6 hours and 24 hours post-infection for two individual donors. Panel D depicts corresponding mean ± SEM lactate concentration as measured in supernatants for two individual donors.

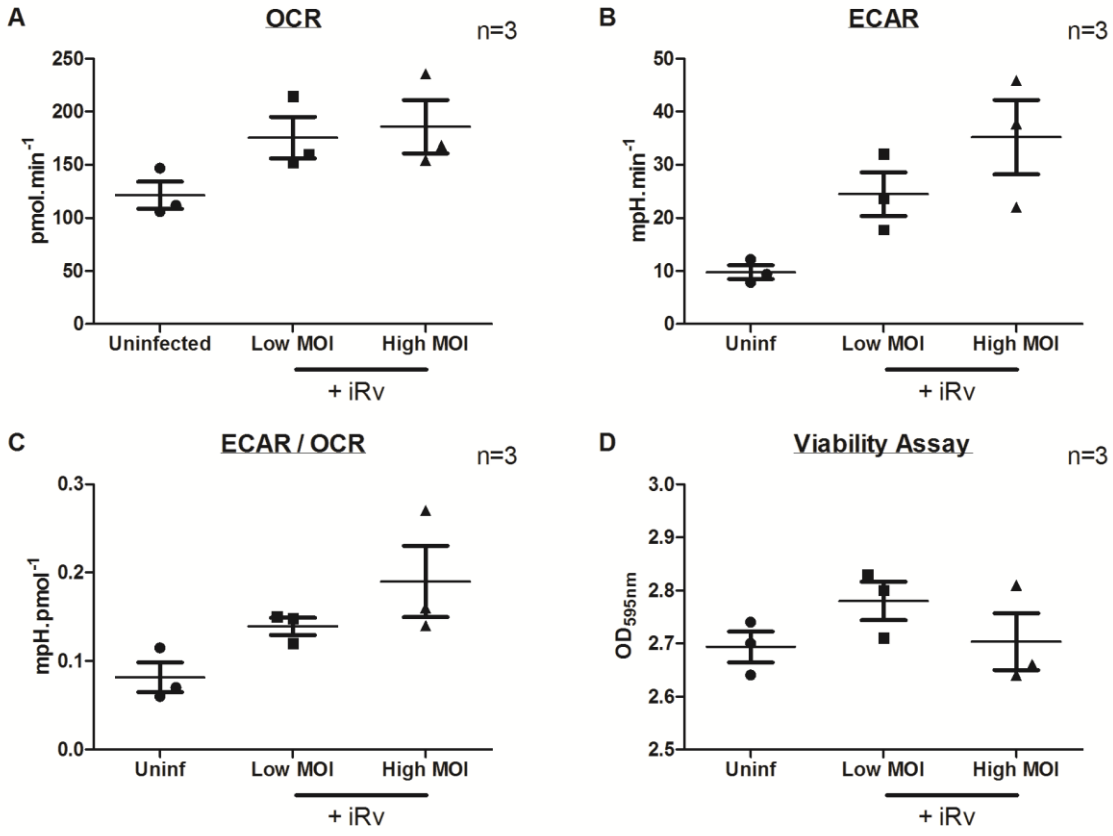

FIGURE 3.28 iMtb-induced glycolytic reprogramming in human AM is MOI-dependent. Human AM were infected with iH37Rv at low MOI, iH37Rv at high MOI or left uninfected (control). At 24 hours post-infection, extracellular flux analysis was performed with data normalised using CV assay. Panels A – C depict mean ± SEM OCR (A), ECAR (B) and calculated ECAR/OCR ratio (C) for three individual donors. Panel D depicts corresponding absorbance following CV staining for three individual donors. Statistical analyses were performed using the paired Student's t-test; statistical significance was set at $p<0.05$.

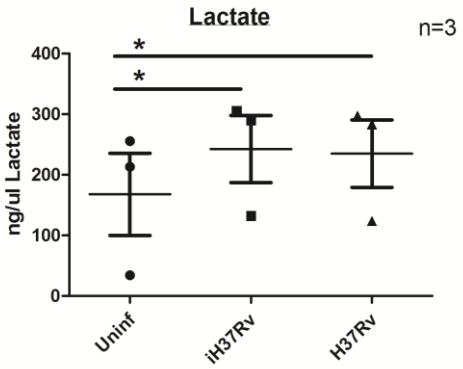

FIGURE 3.29 Live and killed Mtb induce glycolysis in human AM. Human AM were infected with live H37Rv at low MOI, γ-irradiation killed iH37Rv at low MOI, or left uninfected (control). At 24 hours post-infection, supernatants were removed, extracellular bacilli and cell debris removed by centrifugation, and lactate concentration measured. Data depicts mean ± SEM lactate concentration for three individual donors. Statistical analyses were performed using the paired Student's t-test; *$p<0.05$.

3.2.7 Mtb-induced glycolytic reprogramming is mediated through TLR2/6

Stimulation of various TLRs has been shown to induce glycolysis in macrophages and dendritic cells [174,238-240,247,250], and glycolytic reprogramming has been directly linked to IL-1β production in macrophages [174,297]. Mtb PAMPs are known to stimulate TLR2, TLR4 and TLR9. Furthermore, TLR2 stimulation is required for IL-1β production in Mtb infection. Thus, it was hypothesised that Mtb-induced glycolytic reprogramming of human macrophages (and consequent IL-1β production, described in **Chapter 4**) is mediated through TLR2.

First, the role of TLR2 stimulation in murine BMDM glycolytic reprogramming was confirmed using the TLR1/2 agonist P3C, a synthetic triacylated lipopeptide. Murine BMDM were isolated and prepared as described in **Chapter 2 (Section 2.1.3)**. 24 hours after plating, cells were infected with iH37Rv, treated with LPS or P3C or left untreated (control). At 24 hours post-infection/treatment, supernatants were harvested and lactate measured. Similar to LPS treatment or Mtb infection, P3C induced lactate production in murine BMDM (**Figure 3.30**). Furthermore, pre-treatment of cells with anti-TLR1/2 IgG for one hour prior to infection or treatment abrogated lactate production in Mtb-infected murine BMDM, suggesting that the shift towards glycolysis induced by Mtb is partly mediated through TLR1/2 signalling (**Figure 3.30**). As expected, TLR1/2 inhibition also abrogated P3C-induced lactate production, but LPS-induced glycolysis (which is mediated through TLR4) was not affected (**Figure 3.30**).

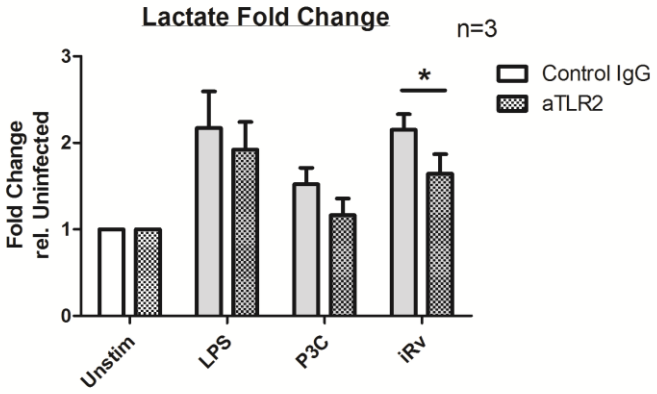

FIGURE 3.30 iMtb-induced glycolytic reprogramming of murine BMDM is partly mediated through TLR2. Murine BMDM were pre-treated with anti-TLR2 antibody or with control IgG for 1 hour prior and throughout the duration of the experiment. Cells were treated with LPS (final concentration 100ng/mL), P3C (final concentration 100ng/mL), infected with iH37Rv at low MOI, or left uninfected (control). At 24 hours post-treatment/infection, supernatants were removed and lactate concentration quantified. Data depicts fold change in lactate concentration (grey bars) relative to uninfected control (white bars) for three individual mice. Statistical analyses were performed using the unpaired Student's t-test; *p<0.05.

Next, the impact of P3C on human MDM metabolism was examined. Human MDM were isolated and prepared as previously described. On Day 6, cells were treated with LPS, P3C or left untreated (control). At 24 hours post-treatment, supernatants were harvested and lactate measured. P3C was observed to induce lactate production in a dose-dependent manner (**Figure 3.31**).

Extracellular flux analyses was performed as before, with P3C treatments applied to designated wells in parallel with iH37Rv infection, 24 hours prior to interrogation. Unexpectedly, P3C did not induce a shift towards glycolytic metabolism in human MDM (**Figure 3.32**), in contrast to Mtb infection, despite measurement of TNF-α concentration in supernatants confirming adequate stimulation.

To further investigate the role of TLR2 signalling in Mtb-induced glycolytic reprogramming, anti-TLR1/2 IgA was employed. First, extracellular flux analyses was performed on uninfected cells treated with anti-TLR1/2 IgA or with control IgA for 24 hours to confirm similar baseline metabolic profile and reserves (**Figure 3.33**). Next, cells were pre-treated with anti-TLR1/2 IgA or with control IgA for 1 hour prior to (and for the duration of) infection with iH37Rv. Anti-TLR1/2 IgA attenuated the Mtb-induced increase in ECAR (**Figure 3.34B**), ECAR/OCR ratio (**Figure 3.34C**) and lactate production (**Figure 3.34D**), suggesting that glycolytic reprogramming in Mtb infection is mediated in part through TLR2.

Thus, despite inability of TLR-2 stimulation in isolation to induce glycolysis in human MDM (**Figure 3.32**), TLR-2 signalling plays a crucial role in Mtb-induced metabolic reprogramming (**Figure 3.34**).

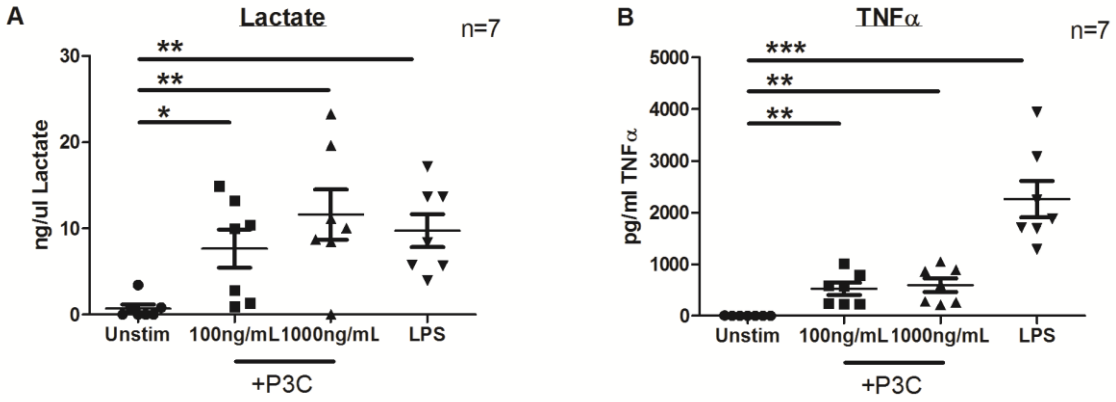

FIGURE 3.31 TLR2 stimulation induces lactate production in human MDM. MDM were treated with P3C (final concentration 100ng/mL or 1000ng/mL), LPS (final concentration 100ng/mL) or left untreated (control). At 24 hours post-infection, supernatants were removed and lactate and TNF-α concentration quantified. Panels depict measured lactate (A) and TNF-α (B) concentration for seven individual donors. Statistical analyses were performed using the paired Student's t-test; *p<0.05, **p<0.01, ***p<0.001.

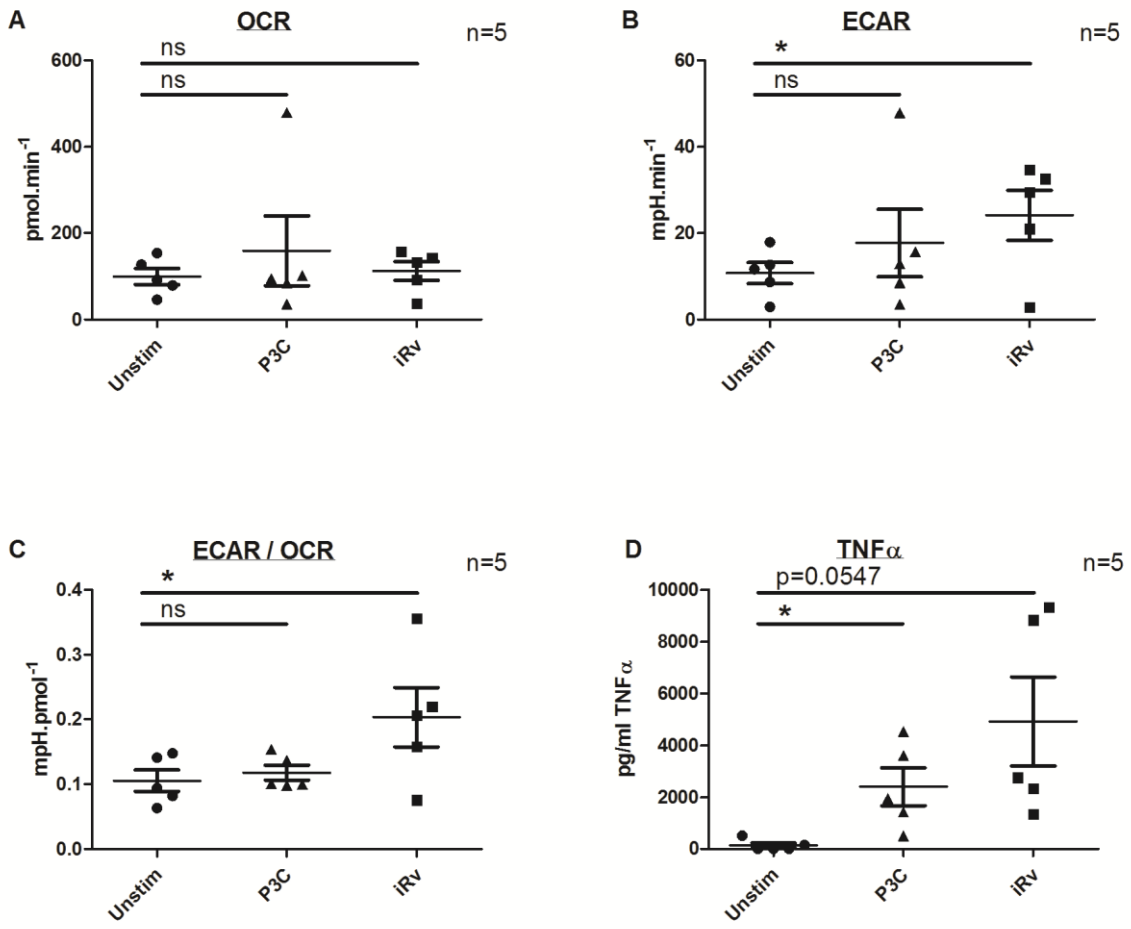

FIGURE 3.32 TLR2 stimulation does not induce glycolytic reprogramming in human MDM, as measured by extracellular flux analyses. MDM were treated with P3C (final concentration 100ng/mL) or left untreated (control). 24 hours post treatment, supernatants were removed and retained for TNF-α quantification, and extracellular flux analyses were performed using CV assay to normalise data. Panels A – C depict mean ± SEM OCR (A), ECAR (B) and calculated ECAR/OCR ratio (C) for five individual donors. Panel D depicts corresponding mean ± SEM TNF-α concentration as measured in supernatants of five individual donors. Statistical analyses were performed using the paired Student's t-test; *p<0.05.

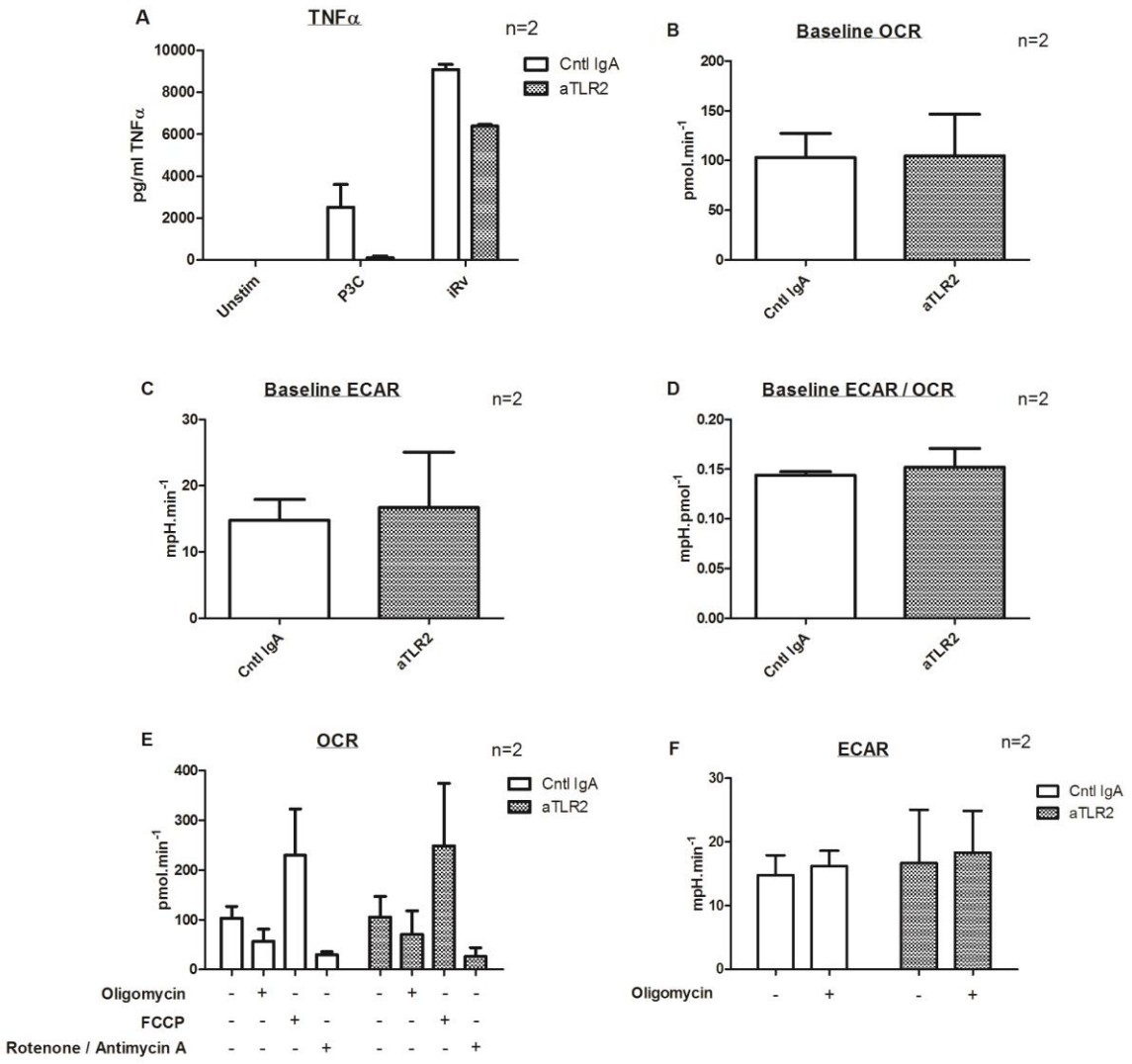

FIGURE 3.33 Antagonism of TLR2 does not alter baseline metabolic profile of human MDM.

Panel A: MDM were pre-treated with anti-TLR2 antibody or with control IgA for 1 hour prior and throughout the duration of the experiment. Cells were treated with P3C (final concentration 100ng/mL), infected with iH37Rv at low MOI, or left uninfected (control). At 24 hours post-treatment/infection, supernatants were removed and TNF-α concentration quantified. Data depicts mean ± SEM TNF-α concentration for two individual donors (A).

Panels B – F: MDM were treated with aTLR2 antibody or control IgA (control). 24 hours post-treatment, extracellular flux analyses were performed with sequential addition of mitochondrial inhibitors and data normalised using CV assay. Panels B – D depict baseline mean ± SEM OCR (B), ECAR (C) and calculated ECAR/OCR ratio (D) for two individual donors. Panels E – F depict mean ± SEM OCR (E), ECAR (F) following interrogation with mitochondrial inhibitors for two individual donors.

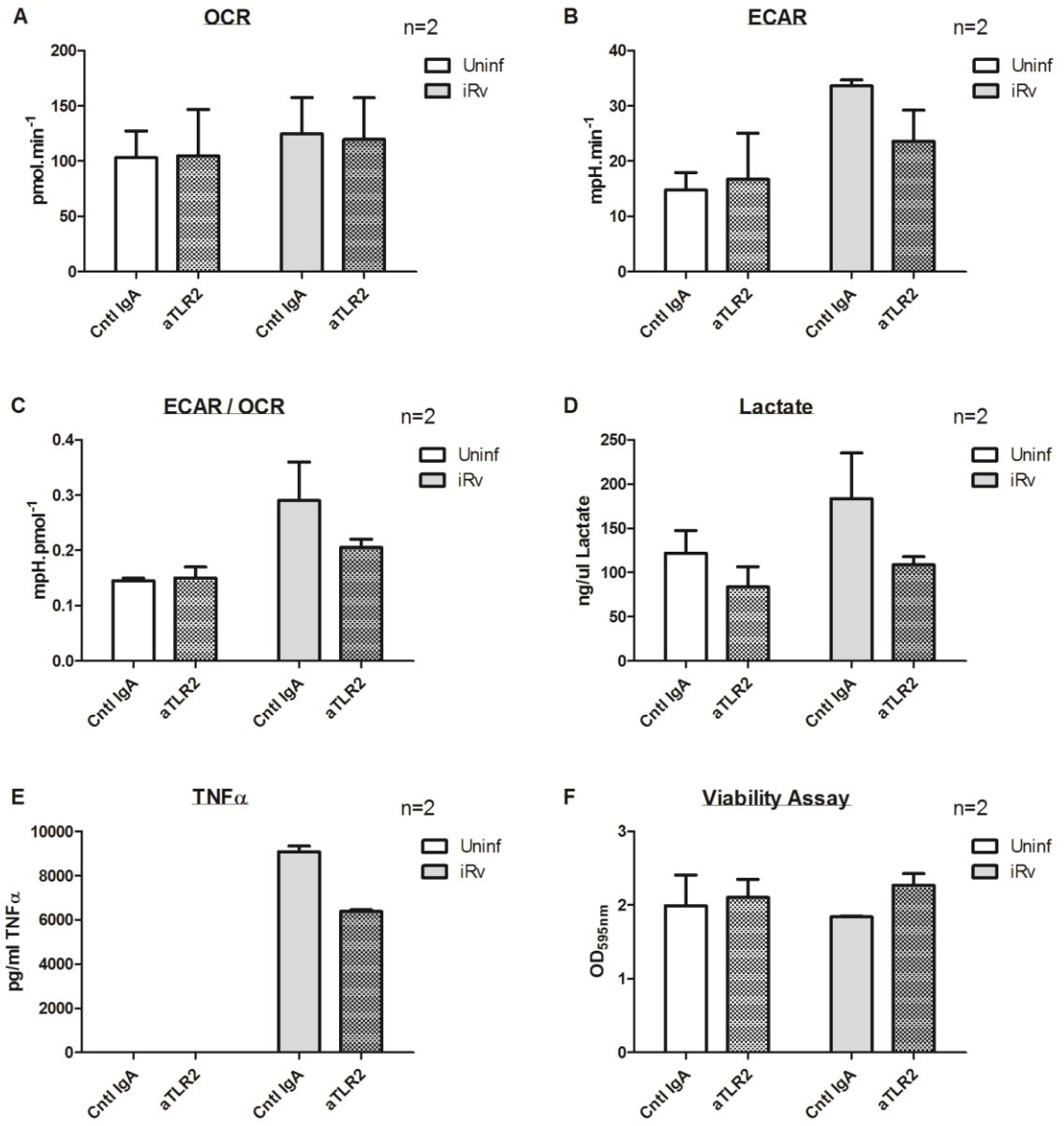

FIGURE 3.34 iMtb-induced glycolytic reprogramming of human MDM is requires TLR2. MDM were pre-treated with anti-TLR2 antibody or with control IgA for 1 hour prior and throughout the duration of the experiment. Cells were infected with iH37Rv at low MOI, or left uninfected (control). At 24 hours post-infection, supernatants were removed and retained for lactate and TNF-α quantification and extracellular flux analyses were performed using CV assay to normalise data. Panels A – C depict mean ± SEM OCR (A), ECAR (B) and calculated ECAR/OCR ratio (C) for three individual donors. Panels D – E depict corresponding mean ± SEM lactate (D) and TNF-α (E) concentration as measured in supernatants of three individual donors. Panel F depicts corresponding absorbance following CV staining, indicative of cell viability, for three individual donors. Statistical analyses were performed using the paired Student's t-test; statistical significance was set at $p<0.05$.

Given the discrepancy seen between the failure of TLR2 stimulation to induce glycolysis in human MDM (**Figure 3.33**) and the evident role for TLR2 in Mtb-induced glycolysis (**Figure 3.34**), it is possible that Mtb-mediated TLR2 stimulation synergises with Mtb-mediated stimulation of another pathway in order to induce metabolic reprogramming in human macrophages. TLR2 is known to dimerise with TLR6 [177], and a TLR2/TLR6 pathway has been implicated in Mtb-induced IL-1β production [131]. Thus, it was hypothesised that combined TLR2/TLR6 stimulation would induce glycolysis in human MDM where TLR2 stimulation alone did not. FSL-1, a synthetic lipoprotein derived from *Mycoplasma salivarium*, acts as a TLR2/TLR6 agonist. Human MDM were again isolated, cultured and plated on Seahorse Biosciences plates as previously described. 24 hours after plating, cells were stimulated with FSL-1, infected with iH37Rv or left untreated (control). At 24 hours post-infection/treatment, extracellular flux analysis and lactate measurement was performed. In contrast to observations with P3C, FSL-1 treatment induced an increase in ECAR and in ECAR/OCR ratio similar to that observed with Mtb infection (**Figure 3.35**).

To investigate the effect of dual blockade of TLR2 and TLR6 signalling, a combination of anti-TLR2 IgA and anti-TLR6 IgG, or control Ig, was applied to cells one hour prior to and for the duration of iH37Rv infection. First, metabolic profile and reserve of uninfected cells treated with combined anti-TLR2 and anti-TLR6 was compared to that of uninfected cells treated with control Ig (**Figure 3.36**), with no differences evident.

Following infection with iH37Rv, however, cells in which TLR2/TLR6 activity was inhibited demonstrated abrogation of increases in ECAR, ECAR/OCR ratio and lactate production (**Figure 3.37**). Though this did not reach statistical significance, this trend supports the hypothesis that Mtb-induced glycoylytic shift is mediated through TLR2/6 signalling.

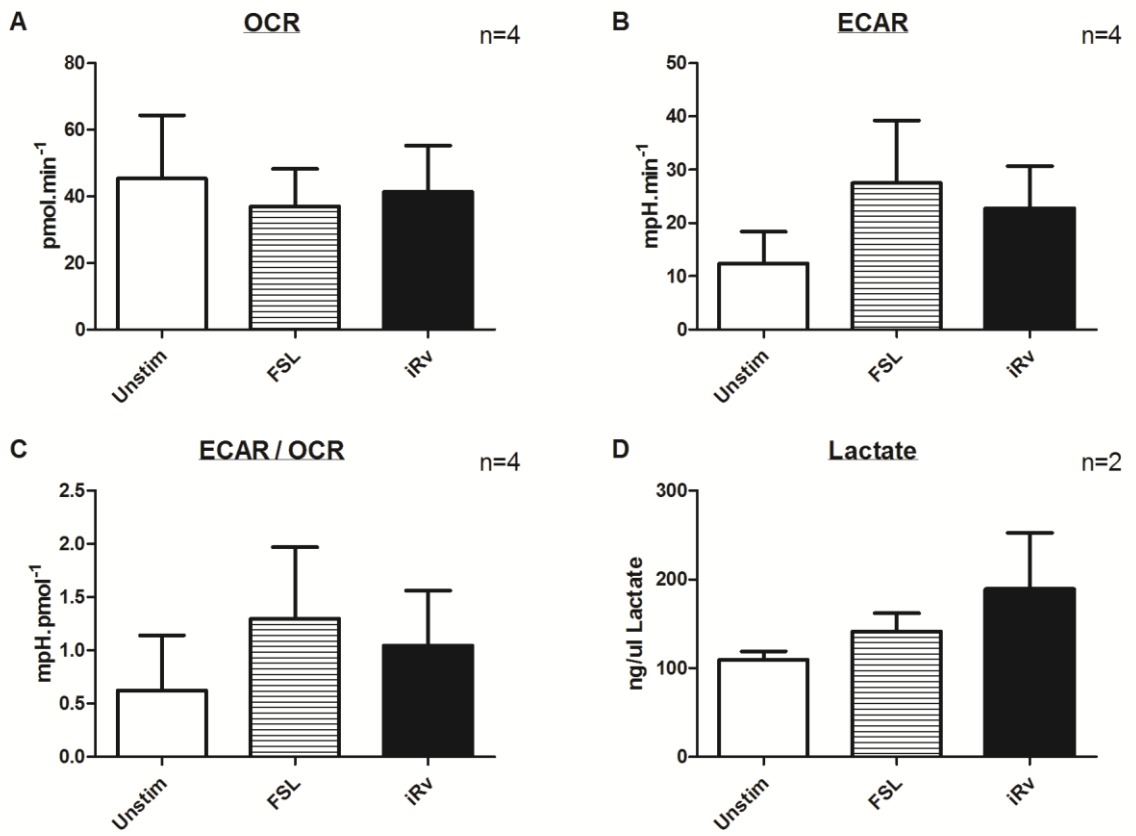

FIGURE 3.35 TLR2/6 stimulation induces glycolytic reprogramming in human MDM. MDM were treated with FSL-1 (final concentration 100ng/mL) or left untreated (control). 24 hours post treatment, supernatants were removed and retained for lactate quantification, and extracellular flux analyses were performed using CV assay to normalise data. Panels A – C depict mean ± SEM OCR (A), ECAR (B) and calculated ECAR/OCR ratio (C) for four individual donors. Panel D depicts mean ± SEM lactate concentration as measured in supernatants of two individual donors. Statistical analyses were performed using the paired Student's t-test; statistical significance was set at $p<0.05$.

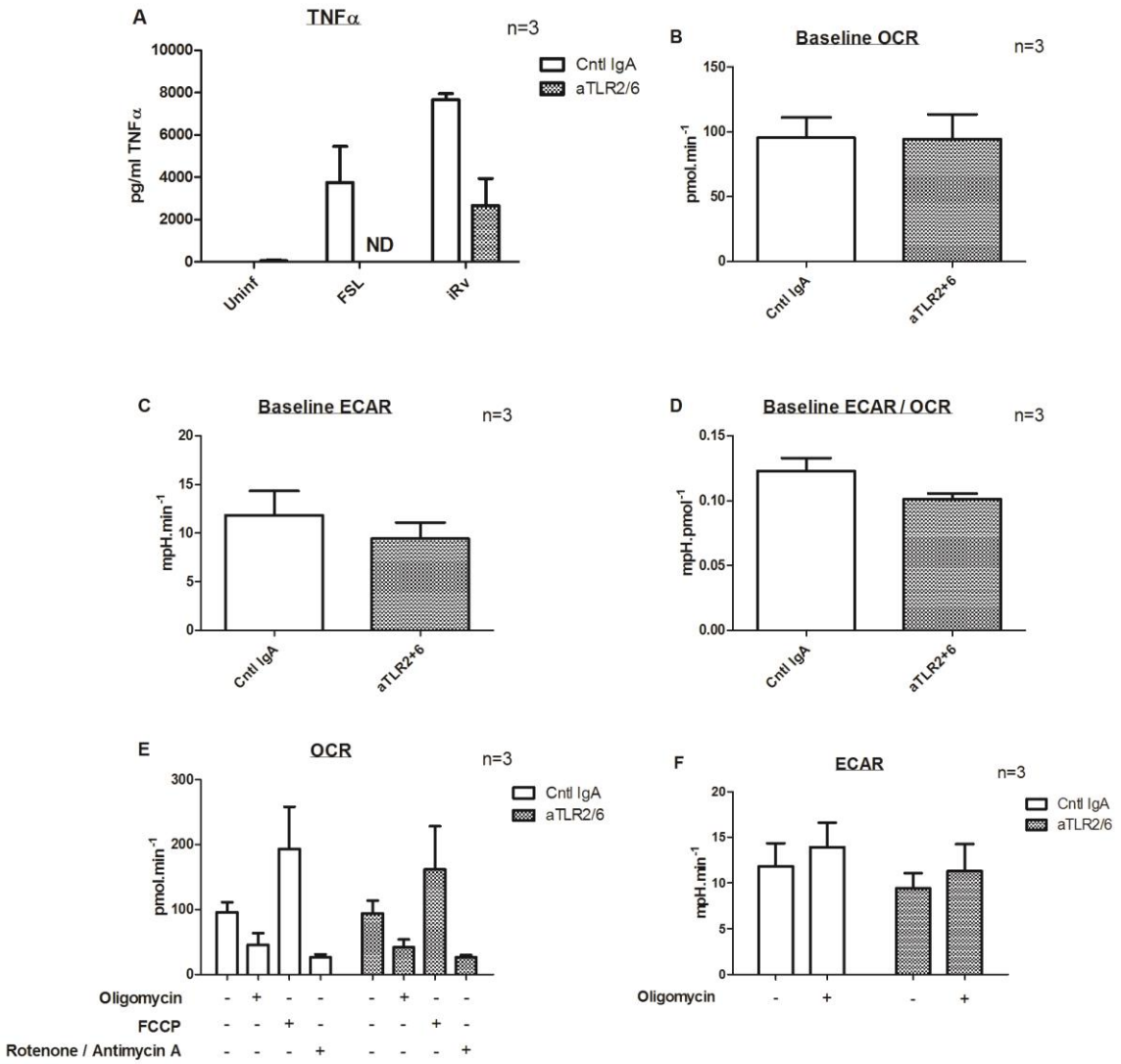

FIGURE 3.36 Antagonism of TLR2/6 does not alter baseline metabolic profile of human MDM.

Panel A: MDM were pre-treated with combined anti-TLR2 antibody and anti-TLR6 antibody or with control IgA for 1 hour prior and throughout the duration of the experiment. Cells were treated with FSL-1 (final concentration 100ng/mL), infected with iH37Rv at low MOI, or left uninfected (control). At 24 hours post-treatment/infection, supernatants were removed and TNF-α concentration quantified. Data depicts mean ± SEM TNF-α concentration for three individual donors (A).

Panels B – F: MDM were treated with combined anti-TLR2 antibody and anti-TLR6 antibody or control IgA (control). 24 hours post-treatment, extracellular flux analyses were performed with sequential addition of mitochondrial inhibitors and data normalised using CV assay. Panels B – D depict baseline mean ± SEM OCR (B), ECAR (C) and calculated ECAR/OCR ratio (D) for three individual donors. Panels E – F depict mean ± SEM OCR (E), ECAR (F) following interrogation with mitochondrial inhibitors for three individual donors. Statistical analyses were performed using the paired Student's t-test; statistical significance was set at $p<0.05$.

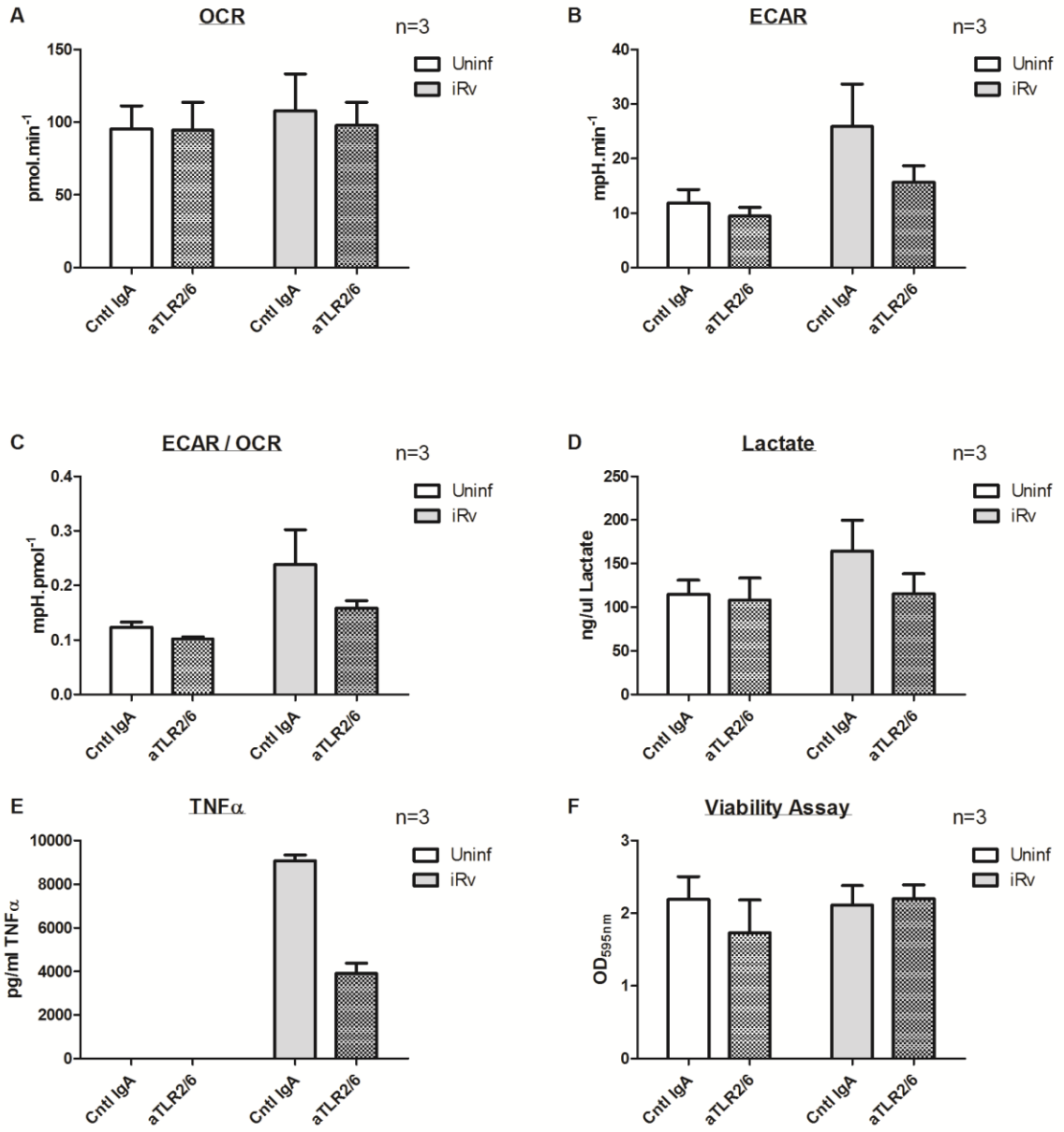

FIGURE 3.37 iMtb-induced glycolytic reprogramming of human AM is partly mediated through TLR2/6. MDM were pre-treated with combined anti-TLR2 antibody and anti-TLR6 antibody or with control IgA for 1 hour prior and throughout the duration of the experiment. Cells were infected with iH37Rv at low MOI, or left uninfected (control). At 24 hours post-infection, supernatants were removed and retained for lactate and TNF-α quantification and extracellular flux analyses were performed using CV assay to normalise data. Panels A – C depict mean ± SEM OCR (A), ECAR (B) and calculated ECAR/OCR ratio (C) for three individual donors. Panels D – E depict corresponding mean ± SEM lactate (D) and TNF-α (E) concentration as measured in supernatants of three individual donors. Panel F depicts corresponding absorbance following CV staining, indicative of cell viability, for three individual donors. Statistical analyses were performed using the paired Student's t-test; statistical significance was set at $p<0.05$.

3.3 DISCUSSION

Links between metabolic profile and functional polarisation of macrophages are increasingly recognised. Glycolytic reprogramming in response to TLR agonists is necessary for key pro-inflammatory functions in murine macrophages. However, to date the role of this metabolic response to stimulation has not been examined in the context of host defence. Macrophage polarisation represents a crucial component of the host immune response to Mtb, with initial alveolar macrophage inflammatory responses playing an important part in determination of disease course. The Mtb bacillus has evolved mechanisms for evasion of this early host response, inducing anti-inflammatory macrophage responses (such as secretion of IL-10) that are traditionally associated with alternative M2 activation of macrophages. In this Chapter, therefore, the impact of Mtb infection of macrophage metabolism was investigated.

3.3.1 Baseline metabolic parameters of human MDM

Seahorse Bioscience technology permits real-time simultaneous measurement of extracellular acidification rate (ECAR; representative of glycolytic rate) and oxygen consumption rate (OCR; representative of oxidative phosphorylation) of live cells, and is becoming a standard technology for the interrogation of cellular energy metabolism, used in work contributing to more than 1,500 publications since its inception 10 years ago. Prior to investigating the impact of stimulation or infection on macrophage metabolism, baseline bioenergetics profile of human MDM within the model were established using the Seahorse XF24e Analyzer (**Figure 3.1**), demonstrating median OCR and ECAR of 109.7 pmol.min^{-1} and 10.6 mpH.min^{-1}, respectively, correlating well with M-CSF-treated human MDM metabolic rates reported by Izquierdo et al [472]. Sequential real-time addition of mitochondrial inhibitors, described in detail in **Chapter 2 (Section 2.3.1)** and depicted in **Figure 2.2**, was utilised to establish baseline metabolic reserves of human MDM within our model (**Figure 3.2**), with median SRC and GR of 16.7 pmol.min^{-1} and 3.6 mpH.min^{-1} respectively observed, again correlating well with published data from Izquierdo et al [472]. Others have conversely reported negligible SRC in human MDM [473,474], however these studies utilised lower doses of FCCP than those employed in this work, which may explain this discordance.

LPS has been observed to induce Warburg metabolism in a range of cell types, including murine macrophages and dendritic cells [174,238-240,247]. Similarly, human MDM demonstrated increased ECAR following LPS stimulation for 24 hours, with OCR unchanged, resulting in significant increase in the ECAR/OCR ratio (**Figure 3.3**). Increased lactate production in these cells provides further evidence for a shift towards glycolytic metabolism (**Figure 3.3**). LPS-stimulated

murine macrophages have been previously shown to demonstrate reduced OCR, in contrast with the unchanged OCR observed in our model. Interestingly, one proposed mechanism for this reduction in OCR is the NO-mediated nitrosylation of ETC complexes leading to inhibition of mitochondrial function and decreased membrane potential [238,265]. Evidence exists for species-specific differences in *NOS2* induction and NO production [32], with human macrophages demonstrating substantially lower levels of expression compared to murine macrophages, providing a plausible explanation for the results observed in this human model. In parallel with observed increased in glycolysis following LPS stimulation, Glycolytic Reserve was abrogated (**Figure 3.4**), suggesting that activated human MDM accelerate glycolytic metabolism to near-maximal rates. SRC and PL were not substantially altered, again indicating that mitochondrial function is not significantly inhibited in human MDM (**Figure 3.4**).

IL-4 stimulation has been shown to antagonise the glycolytic switch within murine macrophages, with inhibition of mTOR signalling, HIF-1α induction and glycolytic enzyme induction [241,242,270,271]. In human MDM, IL-4 treatment similarly reduced ECAR, lactate production and ECAR/OCR ratio without significantly altering OCR (**Figure 3.5**). This model does not reflect true M2-polarised macrophages as cells are derived from *ex vivo* monocytes, however, the reduced glycolytic rate suggests a similar skewing away from this pathway of energy production as that reported in murine macrophages [241,242]. Transcriptomic and metabolomic work by Jha et al suggests sequestration of glucose from central metabolism to permit glycosylation of M2 mediators in IL-4-treated BMDM [244], with cells instead fuelling OXPHOS through β-oxidation of fatty acids. Interestingly, Eisele et al have identified a role for PPARδ-mediated fatty acid oxidation in permitting the establishment of persistent *S. typhimurium* infection in murine macrophages [313], indicating subversion of glycolytic reprogramming as a possible virulence mechanism of this intracellular pathogen. Similarly, Mtb is capable of hijacking M2-polarised macrophages to facilitate the development of granulomata that permit the establishment of persistent infection [475], raising the possibility of manipulation of macrophage intracellular energy metabolism as a mechanism for bacillary survival and replication.

3.3.2 Mtb infection induces glycolysis in human MDM

Preliminary experiments confirmed glycolytic reprogramming, as indicated by increased lactate production, following murine macrophage infection with live virulent (H37Rv), live avirulent (H37Ra) and non-viable (iH37Rv) Mtb strains (**Figure 3.6**), though inter-strain comparisons were not possible as infections were not performed in parallel. Increased lactate production may alternatively be the result of overall increase in metabolic turnover following infection, however

increases in glycolytic rate matched to increases in OXPHOS rate should not result in substantial changes in lactate production in a metabolically efficient cell. Interpretation of results in infections involving viable bacilli is confounded by the presence of metabolically active bacilli within the experimental well, as metabolically active bacilli may also contribute to cumulative lactate concentration in supernatants. However, increased lactate production was also observed in cells infected with non-viable iH37Rv, reflective of macrophage metabolism in isolation. iH37Rv infections further confirm that bacillary viability is not a pre-requisite for induction of glycolytic reprogramming, suggesting a role for mycobacterial PAMPs. TLR4, with and without ATP, has been implicated in the glycolytic shift observed in activated murine macrophages [174,247,250]. Likewise, TLR2, TLR3, TLR4, TLR7/8 and TLR9 have been shown to induce glycolysis in murine dendritic cells [238-240]. Mtb PAMPs stimulate a range of TLRs, including TLR2, TLR4 and TLR9 [20].

In human MDM, iH37Rv induced a shift towards glycolytic metabolism, indicated by significant increases in ECAR, ECAR/OCR ratio and lactate production following infection (**Figure 3.7**). This is similar to results observed in previous LPS experiments (**Figure 3.3**). Again, OCR was not down-regulated as previously demonstrated in M1-polarised murine macrophages (**Figure 3.7**). Interestingly, perturbation of mitochondrial function following Mtb infection has been described in both human lymphocytes and PMA-differentiated THP-1 cells [336,338]. Evidence exists for strain-specificity in terms of this effect, however, with avirulent H37Ra infection inducing downregulation of mitochondrial activity but virulent H37Rv infection causing contrasting upregulation in work by Jamwal et al [338]. Thus the apparent minimal impact of Mtb infection on OCR could be specific to human MDM or specific to the non-viable gamma-irradiated iH37Rv strain used in our experiments. It is notable, however, that readouts of mitochondrial function employed by Jamwal et al did not include OCR, but rather relied on measurement of membrane potential and ATP generation [338]. As outlined below, Mills et al suggest repurposing of macrophage mitochondria following stimulation with LPS [269], meaning that though mitochondria remain active they are no longer producers of ATP.

Infection induced overall upregulation in intracellular metabolic activity (**Figure 3.8**), as well as increased glucose consumption (**Figure 3.9**), likely indicative of increased ATP requirements of infected cells due to increased signalling and biosynthetic demands. However, skewing towards glycolytic metabolism was clearly evident (**Figure 3.8**). A simple bioenergetic explanation for this increased reliance on glycolytic metabolism is the dependence of the cell on glycolytically-derived ATP in the setting of reduced mitochondrial efficiency [238]. However, recent work by Mills et al describes a fundamental functional role for this increase in glycolytic activity, with ATP derived from the glycolytic pathway required to fuel ATP synthase (Complex V) in order to generate high

mitochondrial membrane potential, permitting pro-inflammatory mitochondrial ROS production via Complex I [269]. Mehrota et al have suggested strain-specific increases in glycolytic shift in PMA-treated THP-1 cells, with virulent strains inducing more substantial increases in glycolytic activity [356]. This work must be interpreted with caution, however, as these cells are highly dependent on glycolysis, with inhibition of mitochondrial respiration using rotenone not impacting ATP production, suggesting redundancy of OXPHOS even at uninfected baseline. Furthermore, their experiments utilise viable bacilli rendering it difficult to differentiate host macrophage metabolism from pathogen metabolism.

Concurrent with increased glycolytic activity, GR of human MDM was essentially abrogated following infection with iH37Rv (**Figure 3.10**), similar to results observed following LPS stimulation, indicating acceleration of glycolytic metabolism to near maximal rates. While increased ECAR was evident as early as 6 hours post-infection, this was coupled to similar increases in OCR initially, with no substantial shift towards glycolytic metabolism as indicated by ECAR/OCR ratio (**Figure 3.11**). Continued increases in ECAR up to 24 hours post-infection occurred concomitant with slight reduction in OCR, with substantial increase in ECAR/OCR ratio observed (**Figure 3.11**), indicating a shift towards glycolysis. In a murine dendritic cell model, Everts et al demonstrate NO-mediated inhibition of mitochondrial respiration, occurring at later than 6 hours post-stimulation [238]. Though NO production by human macrophages is substantially lower than that of murine macrophages [32], it is possible that low level NO production is responsible for the failure of OCR to increase in the same order of magnitude as ECAR, resulting in increased reliance on glycolytic metabolism in the infected cell. The magnitude of the shift towards glycolysis did not differ between macrophages infected at low MOI versus high MOI (**Figure 3.12**). This suggests that maximal rates of glycolysis were achieved following infection at low MOI as used in our basic experimental model, supporting the previous observation of abrogated Glycolytic Reserve following infection at low MOI (**Figure 3.10**). Conversely, a non-significant trend towards MOI-dependent increase in glucose consumption was observed (**Figure 3.13**).

The primary function of central glucose metabolism is generation of energy in the form of ATP. Following infection or activation, upregulation of numerous signalling and biosynthetic pathways which require energy is observed. Following infection, intracellular ATP levels were increased (**Figure 3.14**), supporting a model whereby the cell increases energy production to meet increased demand. This model is also supported by the observed increase in overall metabolic activity following infection (**Figure 3.8**), and early increases in both glycolytic metabolism and mitochondrial respiration (**Figure 3.11**).

Though results of metabolic interrogation of viable Mtb-infected macrophages are somewhat confounded by the presence of two distinct metabolising entities, it was important to confirm that macrophage metabolic responses in the setting of infection using viable Mtb strains were not vastly different to those using non-viable iH37Rv. Mehrotra et al have previously demonstrated a shift towards glycolytic metabolism using ^{13}C-glucose labelling in PMA-differentiated THP-1 cells infected with various live Mtb strains [356], though these results must be interpreted with caution for the reasons outlined above. Following infection with viable H37Ra, a shift towards glycolytic metabolism was evident through significantly increased lactate production and a non-significant trend towards increased glucose consumption (**Figure 3.15**).

Glycolytic reprogramming in macrophages is associated with upregulation of glycolytic genes. In their transcriptomic analysis of homogenised lungs from Mtb-infected mice, Shi et al demonstrated broad upregulation of glucose transporters, glycolytic enzymes, PPP enzymes, HIF-1α and lactate exporters evident from Day 0 following aerosolised H37Rv infection [334]. At Day 0 post-infection, they report a four-fold increase in induction of the glucose transporter *Glut1*, a 10-fold increase of the glycolytic enzyme *Hk1*, a 50-fold increase in the enzyme responsible for converting pyruvate to lactate *Ldha*. In human macrophages, substantial upregulation of *SCL2A1* (the gene coding for the glucose transporter GLUT1) and *LDHA* was observed at 24 hours post-infection with iH37Rv, though this was not evident following infection with H37Ra (**Figure 3.16**). Substantial upregulation of *HK1* (the gene coding for hexokinase, the first rate-limiting step of the glycolytic pathway) was observed following infection with either viable H37Ra and non-viable iH37Rv infection (**Figure 3.16**). We also examined transcription of *PDK3* (the gene coding for pyruvate dehydrogenase kinase 3, responsible for preventing pyruvate generated through the glycolytic pathway from entering the TCA cycle) and found it to be substantially increased following infection with both H37Ra and iH37Rv (**Figure 3.16**). These results indicate that glycolytic reprogramming occurs as a result of mycobacterial PAMP-induced upregulation of glycolytic enzymes.

3.3.3 Baseline metabolic parameters of human AM

Baseline metabolic parameters of human AM as observed using extracellular flux analysis have not previously been described and were characterised by interrogation of non-smokers' AM using Seahorse XFe Analyzer. Median OCR and ECAR were 135.4 pmol.min^{-1} and 8.645 mpH.min^{-1}, respectively (**Figure 3.17**). In contrast, human MDM demonstrated a lower mean OCR and a higher mean ECAR at baseline (**Figure 3.1**), suggesting that human AM are more reliant on mitochondrial respiration rather than glycolytic metabolism, compatible with the concept of AM

demonstrating an M2-like phenotype at rest [103]. Following treatment with mitochondrial inhibitors, human AM were found to have a median SRC and GR of 147.2 pmol.min^{-1} and 7.725 mpH.min^{-1}, respectively (**Figure 3.18**), both substantially higher than those observed in human MDM experiments (**Figure 3.2**). The higher metabolic reserve of human AM may reflect the reduced *ex vivo* manipulation used in this model compared to the human MDM model, with cells plated directly onto Seahorse Biosciences plates following isolation from BAL fluid and metabolic interrogation performed 48 hours after plating (outlined in **Chapter 2, Section 2.1.1**). In the human MDM model, contrastingly, isolation from buffy coats involved a more complex protocol (outlined in **Chapter 2, Section 2.1.2**), with cells initially plated onto 12-well plates to allow differentiation over 5 days before transfer onto Seahorse Biosciences plates for metabolic interrogation on Day 7. Though similar cell viability assay was used to normalise results in both human AM and human MDM experiments, it is possible that reduced metabolic reserves of human MDM – though still viable – is a reflection of increased *ex vivo* manipulation and duration prior to interrogation. In order to further assess these observed differences in these models, parallel experiments were conducted using human AM and human MDM (**Figure 3.19**). IL-4-treated MDM were included in these experiments as previous observations demonstrated skewing away from glycolytic metabolism in these cells suggestive of an M2-like metabolic response (**Figure 3.5**). Thus it was hypothesised that human AM metabolism may correlate with that of IL-4-treated MDM, as they too are considered to behave in an M2-like fashion. In fact, results demonstrated overall increased metabolic activity in human AM compared to both untreated MDM and IL-4-treated MDM (**Figure 3.19**). However, when the ECAR/OCR ratio was calculated, human AM demonstrated similar skewing away from glycolytic metabolism at rest as IL-4-treated MDM (**Figure 3.19**). Upon interrogation of metabolic reserves, however, human AM were observed to have a substantially higher SRC and GR than both untreated and IL-4-treated MDM (**Figure 3.20**). This suggests that though human AM metabolically behave in an M2-like fashion at rest, they have substantial metabolic reserves, and are capable of increasing metabolic activity including glycolytic activity when stressed.

In agreement with this observation, stimulation with the TLR4 agonist LPS induced a shift towards glycolytic metabolism in human AM, as evidenced by significant increases in ECAR, ECAR/OCR ratio and lactate production (**Figure 3.21**). Similar to observations with human MDM, OCR was not significantly elevated but neither was it reduced as previously reported in murine macrophages (**Figure 3.21**). Correspondingly, LPS treatment induced transcriptional upregulation of glycolytic genes *SCL2A1*, *LDHA*, *PDK3* and *HK1* at 24 hours post-infection (**Figure 3.22**).

3.3.4 Mtb infection induces glycolysis in human AM

Mtb infection also induced a shift toward glycolytic metabolism in human AM, with significant increases in ECAR/OCR ratio and in lactate production observed at 24 hours post-infection (**Figure 3.23**). This shift towards glycolysis occurred in the context of increased overall metabolic activity (**Figure 3.24**), with a trend towards both increased OCR and ECAR observed (**Figure 3.23**). Again this contrasts with observations in stimulated murine macrophages, where OCR decreases as ECAR increases. Furthermore, the observed trend towards increased OCR was greater in human AM experiments (**Figure 3.23**) compared to human MDM experiments (**Figure 3.7**). One explanation for this may be the greater metabolic reserves of human AM, allowing them to accelerate overall metabolic activity to a greater extent when activated by mycobacterial PAMPs. As discussed above, this may be a result of differing experimental conditions between the two models. An alternative explanation is that the Mtb bacillus impacts intracellular metabolism in a different way in these M2-like macrophages. As mentioned, Mtb has been shown to induce M2-like responses in macrophages to allow hijacking of the cell, facilitating bacillary replication. Induction of mitochondrial respiration may therefore represent a pro-bacillary response in contrast to induction of glycolysis as an anti-bacillary mechanism.

However, following application of inhibitors, though GR was shown to be substantially reduced by infection with iH37Rv (a consequence of increased glycolytic rate), no change was observed in SRC (**Figure 3.25**). Rather, a substantial increase in Non-Mitochondrial OCR was observed (**Figure 3.25**). In fact, when Non-Mitochondrial OCR was subtracted from overall OCR, no substantial difference in Mitochondrial OCR was observed in uninfected and infected AM (**Figure 3.26**), suggesting that the observed increase in OCR is a consequence of increased Non-Mitochondrial OCR alone. Non-Mitochondrial OCR reflects all residual oxygen consumption following complete irreversible inhibition of mitochondrial respiration by addition of the Complex I and Complex III inhibitors Rotenone and Antimycin A, as outlined in **Chapter 2 (Section 2.3.1)**. It represents oxygen consumption by various intracellular oxidases, including NADPH oxidase and xanthine oxidase, both of which are upregulated in activated macrophages and serve to generate ROS and RNS, a cornerstone of the anti-microbial response. Interestingly, xanthine oxidase has been linked to IL-1β secretion in human MDM activated with various TLR agonists [476]. NADPH oxidase has previously been shown to induce macrophage cytokine secretion in response to the Mtb antigen ESAT-6 [477]. Thus the observed increases in human AM OCR following infection with Mtb likely reflect upregulation of anti-microbial cytosolic oxidase activity, with mitochondrial respiration relatively unchanged, similar to our human MDM model.

In contrast to results observed with human MDM, the shift towards glycolytic metabolism was evident from 6 hours post-infection in human AM (**Figure 3.27**). This may reflect increased sensitivity of human AM to stimulation with mycobacterial PAMPs due to baseline skewing towards mitochondrial respiration. Human MDM, conversely, are more skewed towards glycolytic metabolism at uninfected baseline (**Figure 3.19**), therefore the impact of stimulation may not become evident until later timepoints. Again contrasting to results observed in human MDM, increasing MOI resulted in a trend towards increased glycolytic reprogramming in human AM (**Figure 3.28**). This likely reflects the greater metabolic reserves of human AM (**Figure 3.20**), whereby the low MOI utilised in the basic experimental model does not increase glycolysis to maximal rates as it does in the human MDM model (**Figure 3.10**). Parallel infections with non-viable iH37Rv and with viable H37Rv were performed in human AM (**Figure 3.29**), confirming glycolytic reprogramming following infection with live Mtb in line with that observed in our iH37Rv experiments. Interestingly, similar increases in lactate production were observed with both live and killed Mtb strains in these experiments, again supporting the hypothesis that glycolytic reprogramming is a PAMP-driven phenomenon and bacillary viability is non-contributory.

3.3.5 Mtb-induced glycolytic reprogramming is mediated through TLR2/6

Mycobacterial PAMPs are known to stimulate TLR2, TLR4 and TLR9, leading to MyD88 recruitment to the intracellular TIR domain and activation of downstream signalling cascades [20]. Stimulation of TLR2, TLR3, TLR4, TLR7/8 and TLR9 have all been linked to glycolytic reprogramming in immune cells [174,238-240,247,250], thus it was hypothesised that induction of glycolysis by Mtb infection is mediated through TLR signalling. Glycolytic reprogramming has been shown specifically to play a role in IL-1β production in murine macrophages [174], and Kleinnijenhuis et al have suggested a non-redundant role for TLR2 signalling in IL-1β production in response to Mtb infection [131], with signalling through other TLRs found to be dispensable, thus investigations were targeted to TLR2.

Preliminary experiments using murine BMDM demonstrated significant impairment of infection-induced glycolytic reprogramming when TLR2 signalling was inhibited, as measured by lactate production (**Figure 3.30**). Using our human MDM model, we confirmed increased lactate production following stimulation of TLR2 using the TLR1/2 agonist P3C (**Figure 3.31**), in line with previous reports of TLR2-mediated induction of metabolic reprogramming in murine dendritic cells from the Pearce laboratory [239,240]. However, extracellular flux analyses failed to confirm this TLR2-induced glycolytic shift (**Figure 3.32**), despite TNF-α induction confirming successful

stimulation of the cells. Correspondingly, antagonism of TLR2 signalling did not alter metabolic parameters of uninfected human MDM (**Figure 3.33**). Despite this, in the setting of Mtb infection, antagonism of TLR2 signalling was observed to attenuate the shift towards glycolytic metabolism (**Figure 3.34**). This suggested that though TLR2 signalling in isolation was did not impact upon human MDM metabolism, it did play a contributory role in Mtb-induced glycolytic reprogramming.

TLR2 is known to heterodimerise with both TLR1 and TLR6 to expand its ligand spectrum [177]. As the TLR1/2 agonist P3C was not observed to induce increased glycolytic metabolism in human MDM in extracellular flux experiments, it was hypothesised that co-stimulation of TLR2 and TLR6 was required to induce glycolytic reprogramming. Stimulation of human MDM with the TLR2/6 agonist FSL-1 resulted in an increase in ECAR, ECAR/OCR ratio and lactate production (**Figure 3.35**), consistent with a shift towards glycolytic metabolism. Though dual inhibition of TLR2 and TLR6 did not significantly alter human MDM at uninfected baseline (**Figure 3.36**), Mtb-induced glycolytic reprogramming was essentially abrogated in the absence of TLR2/6 signalling (**Figure 3.37**). Thus, the glycolytic response to Mtb infection requires co-stimulation of TLR2 and TLR6.

Since completion of this work, a similar role for TLR2 in the induction of glycolytic reprogramming in PBMCs following Mtb infection has been reported by Lachmandas et al [335]. This study demonstrates that TLR2 signalling, acting through an Akt/mTOR pathway, is essential for both the shift to aerobic glycolysis and for induction of pro-inflammatory cytokines [335], supporting early observations of an essential role for Akt in glycolytic reprogramming of immune cells [239,240], as well as complimenting recent reports of mTORC-driven upregulation of glycolytic activity in activated macrophages [250]. A number of mycobacterial PAMPS including lipoarrabinomannan (LAM), phosphatidylinositol mannoside (PIM), lipoproteins and glycoproteins have been shown to stimulate these TLRs [20,178], thus further interrogation of these antigens may help elucidate the mechanism of metabolic reprogramming in Mtb infection.

3.4 CONCLUSION

The results presented in Chapter 3 offer new insights into the metabolic characteristics of primary human macrophages and their metabolic response following activation. This work demonstrates differences in baseline metabolic parameters between human MDM and human AM, with the latter relying more heavily on mitochondrial respiration at uninfected baseline – in line with paradigms aligning these cells with M2-polarised macrophages – but retaining substantial metabolic reserves that allow for a robust metabolic response following stimulation. Crucially, these results demonstrate for the first time that glycolytic reprogramming occurs in response to infection with Mtb in both human MDM and human AM *ex vivo* models, and demonstrate that this metabolic response requires co-stimulation of TLR2 and TLR6. In **Chapter 4**, interrogation of the functional consequences of this observed glycolytic shift in the human macrophage following infection with Mtb will be discussed.

CHAPTER 4:

The Functional Impact of Glycolytic Reprogramming in the Macrophage Response to Mtb Infection

4.1 Introduction

4.1.1 Hypothesis: Glycolytic reprogramming has functional consequences for Mtb-infected macrophages

Macrophage glycolytic reprogramming has been shown to play a role in a number of important macrophage functions, as summarised in **Figure 1.5**. Tannahill et al demonstrated LPS-induced aerobic glycolysis to be required for optimal IL-1β production in murine BMDM [174], and work by Palsson-McDermott et al implicates glycolytic reprogramming in both induction of IL-1β and in suppression of anti-inflammatory IL-10, again in murine BMDM [247]. Using human PBMCs, Infantino et al link citrate accumulation, a hallmark of glycolytic reprogramming, to important macrophage functions including PGE2 production, NO generation and cellular ROS generation [262]. More recently, Moon et al have described a role for glycolytic reprogramming in the generation of mROS in both murine cell line and murine peritoneal macrophage models [250]. Finally, directly anti-microbial itaconic acid is observed to accumulate in macrophages following glycolytic reprogramming [244]. The results presented in **Chapter 3** demonstrate Mtb-induced glycolytic reprogramming in human macrophages. In **Chapter 4**, the functional implication of this metabolic shift on macrophage responses to the bacillus is investigated.

4.2 Results

4.2.1 Inhibition of glycolytic reprogramming using galactose

Inhibition of glycolytic reprogramming was utilised in order to examine the functional consequences of this phenomenon. Others have utilised 2-DG, a competitive inhibitor of glycolytic enzyme HK1, to assess the role of glycolysis in macrophage function [174]. However, as outlined in **Chapter 2 (Section 2.5.1)**, preliminary experiments demonstrated significant reductions in human macrophage viability in the presence of 2-DG (**Figure 2.7**), likely to render results difficult to interpret. Galactose has successfully been used to inhibit glycolytic shift in human T cells previously [465], and initial viability studies suggested no significant differences between human MDM cultured in glucose-supplemented or galactose-supplemented media (**Figure 2.9**).

Galactose, a 6-carbon monosaccharide, must be metabolised via the cumbersome and ATP-requiring Leloir pathway in order to enter glycolysis, thus cells cultured in glucose-free galactose-supplemented media are reported to rely on glutamine-driven oxidative phosphorylation to produce ATP rather than glycolysis (summarised in **Figure 2.8**). In order to confirm this, extracellular flux analyses was utilised to investigate the baseline metabolic phenotype of human MDM cultured in glucose- or galactose-supplemented media, described in detail in **Chapter 2 (Section 2.5.2)**. Plots of ECAR relative to OCR were generated (**Figure 4.1**), demonstrating increased utilisation of oxidative phosphorylation rather than glycolysis in cells cultured in galactose-supplemented media in comparison to those cultured in glucose-supplemented media, suggesting reduced reliance on glycolytic metabolism in the presence of galactose-supplemented media.

Next, the impact of galactose-supplemented media on macrophage metabolic reserves was interrogated. As before, mitochondrial inhibitors oligomycin, FCCP and rotenone/antimycin A were added sequentially at pre-designated intervals during interrogation (**Figure 4.2**). Pooled analysis of data from 3 individual donors suggested a reduced GR in cells cultured in galactose-supplemented media, though this did not reach statistical significance (**Figure 4.2F**).

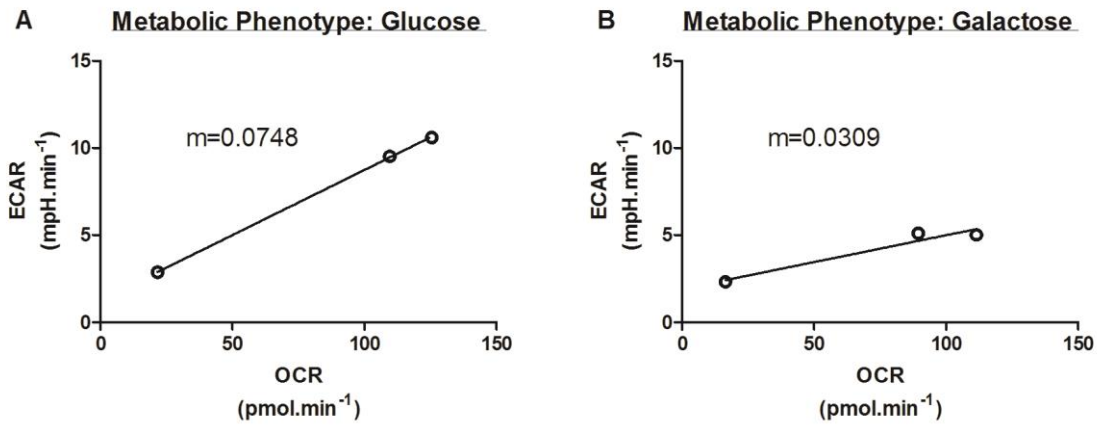

FIGURE 4.1 Cells cultured in Galactose demonstrate an altered baseline metabolic phenotype. MDM isolated from IBTS buffy coats were cultured for 5 days, scraped, and plated on Seahorse Biosciences 24-well plates at 200,000 cells/well in cRPMI. On Day 6, culture media was replaced with glucose-free RPMI supplemented with 10% human serum and with either 10mM glucose or 10mM galactose. On Day 7, cRPMI was removed and cells incubated in Seahorse media supplemented with 2mM glutamine and either 10mM glucose or 10mM galactose in a non-CO_2 incubator for 30 minutes prior to interrogation using the Seahorse XF Flux Analyzer. Following interrogation, CV assay was performed and used to normalise results. Panel A depicts baseline ECAR (y-axis) relative to OCR (x-axis) of cells cultured in Glucose-supplemented media for three individual donors. Panel B depicts baseline ECAR (y-axis) relative to OCR (x-axis) of cells cultured in Galactose-supplemented media for the same three donors.

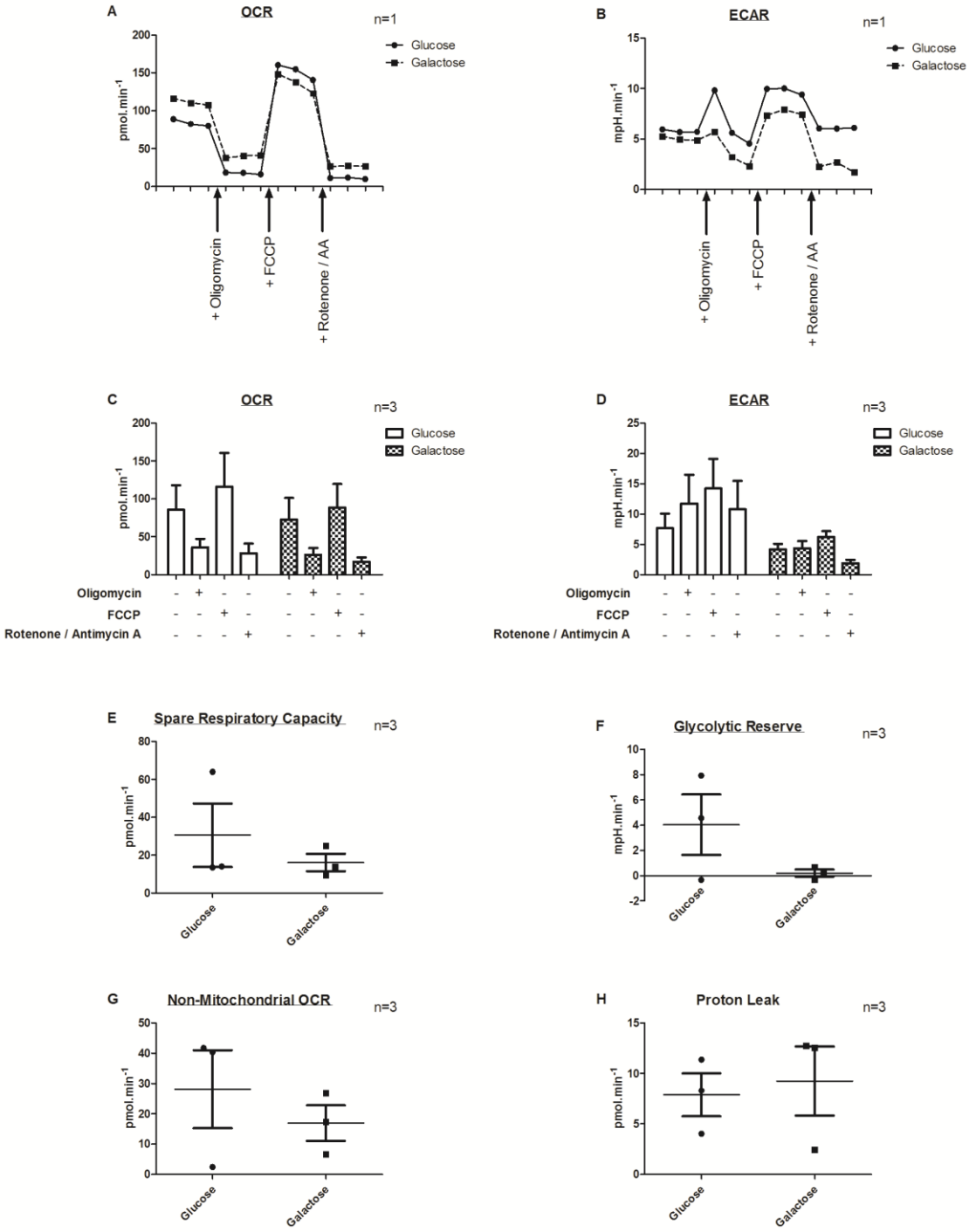

FIGURE 4.2 Cells cultured in Galactose demonstrate a reduced Glycolytic Reserve. MDM were cultured in cRPMI as before. On Day 6, culture media was replaced with either glucose- or galactose-containing media. On Day 7, extracellular flux analyses was performed in the presence of glucose- or galactose-containing Seahorse media with sequential addition of mitochondrial inhibitors oligomycin (1µM), FCCP (2µM) and rotenone/antimycin A (0.5µM), with data normalised using CV assay. Panels A and B depict real-time OCR (A) and ECAR (B) for one representative donor. Panels C and D depict normalised mean ± SEM OCR (C) and ECAR (D) for three individual donors. Panels E – H depict normalised mean ± SEM SRC (E), GR (F), Non-Mitochondrial OCR (G) and PL (H) of three individual donors. Statistical analyses were performed using the Student's t-test; statistical significance was set at $p<0.05$.

In order to confirm that use of galactose-supplemented media could be utilised to inhibit glycolytic reprogramming in activated macrophages, cells were stimulated with LPS in the presence of glucose-supplemented or galactose-supplemented media. In concordance with results presented in **Chapter 3** (**Figure 3.3**), LPS induced a trend towards increased ECAR (**Figure 4.3B**), increased ECAR/OCR ratio (**Figure 4.3C**) and increased lactate production (**Figure 4.3D**) in cells cultured in glucose-supplemented media. However, no such shift towards glycolysis was observed in galactose-treated cells (**Figure 4.3**), suggesting successful inhibition of glycolytic reprogramming. Similarly, cells cultured in glucose-supplemented media demonstrated increased lactate production following iH37Rv infection and this effect was reduced in galactose-treated cells (**Figure 4.4A**), despite similar levels of TNF-α induction confirming successful infection (**Figure 4.4B**). Galactose was also confirmed to successfully inhibit glycolytic reprogramming following infection with live H37Ra, with infection-induced increases in lactate production abrogated in cells cultured in galactose-supplemented media (**Figure 4.5**).

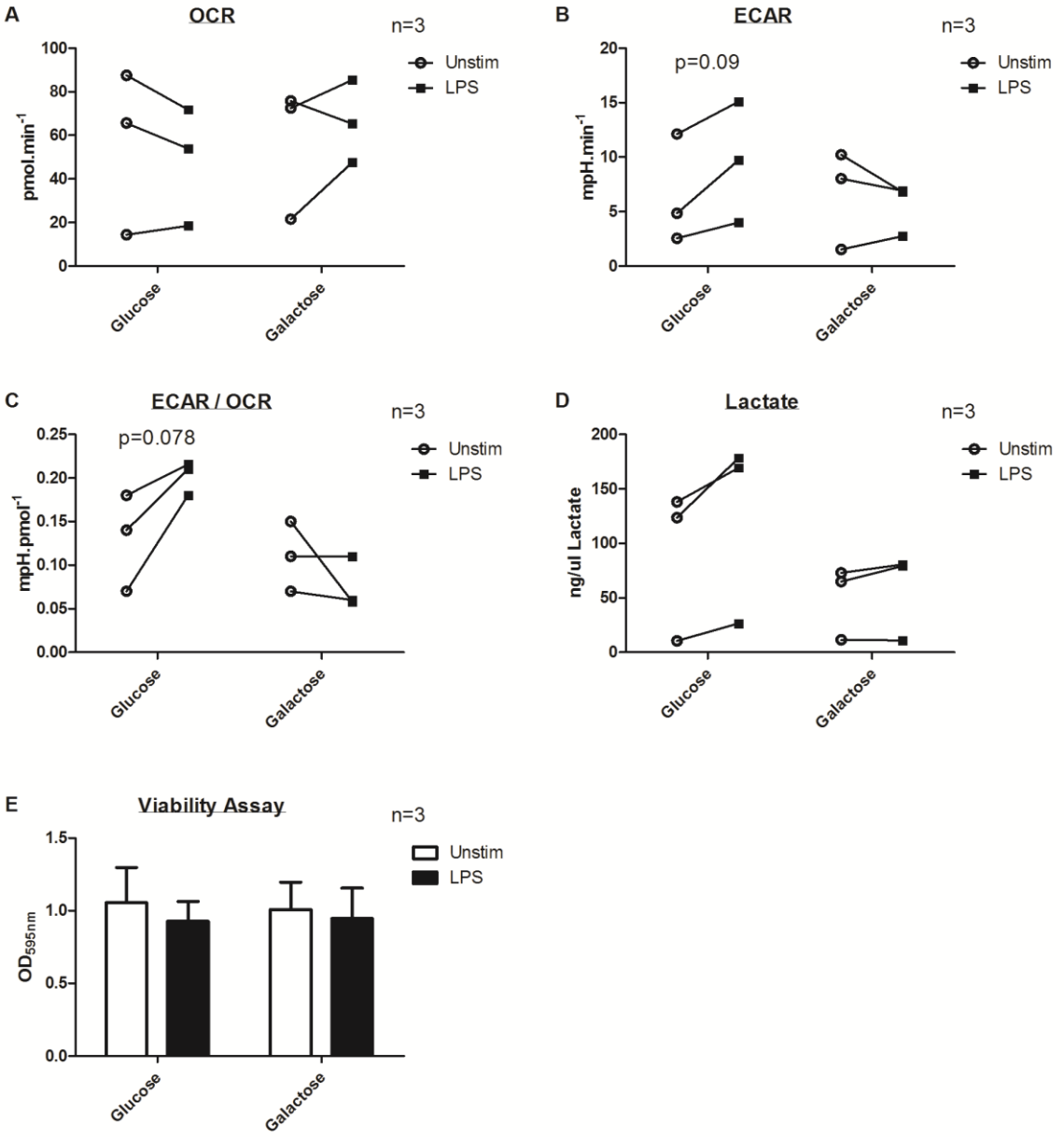

FIGURE 4.3 Cells cultured in Galactose demonstrate attenuated glycolytic response to LPS stimulation. MDM were cultured in cRPMI as before. On Day 6, culture media was replaced with either glucose- or galactose-containing media. 24 hours later, cells were treated with LPS (100ng/mL) or untreated (control). At 24 hours post-treatment, supernatants were removed and retained for lactate quantification, and extracellular flux analyses performed in glucose- or galactose-containing media, with data normalised using CV assay. Panels A – C depict OCR (A), ECAR (B) and calculated ECAR/OCR ratio (C) for three individual donors. Panel D depicts corresponding lactate concentration as measured in supernatants for three individual donors. Panel E depicts corresponding mean ± SEM absorbance following CV staining for three individual donors. Statistical analyses were performed using the paired Student's t-test; statistical significance was set at $p<0.05$.

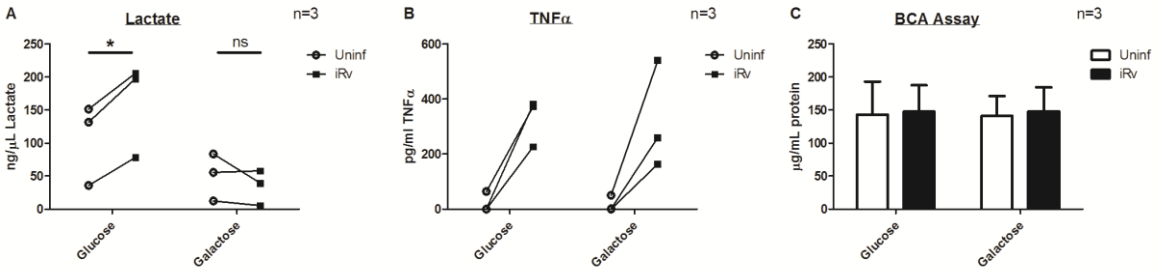

FIGURE 4.4 Cells cultured in Galactose demonstrate attenuated glycolytic response to iH37Rv infection. MDM were cultured in cRPMI as before. On Day 6, culture media was replaced with either glucose- or galactose-containing media. 24 hours later, cells were infected with iH37Rv at low MOI or left uninfected (control). At 24 hours post-infection, supernatants were removed and lactate and TNF-α concentration quantified. Cells were lysed in RIPA buffer and BCA assay used to quantify protein concentration, an indicator of cell number. Panels A and B depict measured lactate (A) and TNF-α (B) concentration for three individual donors. Panel C depicts corresponding mean ± SEM protein concentration as measured by BCA assay for the same three donors.

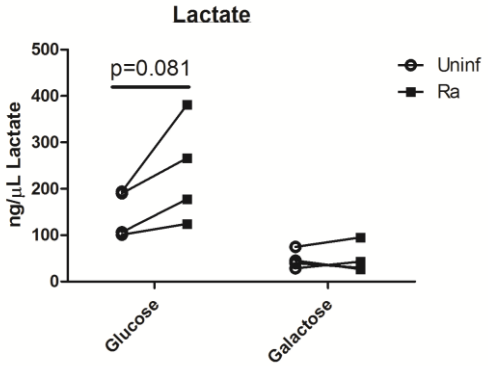

FIGURE 4.5 Cells cultured in Galactose demonstrate attenuated glycolytic response to live H37Ra infection. MDM were cultured in cRPMI as before. On Day 6, culture media was replaced with either glucose- or galactose-containing media. 24 hours later, cells were infected with H37Ra at low MOI or left uninfected (control). At 24 hours post-infection, supernatants were removed and lactate concentration quantified. Data is presented as measured lactate concentration for three individual donors. Statistical analyses were performed using the paired Student's t-test; statistical significance was set at $p<0.05$.

4.2.2 Glycolysis is required for increased intracellular ATP generation in infected human MDM

The primary role of intracellular metabolism is generation of ATP, and results presented in **Chapter 3** demonstrate increased intracellular ATP levels in human MDM following infection with Mtb (**Figure 3.14**). Thus, the impact of galactose-supplemented media on cellular ATP production was next examined, as described in **Chapter 2 (Section2.3.4)**. Cells cultured in galactose-supplemented media did not exhibit an increase in intracellular ATP levels following infection with Mtb (**Figure 4.6**), suggesting an important role for glycolysis in meeting increased energy requirements of the infected cell.

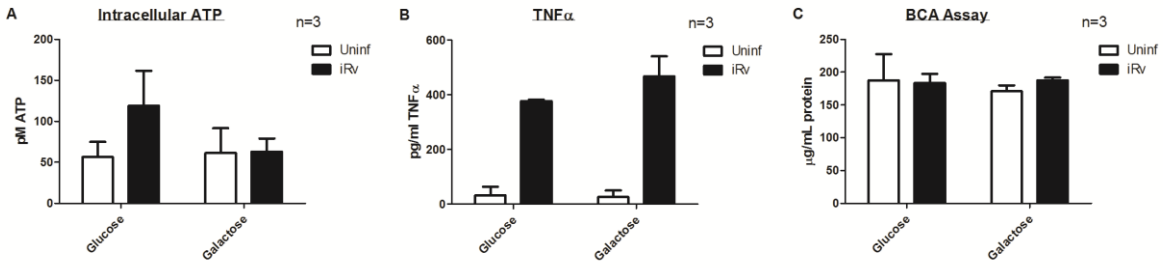

FIGURE 4.6 Cells cultured in Galactose demonstrate an attenuated increase in ATP production following iH37Rv infection. MDM were cultured in cRPMI as before. On Day 6, culture media was replaced with either glucose- or galactose-containing media. 24 hours later, cells were infected with iH37Rv at low MOI or left uninfected (control). At 24 hours post-infection, supernatants were removed and TNF-α concentration quantified. Cells were lysed and intracellular ATP concentration measured by ATP bioluminescence assay. Protein concentration in lysate was quantified by BCA assay. Panel A depicts mean ± SEM intracellular ATP concentration for three individual donors. Panels B and C depict mean ± SEM TNF-α (B) and protein (C) concentration measured in corresponding supernatants and lysates, respectively. Statistical analyses were performed using the paired Student's t-test; statistical significance was set at $p<0.05$.

4.2.3 Glycolytic reprogramming does not play a role in phagocytosis of Mtb

Next, the role of glycolysis in phagocytosis of mycobacteria was examined. 3 hours following infection with H37Ra, cells were washed to remove extracellular bacilli and lysed in 0.1% Triton X. Serial dilutions were performed, lysates plated on Middlebrook 7H10 agar and incubated in a non-CO_2 incubator at 37°C for 14 – 28 days, as described in **Chapter 2 (Section 2.4.5)**. CFU were then enumerated by counting, reflecting the number of bacilli phagocytosed by the macrophages at 3 hours post-infection. Using this approach, no difference in phagocytosis was observed between cells cultured in glucose- or galactose-supplemented media (**Figure 4.7**). This observation was further confirmed by microscopy, with iH37Rv-infected cells washed, fixed and stained using the TB Modified Auramine O Stain Kit and Hoechst 33358 (10µg/mL) in order to allow quantification of MOI, as described in **Chapter 2 (Section 2.2.1)**. **Table 4.1** summarises parameters assessed in determining MOI at 3 hours post-infection, demonstrating no difference in bacillary uptake between cells cultured in glucose- or galactose-supplemented media.

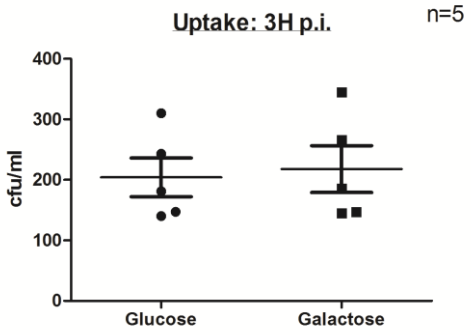

Figure 4.7: Cells cultured in Glucose and Galactose demonstrate similar levels of phagocytosis of H37Ra. MDM were cultured in cRPMI as before. On Day 6, culture media was replaced with either glucose- or galactose-containing media. 24 hours later, cells were infected with H37Ra at low MOI or left uninfected (control). At 3 hours post-infection, cells were washed to remove extracellular bacilli and lysed in sterile 0.1% Triton-X. Lysates were serially diluted in 7H9 Middlebrook Broth and plated on 7H10 Middlebrook agar in triplicate. Agar plates were incubated for 14 – 28 days and CFU enumerated by counting. Data is presented as mean ± SEM CFU for five individual donors. Statistical analyses were performed using the paired Student's t-test; statistical significance was set at $p<0.05$.

	GLUCOSE				GALACTOSE			
Donor	*D1*	*D2*	*D3*	*Mean*	*D1*	*D2*	*D3*	*Mean*
No. Cells	10.7	8.7	17.0	**12.1**	10.3	8.3	15.0	**11.2**
% Infected	60.0	67.7	46.7	**58.1**	44.3	60.3	57.0	**53.9**
Bugs/Cells	1.1	1.2	1.0	**1.1**	1.2	1.1	1.1	**1.1**
Range	0 - 5	0 - 4	0 - 5	**0 - 5**	0 - 6	0 - 6	0 - 5	**0 - 6**

Table 4.1: Cells cultured in Glucose and Galactose demonstrate similar levels of phagocytosis of iH37Rv. MDM were cultured in cRPMI as before. On Day 6, culture media was replaced with either glucose- or galactose-containing media. 24 hours later, cells were infected with iH37Rv at low MOI or left uninfected (control). At 3 hours post-infection, cells were washed to remove extracellular bacilli and fixed with 2% paraformaldehyde. Cells were stained with the TB Modified Auramine O Stain Kit and Hoechst 33358 (10µg/mL), and microscopy was performed using an inverted fluorescent microscope. Multiplicity of infection (MOI) determined through examination of five separate fields for each donor. Table depicts parameters used in assessing multiplicity of infection for three individual donors.

4.2.4 Glycolytic reprogramming is required for optimal IL-1β production in Mtb-infected human MDM and AM

Glycolytic reprogramming has been implicated in IL-1β production in murine macrophages, both at a transcriptional level [174] and for post-translational modification into mature IL-1β [250]. Given that IL-1β is a crucial cytokine in the macrophage response to Mtb infection [133,134,139,143-146], the role of infection-induced glycolytic reprogramming on its induction and secretion was investigated.

Human MDM were isolated and cultured in 12-well plates, treated with glucose- or galactose-supplemented media on Day 6, and infected with Mtb on Day 7 as previously described. Cells were lysed 24 hours post-infection, relative mRNA expression quantified as described in **Chapter 2 (Section 2.4.1)**, and secreted cytokine levels measured in retained supernatants. Glycolytic inhibition using galactose resulted in attenuated transcription of *IL1B* (**Figure 4.8A**) and attenuated levels of mature IL-1β (**Figure 4.8C**) in human MDM infected with either live avirulent H37Ra or killed iH37Rv. As previously observed by Tannahill et al in murine BMDM [174], glycolytic inhibition did not impact upon *TNFA* transcription (**Figure 4.8B**), nor were secreted TNF-α levels affected (**Figure 4.8D**). This effect of glycolytic inhibition on IL-1β levels was evident up to 72 hours post-infection (**Figure 4.9A**). Interestingly, while glycolytic inhibition did not affect TNF-α levels at earlier timepoints post-infection, increased production of TNF-α was observed in galactose-treated cells at 72 hours post-infection (**Figure 4.9B**).

Similarly, glycolytic inhibition using galactose-supplemented media was associated with a trend towards attenuated IL-1β production in human AM infected with H37Ra or treated with LPS (100ng/mL) (**Figure 4.10A**), while TNF-α levels were not affected (**Figure 4.10B**).

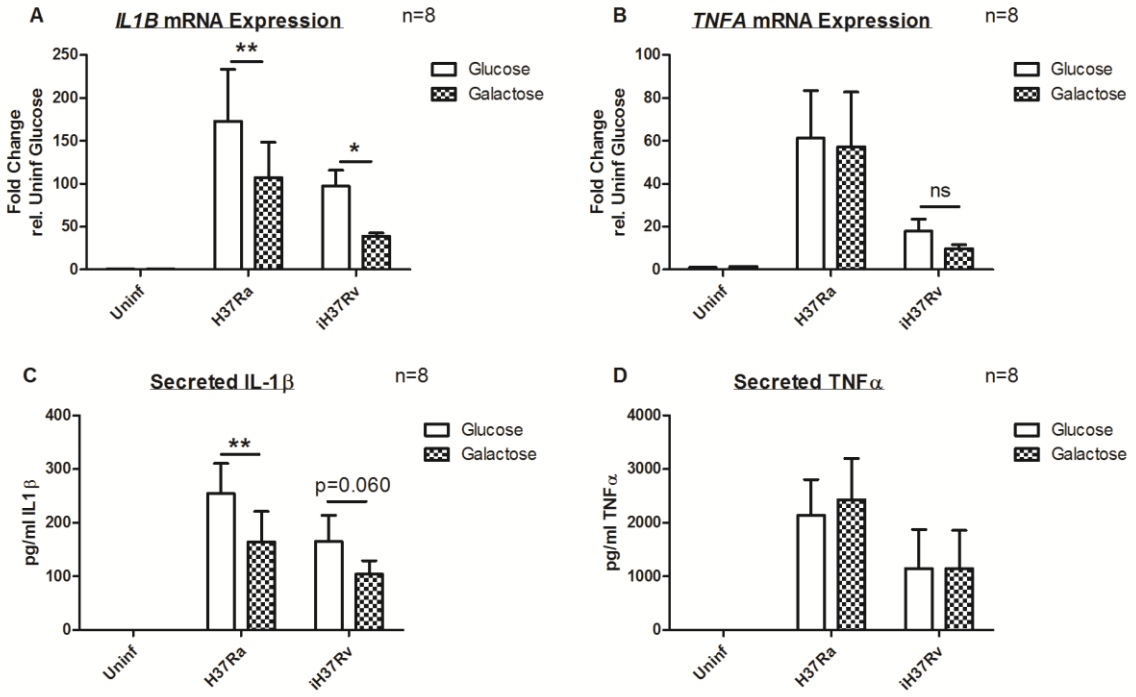

FIGURE 4.8 Glycolysis is required for optimal production of IL-1β in Mtb-infected human MDM. MDM were cultured in cRPMI as before. On Day 6, culture media was replaced with either glucose- or galactose-containing media. 24 hours later, cells were infected with H37Ra at low MOI, iH37Rv at low MOI or left uninfected (control). At 24 hours post-infection, supernatants were removed and retained for IL-1β and TNF-α concentration quantification. Cells were lysed in RLT buffer, RNA extracted and cDNA generated, and qPCR was performed. Data was normalised to *18S* and mRNA expression fold-change relative to uninfected calculated using the $2^{-\Delta\Delta Ct}$ method. Panels A and B depict relative mRNA expression of IL1B (A) and TNFA (B). Panels C and D depict corresponding IL-1β (C) and TNF-α (D) concentrations measured in retained supernatants by ELISA. Data is presented as mean ± SEM results for 8 individual donors. Statistical analyses were performed using the paired Student's t-test. *p<0.05, **p<0.01.

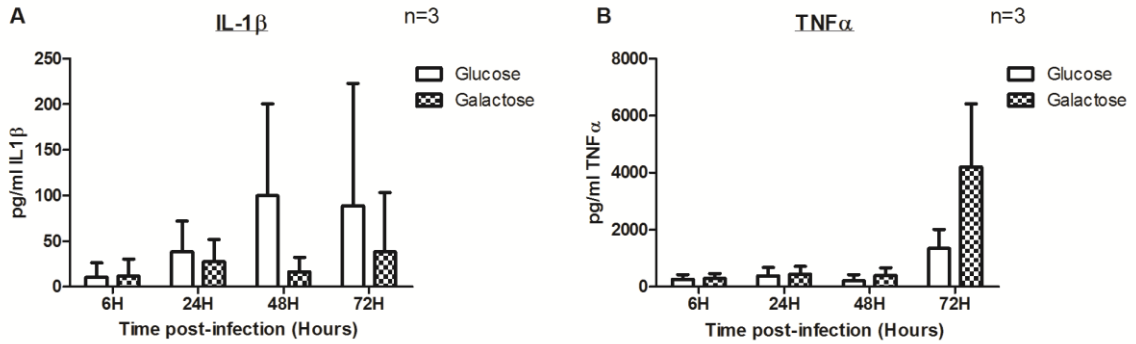

FIGURE 4.9 Glycolysis is required for optimal production of IL-1β up to 72 hours post-infection. MDM were cultured in cRPMI as before. On Day 6, culture media was replaced with either glucose- or galactose-containing media. 24 hours later, cells were infected with H37Ra at low MOI or left uninfected (control). At indicated timepoints post-infection, supernatants were removed and cytokine concentrations quantified by ELISA. Panels A and B depict mean ± SEM IL-1β (A) and TNF-α (B) concentration for three individual donors. Statistical analyses were performed using the paired Student's t-test; statistical significance was set at $p<0.05$.

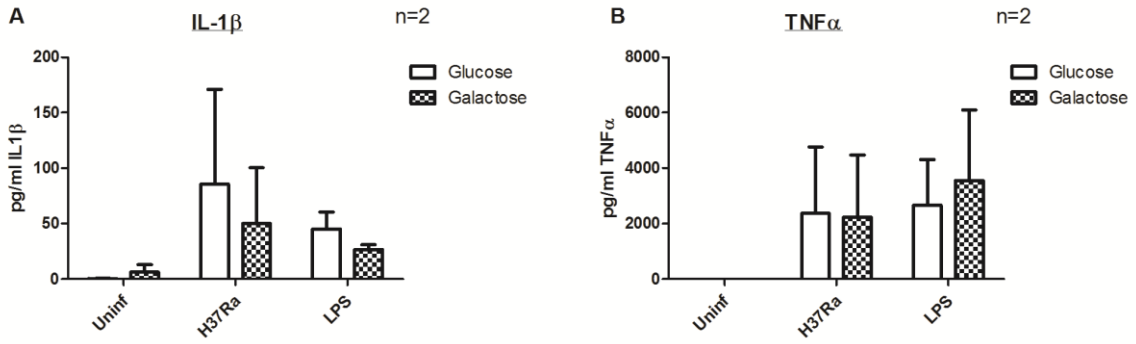

FIGURE 4.10 Glycolysis is required for optimal production of IL-1β in Mtb-infected human AM. Human AM were isolated and cultured in cRPMI supplemented with cefotaxime (50µg/mL) and fungizone (50U/mL). 24 hours after plating, culture media was replaced with either glucose- or galactose-containing antibiotic-supplemented media. 24 hours later, cells were treated with LPS (100ng/mL), infected with H37Ra at low MOI or left unstimulated (control). At 24 hours post-treatment/infection, supernatants were removed and cytokine concentrations quantified by ELISA. Panels A and B depict mean ± SEM IL-1β (A) and TNF-α (B) concentration for 2 individual donors.

In order to rule out IL-1-mediated induction of glycolytic reprogramming as a potential explanation for the observed association between glycolysis and increased IL-1β production, experiments were performed using an anti-IL-1β antibody, as described in **Chapter 2 (Section 2.6.2)**. Briefly, glucose- or galactose-cultured human MDM were treated with anti-IL-1β or with control IgG for one hour prior to infection with H37Ra, and these treatments were reapplied following the 3-hour wash step of infection. At 24 hours post-infection, supernatants were removed and lactate quantified by Lactate Assay. Inhibition of IL-1β signalling did not impact upon lactate production (**Figure 4.11**), confirming that increased IL-1β production occurs downstream of glycolytic reprogramming.

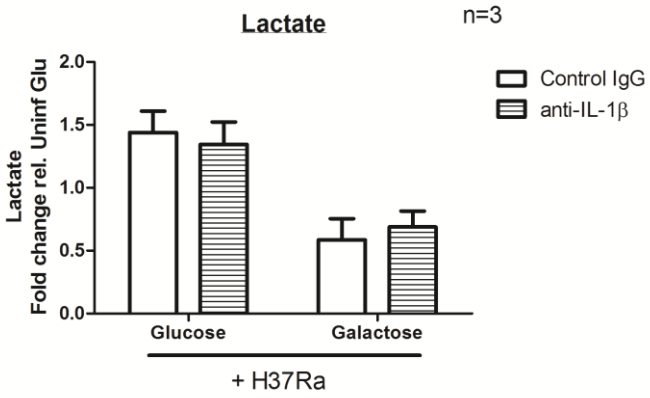

FIGURE 4.11 IL-1β signalling is not required for glycolytic reprogramming following Mtb infection. MDM were cultured in cRPMI as before. On Day 6, culture media was replaced with either glucose- or galactose-containing media. 24 hours later, cells were treated with anti-IL-1β antibody (0.1µg/mL) or IgG control antibody (0.1µg/mL). One hour later, cells were infected with H37Ra at low MOI or left uninfected (control). 24 hours post infection, supernatants were removed and lactate concentration quantified. Data is presented as mean ± SEM lactate concentration for 3 individual donors. Statistical analyses were performed using the paired Student's t-test; statistical significance was set at $p<0.05$.

Extracellular ATP is known to activate the NLRP3 inflammasome via P2RX7 stimulation [185,186]. Although extracellular ATP was undetectable in this model – possibly the result of a low MOI inducing minimal cell death – glycolysis was implicated in upregulation of intracellular ATP generation following Mtb infection (**Figure 4.6**). Thus, in order to confirm that this increased intracellular ATP generation was not responsible for increased IL-1β production, infections were performed in the presence of oxidised ATP (oATP), an irreversible inhibitor of P2RX7. IL-1β production was unaffected by inhibition of P2RX7 (**Figure 4.12**), confirming that this pathway is not required for IL-1β production within this model. Contrastingly, inhibition of caspase-1 YVAD did attenuate IL-1β production, confirming the inflammasome-dependence of the observed IL-1β production (**Figure 4.12**).

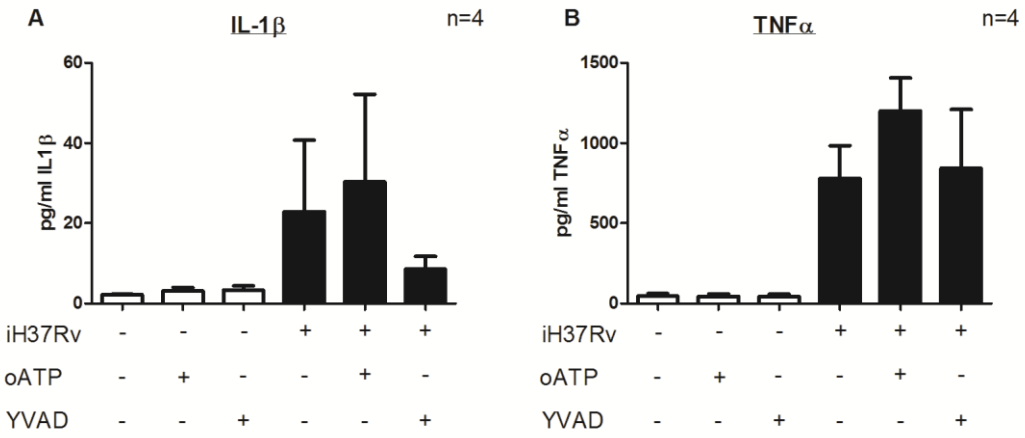

FIGURE 4.12 IL-1β production does not require ATP signalling in Mtb infected macrophages. MDM were cultured in cRPMI as before. On Day 7, cells were treated with oATP (300μM), YVAD (100μM) or left untreated (control) one hour prior to infection with iH37Rv at low MOI. At 24 hours post-infection, supernatants were removed and cytokine concentration quantified by ELISA. Panels A and B depict mean ± SEM IL-1β (A) and TNF-α (B) concentration for 4 individual donors. Statistical analyses were performed using the paired Student's t-test; statistical significance was set at $p<0.05$.

4.2.5 Glycolysis-driven IL-1β augments PGE2 production and suppresses IL-10 production in Mtb-infected human MDM

Next, a panel of genes important in early M1 macrophage function was investigated in order to determine the role of glycolytic reprogramming on their expression (**Figure 4.13**). *PTGS2*, which codes for the enzyme COX2 (responsible for PGE2 generation), has recently been implicated downstream of IL-1β in early macrophage responses to Mtb infection [146]. *IL1A* codes for pro-inflammatory IL-1α, a member of the IL-1 family of cytokines alongside IL-1β [138], and it is likely that IL-1α and IL-1β synergistic signalling is required for optimal host defence in Mtb infection [139], though various studies have suggested the importance of one above the other [134,149]. *IL12A*, coding for IL-12, is crucial for the development of adaptive immunity and has previously been implicated as a downstream target of IL-1 signalling [133,134,188]. *IL18*, coding for IL-18, similarly plays a role in activation of Th1 cell responses to mycobacterial infection [478], and recently a role for glycolytic reprogramming in its production has been described [250]. *IL10*, coding for anti-inflammatory IL-10, appears to be suppressed by glycolysis, with PKM2 activators inducing upregulation of this cytokine concomitant with downregulation of IL-1β in LPS-stimulated murine macrophages [247]. Finally, *NOS2*, the gene coding for iNOS, plays an important role in generation of mycobactericidal NO.

As before, cells were pre-treated for 24 hours with glucose- or galactose-supplemented media prior to infection with H37Ra (**Figure 4.13A**) or iH37Rv (**Figure 4.13B**), cells lysed at 24 hours post-infection, and relative mRNA expression quantified , as described in **Chapter 2 (Section 2.4.1)**. At the timepoint assessed, induction of the majority of these genes was minimal with no substantial differences observed between glucose- and galactose-treated cells (**Figure 4.13**). However, a trend towards decreased *PTGS2* following glycolytic inhibition with galactose was observed for both H37Ra- and iH37Rv-infected macrophages (**Figure 4.13; Figure 4.14**).

In order to further assess this observed trend towards reduced *PTGS2* transcription when glycolytic reprogramming was inhibited, experiments assessing PGE2 production were performed. PGE2 is the eicosanoid product of the reaction catalysed by COX2 (the enzyme coded for by *PTGS2*). As before, cells were treated with glucose- or galactose-supplemented media for 24 hours, infected with H37Ra, and supernatants harvested at 24 hours post-infection. PGE2 concentration was measured using ELISA, as described in **Chapter 2 (Section 2.4.3)**. Glycolytic inhibition was associated with attenuated PGE2 production (**Figure 4.15A**), concomitant with observed reduction in IL-1β production (**Figure 4.15B**), while TNF-α levels remained unaffected (**Figure 4.15C**), suggesting that aerobic glycolysis is required for optimal production of PGE2.

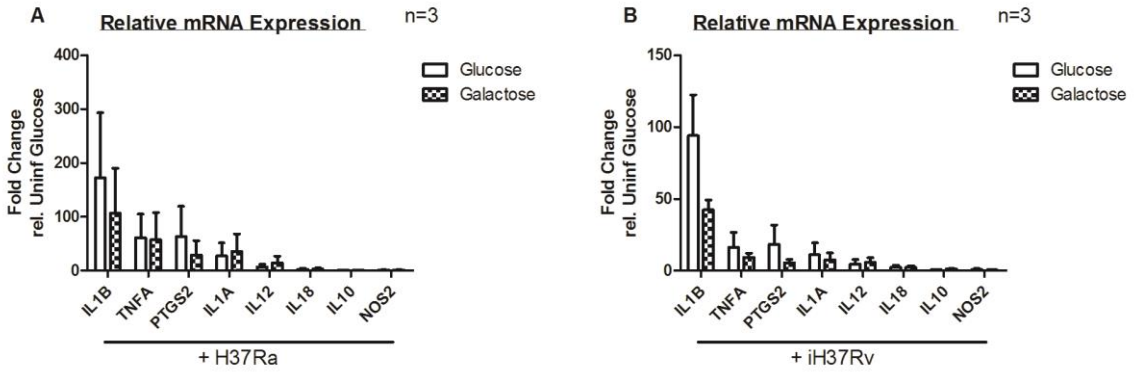

FIGURE 4.13 Inhibition of glycolytic reprogramming does not significantly alter the transcription of other important macrophage cytokines in Mtb infection. MDM were cultured in cRPMI as before. On Day 6, culture media was replaced with either glucose- or galactose-containing media. 24 hours later, cells were infected with H37Ra at low MOI, iH37Rv at low MOI or left uninfected (control). At 24 hours post-infection, cells were lysed in RLT buffer, RNA extracted and cDNA generated, and qPCR was performed. Data was normalised to *18S* and mRNA expression fold-change relative to uninfected calculated using the $2^{-\Delta\Delta Ct}$ method. Panels A and B depict mean ± SEM relative mRNA expression fold-change of indicated genes following infection with H37Ra (A) or iH37Rv (B) for three individual donors. Statistical analyses were performed using the paired Student's t-test; statistical significance was set at $p<0.05$.

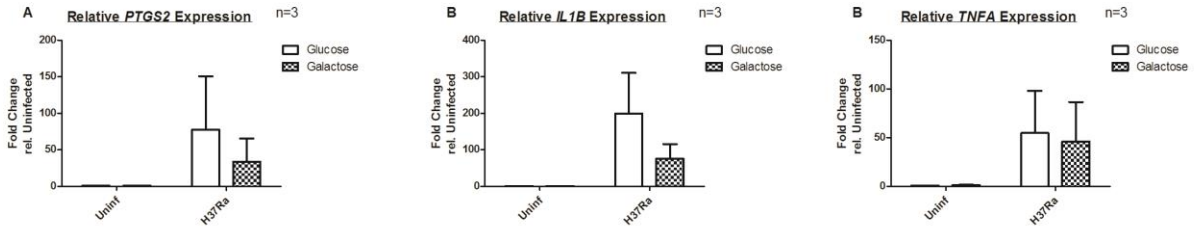

FIGURE 4.14 Glycolysis is required for optimal PTGS2 transcription in Mtb-infected macrophages. MDM were cultured in cRPMI as before. On Day 6, culture media was replaced with either glucose- or galactose-containing media. 24 hours later, cells were infected with H37Ra at low MOI or left uninfected (control). At 24 hours post-infection, cells were lysed in RLT buffer, RNA extracted and cDNA generated, and qPCR was performed. Data was normalised to *18S* and mRNA expression fold-change relative to uninfected calculated using the $2^{-\Delta\Delta Ct}$ method. Panels A – C depict mean ± SEM relative mRNA expression fold-change of PTGS2 (A), IL1B (B) and TNFA (C) for 3 individual donors. Statistical analyses were performed using the paired Student's t-test; statistical significance was set at $p<0.05$.

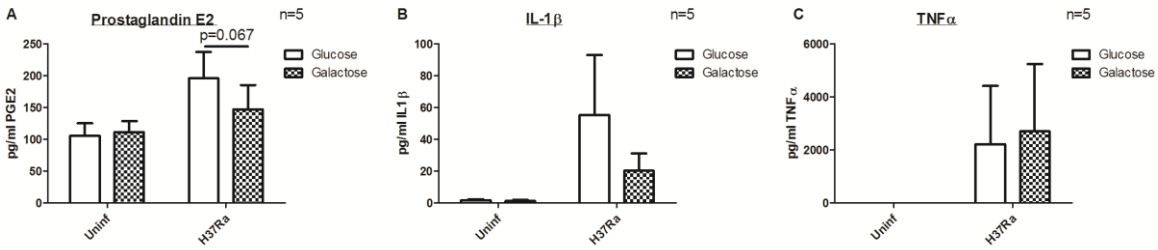

FIGURE 4.15 Glycolysis is required for optimal PGE2 production by Mtb-infected macrophages. MDM were cultured in cRPMI as before. On Day 6, culture media was replaced with either glucose- or galactose-containing media. 24 hours later, cells were infected with H37Ra at low MOI or left uninfected (control). At 24 hours post-infection, supernatants were removed and eicosanoid and cytokine concentration quantified by ELISA. Panels A – C depict mean ± SEM PGE2 (A), IL-1β (B) and TNF-α (C) concentration for 5 individual donors. Statistical analyses were performed using the paired Student's t-test; statistical significance was set at $p<0.05$.

Mayer-Barber et al have previously described IL-1β-mediated upregulation of PGE2, which they demonstrated to be necessary for control of both intracellular and extracellular bacillary growth by infected macrophages [146]. Thus, it was hypothesised that the impact of glycolytic reprogramming on PGE2 production may in fact be mediated via alteration in IL-1β levels. To investigate this, macrophages were again pre-treated with glucose- or galactose-supplemented media for 24 hours prior to infection with H37Ra. One hour prior to infection, cells were treated with anti-IL-1β antibody to inhibit IL-1 signalling, or with control IgG. Treatments were reapplied following the 3-hour wash step of the infection protocol, and supernatants were removed and PGE2 levels quantified at 24 hours post-infection. Inhibition of glycolysis using galactose and inhibition of IL-1 signalling using anti-IL-1β antibody reduced PGE2 production to a similar extent (**Figure 4.16**). Similarly, the impact of glycolytic inhibition on PGE2 production was attenuated – though not completely abrogated – in the absence of IL-1β signalling (**Figure 4.16**), suggesting that glycolytic induction of PGE2 is at least partly mediated through increased IL-1β production.

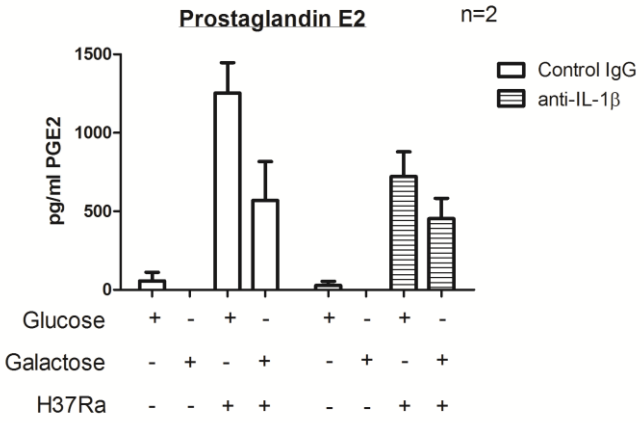

FIGURE 4.16 Glycolytic induction of PGE2 secretion is mediated through increased IL-1β signalling. MDM were cultured in cRPMI as before. On Day 6, culture media was replaced with either glucose- or galactose-containing media. 24 hours later, cells were treated with anti-IL-1β antibody (0.1µg/mL) or IgG control antibody (0.1µg/mL). One hour later, cells were infected with H37Ra at low MOI or left uninfected (control). 24 hours post-infection, supernatants were removed and PGE2 concentration quantified by ELISA. Data is presented as mean ± SEM PGE2 concentration for 2 individual donors.

Though *IL10* mRNA was not detectable at 24 hours post-infection, others have described upregulation of IL-10 following glycolytic inhibition with reciprocal downregulation of IL-1β. In order to investigate this further, secreted IL-10 levels were measured by ELISA in supernatants of glucose- and galactose-treated human MDM 24 hours post-infection with H37Ra or iH37Rv. In both cases, significant induction of IL-10 was observed following glycolytic inhibition (**Figure 4.17A**) and this was coupled to downregulation of IL-1β (**Figure 4.17B**), with no change in TNF-α levels (**Figure 4.17C**). In order to investigate a possible role for IL-1 signalling in this apparent suppression of IL-10 by aerobic glycolysis, experiments were performed using an anti-IL-1β antibody, as described above. Firstly, we demonstrated that inhibition of IL-1β signalling induces IL-10 production (**Figure 4.18**), confirming a role for IL-1β in suppression of the anti-inflammatory cytokine. Proceeding to experiments involving inhibition of glycolysis and inhibition of IL-1 signalling, both galactose and anti-IL-1β treatment induced IL-10 production to a similar extent (**Figure 4.19**). Furthermore, the impact of glycolytic inhibition on IL-10 production was completely abrogated in the absence of IL-1β signalling (**Figure 4.19**), suggesting that suppression of IL-10 production by glycolysis is mediated through increased IL-1β levels.

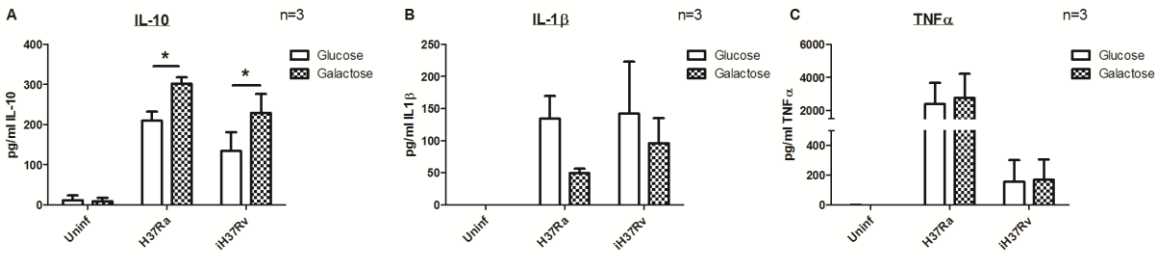

FIGURE 4.17 Glycolysis suppresses IL-10 production in Mtb-infected macrophages. MDM were cultured in cRPMI as before. On Day 6, culture media was replaced with either glucose- or galactose-containing media. 24 hours later, cells were infected with H37Ra at low MOI, iH37Rv at low MOI or left uninfected (control). At 24 hours post-infection, supernatants were removed and cytokine concentration quantified by ELISA. Paenls A – C depict mean ± SEM IL-10 (A), IL-1β (B) and TNF-α (C) concentration for 3 individual donors. Statistical analyses were performed using the paired Student's t-test; *p<0.05.

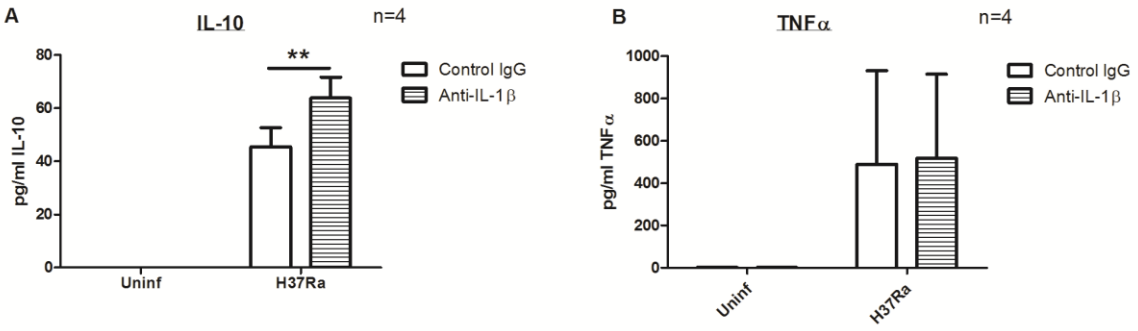

FIGURE 4.18 IL-1β signalling suppresses IL-10 production in Mtb-infected macrophages. MDM were cultured in cRPMI as before. On Day 7, cells were treated with anti-IL-1β antibody (0.1μg/mL) or IgG control antibody (0.1μg/mL). One hour later, cells were infected with H37Ra at low MOI or left uninfected (control). 24 hours post-infection, supernatants were removed and cytokine concentration quantified by ELISA. Panels A and B depict mean ± SEM IL-10 (A) and TNF-α (B) concentration for 4 individual donors. Statistical analyses were performed using the paired Student's t-test; **p<0.01.

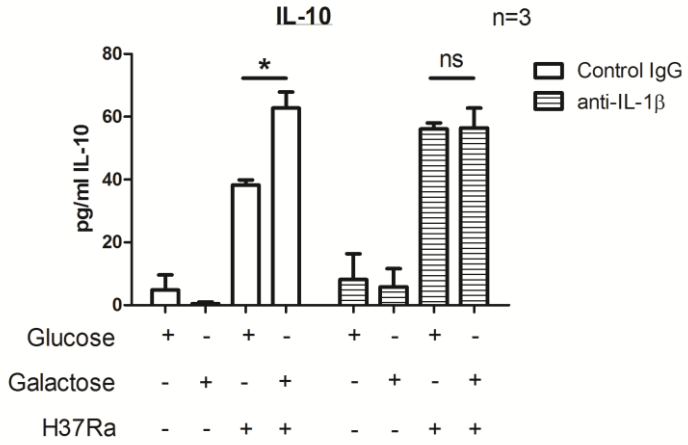

FIGURE 4.19 Glycolytic suppression of IL-10 production is mediated through increased IL-1β signalling. MDM were cultured in cRPMI as before. On Day 6, culture media was replaced with either glucose- or galactose-containing media. 24 hours later, cells were treated with anti-IL-1β antibody (0.1μg/mL) or IgG control antibody (0.1μg/mL). One hour later, cells were infected with H37Ra at low MOI or left uninfected (control). 24 hours post-infection, supernatants were removed and IL-10 concentration quantified by ELISA. Data is presented as mean ± SEM IL-10 concentration for 3 individual donors. Statistical analyses were performed using the paired Student's t-test; *p<0.05.

4.2.6 Glycolysis induces cellular ROS generation in Mtb-infected human MDM

Cellular ROS can have both bactericidal effects and host-damaging effects. In order to investigate the role of glycolytic reprogramming in the generation of cellular ROS in Mtb-infected macrophages, a DFCDA Cellular ROS Detection Assay was utilised. The methodology employed is described in detail in **Chapter 2 (Section 2.4.4)**. Infection with iH37Rv induced a 2-fold increase in cellular ROS detected, and this was almost completely abrogated when glycolytic reprogramming was inhibited using galactose (**Figure 4.20**), suggesting a crucial role for the glycolytic shift in ROS generation.

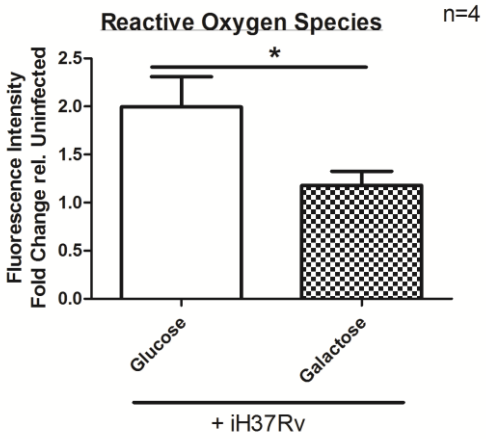

FIGURE 4.20 Glycolysis is required for optimal production of reactive oxygen species in Mtb infected macrophages. MDM were cultured in cRPMI as before. On Day 6, culture media was replaced with either glucose- or galactose-containing media. 24 hours later, cells were infected with iH37Rv at low MOI. At 24 hours post-infection, cells were transferred to a black clear-bottomed 96-well plate and allowed to adhere overnight prior to quantification of ROS activity using the DCFDA Cellular ROS Detection Assay Kit (Abcam). Data depict mean ± SEM fold change in detected fluorescence intensity relative to uninfected control for that condition for 4 individual donors. Statistical analyses were performed using the paired Student's t-test; *$p<0.05$.

4.2.7 Glycolysis is required for optimal bacillary clearance by infected human MDM and AM

Having established a role for glycolysis in induction of IL-1β and PGE2, and in suppression of IL-10, in Mtb-infected macrophages, the functional significance of these effects in terms of early bacillary clearance by the cell was next examined. First the direct impact of our glycolytic inhibitor, galactose, on H37Ra growth in culture was assessed, as this could prove a potential confounder in bacillary killing assays. H37Ra was prepared as previously described, and applied to tissue-culture plate wells containing glucose-free RPMI supplemented with 10mM glucose or 10mM galactose, in the absence of macrophages, and incubated at 37°C. At 3 hours and at 72 hours following application, a sample from each well was removed, diluted, and plated on Middlebrook 7H10 agar. CFU were enumerated 14 – 28 days later, and fold change at 72H relative to 3H calculated for each condition. No difference in H37Ra growth between glucose- and galactose-supplemented RPMI was observed at 72 hours (**Figure 4.21**).

Next, bacillary killing assays were performed, as outlined in detail in **Chapter 2 (Section 2.4.6)**. Inhibition of glycolysis using galactose substantially impaired clearance of H37Ra by human MDM as evidenced by significantly increased absolute CFU count at 72 hours post-infection (**Figure 4.22A**), significantly increased CFU fold change at 72 hours (**Figure 4.22B**) and significantly increased fold change in 72 hour CFU count relative to 72 hour CFU count of glucose control (**Figure 4.22C**). Similarly a trend towards impaired clearance of both avirulent H37Ra (**Figure 4.23**) and virulent H37Rv (**Figure 4.24**) following inhibition of glycolysis was observed in infected human AM.

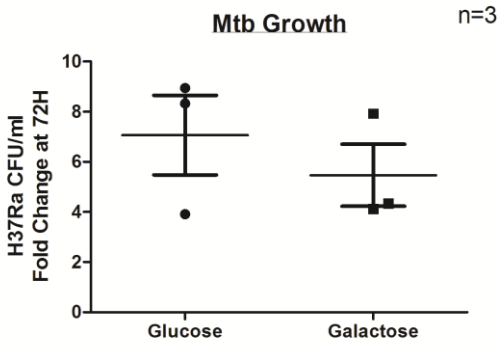

FIGURE 4.21 Galactose-supplemented media does not directly impact upon Mtb growth. H37Ra was grown to log phase in Middlebrook 7H9 broth. Mtb were centrifuged, resuspended in glucose-free RPMI, and passed through a 25-guage needle 10 times to remove clumps. 5µL of the prepared Mtb suspension was added to each well of a 12-well plate containing either glucose- or galactose-supplemented RPMI with no cells. 3 hours later, 50µL was removed from each well, serial dilutions performed, and suspension plated on Middlebrook 7H10 agar. Mtb was incubated for 72 hours at 37°C and then a further 50µL removed from each well, serial dilutions performed, and suspension plated on Middlebrook 7H10 agar. Agar plates were incubated for 14 days in a non-CO_2 incubator before enumeration of CFU by counting. Data is presented as mean ± SEM fold change in CFU at 72 hours relative to 3 hours for three separate experiments. Statistical analyses were performed using the unpaired Student's t-test; statistical significance was set at $p<0.05$.

FIGURE 4.22 Glycolysis is required for optimal clearance of H37Ra by human MDM. MDM were cultured in cRPMI as before. On Day 6, culture media was replaced with either glucose- or galactose-containing media. 24 hours later, cells were infected with H37Ra at low MOI. At 3 hours post-infection, all cells were washed to remove extracellular bacilli. Designated cells were lysed in sterile 0.1% Triton-X and lysates were serially diluted in 7H9 Middlebrook Broth and plated on 7H10 Middlebrook agar in triplicate. The remaining cells were incubated for 72 hours prior to lysis, dilution and plating. Agar plates were incubated for 14 – 28 days and CFU enumerated by counting. Panels depict absolute CFU count for 3H and 72H (A), fold change in CFU count for 72H relative to corresponding 3H count (B) and fold change in 72H CFU count relative to 72H glucose control CFU count (C). Data depict mean ± SEM for 9 individual donors. Statistical analyses were performed using the paired Student's t-test; *$p<0.05$, **$p<0.01$.

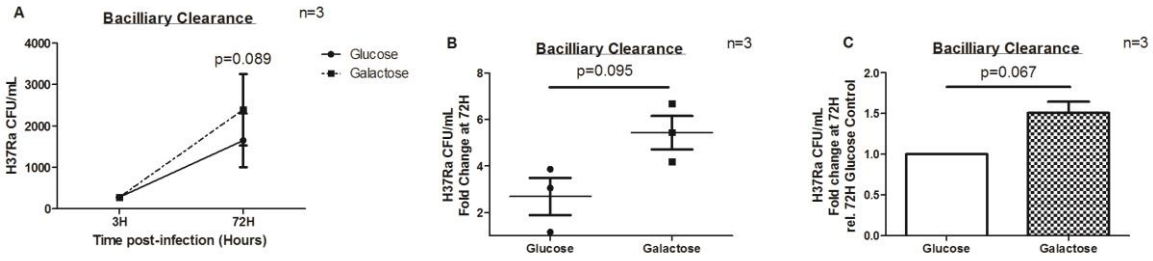

FIGURE 4.23 Glycolysis is required for optimal clearance of H37Ra by human AM. Human AM were plated in antibiotic-supplemented cRPMI as before. 24 hours after plating, culture media was replaced with either glucose- or galactose-containing antibiotic-free media. 24 hours later, cells were infected with H37Ra at low MOI. At 3 hours post-infection, all cells were washed to remove extracellular bacilli. Designated cells were lysed in sterile 0.1% Triton-X and lysates were serially diluted in 7H9 Middlebrook Broth and plated on 7H10 Middlebrook agar in triplicate. The remaining cells were incubated for 72 hours prior to lysis, dilution and plating. Agar plates were incubated for 14 – 28 days and CFU enumerated by counting. Panels depict absolute CFU count for 3H and 72H (A), fold change in CFU count for 72H relative to corresponding 3H count (B) and fold change in 72H CFU count relative to 72H glucose control CFU count (C). Data depict mean ± SEM for 3 individual donors. Statistical analyses were performed using the paired Student's t-test; statistical significance was set at $p<0.05$.

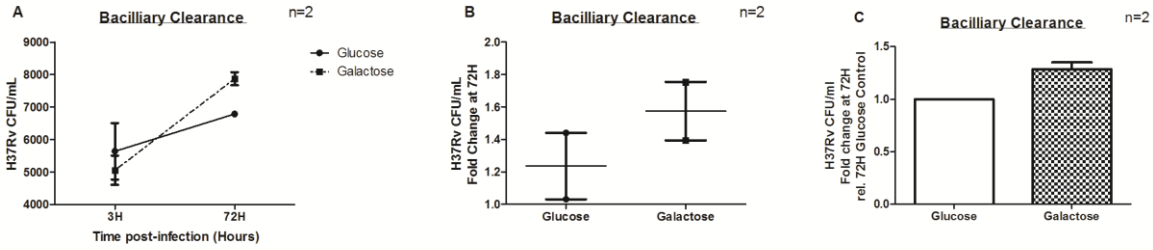

FIGURE 4.24 Glycolysis is required for optimal clearance of H37Rv by human AM. Human AM were plated in antibiotic-supplemented cRPMI as before. 24 hours after plating, culture media was replaced with either glucose- or galactose-containing antibiotic-free media. 24 hours later, cells were infected with H37Rv at low MOI. At 3 hours post-infection, all cells were washed to remove extracellular bacilli. Designated cells were lysed in sterile 0.1% Triton-X and lysates were serially diluted in 7H9 Middlebrook Broth and plated on 7H10 Middlebrook agar in triplicate. The remaining cells were incubated for 72 hours prior to lysis, dilution and plating. Agar plates were incubated for 14 – 28 days and CFU enumerated by counting. Panels depict absolute CFU count for 3H and 72H (A), fold change in CFU count for 72H relative to corresponding 3H count (B) and fold change in 72H CFU count relative to 72H glucose control CFU count (C). Data depict mean ± SEM for two individual donors. Statistical analyses were performed using the paired Student's t-test; statistical significance was set at $p<0.05$.

4.2.8 Glycolysis-induced bacillary clearance is mediated through IL-1β induction

Next, the potential functional link between glycolysis-induced IL-1β production and glycolysis-induced bacillary clearance was assessed. First, bacillary killing assays were performed in the presence or absence of exogenous recombinant human IL-1β. A similar protocol was utilised to that described in **Chapter 2 (Section 2.4.6)**, however following the 3-hour wash step, recombinant human IL-1β (at 100pg/mL) or endotoxin-free PBS (control) was applied to wells prior to 72 hour incubation. IL-1β-treated macrophages demonstrated substantially enhanced bacillary clearance at 72 hours compared to PBS-treated macrophages (**Figure 4.25**), confirming a role for IL-1β in early mycobactericidal activity of human macrophages.

To further confirm a role for IL-1β in bacillary killing by macrophages, IL-1 signalling was inhibited by pre-treating cells one hour prior to infection with anti-IL-1β antibody or with control IgG. Treatments were reapplied following the 3-hour wash step. Macrophages treated with anti-IL-1β demonstrated a trend towards impaired bacillary clearance at 72 hours (**Figure 4.26**), again supporting a critical role for IL-1β signalling in early macrophage responses to Mtb infection.

Finally, we sought to investigate whether the observed requirement for glycolysis (**Figure 4.22**) resulted from the observed requirement for IL-1 signalling (**Figure 4.25; Figure 4.26**). Human MDM were isolated, cultured and treated with glucose- or galactose-supplemented media 24 hours prior to infection, as previously described. One hour prior to infection with H37Ra, cells were pre-treated with anti-IL-1β antibody or with control IgG. As for other killing assay experiments, cells were washed at 3 hours to remove extracellular bacilli and designated wells were lysed, diluted and plated on Middlebrook 7H10 agar. Treatments were reapplied to the remainder of the cells, and cells were incubated for 72 hours prior to lysis, dilution and plating on agar. CFU were enumerated 14 – 28 days later. Absence of IL-1β signalling completely abrogated the impact of glycolytic inhibition on early bacillary clearance (**Figure 4.27B – C**), suggesting that glycolytic reprogramming enhances macrophage mycobactericidal activity via induction of IL-1β.

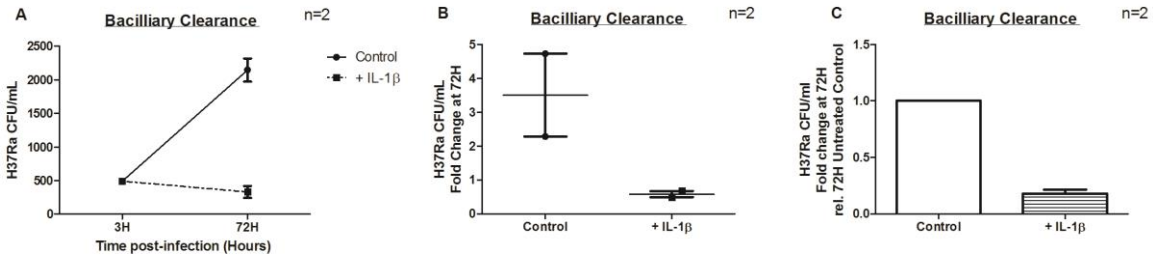

FIGURE 4.25 IL-1β enhances clearance of H37Ra by human MDM. MDM were cultured in cRPMI as before. On Day 7, cells were infected with H37Ra at low MOI. At 3 hours post-infection, all cells were washed to remove extracellular bacilli. Designated cells were lysed in sterile 0.1% Triton-X and lysates were serially diluted in 7H9 Middlebrook Broth and plated on 7H10 Middlebrook agar in triplicate. The remaining cells were treated with recombinant human IL-1β (100pg/mL) or with endotoxin-free PBC (control) and incubated for 72 hours prior to lysis, dilution and plating. Agar plates were incubated for 14 – 28 days and CFU enumerated by counting. Panels depict absolute CFU count for 3H and 72H (A), fold change in CFU count for 72H relative to corresponding 3H count (B) and fold change in 72H CFU count relative to 72H glucose control CFU count (C). Data depict mean ± SEM for two individual donors.

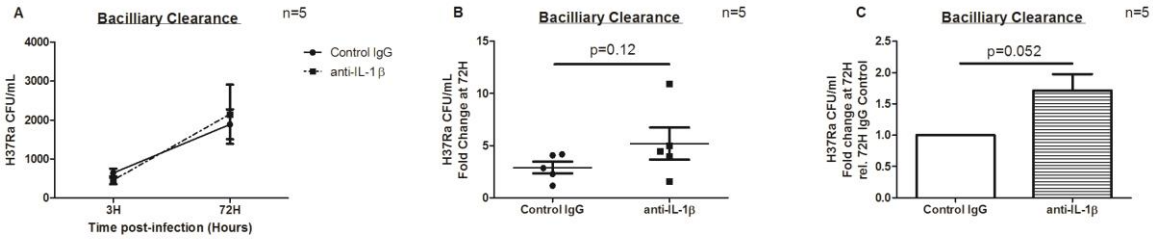

FIGURE 4.26 IL-1β signalling is required for clearance of H37Ra by human MDM. MDM were cultured in cRPMI as before. On Day 7, cells were treated with anti-IL-1β antibody (0.1μg/mL) or IgG control antibody (0.1μg/mL). One hour later, cells were infected with H37Ra at low MOI. At 3 hours post-infection, all cells were washed to remove extracellular bacilli. Designated cells were lysed in sterile 0.1% Triton-X and lysates were serially diluted in 7H9 Middlebrook Broth and plated on 7H10 Middlebrook agar in triplicate. The remaining cells were incubated for 72 hours prior to lysis, dilution and plating. Agar plates were incubated for 14 – 28 days and CFU enumerated by counting. Panels depict absolute CFU count for 3H and 72H (A), fold change in CFU count for 72H relative to corresponding 3H count (B) and fold change in 72H CFU count relative to 72H glucose control CFU count (C). Data depict mean ± SEM for 5 individual donors. Statistical analyses were performed using the paired Student's t-test; statistical significance was set at $p<0.05$.

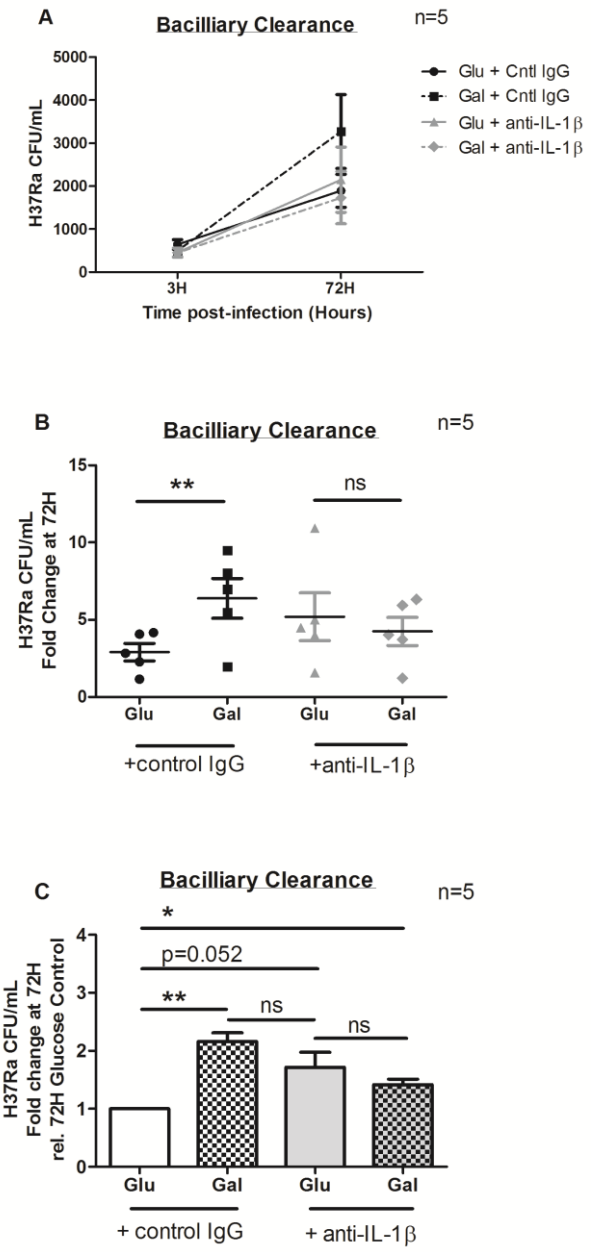

FIGURE 4.27 Glycolytic induction of bacillary clearance is mediated through enhanced IL-1β signalling in human MDM. MDM were cultured in cRPMI as before. On Day 6, culture media was replaced with either glucose- or galactose-containing media. 24 hours later, cells were treated with anti-IL-1β antibody (0.1µg/mL) or IgG control antibody (0.1µg/mL). One hour later, cells were infected with H37Ra at low MOI. At 3 hours post-infection, all cells were washed to remove extracellular bacilli. Designated cells were lysed in sterile 0.1% Triton-X and lysates were serially diluted in 7H9 Middlebrook Broth and plated on 7H10 Middlebrook agar in triplicate. The remaining cells were incubated for 72 hours prior to lysis, dilution and plating. Agar plates were incubated for 14 – 28 days and CFU enumerated by counting. Panels depict absolute CFU count for 3H and 72H (A), fold change in CFU count for 72H relative to corresponding 3H count (B) and fold change in 72H CFU count relative to 72H glucose control CFU count (C). Data depict mean ± SEM for 5 individual donors. Statistical analyses were performed using the paired Student's t-test; *p<0.05, **p<0.01.

4.2.9 Glycolysis enhances IL-1β production and bacillary clearance in Mtb-infected murine BMDM

As outlined above, preliminary experiments revealed glycolytic inhibitor 2-DG to significantly reduce viability of human macrophages (**Figure 2.7**), thus galactose was employed as a glycolytic inhibitor for interrogation of human macrophage metabolic functions. 2-DG has been successfully employed to inhibit glycolysis in murine BMDM [174], thus this inhibitor was employed in the interrogation of murine BMDM. Murine BMDM were isolated and prepared for experimentation as described in **Chapter 2 (Section 2.1.3)**. 3 hours prior to infection, cells were treated with 2-DG (at 5mM) or left untreated (control). Infections were performed with 2-DG treatment reapplied following 3-hour wash step, and supernatants were harvested at 24 hours post-infection. Firstly, lactate quantification was used to confirm successful inhibition of glycolytic reprogramming following H37Ra and iH37Rv infection (**Figure 4.28A**). Inhibition of glycolysis using 2-DG resulted in attenuation of IL-1β production in H37Ra-infected BMDM (**Figure 4.28B**). TNF-α levels were less substantially reduced following 2-DG treatment (**Figure 4.28C**).

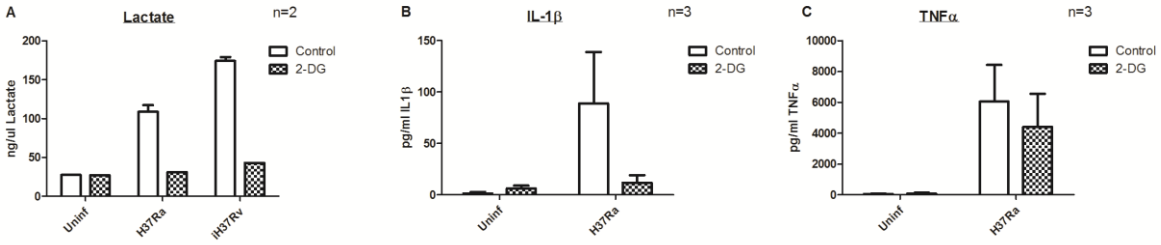

FIGURE 4.28 Glycolysis is required for optimal production of IL-1β in Mtb-infected murine BMDM. Murine BMDM were cultured for 5 days in M-CSF supplemented DMEM as before. On Day 6, MCSF supplementation was discontinued and cells were pre-treated with 2-DG (5mM) or left untreated (control) for 3 hours prior to infection with H37Ra at low MOI or iH37Rv at low MOI. At 3 hours post-infection, cells were washed to remove extracellular bacilli and 2-DG treatment reapplied. At 24 hours post-infection, supernatants were removed and lactate and cytokine concentrations quantified. Panel A depicts mean ± SEM lactate concentration for 2 individual mice. Panels B and C depict mean ± SEM IL-1β (B) and TNF-α (C) concentration for 3 individual mice. Statistical analyses were performed using the unpaired Student's t-test; statistical significance was set at $p<0.05$.

Having elucidated a role for IL-1 signalling in both induction of PGE2 and suppression of IL-10 in human MDM, this axis was investigated in a murine macrophage model. BMDM from wild type (WT) and IL-1R-KO mice were isolated and prepared as before, and infected with H37Ra as previously described. Relative mRNA expression at 24 hours post-infection was quantified as before. Absence of IL-1 signalling was associated with attenuated *Ptgs2* transcription (**Figure 4.29A**) and enhanced *Il10* transcription (**Figure 4.29B**), in line with observations in human MDM.

Next, the role of glycolytic reprogramming in early bacillary clearance by murine macrophages was examined. Murine BMDM were prepared and pre-treated with 2-DG 3 hours prior to infection with H37Ra, as described above. Killing assays were performed as outlined for human macrophages and as described in detail in **Chapter 2 (Section 2.4.6)**, with 2-DG treatment reapplied following the 3-hour wash step. Similar to galactose-treated human macrophages, glycolytic inhibition using 2-DG resulted in significantly impaired bacillary clearance by murine BMDM at 72 hours post-infection (**Figure 4.30**).

In order to investigate the role of IL-1β in early macrophage mycobactericidal activity, killing assays were performed in the presence or absence of recombinant mouse IL-1β (at 100pg/mL), using the same protocol as that described for human macrophage experiments. Again, cells treated with exogenous IL-1β demonstrated enhanced bacillary clearance at 72 hours compare to those treated with PBS (control) (**Figure 4.31**), demonstrating a critical role for IL-1β in early macrophage response to infection. Side-by-side killing assays performed in WT and IL-1R-KO BMDM further supported this hypothesis, with absence of IL-1 signalling associated with significantly impaired bacillary clearance at 72 hours compared to WT controls (**Figure 4.32**).

Finally, we investigated the role of IL-1β in glycolysis-driven enhanced bacillary clearance. As before, BMDM were isolated from WT and IL-1R-KO mice and prepared for experimentation. Cells were pre-treated with 2-DG (at 5mM) or left untreated (control) 3 hours prior to infection with H37Ra. Killing assays were performed as outlined above, with 2-DG treatment reapplied following the 3-hour wash step. As seen in human macrophage experiments, absence of IL-1 signalling completely abrogated the effect of glycolytic inhibition on early bacillary clearance in murine BMDM (**Figure 4.33**), implicating increased IL-1β production in the glycolysis-induced enhanced bacillary clearance observed in infected cells.

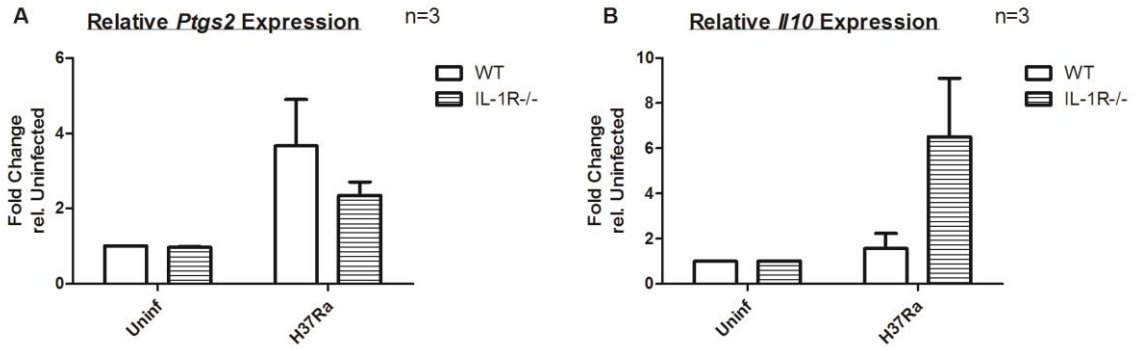

FIGURE 4.29 IL-1 signalling enhances *PTGS2* transcription and suppresses *IL-10* transcription in Mtb-infected murine BMDM. BMDM were isolated from CS57BL/6 mice (WT control) and CS57BL/6 background IL-1R-KO mice and cultured in DMEM supplemented with 15% MCSF for 5 days, as previously described. On Day 6, MCSF supplementation was discontinued and cells infected with H37Ra at low MOI. At 24 hours post-infection, cells were lysed in RLT buffer, RNA extracted, cDNA generated and qPCR performed with data normalised to *18S*. mRNA expression fold-change relative to uninfected was calculated using the $2^{-\Delta\Delta Ct}$ method. Panels A and B depict mean ± SEM relative mRNA expression of *Ptgs2* (A) and *Il10* (B) for 3 individual mice. Statistical analyses were performed using the unpaired Student's t-test; statistical significance was set at $p<0.05$.

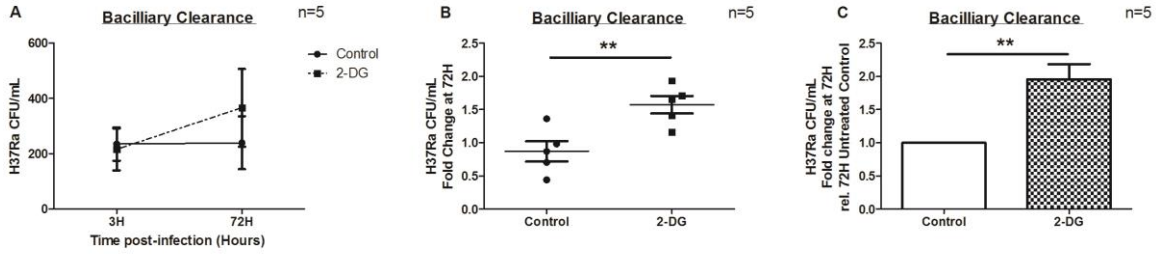

FIGURE 4.30 Glycolysis is required for optimal clearance of H37Ra by murine BMDM. Murine BMDM were cultured for 5 days in M-CSF supplemented DMEM as before. On Day 6, MCSF supplementation was discontinued and cells were pre-treated with 2-DG (5mM) for 3 hours prior to infection with H37Ra at low MOI. At 3 hours post-infection, all cells were washed to remove extracellular bacilli. Designated cells were lysed in sterile 0.1% Triton-X and lysates were serially diluted in 7H9 Middlebrook Broth and plated on 7H10 Middlebrook agar in triplicate. 2-DG or control treatments were reapplied to remaining cells. Cells were incubated for 72 hours prior to lysis, dilution and plating. Agar plates were incubated for 14 – 28 days and CFU enumerated by counting. Panels depict absolute CFU count for 3H and 72H (A), fold change in CFU count for 72H relative to corresponding 3H count (B) and fold change in 72H CFU count relative to 72H glucose control CFU count (C). Data depict mean ± SEM for 5 individual mice. Statistical analyses were performed using the unpaired Student's t-test; $^{**}p<0.01$.

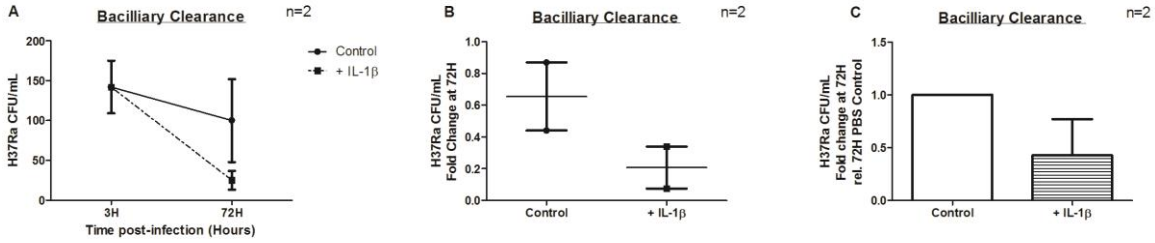

FIGURE 4.31 IL-1β enhances clearance of H37Ra by murine BMDM. Murine BMDM were cultured as before. On Day 6, MCSF supplementation was discontinued and cells were infected with H37Ra at low MOI. At 3 hours post-infection, all cells were washed to remove extracellular bacilli. Designated cells were lysed in sterile 0.1% Triton-X and lysates were serially diluted in 7H9 Middlebrook Broth and plated on 7H10 Middlebrook agar in triplicate. The remaining cells were treated with recombinant human IL-1β (100pg/mL) or with endotoxin-free PBC (control) and incubated for 72 hours prior to lysis, dilution and plating. Agar plates were incubated for 14 – 28 days and CFU enumerated by counting. Panels depict absolute CFU count for 3H and 72H (A), fold change in CFU count for 72H relative to 3H count (B) and fold change in 72H CFU count relative to 72H PBS control CFU count (C). Data depict mean ± SEM for 2 individual mice.

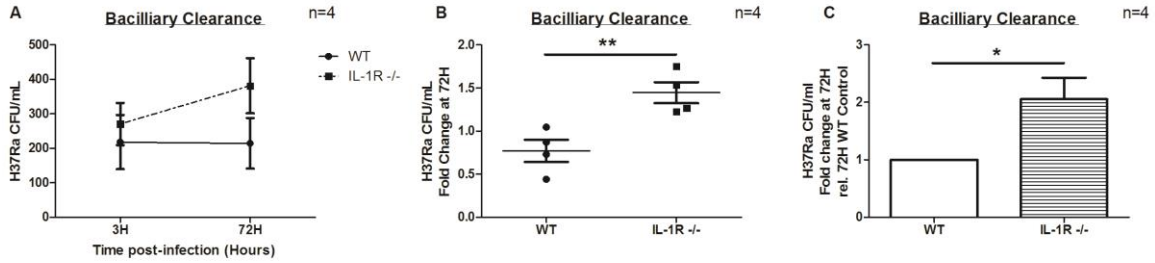

FIGURE 4.32 IL-1 signalling is required for optimal clearance of H37Ra by murine BMDM. BMDM were isolated from CS57BL/6 mice (WT control) and CS57BL/6 background IL-1R-KO mice and cultured in DMEM supplemented with 15% MCSF for 5 days, as previously described. On Day 6, MCSF supplementation was discontinued and cells infected with H37Ra at low MOI. At 3 hours post-infection, all cells were washed to remove extracellular bacilli. Designated cells were lysed in sterile 0.1% Triton-X and lysates were serially diluted in 7H9 Middlebrook Broth and plated on 7H10 Middlebrook agar in triplicate. The remaining cells were incubated for 72 hours prior to lysis, dilution and plating. Agar plates were incubated for 14 – 28 days and CFU enumerated by counting. Panels depict absolute CFU count for 3H and 72H (A), fold change in CFU count for 72H relative to corresponding 3H count (B) and fold change in 72H CFU count relative to 72H WT control CFU count (C). Data depict mean ± SEM for 4 individual mice. Statistical analyses were performed using the paired Student's t-test; *p<0.05, **p<0.01.

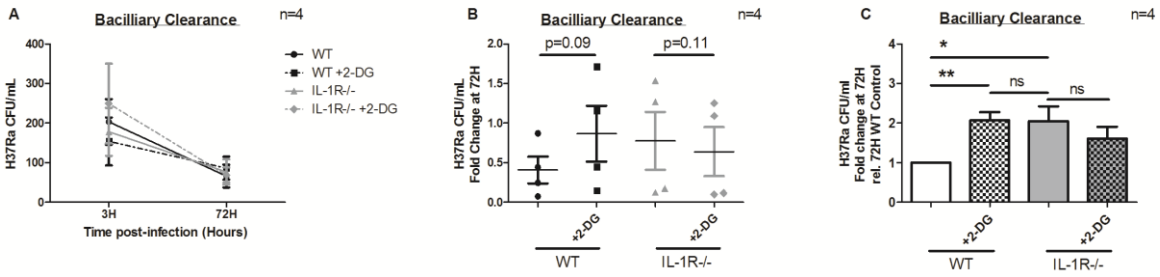

FIGURE 4.33 Glycolytic induction of bacillary clearance is mediated through enhanced IL-1 signalling in murine BMDM. BMDM were isolated from CS57BL/6 mice (WT control) and CS57BL/6 background IL-1R-KO mice and cultured in DMEM supplemented with 15% MCSF for 5 days, as previously described. On Day 6, MCSF supplementation was discontinued and cells were pre-treated with 2-DG (5mM) or left untreated (control) for 3 hours prior to infection with H37Ra at low MOI. At 3 hours post-infection, all cells were washed to remove extracellular bacilli. Designated cells were lysed in sterile 0.1% Triton-X and lysates were serially diluted in 7H9 Middlebrook Broth and plated on 7H10 Middlebrook agar in triplicate. 2-DG or control treatments were reapplied to remaining cells. Cells were incubated for 72 hours prior to lysis, dilution and plating. Agar plates were incubated for 14 – 28 days and CFU enumerated by counting. Panels depict absolute CFU count for 3H and 72H (A), fold change in CFU count for 72H relative to corresponding 3H count (B) and fold change in 72H CFU count relative to 72H WT control CFU count (C). Data depict mean ± SEM for 4 individual mice. Statistical analyses were performed using the paired Student's t-test; *p<0.05, **p<0.01.

4.2.10 PKM2 activation suppresses IL-1β production and impairs bacillary clearance in Mtb-infected and *S.typhi*-infected murine BMDM

The enzyme PKM2 can exist as an enzymatically-active tetrameric form or an enzymatically-inactive dimeric form. Dimeric PKM2 translocates to the cell nucleus where it serves to upregulate glycolysis [260]. PKM2 activators, such as the cell-permeable allosteric PKM2 activator TEPP-46, induce its enzymatic activation and prevent its translocation to the nucleus, with the net effect of reducing glycolytic flux.

In order to assess the impact of PKM2 activation on macrophage Mtb responses, murine BMDM were treated with TEPP-46 or with DMSO (control) one hour prior to infection. Infections were performed as previously, with TEPP-46 or DMSO treatments reapplied following the 3-hour was step. Supernatants were harvested at 24 hours post-infection for measurement of cytokines and killing assays performed. Cytokine analyses demonstrated dose-dependent attenuation of IL-1β production, a less pronounced attenuation TNF-α production, as well as an increase in IL-10 production at lower doses, in H37Ra-infected murine BMDM treated with TEPP-46 (**Figure 4.34A – C**), similar to results observed with glycolytic inhibition using 2-DG (**Figure 4.28**). Similarly, killing assays demonstrated impaired clearance of H37Ra by murine BMDM following TEPP-46 treatment (**Figure 4.34D – F**), demonstrating that dimeric PKM2 is required for optimal macrophage anti-mycobacterial responses.

Finally, in order to investigate the importance of this elucidated pathway in macrophage responses to non-mycobacterial intracellular pathogens, murine BMDM were infected with *S. typhi* following pre-treatment with TEPP-46 or DMSO (control), as described in **Chapter 2 (Section 2.2.2)**. Killing assays were performed, with cells washed and lysed at 30 minutes post infection, serial dilutions performed and lysates plated on agar. The remainder of cells were washed at 30 minutes post-infection to remove extracellular bacteria, TEPP-46 and DMSO treatments reapplied, and incubated for 24 hours prior to lysis, dilution and plating on agar. Agar plates were incubated for 24 to 72 hours and CFU enumerated by counting. Counts from 30 minute timepoints indicated no difference in bacterial uptake by macrophages with TEPP-46 treatment (**Figure 4.35A**), however 24 hour timepoints demonstrated impaired bacterial clearance by BMDM following TEPP-46 treatment (**Figure 4.35B**), similar to results observed in Mtb experiments (**Figure 4.34**), and confirming a broader role for glycolytic reprogramming in macrophage responses to other intracellular pathogens.

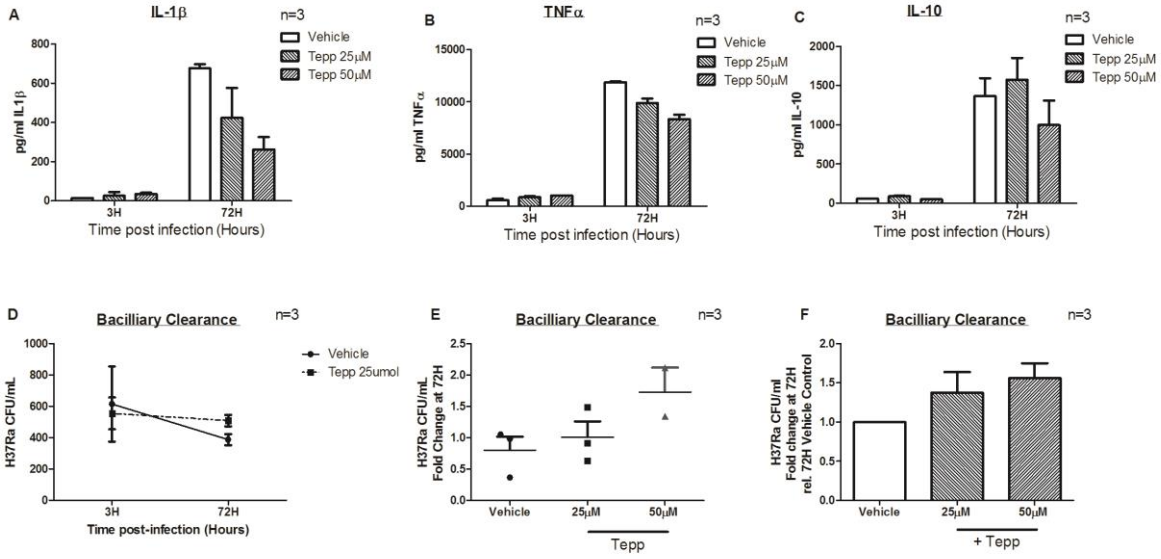

FIGURE 4.34 PKM2 activation alters cytokine profile and impairs bacillary clearance in Mtb-infected murine BMDM. Murine BMDM were cultured for 5 days in M-CSF supplemented DMEM as before. On Day 6, MCSF supplementation was discontinued and cells were pre-treated with TEPP-46 (at indicated concentration) or DMSO (control) for 3 hours prior to infection with H37Ra at low MOI. At 3 hours post-infection, all cells were washed to remove extracellular bacilli. Designated cells were lysed in sterile 0.1% Triton-X and lysates were serially diluted in 7H9 Middlebrook Broth and plated on 7H10 Middlebrook agar in triplicate. TEPP-46 or control treatments were reapplied to remaining cells. Cells were incubated for 72 hours prior to lysis, dilution and plating. Agar plates were incubated for 14 – 28 days and CFU enumerated by counting. Supernatants were retained at 3 hours and at 72 hours to allow quantification of cytokines by ELISA. Panels A – C depict IL-1β (A), TNF-α (B) and IL-10 (C) concentration measured in supernatants. Panels D – F depict absolute CFU count for 3H and 72H (D), fold change in CFU count for 72H relative to corresponding 3H count (E) and fold change in 72H CFU count relative to 72H vehicle control CFU count (F). Data depict mean ± SEM for 3 individual mice. Statistical analyses were performed using the 1-way ANOVA; statistical significance was set at $p<0.05$.

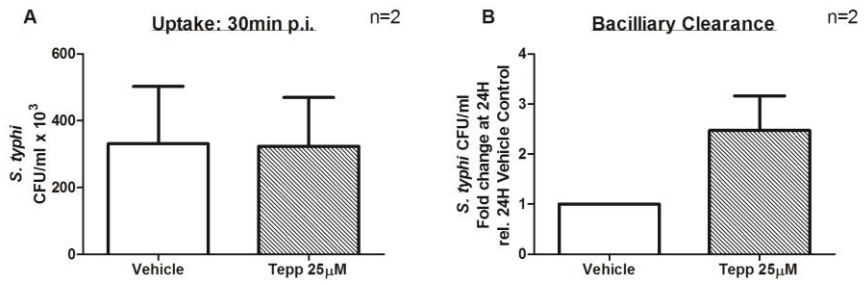

FIGURE 4.35: PKM2 activation impairs clearance of *Salmonella typhi* by murine BMDM. Murine BMDM were cultured for 5 days in M-CSF supplemented DMEM as before. On Day 6, MCSF supplementation was discontinued and cells were pre-treated with TEPP-46 (25μM) or DMSO (control) for 1 hour prior to infection with *S.typhi* at low MOI. At 30 minutes post-infection, all cells were washed to remove extracellular bacilli. Designated cells were lysed in sterile 0.1% Triton-X and lysates were serially diluted in sterile PBS and plated on LB agar in triplicate. TEPP-46 or control treatments were reapplied to remaining cells. Cells were incubated for 24 hours prior to lysis, dilution and plating. Agar plates were incubated for 1 – 3 days and CFU enumerated by counting. Panel A depicts CFU count for 30 minute post-infection timepoint, representative of uptake. Panel B depicts fold change in 24H CFU count relative to 24H vehicle control CFU count, representative of clearance. Data depict mean ± SEM for 2 individual mice.

4.2.11 Meclizine enhances IL-1β production and bacillary clearance in Mtb-infected human MDM

Meclizine, an over-the-counter antihistamine that is used as an anti-emetic, has recently been demonstrated to shift cellular energy metabolism from oxidative phosphorylation to glycolysis [464]. This is mediated through its direct inhibition of the cytosolic enzyme CTP:phosphoethanolamine cytidylyltransferase (PCYT2), leading to accumulation of phosphoethanolamine, an inhibitor of State 3 mitochondrial respiration [468]. It was hypothesised, therefore, that meclizine may enhance the glycolytic shift observed in macrophages infected with Mtb.

Firstly, uninfected MDM were treated with meclizine dihydrochloride or with DMSO (control) for 24 hours and extracellular flux analyses performed, as described in **Chapter 2 (Section 2.5.4)**. Meclizine treatment induced a shift towards glycolysis in uninfected macrophages, as demonstrated by increased ECAR/OCR ratio (**Figure 4.36C**) and increased lactate production (**Figure 4.36D**). Next, cells were pre-treated with meclizine or DMSO for 24 hours prior to infection with iH37Rv and metabolic analyses performed at 24 hours post-infection. Both extracellular flux analysis and lactate measurement at 24 hours demonstrated enhanced infection-induced glycolytic shift in the presence of meclizine (**Figure 4.37A – D**). Enhanced IL-1β production was also observed, with TNF-α production unaffected (**Figure 4.37E – F**). Viability was not substantially altered with treatment (**Figure 4.37G**).

The impact of meclizine pre-treatment on glycolytic reprogramming with live Mtb infection was also interrogated using the live avirulent strain H37Ra. In unexpected contrast to iH37Rv infection, meclizine pre-treatment did not enhance lactate production in H37Ra-infected MDM (**Figure 4.38A**). Conversely, meclizine enhanced IL-1β production following H37Ra infection (**Figure 4.38B**). Furthermore, bacillary clearance experiments suggested enhanced mycobactericidal activity of human MDM pre-treated with meclizine at doses of 25μM or 50μM in comparison to DMSO-treated control cells (**Figure 4.39**), although this failed to reach significance.

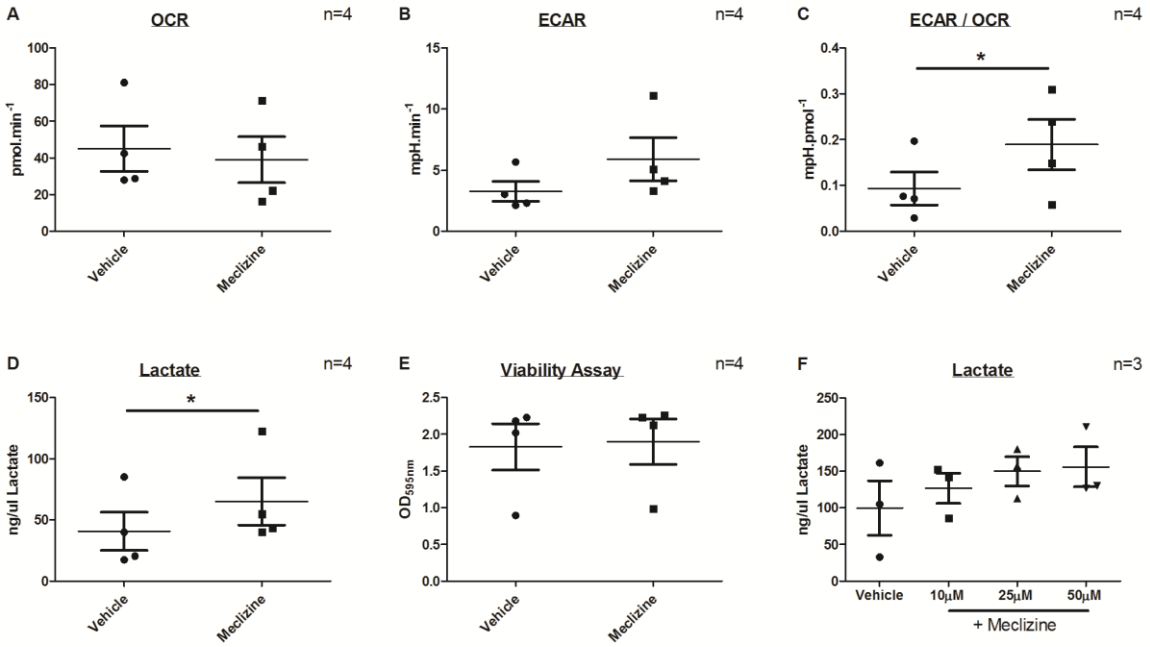

FIGURE 4.36 Meclizine induces glycolysis in uninfected human MDM. MDM were cultured in cRPMI as before. On Day 6, cells were treated with meclizine dihydrochloride (25µM) or DMSO (control). 24 hours after treatment, supernatants were removed and retained for quantification of lactate, and extracellular flux analyses was performed in Seahorse media, with CV assay used to normalise data. Panels A – E depict mean ± SEM OCR (A), ECAR (B), ECAR/OCR ratio (C), measured lactate concentration (D) and corresponding absorbance following CV staining (E) for 4 individual donors. Panel F depicts mean ± SEM lactate concentration from cells treated with varying concentrations of meclizine dihydrochloride for 3 individual donors. Statistical analyses were performed using the paired Student's t-test; *$p<0.05$.

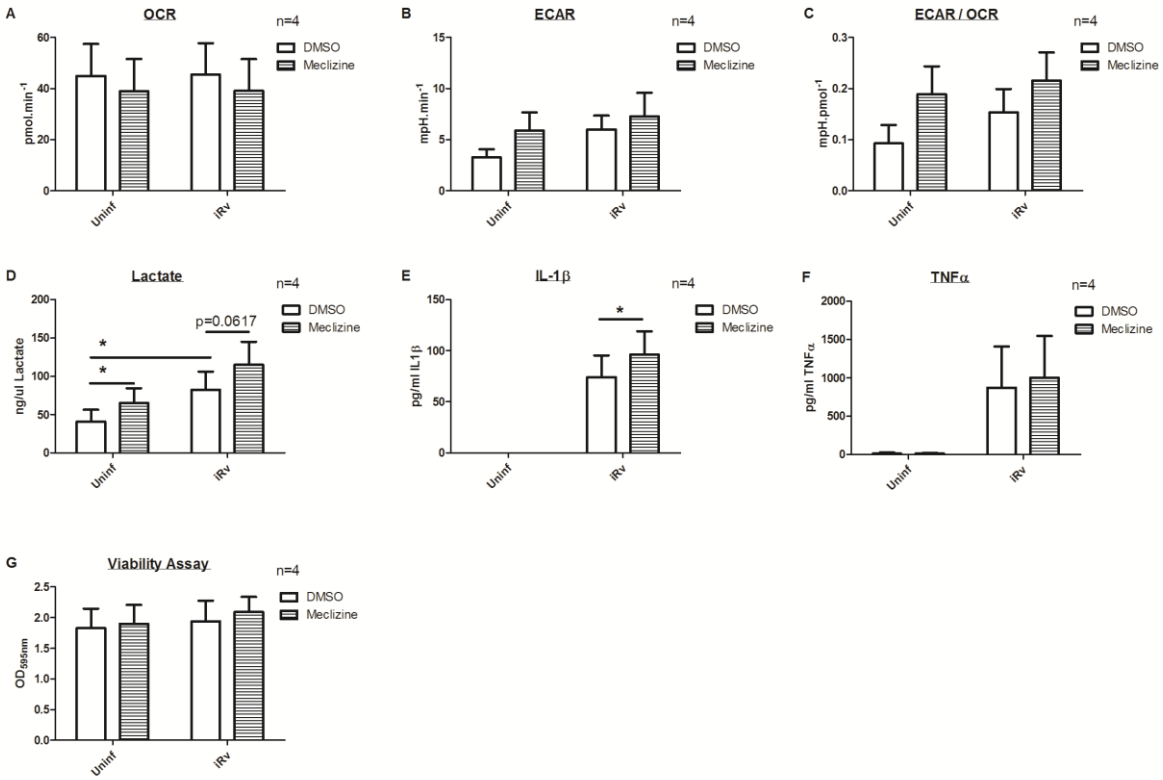

FIGURE 4.37 Meclizine enhances glycolytic reprogramming and IL-1β production in iMtb-infected human MDM. MDM were cultured in cRPMI as before. On Day 6, cells were treated with meclizine dihydrochloride (25μM) or DMSO (control) for one hour prior to infection with iH37Rv at low MOI. 24 hours post infection, supernatants were removed and retained for quantification of lactate and cytokines. Extracellular flux analyses were performed in Seahorse media, with CV assay used to normalise data. Panels A – G depict mean ± SEM OCR (A), ECAR (B), ECAR/OCR ratio (C), measured lactate concentration (D), IL-1β concentration (E), TNF-α concentration (F) and corresponding absorbance following CV staining (G) for 4 individual donors. Statistical analyses were performed using the paired Student's t-test; *p<0.05.

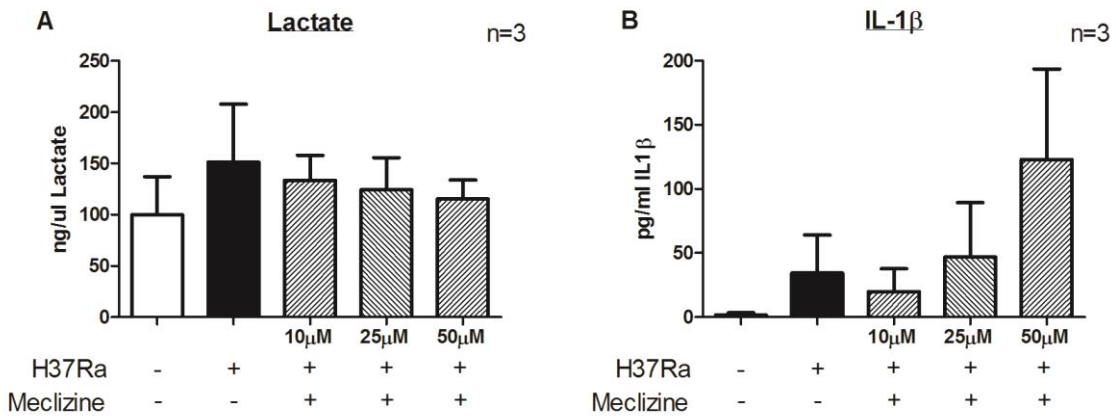

FIGURE 4.38 Meclizine does not enhance lactate production in H37Ra-infected human MDM, but does enhance IL-1β production. MDM were cultured in cRPMI as before. On Day 6, cells were treated with meclizine dihydrochloride (at indicated concentration) or DMSO (control) for one hour prior to infection with H37Ra at low MOI. 24 hours post infection, supernatants were removed and retained for quantification of lactate and cytokines. Panels A and B depict mean ± SEM measured lactate (A) and IL-1β (B) concentration for 3 individual donors. Statistical analyses were performed using the paired Student's t-test; statistical significance was set at $p<0.05$.

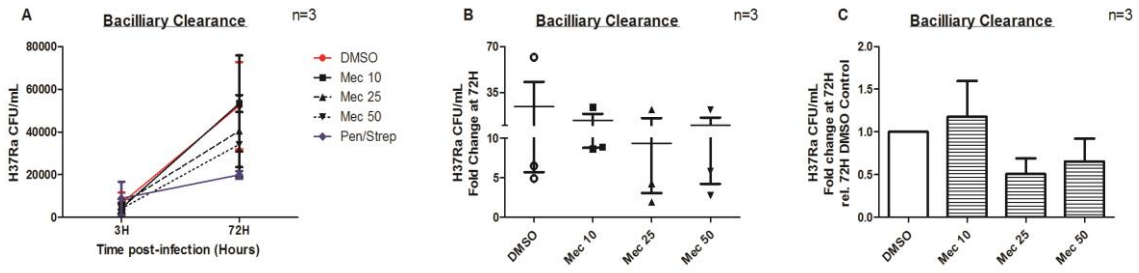

FIGURE 4.39 Meclizine enhances early bacillary clearance of H37Ra by human MDM. MDM were cultured in cRPMI as before. On Day 6, cells were treated with meclizine dihydrochloride (at indicated concentration) or DMSO (control) for one hour prior to infection with H37Ra at low MOI. At 3 hours post-infection, all cells were washed to remove extracellular bacilli. Designated cells were lysed in sterile 0.1% Triton-X and lysates were serially diluted in 7H9 Middlebrook Broth and plated on 7H10 Middlebrook agar in triplicate. Meclizine or control treatments were reapplied to the remaining cells. Cells were incubated for 72 hours prior to lysis, dilution and plating. Agar plates were incubated for 14 – 28 days and CFU enumerated by counting. Panels A – C depict absolute CFU count for 3H and 72H (A), fold change in CFU count for 72H relative to corresponding 3H count (B) and fold change in 72H CFU count relative to 72H vehicle control CFU count (C). Data is presented as mean ± SEM for 3 individual donors. Statistical analyses were performed using the paired Student's t-test; statistical significance was set at $p<0.05$.

4.3 Discussion

Glycolytic reprogramming in macrophages has been linked to key pro-inflammatory functions [174,244,247,250,262]. Work to date has centred on activation of macrophages using TLR agonists such as LPS, thus the role of this metabolic shift in the context of functional implications for host defence have not been examined. Having demonstrated a shift towards glycolytic metabolism in macrophages following infection with intracellular Mycobacterium tuberculosis, as outlined in **Chapter 3**, the role of this metabolic shift in the host response to infection is explored in **Chapter 4**. Given the reported role of Warburg metabolism in production of the pro-inflammatory cytokine IL-1β in LPS-activated murine macrophages [174], it was hypothesised that the Mtb-induced shift toward glycolytic metabolism is required for optimal IL-1β production in the context of infection. As IL-1β has been demonstrated to play a vital role in the host response to infection [134,146], it was further hypothesised that inhibition of the Mtb-induced glycolytic shift would impair macrophage anti-mycobacterial function.

4.3.1 Inhibition of glycolytic metabolism

Numerous studies have utilised the HK1 inhibitor 2-DG in order to explore the functional role of glycolytic reprogramming in murine macrophages [174,247,250]. Preliminary studies suggested significant reductions in human macrophage viability in the presence of 2-DG (**Figure 2.7**), however. Chang et al successfully utilised glucose-free galactose-supplemented media to inhibit the shift towards glycolysis in activated human T cells [465], with cells cultured in this environment essentially forced to rely on glutamine-driven oxidative phosphorylation for ATP production [464]. In the work presented in this thesis, glucose-free galactose-supplemented media skewed human macrophage metabolism towards oxidative phosphorylation and away from glycolysis at baseline (**Figure 4.1**), with impaired GR confirming effective inhibition of glycolysis (**Figure 4.2**), without any significant impact on macrophage viability demonstrated (**Figure 2.9**). The observed trend towards reduced SRC in the presence of galactose (**Figure 4.2**) is likely related to the presence of a single outlier. Alternatively, increased dependence on oxidative phosphorylation at baseline may limit the cell's ability to increase rates of mitochondrial respiration when stressed.

The previously demonstrated shift towards glycolytic metabolism following stimulation with LPS was inhibited in the presence of galactose (**Figure 4.3**), as was glycolytic reprogramming in response to non-viable iH37Rv (**Figure 4.4**) and viable H37Ra (**Figure 4.5**) infection. These

experiments confirmed glucose-free galactose-supplemented media as a suitable approach to inhibiting glycolytic reprogramming in human macrophages.

Interestingly, cells cultured in galactose did not demonstrate an increase in ATP production following infection, in contrast to those cultured in glucose in which glycolytic reprogramming was allowed to occur (**Figure 4.6**). Others have similarly demonstrated a role for glycolytic metabolism in meeting ATP requirements in activated murine dendritic cells [238,240], particularly in the context of NO-mediated inhibition of oxidative phosphorylation. As outlined in **Section 3.3.1**, species-specific variation in NO production may potentially render inhibition of oxidative phosphorylation less complete in human macrophages following activation [32]. However, glycolytically-derived ATP has recently been postulated to play a role in maintenance of mitochondrial membrane potential in order to facilitate RET and mROS production via Complex I [269], thus reduced ATP production resulting from glycolytic inhibition is likely to impact upon pro-inflammatory function of human macrophages.

4.3.2 Glycolytic reprogramming is required for optimal production of IL-1β

Phagocytosis of the bacillus by the macrophage is a central plank in the host-bug interaction for Mtb infection. This occurs with a series of co-ordinated membrane invaginations and fusions, resulting in the formation of a phagosome which can paradoxically provide both a nidus for survival and replication for the bug and also drive antigen presentation and permit bug killing through the process of phagosome-lysosomal fusion [19]. Enhanced phagocytic activity has been described in M2-polarised macrophages [102,103], as well as links to cholesterol metabolism [19], however the role of glycolytic reprogramming has never been studied in macrophage phagocytosis of Mtb. In this study, no difference in phagocytosis is observed in the presence of glycolytic inhibitor galactose (**Figure 4.7** and **Table 4.1**), as indicated by similar uptake of bacilli at 3 hours post-infection.

Mtb-driven induction of *IL-1B* transcription, however, was significantly reduced following infection of human MDM with either viable H37Ra or non-viable iH37Rv in the presence of the glycolytic inhibitor galactose (**Figure 4.8A**). This is consistent with work in murine macrophages stimulated with LPS [174]. Similar to the findings of Tannahill et al, no significant reduction in *TNFA* induction was observed (**Figure 4.8B**). Warburg-driven transcription of *IL1B* is postulated to occur secondary to stabilisation of HIF-1α, thus *TNFA* induction is not affected. Additionally, HIF-1α drives upregulation of glycolytic genes and glucose transporters, potentiating the shift towards glycolytic metabolism [256-258]. Work by Shi et al supports a role for HIF-1α in the context of

Mtb-driven glycolytic reprogramming [334], with homogenised lungs from mice infected with H37Rv demonstrating increased levels of the transcription factor.

In addition to enhancing transcription of *IL1B*, this work also demonstrates a role for glycolytic reprogramming in production of mature IL-1β from Mtb-infected human MDM (**Figure 4.8**) and human AM (**Figure 4.10**). As described in detail in **Section 1.2.3**, production of IL-1β is a two-step process, requiring induction of pro-IL-1β as a priming step and subsequent cleavage of this protein to form mature IL-1β. Mtb is capable of triggering both steps required for IL-1β production. Results presented in **Chapter 4** indicate a requirement for glycolytic reprogramming in order to facilitate production of pro-IL-1β, demonstrated by reduced transcription of IL1B following glycolytic inhibition (**Figure 4.8A**). It is reasonable that reduction in IL1B transcription therefore would lead to downstream reduction in mature IL-1β. However, mature IL-1β may also be regulated by glycolytic reprogramming at the level of protein cleavage. Moon et al demonstrate upregulation of the glycolytic enzyme HK1 to be required for NLRP3 inflammasome activation, with glycolytic inhibition using 2-DG resulting in reduced cleavage of pro-IL-1β to form the mature protein [250]. This observed inflammasome activation may be mediated by mROS induction [250], a phenomenon recently linked to macrophage glycolytic reprogramming by Mills et al [269]. In **Chapter 3**, upregulation of HK1 in human MDM infected with Mtb is demonstrated (**Figure 3.16**). Thus, glycolytic reprogramming likely regulates IL-1β production at a range of levels, offering some explanation for the specificity of this observation.

In line with the observation that the glycolytic shift does not become evident until 24 hours post-infection (**Figure 3.11**), the impact of glycolytic inhibition on secreted IL-1β levels was not evident at 6 hours post infection but was evident at 24 hours post infection (**Figure 4.9A**). TNF-α levels were again not impacted by glycolytic inhibition up to 48 hours post-infection, however substantial increases in TNF-α were observed in macrophages cultured in galactose at 72 hours post-infection (**Figure 4.9B**). Conflictingly, Jayaraman et al have demonstrated a role for IL-1β in augmenting transcription and secretion of TNF-α in Mtb infection [197]. It is possible therefore that glycolytic reprogramming serves to inhibit TNF-α production by an unknown mechanism, an effect that is counteracted by increases in IL-1β driving TNF-α at earlier timepoints. Given the importance of TNF-α in the host immune response to Mtb, this pathway requires elucidation in order to characterise the role of glycolytic reprogramming in macrophage-bacillus interactions.

HIF-1α has been implicated as both a product and a driver of glycolytic reprogramming [256-258]. However, experiments using anti-IL-1β antibody demonstrated similar increases in lactate production in the presence and absence of IL-1 signalling, as well as similar response to glycolytic inhibition using galactose (**Figure 4.11**), confirming glycolysis-associated increases in IL-1β occur

downstream of glycolytic reprogramming rather than upstream. As outlined above, increases in IL-1β potentially represent the impact of glycolytic reprogramming on a number of steps in the regulation of IL-1β production, including transcription and cleavage. As extracellular ATP signalling via the P2RX7 receptor has been implicated in activation of the NLRP3 inflammasome [185,186], it was hypothesised that reduced mature IL-1β levels in cells cultured in galactose may result from the previously-demonstrated reduced ATP production following infection (**Figure 4.6**). Inhibition of P2RX7 signalling with oATP did not inhibit IL-1β production in this model (**Figure 4.12**). As outlined in **Chapter 3**, no extracellular ATP was detected following infection using the ATP Bioluminescence Assay Kit CLS II (Sigma-Aldrich). Placido et al have described the MOI-dependency of ATP secretion in the context of Mtb infection [479], and Iyer et al have linked increases in extracellular ATP with cell necrosis [185]. Thus, it is likely that the low MOI utilised in our model does not induce sufficient amounts of extracellular ATP to substantially impact upon IL-1β production, rendering the effects of its inhibition negligible.

4.3.3 Downstream impacts of glycolysis-driven increases in IL-1β

A screen of several genes important in the early macrophage response to Mtb highlighted *IL1B* and *PTGS2* as genes impacted by glycolytic reprogramming at a transcriptional level (**Figure 4.13**). Again, the specificity of this regulation was emphasised by the negligible effect of transcription on *TNFA*, *IL1A*, *IL12* and *IL18*, though induction of these genes at the 24 hour timepoint investigated was limited and a different timepoint may have revealed a role for glycolysis. *PTGS2* codes for the enzyme COX2, responsible for generation of the eicosanoid PGE2. Mayer-Barber et al have recently described a mechanism of host defence whereby increases in IL-1β drive induction of PGE2, with reciprocal suppression of Type I Interferons and anti-inflammatory IL-10 [146]. In line with this model, glycolytic inhibition reduced Mtb-induced PTGS2 production (**Figure 4.14**) and PGE2 production (**Figure 4.15**), concurrent with impaired IL-1β production and increased IL-10 production (**Figure 4.17**), and with TNF-α production unaffected. Furthermore, inhibition of IL-1 signalling using an anti-IL-1β antibody negated the effect of glycolytic inhibition on both PGE2 (**Figure 4.16**) and IL-10 (**Figure 4.19**) production. These results support a model whereby Mtb infection induces glycolytic reprogramming which drives IL-1β production, with downstream induction of PGE2 and suppression of IL-10.

ROS generation represents an important anti-mycobacterial mechanism within the macrophage. Decreased induction of cellular ROS following infection was observed in the presence of the glycolytic inhibitor galactose (**Figure 4.20**). Interestingly, recent work by both Moon et al and Mills et al suggest that generation of mROS occurs as a direct consequence of glycolytic reprogramming

in activated macrophages [250,269], and that this increase in mROS drives induction of IL-1β. Though in this study mROS is not specifically measured, mitochondrial ROS generated through Complex I are delivered to the cytosol therefore contribute to overall cellular ROS measured (**Figure 4.20**). Further work examining specific mROS generation in the context of Mtb-induced glycolytic reprogramming is warranted, but this work is supportive of the model suggested by Mills et al whereby glycolytically-derived ATP fuels reverse electron transport within the mitochondrion, permitting mROS induction and consequent increases in IL-1β [269].

As mentioned, macrophage glycolytic reprogramming has never previously been examined in the context of host defence. Shi et al demonstrate broad upregulation of glucose transporters, glycolytic enzymes, HIF-1α and lactate exporters in homogenised lungs from H37Rv-infected mice at Day 0 [334], supporting early glycolytic reprogramming as a feature of the host response to infection. Similarly, since the time of writing Lachmandas et al have confirmed upregulation of glycolytic genes and downregulation of TCA genes in a transcriptional analysis of PBMCs from pulmonary TB patients, which reverses following treatment with anti-tuberculous medication [335]. Neither study, however, examined the functional implication of this shift towards glycolysis following infection. In order to address this, intracellular Mtb growth in macrophages was assessed in the presence of the glycolytic inhibitor galactose, compared to that in the presence of glucose-containing media. As these experiments involved the use of live bacilli, preliminary experiments were performed to confirm no significant difference in Mtb growth in the presence of glucose- or galactose-supplemented media (**Figure 4.21**), ruling out a direct impact of glycolytic inhibition upon bacillary growth that could confound interpretation of its effect on macrophage function in isolation.

Glycolytic inhibition resulted in impaired macrophage early bacillary clearance, indicated by significantly increased H37Ra CFU at 72 hours post infection (**Figure 4.22**). A similar trend towards increased Mtb growth secondary to glycolytic inhibition was demonstrated in human AM infected with avirulent H37Ra (**Figure 4.23**) and virulent H37Rv (**Figure 4.24**). These data demonstrate for the first time that glycolytic reprogramming directly facilitates macrophage clearance of Mtb infection. Conflictingly, Mehrotra et al previously reported enhanced Mtb growth in human MDM in the presence of glycolytic inhibitor 5-thioglucose [356], though no data was presented to confirm viability of these cells in the presence of this HK1 inhibitor.

The centrality of IL-1 signalling in macrophage mycobactericidal function has been demonstrated by Mayer-Barber et al [146], with BMDM from *Il1r1-/-* and *Il1a,Il1b-/-* mice demonstrating increased CFU at 5 days post-infection compared to WT controls. Similarly, in the human MDM model utilised in this work, exogenous IL-1β enhances macrophage clearance of H37Ra (**Figure**

4.25), and that inhibition of IL-1β signalling impairs clearance (**Figure 4.26**). Interestingly, when IL-1β signalling was inhibited using anti-IL-1β antibody, the impact of glycolytic inhibition on macrophage mycobactericidal ability was completely abrogated (**Figure 4.27**). This suggests that the functional impact of glycolytic reprogramming on macrophage early bacillary clearance in Mtb infection is mediated through induction of IL-1β.

These results conflict with those of Singhal et al who demonstrate a role for metformin, and AMPK activator used in the treatment of DM2, in enhancing early mycobacterial clearance [353]. Though metformin induces intracellular glycolysis, this is associated with decreased IL-1β production through inhibition of Complex I of the ETC [297]. However, metformin has a wide range of intracellular effects, and Singhal et al have specifically linked increased mycobactericidal effect with AMPK activation, and do not examine the role of glycolytic reprogramming and IL-1β production in the context of macrophage function.

4.3.4 Glycolytic reprogramming in Mtb infection in a murine macrophage model

One of the strengths of this body of work is the centrality of primary human macrophages. However, as the majority of published data focussing on glycolytic reprogramming centres on murine cells, findings were confirmed in a murine macrophage model also. Using lactate quantification, increased glycolytic activity was observed in murine BMDM following infection with avirulent H37Ra or virulent H37Rv (**Figure 4.28A**), and this was inhibited in the presence of glycolytic inhibitor 2-DG. Similar to results observed in human macrophages (**Figure 4.8**), glycolysis was required for optimal production of IL-1β (**Figure 4.28B**). Interestingly, though TNF-α production was not significantly impacted, a trend towards reduced levels in the presence of the glycolytic inhibitor 2-DG was observed (**Figure 4.28C**), in contrast results observed in human MDM (**Figure 4.8D**). This may reflect inter-species variation or possible off-target effects of 2-DG. Using BMDM taken from an *IL-1R-/-* mice (a kind gift from Professor Kingston Mills, TCD), IL-1 signalling was shown to be necessary for induction of *Ptgs2* and suppression of *Il10* transcription following infection with H37Ra. As both IL-1β and IL-1α signalling is absent in these animals, the specificity of IL-1β signalling cannot be inferred from this data.

Similar to results observed in human MDM and human AM (**Figure4.22; Figure 4.23; Figure 4.24**), murine BMDM early bacillary clearance was significantly impaired when glycolytic reprogramming was inhibited (**Figure 4.30**). As also demonstrated in human MDM (**Figure 4.25; Figure 4.26**), and in observations by Mayer-Barber et al [146], exogenous IL-1β enhanced bacillary clearance by murine macrophages (**Figure 4.31**), and cells deficient in IL-1 signalling demonstrated impaired

clearance of H37Ra at 72 hours post-infection (**Figure 4.32**). Finally, the impact of glycolytic inhibition using 2-DG was completely abrogated in *IL-1R-/-* macrophages (**Figure 4.33**), in line with results observed in human MDM following treatment with anti-IL-1β antibody (**Figure 4.27**), suggesting the importance of the glycolysis/IL-1β axis in early macrophage responses to Mtb infection.

Glycolytic reprogramming in LPS-stimulated macrophages has been linked to increased levels of the enzymatically-inactive dimeric form of the glycolytic enzyme PKM2 [247]. PKM2 can exist in an enzymatically-active tetrameric form or in an enzymatically-inactive dimeric form [260]. Dimeric PKM2 has been shown to translocate to the nucleus within cancer cells, where it upregulates glycolysis in a number of ways, including activation of HIF-1α, thus potentiating the Warburg effect [260]. In work performed in collaboration with Palsson-McDermott et al [247], the PKM2 activator TEPP-46 (which gives rise to increased enzymatic activity and reduced nuclear translocation of the enzyme, with the net effect of reducing glycolytic rate) was shown to reduce IL-1β secretion in murine BMDM following infection with H37Ra (**Figure 4.34A**). Interestingly, a less substantial trend towards decreasing TNF-α production was also observed with increasing doses of TEPP-46 (**Figure 4.34B**), echoing results observed with direct inhibition of glycolysis in murine macrophages using 2-DG (**Figure 4.28C**), but in contrast to observations in human MDM (**Figure 4.8D**). As discussed above, this may reflect species-related variation. Trends towards increased IL-10 production demonstrated with low concentrations of TEPP-46 complimented results observed with LPS stimulation [247], however this effect was not demonstrated at higher concentrations of TEPP-46 (**Figure 4.34C**). Despite this, as observed in 2-DG experiments (**Figure 4.30**), antagonism of the Warburg effect using PKM2 activation resulted in reduced mycobactericidal ability of murine macrophages (**Figure 4.34D–F**), further emphasising the functional importance of the glycolytic shift in host defence. Likewise, clearance of the intracellular pathogen *Salmonella typhimurium* was impaired in the presence of the PKM2 activator TEPP-46 (**Figure 4.35**), suggesting that the role of glycolysis in host defence is not specific to Mtb.

4.3.5 Pharmacological induction of glycolysis boosts macrophages responses to Mtb

Meclizine has been demonstrated to shift cellular energy metabolism from oxidative phosphorylation to glycolysis, via accumulation of the mitochondrial inhibitor phosphoethanolamine due to meclizine-induced inhibition of the Kennedy pathway [464,468]. Other pharmacological agents that inhibit mitochondrial respiration (with consequent upregulation of glycolysis) through direct inhibition of Complex I (NADH:ubiquinone

oxidoreductase), such as metformin and rotenone, have been shown to inhibit mROS and IL-1β production [297]. However, recent work by Gohil et al suggests meclizine-induced inhibition of mitochondrial respiration is not mediated through direct inhibition of ETC complexes [468]. In fact, phosphoethanolamine specifically inhibits State 3 mitochondrial respiration (i.e. ADP-stimulated respiration) without impacting State2/4 mitochondrial respiration (i.e. residual oxygen consumption). Furthermore, this inhibition of mitochondrial respiration is associated with reduced NADH levels [468], a phenomenon that has also been observed in monocytes treated with the yeast product β-glucan [480]. β-glucan induces a state of "trained immunity" in monocytes, a process that involves cell glycolytic reprogramming (characterised by reduced mitochondrial oxygen consumption, increased lactate production and increased glucose consumption) in an Akt/mTOR/HIF-1α-dependent pathway [480]. Importantly, the increased NAD+/NADH ratio induced by β-glucan stimulation contrasts to the decreased NAD+/NADH ratio associated with LPS-induced glycolytic reprogramming [481], and this is postulated to account for the sustained priming of cells exposed to β-glucan as opposed to the tolerance observed following LPS stimulation [482]. In this context, it was hypothesised that meclizine-induced glycolytic reprogramming may help to bolster IL-1β production and hence facilitate clearance of Mtb in human macrophages.

Using extracellular flux analysis, we confirmed a shift towards glycolytic metabolism in uninfected human MDM in the presence of meclizine (**Figure 4.36**), in line with observations by Gohil et al using human fibroblasts [464]. Interestingly, no significant reduction in OCR was observed following treatment with meclizine (**Figure 4.36A**), though this may be reflective of reduced metabolic activity at baseline attenuating the observed impact of inhibition. Following infection with non-viable iH37Rv, meclizine pretreatment was associated with a more substantial shift towards glycolysis and with increased IL-1β production (**Figure 4.37**). Unexpectedly, this trend towards increased glycolytic shift was not confirmed in macrophages infected with live H37Ra as measured by lactate assay (**Figure 4.38A**), though a trend towards increased IL-1β production was observed (**Figure 4.38B**). The reason for this inconsistency is unclear. It is possible that meclizine present in the media interfered indirectly with the lactate assay, though this did not appear to affect results in iH37Rv experiments (**Figure 4.37D**). Finally, a trend towards increased bacillary clearance by macrophages pre-treated with meclizine is observed at higher concentrations (**Figure 4.39**). Though numbers in these experiments remain small, they suggest a potential role for meclizine as a therapeutic adjunct to enhance early clearance of Mtb by macrophages. Furthermore, this work represents the first example of glycolytic manipulation in order to enhance host defence.

4.4 Conclusion

The results presented in **Chapter 4** demonstrate a functional role for glycolytic reprogramming in the host macrophage response to Mtb. Specific glycolysis-driven increases in pro-inflammatory IL-1β enhance PGE2 production, suppress IL-10 production, and ultimately facilitate early bacillary clearance in both human and murine macrophage models, with results withstanding interrogation using various methods of glycolytic inhibition. This work represents the first demonstration of metabolic reprogramming as an integral component of host defence, with robust evidence provided for its role in the macrophage response to Mtb infection and supportive evidence for a similar role in macrophage responses to another intracellular pathogen, *S. typhi*. Finally, this work provides evidence for glycolytic manipulation as a potential tool to enhance early macrophage responses to Mtb, raising the possibility of a new avenue of exploration in the search for host-directed adjuvant therapies. In **Chapter 5**, the integrity of this important host defence mechanism in the setting of cigarette smoke exposure, a significant risk factor for the development of TB disease, is examined.

CHAPTER 5:

The Effect of Cigarette Smoke Exposure on the Macrophage Metabolic Response to Mtb Infection

5.1 Introduction

5.1.1 Hypothesis: Cigarette smoke impairs macrophage glycolytic reprogramming in response to Mtb infection

Smoking is a well-established risk factor for Mtb infection, and our group has previously demonstrated impairments in AM cytokine responses following Mtb infection in smokers compared to non-smokers [411]. Evidence also suggests that cigarette smoke and its components alter metabolic profile of human AM [395,419], although studies have yielded conflicting results in terms of its impact on glucose utilisation [455-457]. To our knowledge, glycolytic rates in smokers' AM and non-smokers' AM have never been compared. Recent work in Type II alveolar epithelial cells, however, suggests that acrolein treatment skews metabolism away from glycolysis towards fatty acid oxidation [458], and Type II alveolar epithelial cells from cigarette smoke-exposed mice demonstrate decreased glycolytic rates compared to unexposed controls [459]. Having established that Mtb infection induces a metabolic shift towards glycolysis in human macrophages and that this shift is required for optimal anti-mycobacterial responses through work outlined in **Chapter 3** and **Chapter 4**, therefore, it was hypothesised that this glycolytic shift may be impaired in smokers' AM and that this may partly explain their attenuated cytokine response to infection, and possibly the increased susceptibility to Mtb infection seen in these individuals.

5.2 Results

5.2.1 CIGARETTE SMOKE EXTRACT REDUCES BASELINE OCR AND ECAR AND ATTENUATES GLYCOLYTIC RESERVES IN HUMAN MDM

Application of cigarette smoke extract (CSE) to cells in vitro is a well-established model for studying the cellular effects of smoking. Thus, the impact of CSE treatment on human MDM metabolic and cytokine responses to Mtb infection was investigated. Generation of CSE was achieved as outlined in **Chapter 2 (Section 2.7)**. Based on Bernhard's original equations, 2.5% CSE was equitable to a smoker of 20 cigarettes / day, 5% equitable to 40 cigarettes / day, and 10% equitable to 80 cigarettes / day. CSE treatment was applied to human MDM as described. Firstly, the impact of CSE on cell viability was assessed using a crystal violet assay, demonstrating a trend towards decreased viability with increasing CSE dose (**Figure 5.1**). Next, extracellular flux analysis were performed, in conjunction with lactate quantification, on human MDM following treatment with CSE for 48 hours at various doses compared to untreated control. Dose-dependent decreases in both OCR and ECAR were evident (**Figure 5.2 A – B**). Calculation ECAR/OCR ratio indicated that ECAR was reduced to a greater extent (**Figure 5.2 C**), suggesting CSE treatment was skewing cells away from glycolytic metabolism, supporting observations by Agarwal et al in Type II alveolar epithelial cells [458]. Interrogation with inhibitors showed substantial reductions in both SRC and GR following CSE treatment (**Figure 5.3**). Taken together, these data imply a global reduction in macrophage metabolic activity and metabolic reserves following CSE treatment, with more pronounced attenuation of glycolysis relative to mitochondrial respiration.

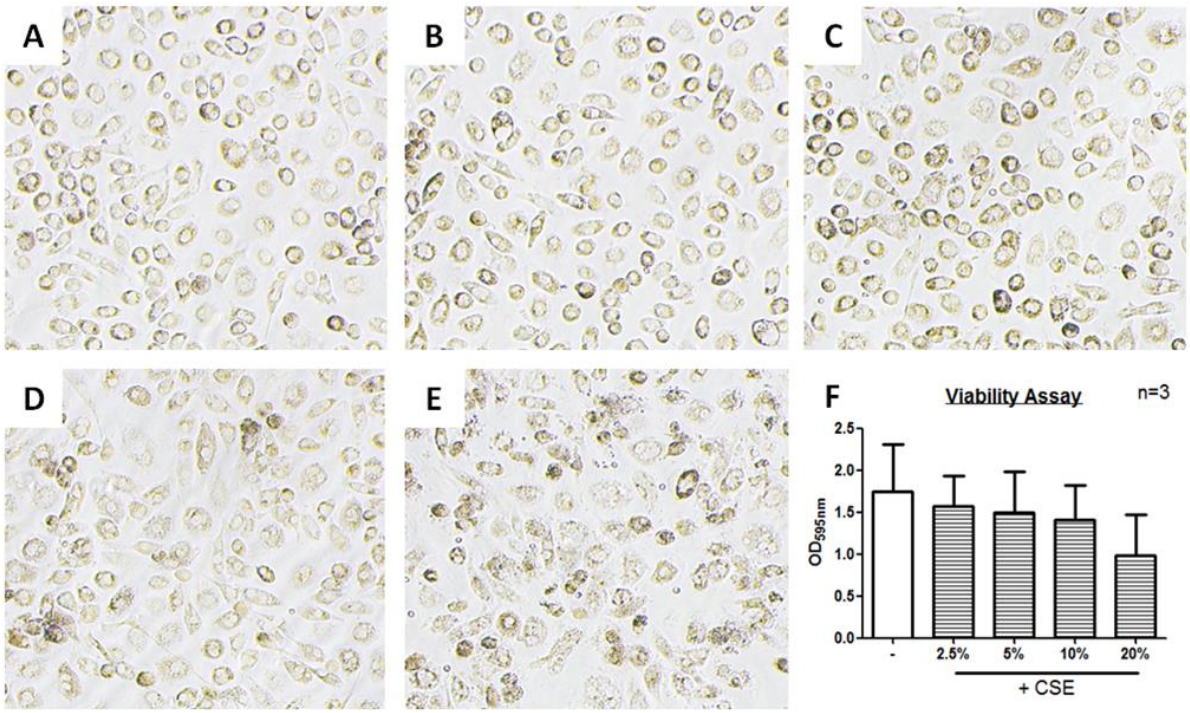

FIGURE 5.1 CSE doses up to 10% do not significantly reduce human MDM viability in vitro. MDM isolated from IBTS buffy coats were cultured for 5 days, scraped, and plated on Seahorse Biosciences 24-well plates at 200,000 cells/well in cRPMI. 24 hours after plating, cells were treated with CSE at varying doses and incubated for 48 hours at 37°C and 5% CO_2. Cells were visualised by light microscopy prior to performance of CV assay. Panels A – E depict light microscopy images of one representative donor after incubation with 0% (A), 2.5% (B), 5% (C), 10% (D) and 20% (E) CSE for 48 hours. Panel F depicts mean ± SEM absorbance at OD_{595nm} following CV staining for three individual donors.

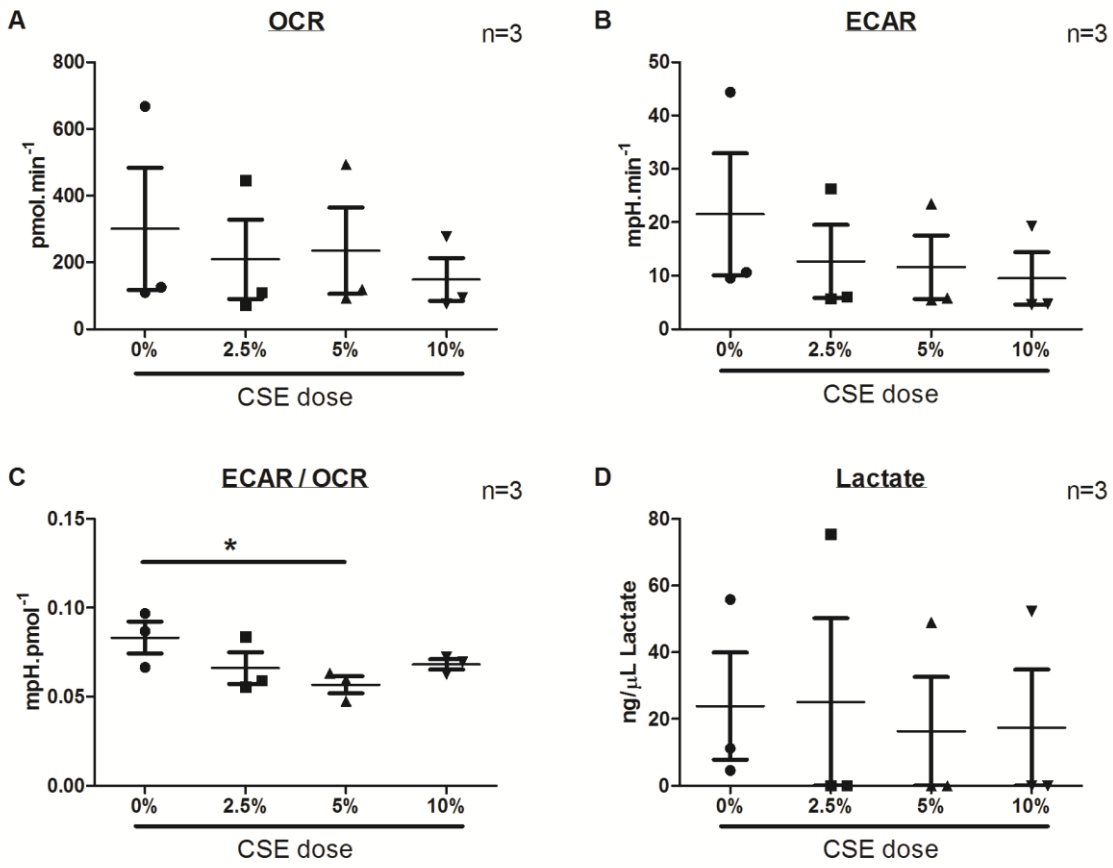

FIGURE 5.2 CSE treatment reduces baseline OCR and ECAR of human MDM. MDM were prepared and treated with varying doses of CSE as previously. 48 hours after CSE treatment, supernatants were removed and retained for quantification of lactate, and extracellular flux analyses were performed with CV assay used to normalise data. Panel A – C depict mean ± SEM OCR (A), ECAR (B) and ECAR/OCR ratio for three individual donors. Panel D depicts corresponding mean ± SEM absorbance at OD_{595nm} following CV staining for three individual donors. Statistical analyses were performed using the paired Student's t-test; *p<0.05.

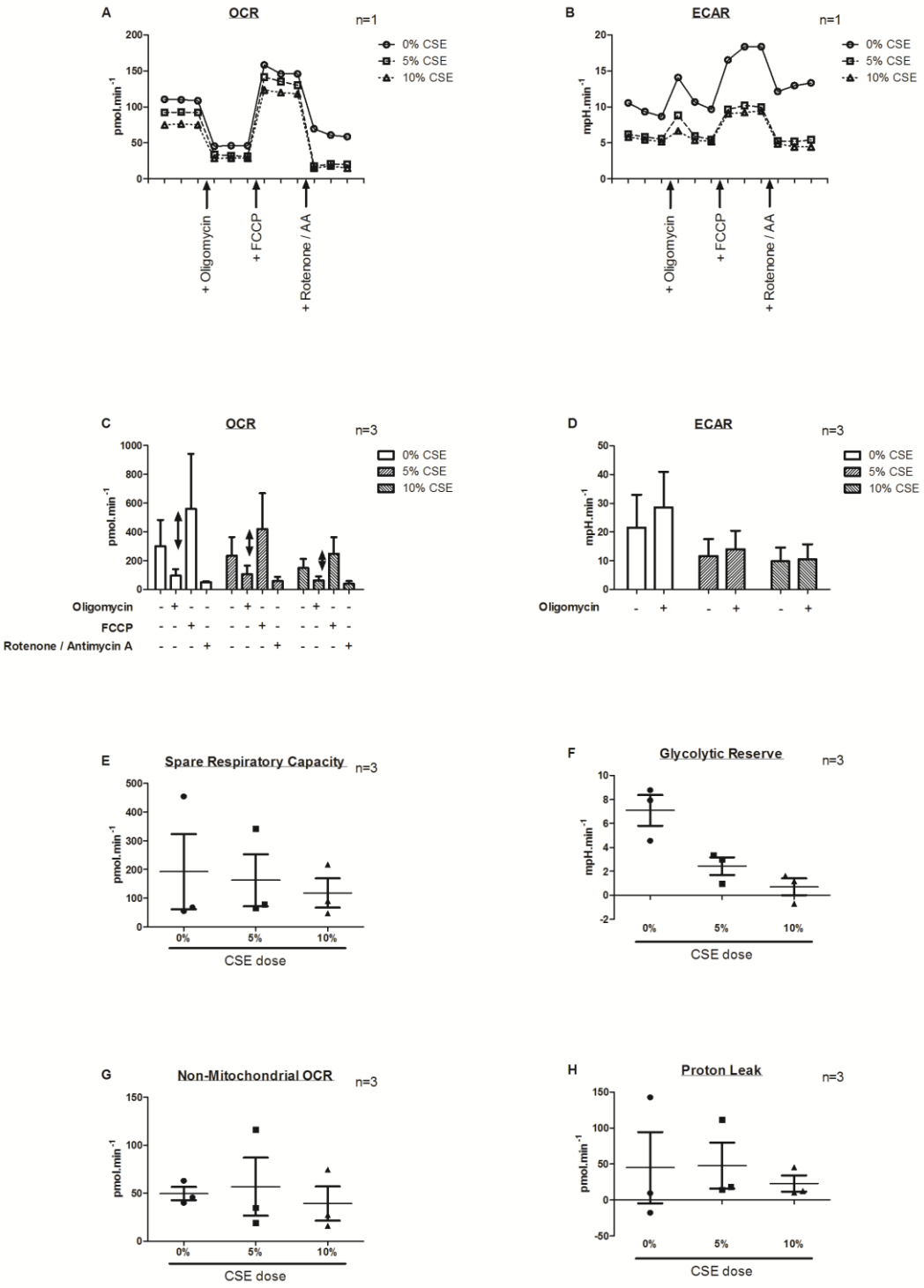

FIGURE 5.3 CSE treatment attenuates Glycolytic Reserve of human MDM. MDM were prepared and treated with varying doses of CSE as previously. 48 hours after CSE treatment, extracellular flux analyses were performed with sequential addition of mitochondrial inhibitors oligomycin (1µM), FCCP (2µM) and rotenone/antimycin A (0.5µM). CV assay was used to normalise data. Panels A and B depict real-time OCR (A) and ECAR (B) for one representative donor. Panels C and D depict normalised mean ± SEM OCR (C) and ECAR (D) for four individual donors. Panels E – H depict normalised mean ± SEM SRC (E), GR (F), Non-Mitochondrial OCR (G) and PL (H) for four individual donors. Statistical analyses were performed using the Student's t-test; statistical significance was set at $p<0.05$.

5.2.2 CSE attenuates glycolytic reprogramming in response to Mtb infection in human MDM

Following the observation that CSE treatment altered human MDM metabolism at baseline, the impact of this treatment on Mtb-induced glycolytic reprogramming was examined next. Human MDM were isolated, cultured and prepared as previously described, and CSE treatments applied 24 hours prior to infection with Mtb. As before, pre-treatment with CSE led to a dose-dependent decrease in both OCR (**Figure 5.4A**) and ECAR (**Figure 5.4B**). The shift towards glycolytic metabolism following infection with Mtb, as demonstrated by increased ECAR / OCR ratio, was attenuated in CSE-treated MDM (**Figure 5.4C**). CSE treatment was also associated with a dose-dependent attenuation in Mtb-induced lactate production (**Figure 5.5**). These data imply impairment of glycolytic reprogramming following Mtb infection in CSE exposed human MDM.

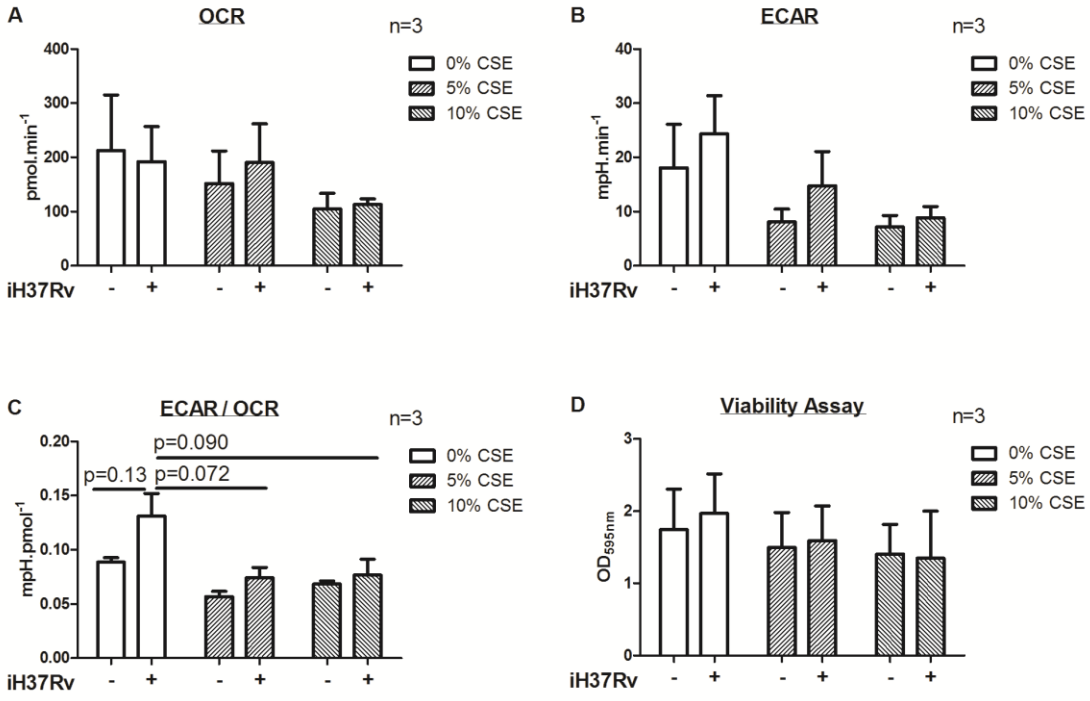

FIGURE 5.4 CSE treatment impairs Mtb-induced increases in the ECAR/OCR ratio in human MDM. MDM were prepared and treated with varying doses of CSE as previously. 24 hours after CSE treatment, cells were infected with iH37Rv at low MOI of left uninfected (control). 24 hours post-infection, extracellular flux analyses were performed with CV assay used to normalise data. Panel A – C depict mean ± SEM OCR (A), ECAR (B) and ECAR/OCR ratio for three individual donors. Panel D depicts corresponding mean ± SEM absorbance at OD_{595nm} following CV staining for three individual donors. Statistical analyses were performed using the paired Student's t-test; statistical significance was set at $p<0.05$.

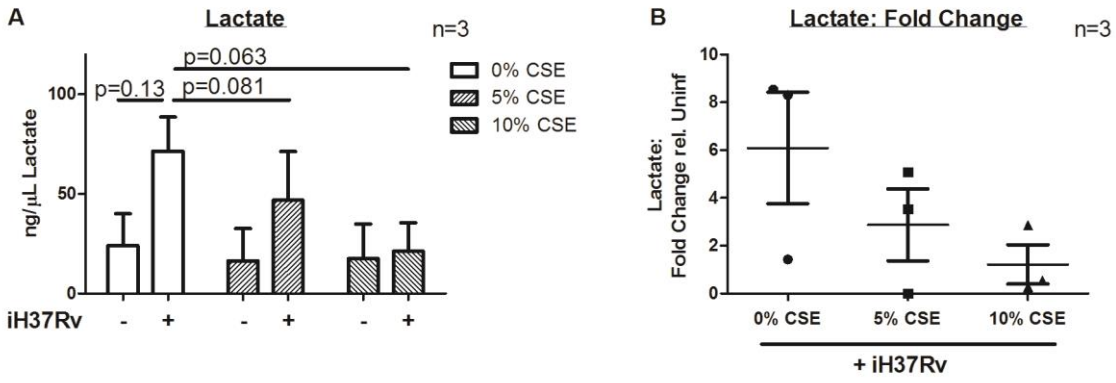

FIGURE 5.5: CSE treatment impairs Mtb-induced increases in lactate production in human MDM. MDM were prepared and treated with varying doses of CSE as previously. MDM were prepared and treated with varying doses of CSE as previously. 24 hours after CSE treatment, cells were infected with iH37Rv at low MOI of left uninfected (control). 24 hours post-infection, supernatants were removed and lactate concentration quantified. Panel A depicts mean ± SEM lactate concentration for three individual donors. Panel B depicts mean ± SEM fold change in lactate concentration in infected cells relative to corresponding uninfected control. Statistical analyses were performed using the paired Student's t-test; statistical significance was set at $p<0.05$.

5.2.3 CSE impairs cytokine production in response to Mtb infection in human MDM

Data presented in **Chapter 4** demonstrate the association between glycolytic reprogramming and IL-1β production in human MDM infected with Mtb, while TNF-α production is not affected. Following the observation that CSE treatment resulted in attenuation of infection-induced glycolytic reprogramming, therefore, the impact of CSE treatment on cytokine production was next investigated. Again, human MDM were treated with varying doses of CSE 24 hours prior to infection with iH37Rv, resulting in a dose-dependent decrease in IL-1β production (**Figure 5.6A**). TNF-α production was also attenuated following CSE treatment (**Figure 5.6B**), however, suggesting that CSE-mediated impairment in cytokine production is not due solely to attenuated glycolytic reprogramming.

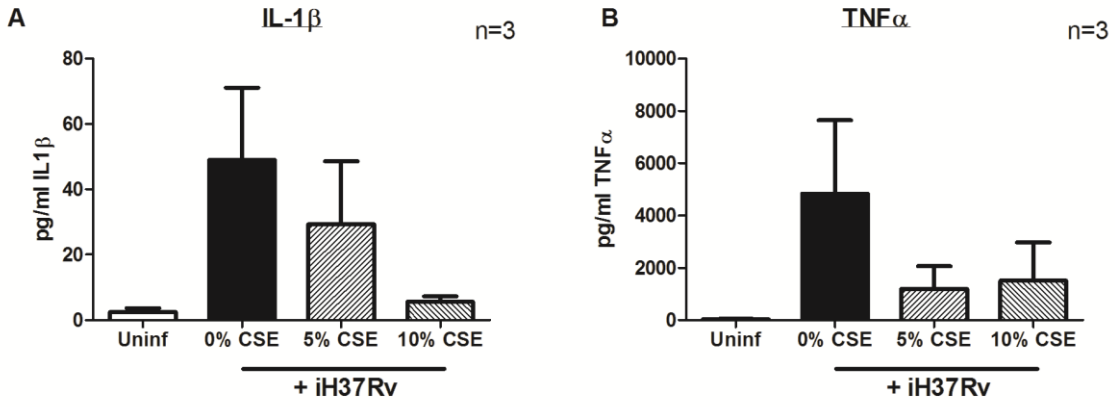

FIGURE 5.6 CSE treatment impairs Mtb-induced production of IL-1β and TNF-α in human MDM. MDM were prepared and treated with varying doses of CSE as previously. MDM were prepared and treated with varying doses of CSE as previously. 24 hours after CSE treatment, cells were infected with iH37Rv at low MOI of left uninfected (control). 24 hours post-infection, supernatants were removed and cytokine concentration quantified by ELISA. Panels A and B depict mean ± SEM IL-1β (A) and TNF-α (B) concentration for three individual donors. Statistical analyses were performed using the paired Student's t-test; statistical significance was set at $p<0.05$.

5.2.4 Addition of meclizine does not restore infection-induced glycolytic reprogramming in CSE-treated human MDM

As presented in **Chapter 4**, pre-treatment with meclizine dihydrochloride induces a shift towards glycolytic reprogramming both at baseline and following infection in human MDM. Thus, it was hypothesised that meclizine could be used to restore the glycolytic response to infection in CSE-treated human MDM, possibly enhancing IL-1β production in response to infection. Human MDM were prepared as before, and treated with 5% CSE or left untreated (control) as in **Chapter 2 (Section 2.7.2)**. 24 hours later, meclizine dihydrochloride at 25μM or DMSO control was applied to designated wells, as described in **Chapter 2 (Section 2.5.4)**. 24 hours after this, infections were performed as previously. As before, CSE treatment attenuated Mtb-induced lactate production (**Figure 5.7A**). Treatment with meclizine did not improve CSE-mediated attenuation in lactate production (**Figure 5.7A**). Similarly, meclizine treatment did not improve CSE-mediated attenuation in IL-1β production (**Figure 5.7B**). Thus, in this model, meclizine could not be used to overcome the impact of CSE treatment on glycolytic reprogramming in Mtb-infected human MDM.

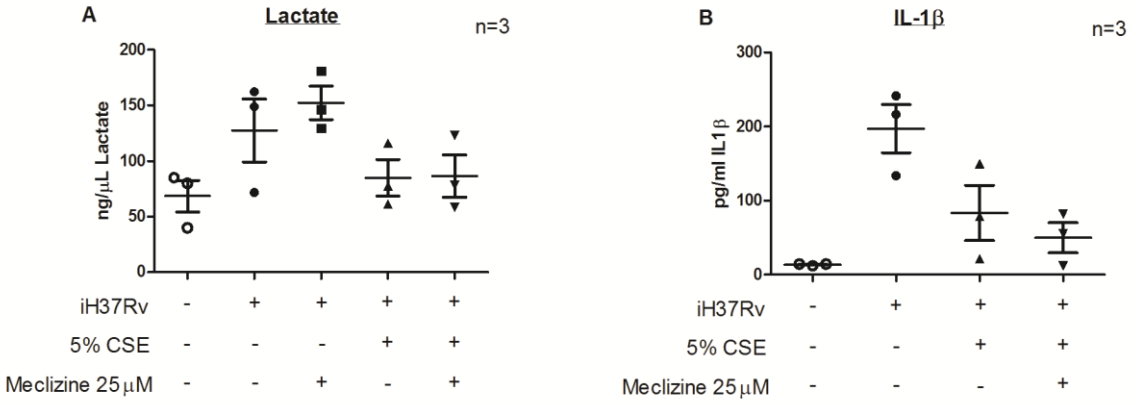

FIGURE 5.7 Meclizine does not enhance lactate or IL-1β production in CSE-treated human MDM infected with iH37Rv. MDM were prepared and treated with CSE (5%). 24 hours after CSE treatment, cells were treated with Meclizine dihydrochloride (25μM) or with DMSO (control). 24 hours later, cells were infected with iH37Rv at low MOI or left uninfected (control). CSE, Meclizine and control treatments were maintained for the duration of the experiment. 24 hours post-infection, supernatants were removed and lactate and IL-1β concentration quantified. Panels A and B depict mean ± SEM lactate (A) and IL-1β (B) concentration for three individual donors. Statistical analyses were performed using the paired Student's t-test; statistical significance was set at $p<0.05$.

5.2.5 Smokers' AM demonstrate attenuated production of pro-inflammatory mediators following infection when compared to non-smokers' AM

Following observations of impaired infection-induced glycolytic reprogramming and cytokine production in human MDM treated with CSE, the effect of cigarette smoke exposure *in vivo* on macrophage metabolic and immune responses was next examined. Human AM were obtained at bronchoscopy as described in **Chapter 2 (Section 2.1.1)**. Donor current and previous smoking status was confirmed by interview prior to bronchoscopy at the time written informed consent was obtained. Based on this information, donors were classified as "smokers", "ex-smokers" or "never-smokers". Due to limited numbers of never-smokers, an alternative classification of "smokers" and "non-smokers" (with non-smokers including both never-smokers and ex-smokers who had ceased smoking more than 2 years prior to sample acquisition) was utilised for the majority of experiments.

Our group has previously demonstrated attenuated IL-1β, TNF-α and IFN-γ production in smokers' AM following infection with H37Ra, as compared to both ex-smokers' AM and never-smokers' AM [411]. In order to confirm this with iH37Rv, smokers' and non-smokers' AM were infected at low MOI as previously, and supernatants harvested at 24 hours post-infection. As before, infection-mediated induction of both IL-1β and TNF-α was reduced in smokers' AM compared to non-smokers' AM (**Figure 5.8 A – B**). Given the requirement for IL-1β signalling in Mtb-induced PGE_2 production demonstrated in **Chapter 4**, iH37Rv-induced PGE_2 production in smokers' and non-smokers' AM was also examined, and similarly found to be attenuated in smokers (**Figure 5.8C**). Viability assay was also performed, as increased cell death has been reported in smokers' AM and this could represent a potential confounder of results. However, CV assay did not demonstrate significant differences in cell viability between smokers' and non-smokers' AM in this model (**Figure 5.8D**).

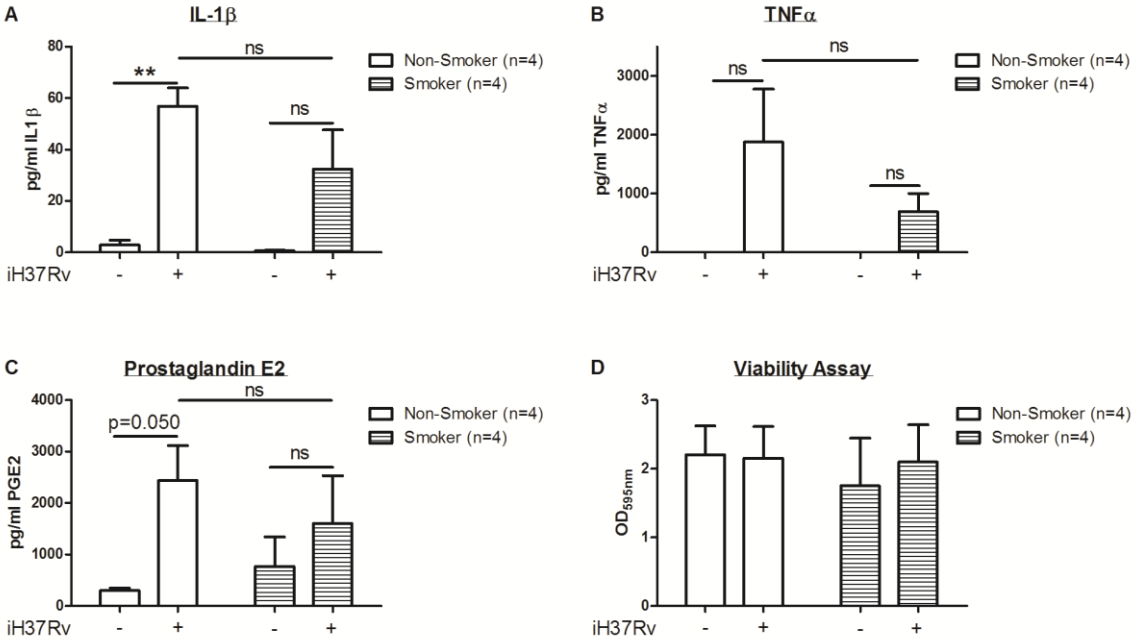

FIGURE 5.8 Smokers' AM demonstrate attenuated production of IL-1β, PGE_2 and TNF-α compared to non-smokers' AM following infection with H37Ra. Human AM were isolated from BAL fluid, plated at $1x10^6$/mL on tissue culture-treated 24-well plates in cRPMI supplemented with cefotaxime (50μg/mL) and fungizone (50U/mL), and non-adherent cells removed by washing. 24 hours after plating, cells were infected with H37Ra at low MOI. At 24 hours post-infection, supernatants were removed and cytokine and eicosanoid concentrations were quantified by ELISA. Panels A – C depict mean ± SEM IL-1β (A), TNF-α (B), and PGE_2 (C) concentrations for 4 individual non-smokers and 4 individual smokers. Panel D depicts corresponding mean ± SEM absorbance at OD_{600nm} detected following CV assay staining. Within-group statistical analyses were performed using the paired Student's t-test; between-group statistical analyses were performed using the Mann Whitney U test; **p<0.01.

5.2.6 At baseline, smokers' AM demonstrate reduced metabolic activity and reduced metabolic reserves compared to non-smokers' AM

Next, differences in baseline metabolic parameters between uninfected smokers' and non-smokers' AM were investigated. Human AM were isolated and plated on Seahorse Biosciences plates as previously described. 48 hours after plating, cells were interrogated by extracellular flux analysis, with results normalised to cell number as before. Plotting ECAR (y-axis) against OCR (x-axis) suggested overall reduced metabolic activity of smokers' AM compared to non-smokers' AM (**Figure 5.9**). Absolute OCR values in smokers' AM were significantly reduced compared to non-smokers' AM (**Figure 5.10A**), reflective of reduced overall metabolic activity in these cells, and absolute ECAR was also reduced in smokers' AM (**Figure 5.10B**). Despite plots of ECAR relative to OCR suggesting a skewing of smokers' AM towards oxidative phosphorylation and away from glycolytic metabolism (**Figure 5.9**), direct comparison of ECAR / OCR ratio (**Figure 5.10C**) and lactate production (**Figure 5.11**) did not reveal any substantial differences between uninfected smokers' and non-smokers' AM. However, interrogation with inhibitors demonstrated significantly reduced SRC (**Figure 5.12E**) and a trend towards reduced GR (**Figure 5.12F**) in smokers' AM relative to non-smokers' AM. Interestingly, Non-Mitochondrial OCR (**Figure 5.12G**) and PL (**Figure 5.12H**) were not substantially different between smokers and non-smokers. Overall, these data imply global reduction in metabolic activity, as well as reduced metabolic reserve, in smokers' AM compared to non-smokers' AM, similar to results observed in CSE-treated human MDM.

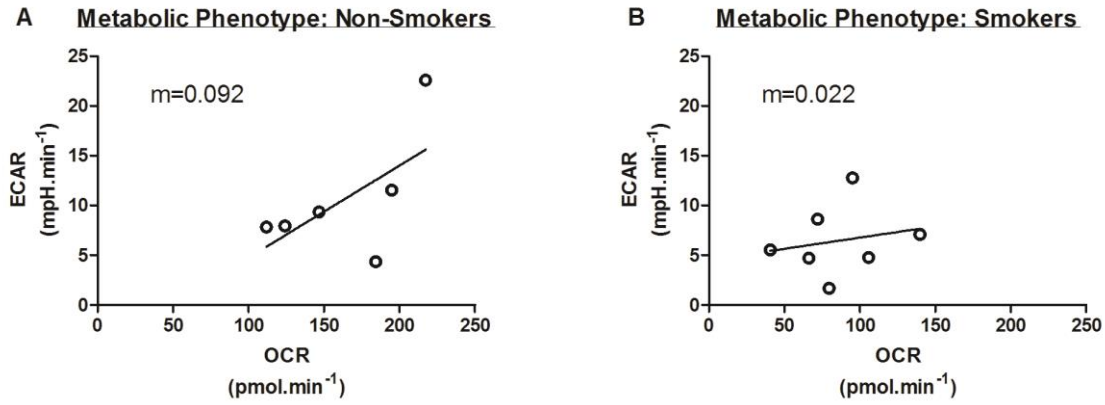

FIGURE 5.9 Smokers' AM demonstrate reduced metabolic activity at baseline compared to non-smokers' AM. Human AM were plated on Seahorse Biosciences 24-well plates at 100,000 cells/well in cRPMI supplemented with cefotaxime (50µg/mL) and fungizone (50U/mL). On Day 1, non-adherent cells were removed by washing. On Day 2, extracellular flux analyses were performed with CV assay used to normalise data. Panels depict normalised ECAR (y-axis; representative of glycolytic activity) relative to OCR (x-axis; representative of mitochondrial respiration) in non-smokers' (A) and smokers' (B) AM. Data are representative of 6 (A) and 7 (B) individual donors.

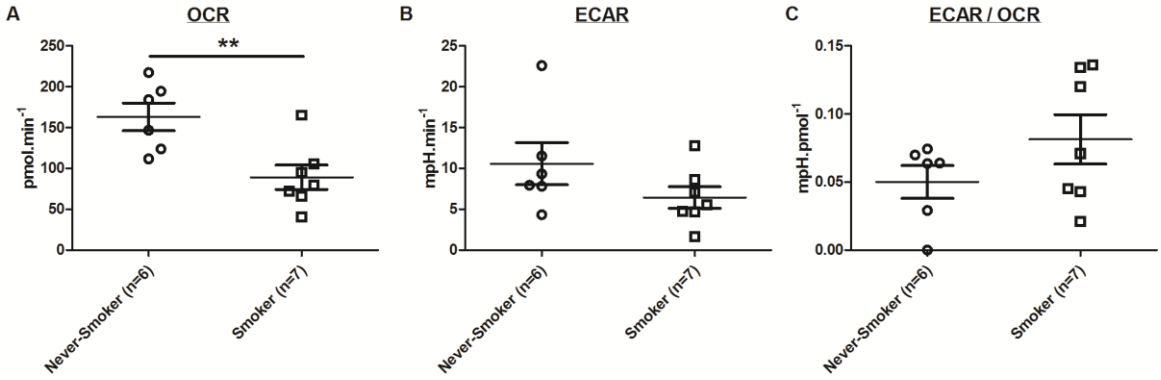

FIGURE 5.10 Smokers' AM demonstrate reduced OCR and ECAR at baseline compared to non-smokers' AM. Human AM were plated on Seahorse Biosciences 24-well plates at 100,000 cells/well in cRPMI supplemented with cefotaxime (50µg/mL) and fungizone (50U/mL). On Day 1, non-adherent cells were removed by washing. On Day 2, extracellular flux analyses were performed with CV assay used to normalise data. Panels A – C depict mean ± SEM OCR (A), ECAR (B) and ECAR/OCR ratio (C) for 6 non-smokers and 7 smokers. Statistical analyses were performed using the Mann Whitney U test; **p<0.01.

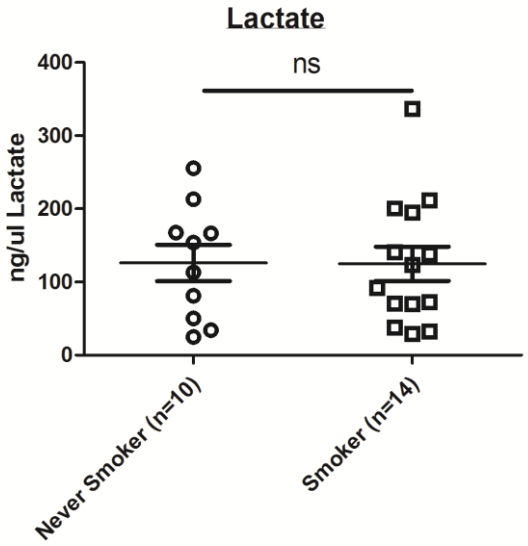

FIGURE 5.11 No difference in lactate production is evident between smokers' and non-smokers' AM at baseline. Human AM were plated on Seahorse Biosciences 24-well plates at 100,000 cells/well in cRPMI supplemented with cefotaxime (50μg/mL) and fungizone (50U/mL). On Day 1, non-adherent cells were removed by washing. On Day 2, supernatants were removed and lactate concentration quantified. Data is presented as mean ± SEM lactate concentration for 10 non-smokers and 14 smokers. Statistical analyses were performed using the Mann Whitney U test; statistical significance was set at $p<0.05$.

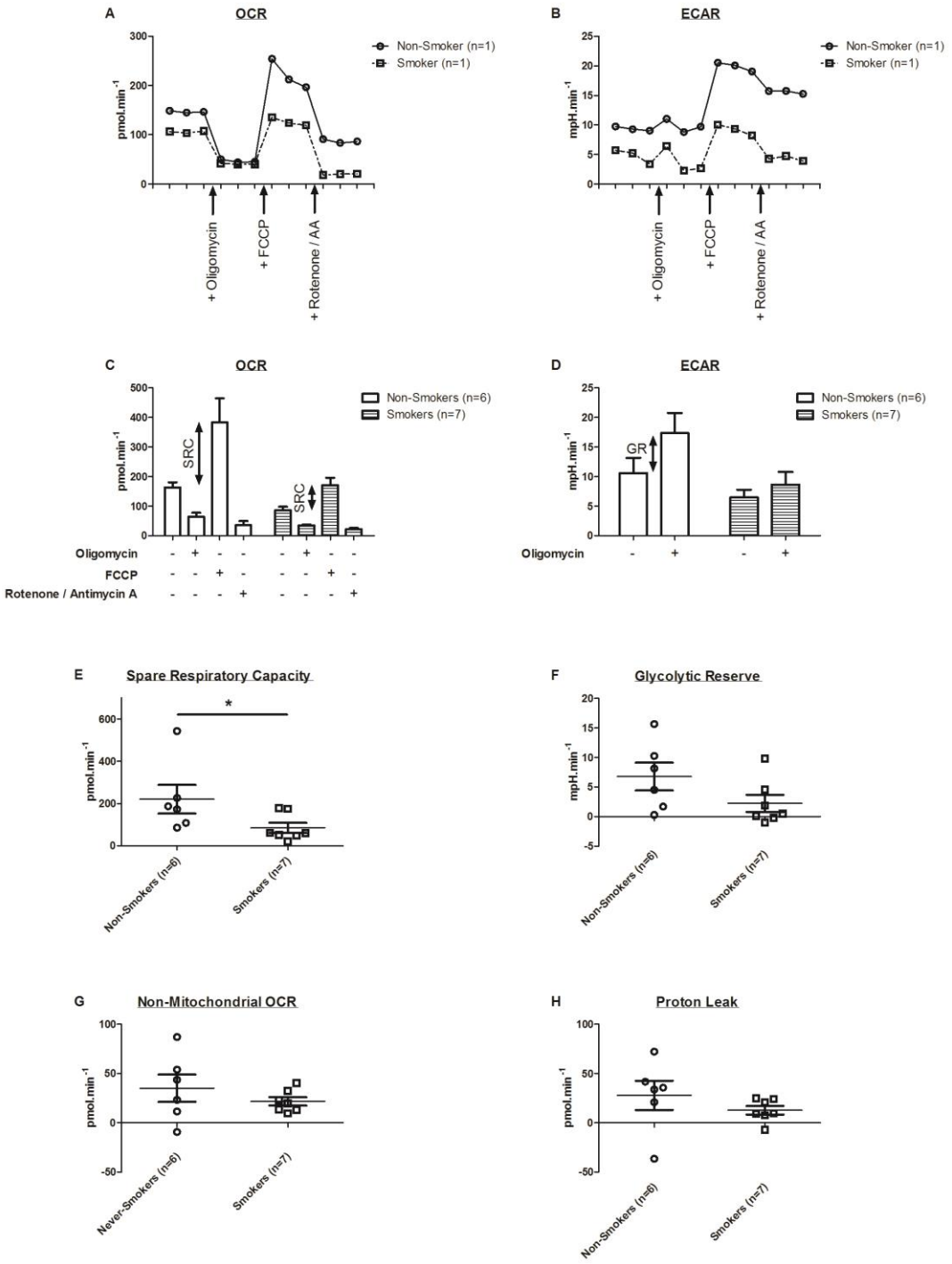

FIGURE 5.12 Smokers' AM have reduced metabolic reserves compared to non-smokers' AM. Extracellular flux analysis was performed on human AM and data normalised using CV assay. Mitochondrial inhibitors were sequentially to achieve final concentrations of 1µM (oligomycin), 2µM (FCCP) and 0.5µM (rotenone/antimycin A). Panels A and B depict real-time OCR (A) and ECAR (B) for two representative donors (one Non-Smoker and one Smoker). Panels C and D depict mean ± SEM OCR (C) and ECAR (D) for 6 non-smokers and 7 smokers. Panels E – H depict normalised mean ± SEM SRC (E), GR (F), Non-Mitochondrial OCR (G) and PL (H) of 6 non-smokers and 7 smokers. Statistical analyses were performed using Mann Whitney U test; *p<0.05.

5.2.7 Smokers' AM demonstrate attenuated glycolytic reprogramming following LPS stimulation compared to non-smokers' AM

Next, the impact of *in vivo* cigarette smoke exposure on human AM glycolytic reprogramming in response to LPS stimulation was investigated. Human AM were isolated as before and LPS treatments applied as previously described. LPS-induced increases in ECAR (**Figure 5.13**) and lactate concentration (**Figure 5.14**) were attenuated in smokers' AM compared to non-smokers' AM. Furthermore, transcriptional analysis revealed attenuated induction of a range of glycolytic genes following LPS stimulation, with *PKD3* and *HK1* mRNA expression most substantially reduced, in smokers' AM compared to non-smokers' AM (**Figure 5.15**).

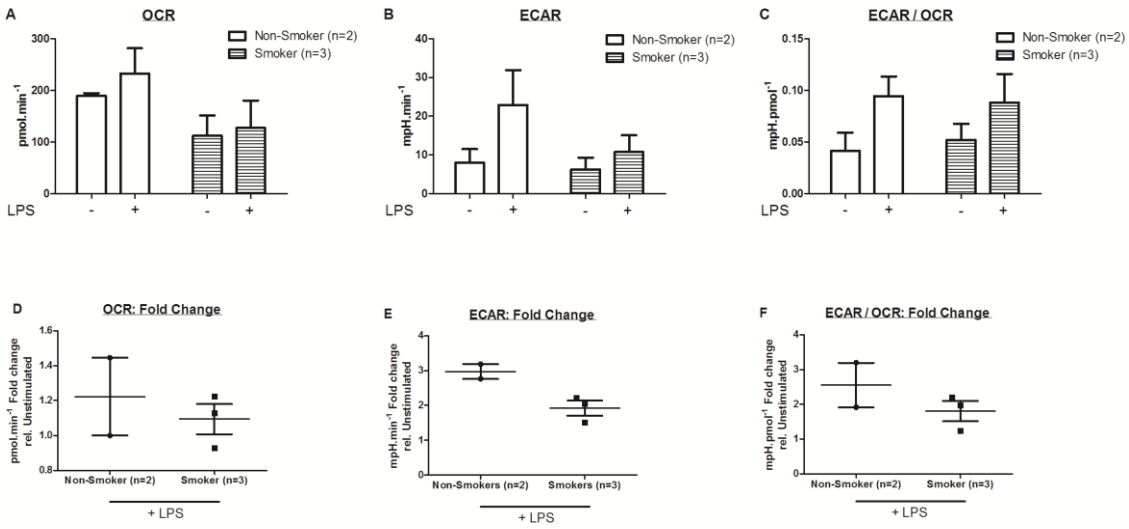

FIGURE 5.13 Smokers' AM demonstrate attenuated glycolytic response to LPS stimulation compared to non-smokers' AM. Human AM were plated as before. 24 hours after plating, cells were treated with LPS (100ng/mL) or left untreated (control). At 24 hours post-treatment, extracellular flux analyses were performed using CV assay to normalise data. Panels A – C depict mean ± SEM OCR (A), ECAR (B) and ECAR/OCR ratio (C) for 2 non-smokers and 3 smokers. Panels D – F depict mean ± SEM fold change in OCR (D), ECAR (E) and ECAR/OCR ratio (F) following LPS stimulation relative to unstimulated control for 2 non-smokers and 3 smokers. Statistical analyses were performed using the Mann Whitney U test; statistical significance was set at $p<0.05$.

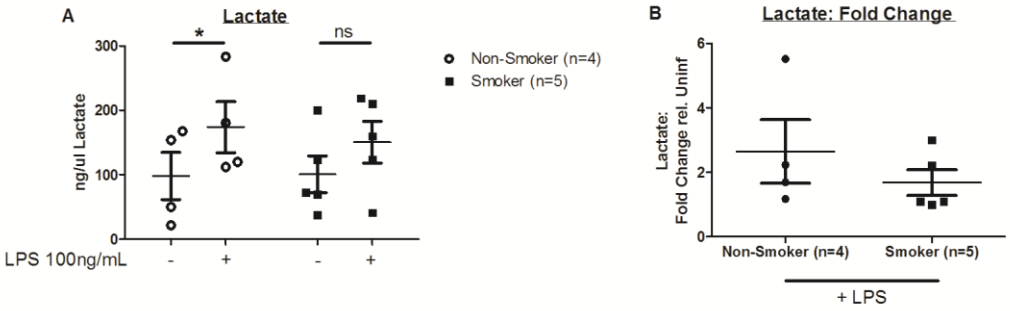

FIGURE 5.14 Smokers' AM demonstrate attenuated lactate production following LPS stimulation compared to non-smokers' AM. Human AM were plated as before. 24 hours after plating, cells were treated with LPS (100ng/mL) or left untreated (control). At 24 hours post-treatment, supernatants were removed and lactate concentration quantified. Panels A and B depict mean ± SEM measured lactate concentration (A) and fold change in lactate concentration following LPS stimulation relative to unstimulated (B) for 4 non-smokers and 5 smokers. Within-group statistical analyses were performed using the paired Student's t-test; between-group statistical analyses were performed using the Mann Whitney U test; *p<0.05.

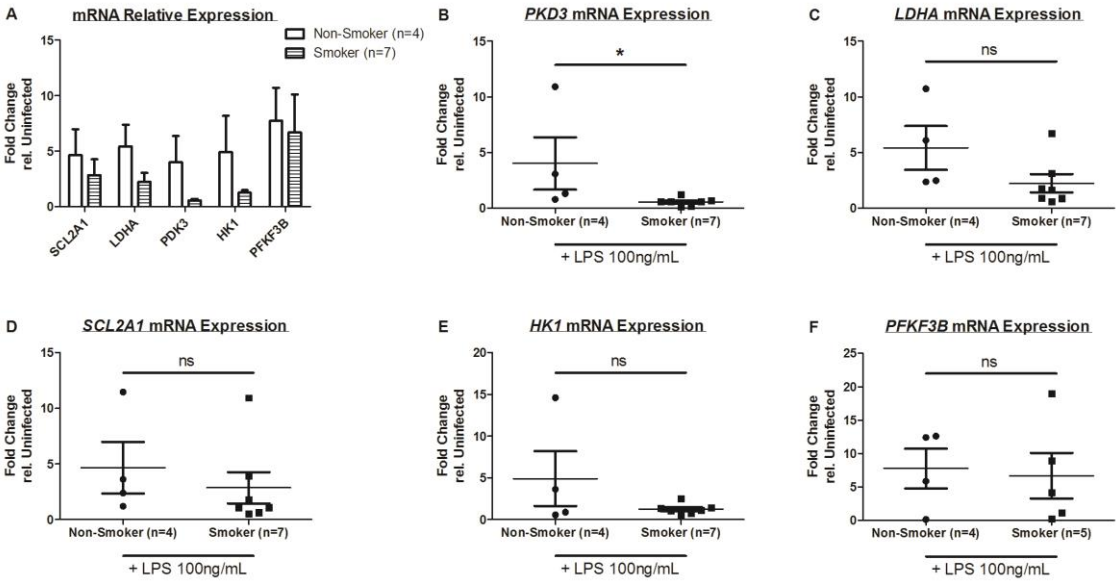

FIGURE 5.15 Smokers' AM demonstrate attenuated glycolytic gene expression following LPS stimulation compared to non-smokers' AM. Human AM were plated as before. 24 hours after plating, cells were treated with LPS (100ng/mL) or left untreated (control). At 24 hours post-treatment, cells were lysed in RLT, RNA extracted and cDNA generated, and qPCR performed. Data was normalised to *18S* and mRNA expression fold-change relative to unstimulated calculated using the $2^{-\Delta\Delta Ct}$ method. Panel A depicts mean ± SEM mRNA expression fold-change for a panel of glycolytic genes for 4 non-smokers and 7 smokers. Panels B – F depict mean ± SEM mRNA expression fold-change for individual genes for the same donors. Statistical analyses were performed using the Mann Whitney U test; *p<0.05.

5.2.8 Smokers' AM demonstrate attenuated glycolytic reprogramming following Mtb infection compared to non-smokers' AM

Thus, smokers' AM demonstrate impaired glycolytic reprogramming in response to LPS stimulation. Next, the metabolic response to Mtb infection in these cells was examined. Human AM were isolated and infected as previously described, and extracellular flux analysis performed as previously described. As before, plotting ECAR relative to OCR demonstrated reduced metabolic activity in uninfected smokers' AM compared to uninfected non-smokers' AM (**Figure 5.16 A, C**). Plots revealed an infection-induced increase in metabolic acitivty, as well as a shift towards glycolytic metabolism, in both smokers' and non-smokers' AM (**Figure 5.16 B, D**). However, both the increase in metabolic activity and the skewing towards glycolysis was substantially attenuated in smokers' AM compared to non-smokers' AM (**Figure 5.16 B, D**), suggesting an impairment in glycolytic reprogramming in response to infection. Direct comparison of absolute OCR and ECAR values confirmed that, despite infection-induced increases in these metabolic parameters being observed in both groups, the increase was substantially attenuated in smokers' AM compared to non-smokers' AM (**Figure 5.17**). Furthermore, while iH37Rv infection induced a significant increase in ECAR/OCR ratio in non-smokers' AM, reflecting a shift towards glycolytic metabolism following infection, this failed to reach significance in smokers' AM (**Figure 5.17**). Similarly, while Mtb infection induced significant increases in lactate production in non-smokers' AM, no such induction of lactate was observed in smokers' AM following infection (**Figure 5.18**). Finally, H37Ra-mediated induction of glycolytic enzymes *PKD3*, *LDHA*, *SCL2A1* and *HK1* was attenuated in smokers' AM compared to non-smokers' AM (**Figure 5.19**). These data suggest that though Mtb infection does induce a metabolic shift in smokers' AM, this effect is substantially attenuated compared to that seen in non-smokers' AM. This potentially reflects the attenuated metabolic reserves of smokers' AM (**Figure 5.12**), which limits the metabolic response to infection that can be achieved.

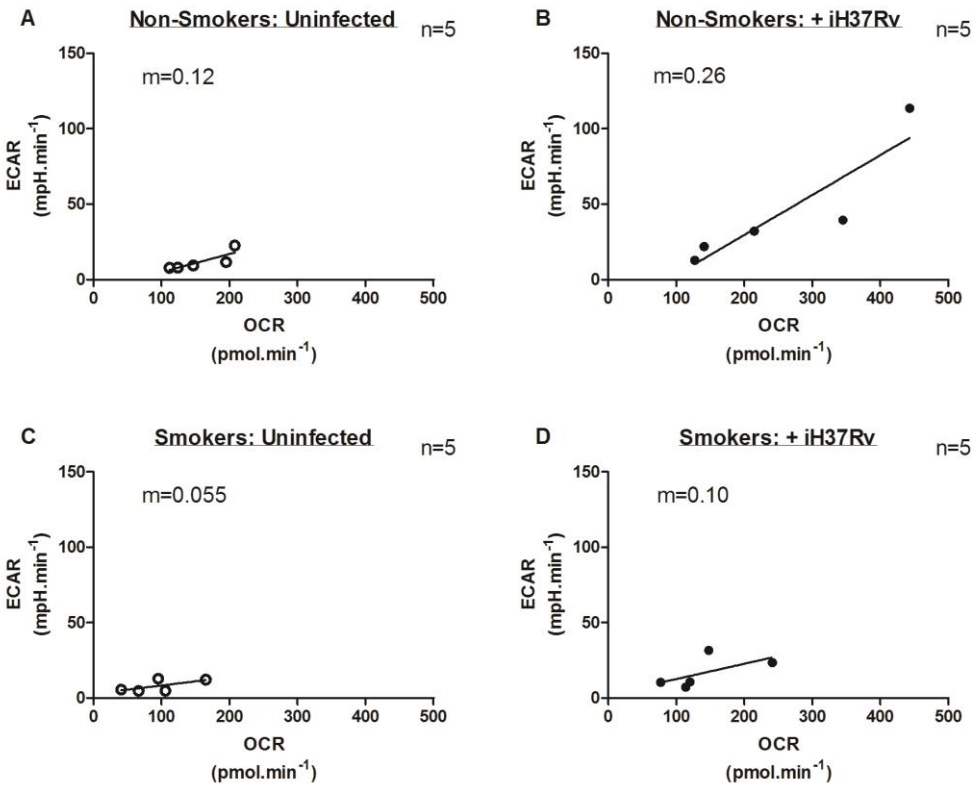

FIGURE 5.16 Smokers' AM do not demonstrate increased metabolic activity following Mtb infection compared to non-smokers' AM. Human AM were plated as before. 24 hours after plating, cells were infected with iH37Rv at low MOI or left uninfected (control). 24 hours post-infection, extracellular flux analyses were performed using CV assay to normalise data. Panels depict ECAR (y-axis; representative of glycolytic activity) relative to OCR (x-axis; representative of mitochondrial respiration) in uninfected Non-smokers' AM (A), infected non-smokers' AM (B), uninfected smokers' AM (C) and infected smokers' AM (D). Data is representative of 5 non-smokers and 5 smokers.

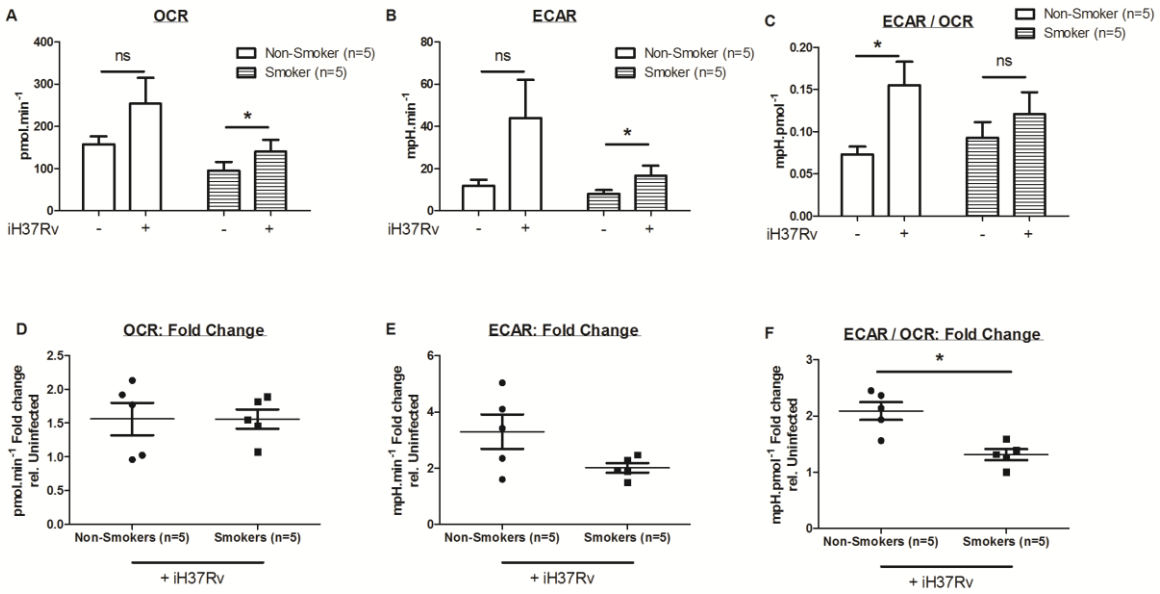

FIGURE 5.17 Smokers' AM demonstrate attenuated glycolytic shift following Mtb infection compared to non-smokers' AM. Human AM were plated as before. 24 hours after plating, cells were infected with iH37Rv at low MOI or left uninfected (control). 24 hours post-infection, extracellular flux analyses were performed using CV assay to normalise data. Panels A – C depict mean ± SEM OCR (A), ECAR (B) and ECAR/OCR ratio (C) for 5 non-smokers and 5 smokers. Panels D – F depict mean ± SEM fold change in OCR (D), ECAR (E) and ECAR/OCR ratio (F) following iH37Rv infection relative to unstimulated control for 5 non-smokers and 5 smokers. Within-group statistical analyses were performed using the paired Student's t-test; between-group statistical analyses were performed using the Mann Whitney U test; *p<0.05.

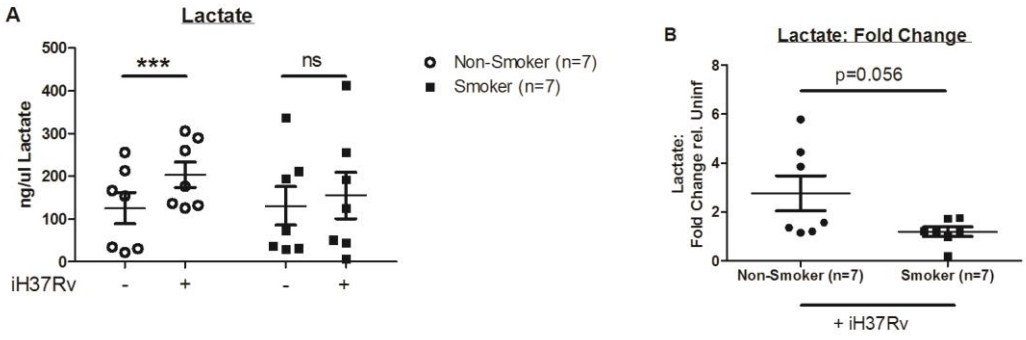

FIGURE 5.18 Smokers' AM demonstrate attenuated lactate production following Mtb infection compared to non-smokers' AM. Human AM were plated as before. 24 hours after plating, cells were infected with iH37Rv at low MOI or left uninfected (control). 24 hours post-infection, supernatants were removed and lactate concentration quantified. Panels A and B depict mean ± SEM measured lactate concentration (A) and fold change in lactate concentration following iH37Rv infection relative to uninfected (B) for 7 non-smokers and 7 smokers. Within-group statistical analyses were performed using the paired Student's t-test; between-group statistical analyses were performed using the Mann Whitney U test; ***p<0.001.

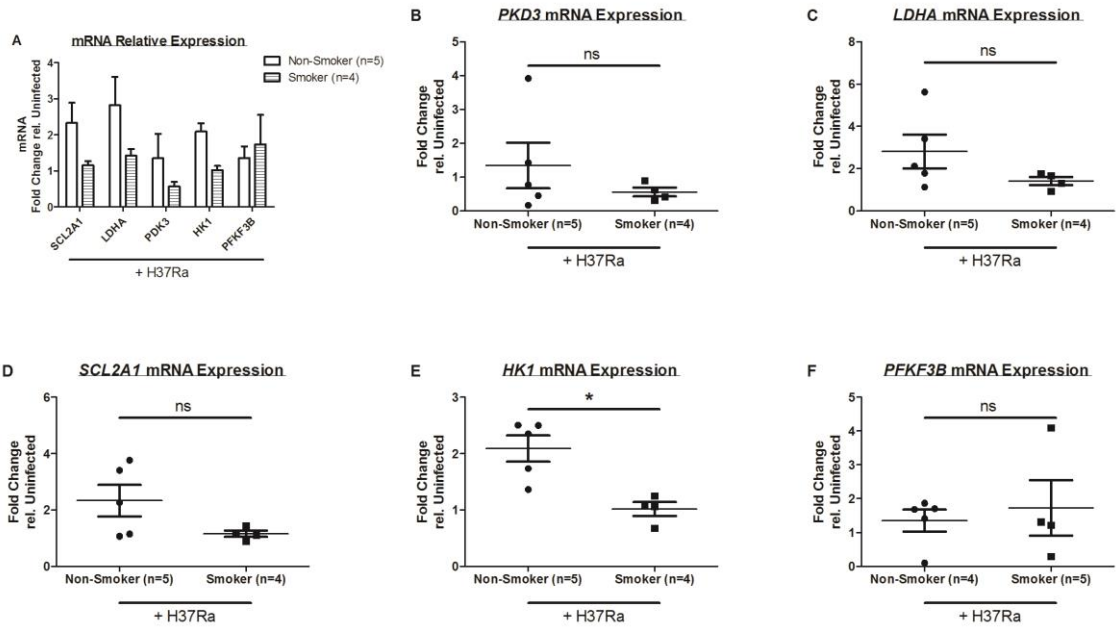

FIGURE 5.19 Smokers' AM demonstrate attenuated glycolytic gene expression following Mtb infection compared to non-smokers' AM. Human AM were plated as before. 24 hours after plating, cells were infected with H37Ra at low MOI or left uninfected (control). At 24 hours post-infection, cells were lysed in RLT, RNA extracted and cDNA generated, and qPCR performed. Data was normalised to *18S* and mRNA expression fold-change relative to uninfected calculated using the $2^{-\Delta\Delta Ct}$ method. Panel A depicts mean ± SEM mRNA expression fold-change for a panel of glycolytic genes for 5 non-smokers and 4 smokers. Panels B – F depict mean ± SEM mRNA expression fold-change for individual genes for the same donors. Statistical analyses were performed using the Mann Whitney U test; *p<0.05.

5.2.9 Glycolysis does not play a role in IL-1β production in Mtb-infected smokers' AM

Despite impairments in cytokine response to Mtb infection, smokers' AM are observed to produce IL-1β at attenuated levels (**Figure 5.8**). To investigate the contribution of glycolytic reprogramming to IL-1β production in smokers' AM, cells were pre-treated with glucose-free RPMI supplemented with 10mM Galactose to inhibit glycolysis (or with 10mM Glucose as a control) 24 hours prior to infection. Infections were performed as previously, with supernatants removed at 24 hours and cytokine concentration measured by ELISA. Consistent with previous observations, non-smokers' AM demonstrated attenuated IL-1β production when glycolysis was inhibited, emphasising the role of glycolytic reprogramming in the production of this cytokine (**Figure 5.20**). However, infection-induced IL-1β production in smokers' AM was unchanged following glycolytic inhibition (**Figure 5.20**), suggesting that the preserved IL-1β production observed in these cells is independent of glycolytic reprogramming. These data imply that attenuation in IL-1β production in smokers' AM is at least partly related to impaired glycolytic reprogramming in these cells.

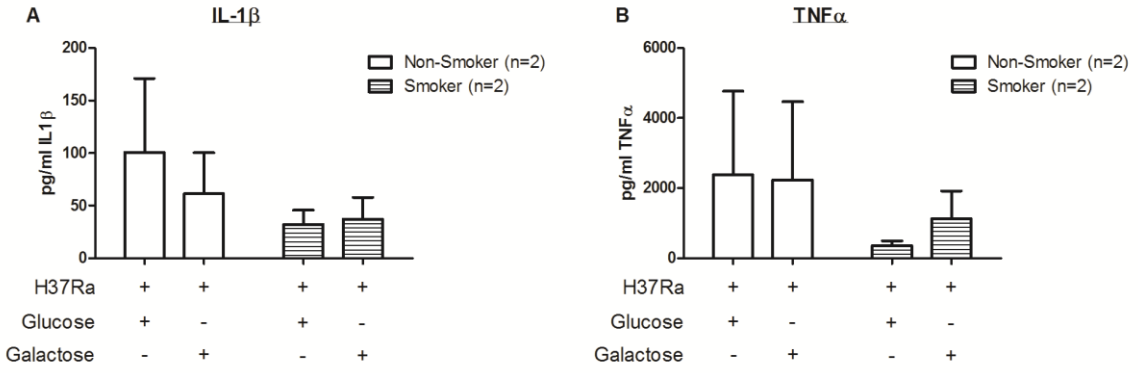

FIGURE 5.20 IL-1β production is not impacted by glycolytic inhibition in Mtb-infected smokers' AM, in contrast to non-smokers' AM. Human AM were plated in antibiotic-supplemented cRPMI as before. 24 hours after plating, culture media was replaced with either glucose- or galactose-containing antibiotic-free media. 24 hours later, cells were infected with H37Ra at low MOI or left uninfected (control). 24 hours post-infection, supernatants were removed and cytokine concentration quantified by ELISA. Panels A and B depict mean ± SEM IL-1β (A) and TNF-α concentration for 2 non-smokers and 2 smokers.

5.2.10 Ex-smokers' AM demonstrate partial recovery in infection-induced glycolytic reprogramming

Finally, in order to investigate the potential for recovery of metabolic responses to infection following cessation of smoking, AM were retrieved from smokers, ex-smokers and never-smokers, culture and infection performed as previously described , and lactate measured in supernatants 24 hours post-infection. Results indicated a partial improvement in lactate responses to infection in ex-smokers' AM compared to smokers' AM, though levels failed to reach those of never-smokers' AM (**Figure 5.21**). However, these results imply that smoking cessation may result in at least partial correction of glycolytic response to infection.

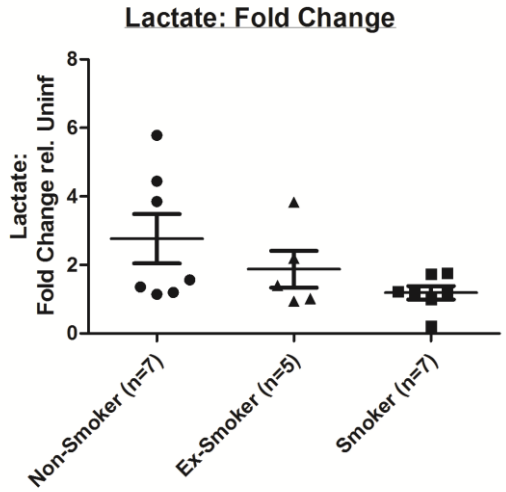

FIGURE 5.21 Ex-smokers' AM demonstrate partial recovery of lactate production in response to Mtb infection. Human AM were plated as before. 24 hours after plating, cells were infected with iH37Rv at low MOI or left uninfected (control). 24 hours post-infection, supernatants were removed and lactate concentration quantified. Data is presented as mean ± SEM fold change in lactate concentration following LPS stimulation relative to uninfected for 7 never-smokers, 5 ex-smokers and 7 smokers. Statistical analyses were performed using the Mann Whitney U test; statistical significance was set at $p<0.05$.

5.3 Discussion

Cigarette-smoke induced inhibition of mitochondrial activity has been reported by numerous groups [419,446-450], and more recently, work by Agarwal et al in Type II alveolar epithelial cells suggests that impaired mitochondrial function following cigarette smoke exposure may be a consequence of reduced glycolytic activity [458,459]. However, the impact of cigarette smoke on glycolytic metabolism in AM has never been investigated. In light of the important functional role for glycolytic reprogramming presented in **Chapter 4**, it was hypothesised that alterations in host macrophage metabolic responses may contribute to impaired cytokine responses to Mtb infection that we have previously observed in smokers [411].

5.3.1 CSE reduces baseline metabolic activity and glycolytic reserve of human MDM

In experiments on Type II alveolar epithelial cells, reductions both glycolytic activity and oxidative phosphorylation were observed following exposure to the cigarette-smoke component acrolein [458]. In concordance with these observations, reductions in both ECAR and OCR in human MDM following treatment with cigarette smoke extract (CSE) were observed (**Figure 5.2**). Interestingly, glycolytic impairment appeared to be more pronounced, as indicated by significant reduction in ECAR/OCR ratio (**Figure 5.2C**). In their work, Agarwal et al suggest that reduction in OCR occurs secondary to impaired glycolysis [458], evidenced by the ability of exogenous pyruvate to rescue mitochondrial respiration and by the preferential utilisation of palmitate oxidation to fuel oxidative phosphorylation in acroelin-exposed cells, which may account for the increased sensitivity of glycolytic metabolism to CSE exposure observed in human MDM. In agreement with this observation, human MDM glycolytic reserves were substantially attenuated following CSE exposure, in dose-dependent fashion (**Figure 5.3**). Though a trend towards decreased SRC was also observed (**Figure 5.3E**), this was again less pronounced and may be attributable to the presence of a single outlier in the data presented. This cigarette smoke glycolytic inhibition is also supported by separate studies in a human alveolar epithelial adenocarcinoma cell line and in a human hepatoma cell line [460,462], though metabolic readouts from immortalised cell lines must be interpreted with caution given the natural skewing of cancer cells towards Warburg metabolism.

Interestingly, a similar generalised defect in metabolism, with reduced levels of both glycolysis and OXPHOS, has been described in leukocytes taken from patients with sepsis and immunoparalysis, supporting a functional connection between muted intracellular metabolism

and impaired host defence [483]. Cheng et al demonstrate a role for IFN-γ in reversing this metabolic senescence in the setting of immunoparalysis.

5.3.2 CSE impairs glycolytic reprogramming in response to Mtb infection

The impact of cigarette smoke on glycolytic reprogramming in stimulated immune cells has never been studied previously. Using human MDM, impaired glycolytic reprogramming following infection with iH37Rv was observed in the presence of CSE, as indicated by attenuated increase in ECAR/OCR ratio (**Figure 5.4C**) and lactate production (**Figure 5.5**). This occurred in concert with reduced IL-1β and TNF-α production in response to infection in CSE-exposed MDM (**Figure 5.6**), consistent with previously published observations in TLR-stimulated macrophages [433,436-438] and work from our group on Mtb-infected AM [411]. These data support the hypothesis that cigarette smoke exposure is associated with impairment in glycolytic reprogramming in response to Mtb infection, with consequent reduction in pro-inflammatory IL-1β production. However, as demonstrated in **Chapter 4**, the impact of glycolytic reprogramming appears to be highly specific to IL-1β production in human macrophages, with TNF-α levels relatively well preserved following glycolytic inhibition (**Figure 4.8**). Thus, the impact of CSE on cytokine response to infection is likely mediated via a multitude of mechanisms, not solely alterations in metabolic reprogramming.

Given the observed effects of meclizine in enhancing glycolytic reprogramming in response to iH37Rv infection described in **Chapter 4** (**Figure 4.37**), it was hypothesised that meclizine may serve to restore the glycolytic response of CSE-treated MDM. However, despite enhanced lactate production once again being demonstrated in non-CSE-exposed infected MDM following meclizine treatment, meclizine did not enhance either lactate or IL-1β production in CSE-exposed infected MDM (**Figure 5.7**). Again, this likely reflects the multifactorial impact of cigarette smoke on macrophage function.

5.3.3 At baseline, smokers' AM demonstrate reduced metabolic activity and reduced metabolic reserves compared to non-smokers' AM

Consistent with previously published results using H37Ra [411], this work demonstrates impaired induction of the pro-inflammatory cytokines IL-1β and TNF-α in smokers' AM compared to non-smokers' AM following infection with iH37Rv (**Figure5.8A–B**). Similar attenuation in pro-inflammatory cytokine production has been demonstrated in smokers' AM following stimulation with various TLR agonists [436-438]. As described by Mayer-Barber et al [146], and as

demonstrated in **Chapter 4** using a human MDM model (**Figure 4.16**), Mtb-induced increases in IL-1β production lead to enhanced production of the eicosanoid mediator PGE2. In concert with attenuated IL-1β responses, smokers' AM also demonstrated reduced levels of PGE2 production in response to iH37Rv infection (**Figure 5.8C**), a phenomenon previously observed in LPS-stimulated smokers' AM [437]. These observations, along with results of CSE-treated MDM experiments, provided support for the hypothesis that smokers' AM demonstrate attenuated glycolytic reprogramming in response to Mtb infection when compared to non-smokers' AM.

Prior to testing this hypothesis, baseline metabolic parameters of smokers' and non-smokers' AM were established and compared. Consistent with work by Monick et al [419], smokers' AM demonstrated attenuated OCR compared to non-smokers' (**Figure 5.10A**). Though Monick et al did not present data on glycolytic activity, a non-significant trend towards decreased ECAR in smokers' AM compared to non-smokers' was observed in these experiments (**Figure 5.10B**), though no difference was detected by use of the less-sensitive lactate assay (**Figure 5.11**), consistent with overall reduced metabolic activity in these cells. This echoes observations in murine Type II alveolar epithelial cells, with acrolein exposure associated with reduced ECAR and reduced OCR [458]. Despite plots of ECAR:OCR suggesting skewing of smokers' AM away from glycolytic metabolism at baseline (**Figure 5.9**) – possibly supporting the model of smokers' AM as more M2-skewed at baseline, as demonstrated by two independent transcriptional studies [415,430] – this skewing was not evident on a plot of mean ECAR/OCR ratio (**Figure 5.10C**), thus no firm conclusion can be drawn from the data in this regard. Significant reduction in SRC (consistent with Monick's observations [419]) are seen in smokers' AM however, as well as a non-significant trend towards reduced GR (**Figure 5.12**). Taken together, these data imply that smokers' AM are less metabolically active at baseline and demonstrate reduced metabolic reserves when stressed, in comparison to non-smokers' AM.

5.3.4 Smokers' AM demonstrate impaired glycolytic reprogramming compared to non-smokers' AM following LPS stimulation or Mtb infection

Following stimulation with TLR4 agonist LPS, smokers' AM demonstrated attenuated glycolytic reprogramming compared to non-smokers' AM, indicated by attenuated increase in ECAR/OCR ratio (**Figure 5.13**) and in lactate production (**Figure 5.14**). This correlated with attenuated induction of key glycolytic genes including *PKD3* and *HK1* (**Figure 5.15**). Similarly, the glycolytic response to Mtb infection was attenuated in smokers' AM in terms of both ECAR/OCR ratio (**Figure 5.17**) and lactate production (**Figure 5.18**). Interestingly, smokers' AM demonstrated an overall attenuation in metabolic response to infection, in terms of both OCR and ECAR (**Figure**

5.16), possibly reflecting the exhausted metabolic reserves of these cells ultimately leading to their failure to increase ATP production in response to this infective challenge. Increased levels of cell death have been described in cigarette smoke-exposed AM [411,426,428,429], which may be a downstream consequence of this metabolic exhaustion. Again, smokers' AM demonstrated attenuated induction of key glycolytic enzymes following Mtb infection (**Figure 5.19**), lending further support to the concept of ineffective glycolytic reprogramming in these cells.

Having established impaired glycolytic reprogramming in smokers' AM, the impact of this dysfunctional metabolic response to infection upon observed reductions in pro-inflammatory cytokine production was investigated. As previously observed, glycolytic inhibition with galactose-supplemented media led to attenuated IL-1β production in response to infection without significant alterations in TNF-α production in non-smokers' AM (**Figure 5.20**). Also consistent with previous observations, smokers' AM demonstrated reduced IL-1β and TNF-α production following infection when compared with non-smokers' AM (**Figure 5.20**). However, glycolytic inhibition did not further attenuate IL-1β production in infected smokers' AM, in contrast to non-smokers' AM (**Figure 5.20A**). Thus, glycolytic reprogramming represents an important mechanism for IL-1β production in non-smokers' AM but does not contribute to production of this cytokine in smokers' AM, consistent with observed impairment in metabolic response in smokers. However, IL-1β production in smokers' AM is suppressed to a greater extent than in non-smokers' AM cultured in galactose (**Figure 5.20A**), and TNF-α production is also suppressed in smokers' AM (**Figure 5.20B**), again emphasising that the impact of cigarette smoke exposure is not limited to altered metabolic responses but is likely multifactorial.

Finally, infection-induced lactate induction between non-smokers, ex-smokers and smokers was compared, demonstrating a trend towards increased glycolytic responses in ex-smokers relative to smokers, and further increased glycolytic response in non-smokers relative to ex-smokers (**Figure 5.21**). These data suggest an element of reversibility in terms of smoking-induced dysfunction in glycolytic reprogramming. However, while this may reflect reversibility of metabolic dysregulation at a cellular level, it is more likely that this represents the presence of non-smoke exposed AM within the cell population retrieved from ex-smokers at bronchoscopy.

5.4 Conclusion

The work presented in **Chapter 5** offers novel insights into the impact of cigarette smoke exposure on macrophage glycolytic metabolism. Using both a CSE-treated human MDM model and a smoker versus non-smoker human AM model, broad attenuation of baseline metabolism and metabolic reserves is shown to be associated with cigarette smoke exposure. For the first time, impaired glycolytic metabolism secondary to cigarette smoke exposure is demonstrated in a human AM model. Also for the first time, cigarette smoke-associated attenuation in the glycolytic response to infection is demonstrated, again using two independent models of cigarette smoke exposure. Finally, cigarette smoke-associated impaired metabolic response is correlated with impaired IL-1β production, suggesting dysfunctional macrophage glycolytic reprogramming as a contributor to the increased susceptibility to Mtb infection observed in the smoking population.

CHAPTER 6:

Concluding Remarks

Today, TB remains a catastrophic global disease. Enhanced understanding of the mechanism of host-bacillus interaction is paramount to developing new therapies and vaccines. In this work, the role of immunometabolism in the macrophage response to Mtb infection is defined for the first time. Mtb-induced glycolysis is shown to be crucial for the production of pro-inflammatory, anti-mycobacterial mediators IL-1β and PGE2, as well as suppression of the anti-inflammatory, pro-mycobacterial cytokine IL-10. Furthermore, glycolytic reprogramming is essential for early bacillary clearance by the macrophage in vitro. Crucially, pharmacological manipulation of this metabolic response using the over-the-counter anti-emetic meclizine boosted the glycolytic response to infection and enhanced mycobactericidal activity of macrophages. These results recommend this metabolic-immune axis as a potential target for host-directed adjunctive therapies in the future.

Though recent years have seen exponential interest in the metabolic shift that occurs in activated immune cells, this work describes a role for this glycolytic reprogramming in the context of host defence for the first time. A similar anti-bacterial role is demonstrated for glycolytic reprogramming in the host response to the intracellular pathogen *Salmonella typhimurium*, suggesting the centrality of this axis in the host response to a range of infectious diseases. As detailed in previous chapters, a range of TLR ligands have been shown to induce a shift towards glycolytic metabolism in macrophages. Tannahill et al demonstrated glycolytic reprogramming in response to *Bordatella pertussis* [174], though its bactericidal role was not examined. Thus, the role of glycolytic reprogramming in host defence is not limited to Mtb infection but is likely applicable to a range of pathogens. Further delineation of this host defence pathway, and crucially, its pharmacological manipulation to enhance anti-bacterial effects, should be prioritised going forward. All the data presented in this thesis represents in vitro experimentation using supra-physiologic glucose concentrations, thus further in vivo work is necessary to confirm the importance of this immune-metabolic axis in a physiologic model. While in vitro work examining the impact of pharmacological induction of glycolysis following direct supplementation with meclizine is promising, a small human trial investigating the impact of orally ingested meclizine on macrophage responses would be helpful in determining the potential clinical impact of this agent. Should pharmacological enhancement of this immune-metabolic axis be achievable by administration of a safe systemic medication, it may prove a useful clinical tool as a post-exposure prophylactic treatment, enhancing early innate immune responses to prevent the development of active or latent TB infection in outbreak situations.

This work further demonstrates that defects in macrophage metabolic response to Mtb infection may contribute to the increased susceptibility to infection observed in certain subpopulations. In both a CSE-treated MDM model and in an *in vivo* smoke-exposed AM model, glycolytic

reprogramming was attenuated following stimulation with LPS or infection with Mtb. Furthermore, the metabolic shift does not drive IL-1β production in smokers' AM, emphasising the metabolic dysfunction of these cells. In light of the significant metabolic alterations observed in smokers' AM in this body of work, further delineation of the metabolic "imprint" of smoking is warranted through transcriptional and metabolomic analyses, as well as investigation of the epigenetic impact of cigarette smoke, particularly given the continued immune and metabolic defects observed in ex-smokers' AM. Though beyond the scope of this work, it is possible that defective glycolytic reprogramming may contribute to the increased susceptibility to Mtb infection observed in DM2 also. DM2 is characterised by resistance to insulin resulting in impaired uptake and utilisation of glucose within cells [346,347]. Thus, it is possible that impaired glycolytic reprogramming may contribute to phenotypic skewing towards M2 polarisation that has been described in macrophages from diabetic rodents [350-352]. Though experiments attempting to restore the glycolytic function of CSE-treated macrophages using meclizine were unsuccessful, further investigation is warranted, with the potential for uncovering subpopulation-specific host-directed adjunctive therapies, providing an economical and efficient means to reduce the burden of TB disease in the era of personalised medicine.

As the scientific community's understanding of immunometabolism grows, it is becoming clear that the metabolic shift known as the Warburg effect is not limited to glycolysis alone. In this work, an Mtb-induced shift towards glycolysis was demonstrated to drive IL-1β production in human macrophages, and subsequent mycobactericidal activity. However, a myriad of metabolic changes have been demonstrated to occur within the cell upon stimulation with various TLRs, allowing one to hypothesise that a similar constellation of metabolic changes occur following Mtb infection. Notably, Jha et al report increases in isocitrate following LPS/IFN-γ treatment of macrophages [244]. This leads to increases in the nonamino organic acid itaconate, a compound that demonstrates direct anti-mycobacterial effects through its inhibition of methylisocitrate lyase [244,304,305]. The emerging link between glycolytic reprogramming an mROS production suggests a further mechanism by which the metabolic shift may enhance mycobactericidal activity of macrophages [250,269]. Thus, glycolytic reprogramming embodies a complex constellation of metabolic changes. Enhanced understanding of these changes and their functional consequences will allow a refined approach to pharmacological manipulation for the development of new therapies for Mtb infection.

In this body of work, therefore, evidence is provided for the central role of glycolytic reprogramming in innate host defence. As the burgeoning field of immunometabolism rapidly progresses, the work presented in this thesis serves as a scaffold upon which to build an

understanding of the complex host-pathogen metabolic interplay and to harness developments to create new therapies and vaccines for the leading infectious disease killer in the world.

CHAPTER 7:

References

1. **WHO Global Tuberculosis Report 2015**. Edited by: World Health Organisation; 2015.
2. O'Garra A, Redford PS, McNab FW, Bloom CI, Wilkinson RJ, Berry MP: **The immune response in tuberculosis**. *Annu Rev Immunol* 2013, **31**:475-527.
3. **WHO Stop TB Strategy**. Edited by: World Health Organisation; 2006.
4. Young DB, Perkins MD, Duncan K, Barry CE: **Confronting the scientific obstacles to global control of tuberculosis**. *J Clin Invest* 2008, **118**:1255-1265.
5. Kaufmann SH: **Tuberculosis vaccine development: strength lies in tenacity**. *Trends Immunol* 2012, **33**:373-379.
6. Kaufmann SH, Lange C, Rao M, Balaji KN, Lotze M, Schito M, Zumla AI, Maeurer M: **Progress in tuberculosis vaccine development and host-directed therapies--a state of the art review**. *Lancet Respir Med* 2014, **2**:301-320.
7. McShane H, Jacobs WR, Fine PE, Reed SG, McMurray DN, Behr M, Williams A, Orme IM: **BCG: myths, realities, and the need for alternative vaccine strategies**. *Tuberculosis (Edinb)* 2012, **92**:283-288.
8. Hawn TR, Shah JA, Kalman D: **New tricks for old dogs: countering antibiotic resistance in tuberculosis with host-directed therapeutics**. *Immunol Rev* 2015, **264**:344-362.
9. Wallis RS, Hafner R: **Advancing host-directed therapy for tuberculosis**. *Nat Rev Immunol* 2015, **15**:255-263.
10. Raviglione MC, Uplekar MW: **WHO's new Stop TB Strategy**. *Lancet* 2006, **367**:952-955.
11. Hopewell PC: **Impact of human immunodeficiency virus infection on the epidemiology, clinical features, management, and control of tuberculosis**. *Clin Infect Dis* 1992, **15**:540-547.
12. Perkins MD, Cunningham J: **Facing the crisis: improving the diagnosis of tuberculosis in the HIV era**. *J Infect Dis* 2007, **196 Suppl 1**:S15-27.
13. Vynnycky E, Fine PE: **Lifetime risks, incubation period, and serial interval of tuberculosis**. *Am J Epidemiol* 2000, **152**:247-263.
14. Getahun H, Matteelli A, Chaisson RE, Raviglione M: **Latent Mycobacterium tuberculosis infection**. *N Engl J Med* 2015, **372**:2127-2135.
15. Verrall AJ, Netea MG, Alisjahbana B, Hill PC, van Crevel R: **Early clearance of Mycobacterium tuberculosis: a new frontier in prevention**. *Immunology* 2014, **141**:506-513.
16. Morrison J, Pai M, Hopewell PC: **Tuberculosis and latent tuberculosis infection in close contacts of people with pulmonary tuberculosis in low-income and middle-income countries: a systematic review and meta-analysis**. *Lancet Infect Dis* 2008, **8**:359-368.
17. O'Connor G, Gleeson LE, Fagan-Murphy A, Cryan SA, O'Sullivan MP, Keane J: **Sharpening nature's tools for efficient tuberculosis control: A review of the potential role and development of host-directed therapies and strategies for targeted respiratory delivery**. *Adv Drug Deliv Rev* 2016.
18. Fennelly KP, Jones-López EC, Ayakaka I, Kim S, Menyha H, Kirenga B, Muchwa C, Joloba M, Dryden-Peterson S, Reilly N, et al.: **Variability of infectious aerosols produced during coughing by patients with pulmonary tuberculosis**. *Am J Respir Crit Care Med* 2012, **186**:450-457.
19. Pieters J: **Mycobacterium tuberculosis and the macrophage: maintaining a balance**. *Cell Host Microbe* 2008, **3**:399-407.
20. Kleinnijenhuis J, Oosting M, Joosten LA, Netea MG, Van Crevel R: **Innate immune recognition of Mycobacterium tuberculosis**. *Clin Dev Immunol* 2011, **2011**:405310.
21. Levine B, Mizushima N, Virgin HW: **Autophagy in immunity and inflammation**. *Nature* 2011, **469**:323-335.
22. Bradfute SB, Castillo EF, Arko-Mensah J, Chauhan S, Jiang S, Mandell M, Deretic V: **Autophagy as an immune effector against tuberculosis**. *Curr Opin Microbiol* 2013, **16**:355-365.
23. Gutierrez MG, Master SS, Singh SB, Taylor GA, Colombo MI, Deretic V: **Autophagy is a defense mechanism inhibiting BCG and Mycobacterium tuberculosis survival in infected macrophages**. *Cell* 2004, **119**:753-766.

24. Armstrong JA, Hart PD: **Response of cultured macrophages to Mycobacterium tuberculosis, with observations on fusion of lysosomes with phagosomes**. *J Exp Med* 1971, **134**:713-740.
25. Clemens DL, Horwitz MA: **Characterization of the Mycobacterium tuberculosis phagosome and evidence that phagosomal maturation is inhibited**. *J Exp Med* 1995, **181**:257-270.
26. Vergne I, Singh S, Roberts E, Kyei G, Master S, Harris J, de Haro S, Naylor J, Davis A, Delgado M, et al.: **Autophagy in immune defense against Mycobacterium tuberculosis**. *Autophagy* 2006, **2**:175-178.
27. Deretic V, Delgado M, Vergne I, Master S, De Haro S, Ponpuak M, Singh S: **Autophagy in immunity against mycobacterium tuberculosis: a model system to dissect immunological roles of autophagy**. *Curr Top Microbiol Immunol* 2009, **335**:169-188.
28. Rovetta AI, Peña D, Hernández Del Pino RE, Recalde GM, Pellegrini J, Bigi F, Musella RM, Palmero DJ, Gutierrez M, Colombo MI, et al.: **IFNG-mediated immune responses enhance autophagy against Mycobacterium tuberculosis antigens in patients with active tuberculosis**. *Autophagy* 2014, **10**:2109-2121.
29. Yuk JM, Shin DM, Lee HM, Yang CS, Jin HS, Kim KK, Lee ZW, Lee SH, Kim JM, Jo EK: **Vitamin D3 induces autophagy in human monocytes/macrophages via cathelicidin**. *Cell Host Microbe* 2009, **6**:231-243.
30. Bustamante J, Arias AA, Vogt G, Picard C, Galicia LB, Prando C, Grant AV, Marchal CC, Hubeau M, Chapgier A, et al.: **Germline CYBB mutations that selectively affect macrophages in kindreds with X-linked predisposition to tuberculous mycobacterial disease**. *Nat Immunol* 2011, **12**:213-221.
31. MacMicking JD, North RJ, LaCourse R, Mudgett JS, Shah SK, Nathan CF: **Identification of nitric oxide synthase as a protective locus against tuberculosis**. *Proc Natl Acad Sci U S A* 1997, **94**:5243-5248.
32. Wink DA, Hines HB, Cheng RY, Switzer CH, Flores-Santana W, Vitek MP, Ridnour LA, Colton CA: **Nitric oxide and redox mechanisms in the immune response**. *J Leukoc Biol* 2011, **89**:873-891.
33. Rich EA, Torres M, Sada E, Finegan CK, Hamilton BD, Toossi Z: **Mycobacterium tuberculosis (MTB)-stimulated production of nitric oxide by human alveolar macrophages and relationship of nitric oxide production to growth inhibition of MTB**. *Tuber Lung Dis* 1997, **78**:247-255.
34. Zwilling BS, Kuhn DE, Wikoff L, Brown D, Lafuse W: **Role of iron in Nramp1-mediated inhibition of mycobacterial growth**. *Infect Immun* 1999, **67**:1386-1392.
35. Scanga CA, Mohan VP, Tanaka K, Alland D, Flynn JL, Chan J: **The inducible nitric oxide synthase locus confers protection against aerogenic challenge of both clinical and laboratory strains of Mycobacterium tuberculosis in mice**. *Infect Immun* 2001, **69**:7711-7717.
36. Nathan C, Shiloh MU: **Reactive oxygen and nitrogen intermediates in the relationship between mammalian hosts and microbial pathogens**. *Proc Natl Acad Sci U S A* 2000, **97**:8841-8848.
37. Nicholson S, Bonecini-Almeida MaG, Lapa e Silva JR, Nathan C, Xie QW, Mumford R, Weidner JR, Calaycay J, Geng J, Boechat N, et al.: **Inducible nitric oxide synthase in pulmonary alveolar macrophages from patients with tuberculosis**. *J Exp Med* 1996, **183**:2293-2302.
38. Nozaki Y, Hasegawa Y, Ichiyama S, Nakashima I, Shimokata K: **Mechanism of nitric oxide-dependent killing of Mycobacterium bovis BCG in human alveolar macrophages**. *Infect Immun* 1997, **65**:3644-3647.
39. Chan J, Fan XD, Hunter SW, Brennan PJ, Bloom BR: **Lipoarabinomannan, a possible virulence factor involved in persistence of Mycobacterium tuberculosis within macrophages**. *Infect Immun* 1991, **59**:1755-1761.
40. Pabst MJ, Gross JM, Brozna JP, Goren MB: **Inhibition of macrophage priming by sulfatide from Mycobacterium tuberculosis**. *J Immunol* 1988, **140**:634-640.

41. Li Z, Kelley C, Collins F, Rouse D, Morris S: **Expression of katG in Mycobacterium tuberculosis is associated with its growth and persistence in mice and guinea pigs**. *J Infect Dis* 1998, **177**:1030-1035.
42. Darwin KH, Ehrt S, Gutierrez-Ramos JC, Weich N, Nathan CF: **The proteasome of Mycobacterium tuberculosis is required for resistance to nitric oxide**. *Science* 2003, **302**:1963-1966.
43. Shin DM, Jeon BY, Lee HM, Jin HS, Yuk JM, Song CH, Lee SH, Lee ZW, Cho SN, Kim JM, et al.: **Mycobacterium tuberculosis eis regulates autophagy, inflammation, and cell death through redox-dependent signaling**. *PLoS Pathog* 2010, **6**:e1001230.
44. Botella H, Peyron P, Levillain F, Poincloux R, Poquet Y, Brandli I, Wang C, Tailleux L, Tilleul S, Charrière GM, et al.: **Mycobacterial p(1)-type ATPases mediate resistance to zinc poisoning in human macrophages**. *Cell Host Microbe* 2011, **10**:248-259.
45. Behar SM, Martin CJ, Booty MG, Nishimura T, Zhao X, Gan HX, Divangahi M, Remold HG: **Apoptosis is an innate defense function of macrophages against Mycobacterium tuberculosis**. *Mucosal Immunol* 2011, **4**:279-287.
46. Oddo M, Renno T, Attinger A, Bakker T, MacDonald HR, Meylan PR: **Fas ligand-induced apoptosis of infected human macrophages reduces the viability of intracellular Mycobacterium tuberculosis**. *J Immunol* 1998, **160**:5448-5454.
47. Winau F, Weber S, Sad S, de Diego J, Hoops SL, Breiden B, Sandhoff K, Brinkmann V, Kaufmann SH, Schaible UE: **Apoptotic vesicles crossprime CD8 T cells and protect against tuberculosis**. *Immunity* 2006, **24**:105-117.
48. Behar SM, Divangahi M, Remold HG: **Evasion of innate immunity by Mycobacterium tuberculosis: is death an exit strategy?** *Nat Rev Microbiol* 2010, **8**:668-674.
49. Keane J, Remold HG, Kornfeld H: **Virulent Mycobacterium tuberculosis strains evade apoptosis of infected alveolar macrophages**. *J Immunol* 2000, **164**:2016-2020.
50. van Crevel R, Ottenhoff TH, van der Meer JW: **Innate immunity to Mycobacterium tuberculosis**. *Clin Microbiol Rev* 2002, **15**:294-309.
51. Schlesinger LS: **Entry of Mycobacterium tuberculosis into mononuclear phagocytes**. *Curr Top Microbiol Immunol* 1996, **215**:71-96.
52. Wolf AJ, Linas B, Trevejo-Nuñez GJ, Kincaid E, Tamura T, Takatsu K, Ernst JD: **Mycobacterium tuberculosis infects dendritic cells with high frequency and impairs their function in vivo**. *J Immunol* 2007, **179**:2509-2519.
53. Eruslanov EB, Lyadova IV, Kondratieva TK, Majorov KB, Scheglov IV, Orlova MO, Apt AS: **Neutrophil responses to Mycobacterium tuberculosis infection in genetically susceptible and resistant mice**. *Infect Immun* 2005, **73**:1744-1753.
54. Henderson RA, Watkins SC, Flynn JL: **Activation of human dendritic cells following infection with Mycobacterium tuberculosis**. *J Immunol* 1997, **159**:635-643.
55. Eum SY, Kong JH, Hong MS, Lee YJ, Kim JH, Hwang SH, Cho SN, Via LE, Barry CE: **Neutrophils are the predominant infected phagocytic cells in the airways of patients with active pulmonary TB**. *Chest* 2010, **137**:122-128.
56. Braian C, Hogea V, Stendahl O: **Mycobacterium tuberculosis- induced neutrophil extracellular traps activate human macrophages**. *J Innate Immun* 2013, **5**:591-602.
57. Andersson H, Andersson B, Eklund D, Ngoh E, Persson A, Svensson K, Lerm M, Blomgran R, Stendahl O: **Apoptotic neutrophils augment the inflammatory response to Mycobacterium tuberculosis infection in human macrophages**. *PLoS One* 2014, **9**:e101514.
58. Tan BH, Meinken C, Bastian M, Bruns H, Legaspi A, Ochoa MT, Krutzik SR, Bloom BR, Ganz T, Modlin RL, et al.: **Macrophages acquire neutrophil granules for antimicrobial activity against intracellular pathogens**. *J Immunol* 2006, **177**:1864-1871.
59. Hedlund S, Persson A, Vujic A, Che KF, Stendahl O, Larsson M: **Dendritic cell activation by sensing Mycobacterium tuberculosis-induced apoptotic neutrophils via DC-SIGN**. *Hum Immunol* 2010, **71**:535-540.

60. Blomgran R, Ernst JD: **Lung neutrophils facilitate activation of naive antigen-specific CD4+ T cells during Mycobacterium tuberculosis infection**. *J Immunol* 2011, **186**:7110-7119.
61. Keller C, Hoffmann R, Lang R, Brandau S, Hermann C, Ehlers S: **Genetically determined susceptibility to tuberculosis in mice causally involves accelerated and enhanced recruitment of granulocytes**. *Infect Immun* 2006, **74**:4295-4309.
62. Elkington PT, Ugarte-Gil CA, Friedland JS: **Matrix metalloproteinases in tuberculosis**. *Eur Respir J* 2011, **38**:456-464.
63. Reece ST, Loddenkemper C, Askew DJ, Zedler U, Schommer-Leitner S, Stein M, Mir FA, Dorhoi A, Mollenkopf HJ, Silverman GA, et al.: **Serine protease activity contributes to control of Mycobacterium tuberculosis in hypoxic lung granulomas in mice**. *J Clin Invest* 2010, **120**:3365-3376.
64. Rivas-Santiago B, Hernandez-Pando R, Carranza C, Juarez E, Contreras JL, Aguilar-Leon D, Torres M, Sada E: **Expression of cathelicidin LL-37 during Mycobacterium tuberculosis infection in human alveolar macrophages, monocytes, neutrophils, and epithelial cells**. *Infect Immun* 2008, **76**:935-941.
65. Valone SE, Rich EA, Wallis RS, Ellner JJ: **Expression of tumor necrosis factor in vitro by human mononuclear phagocytes stimulated with whole Mycobacterium bovis BCG and mycobacterial antigens**. *Infect Immun* 1988, **56**:3313-3315.
66. Law K, Weiden M, Harkin T, Tchou-Wong K, Chi C, Rom WN: **Increased release of interleukin-1 beta, interleukin-6, and tumor necrosis factor-alpha by bronchoalveolar cells lavaged from involved sites in pulmonary tuberculosis**. *Am J Respir Crit Care Med* 1996, **153**:799-804.
67. Ladel CH, Szalay G, Riedel D, Kaufmann SH: **Interleukin-12 secretion by Mycobacterium tuberculosis-infected macrophages**. *Infect Immun* 1997, **65**:1936-1938.
68. Johnson BJ, McMurray DN: **Cytokine gene expression by cultures of human lymphocytes with autologous Mycobacterium tuberculosis-infected monocytes**. *Infect Immun* 1994, **62**:1444-1450.
69. Kasahara K, Tobe T, Tomita M, Mukaida N, Shao-Bo S, Matsushima K, Yoshida T, Sugihara S, Kobayashi K: **Selective expression of monocyte chemotactic and activating factor/monocyte chemoattractant protein 1 in human blood monocytes by Mycobacterium tuberculosis**. *J Infect Dis* 1994, **170**:1238-1247.
70. Zhang Y, Broser M, Cohen H, Bodkin M, Law K, Reibman J, Rom WN: **Enhanced interleukin-8 release and gene expression in macrophages after exposure to Mycobacterium tuberculosis and its components**. *J Clin Invest* 1995, **95**:586-592.
71. Sia JK, Georgieva M, Rengarajan J: **Innate Immune Defenses in Human Tuberculosis: An Overview of the Interactions between Mycobacterium tuberculosis and Innate Immune Cells**. *J Immunol Res* 2015, **2015**:747543.
72. Roca FJ, Ramakrishnan L: **TNF dually mediates resistance and susceptibility to mycobacteria via mitochondrial reactive oxygen species**. *Cell* 2013, **153**:521-534.
73. Dahl KE, Shiratsuchi H, Hamilton BD, Ellner JJ, Toossi Z: **Selective induction of transforming growth factor beta in human monocytes by lipoarabinomannan of Mycobacterium tuberculosis**. *Infect Immun* 1996, **64**:399-405.
74. Shaw TC, Thomas LH, Friedland JS: **Regulation of IL-10 secretion after phagocytosis of Mycobacterium tuberculosis by human monocytic cells**. *Cytokine* 2000, **12**:483-486.
75. Banchereau J, Steinman RM: **Dendritic cells and the control of immunity**. *Nature* 1998, **392**:245-252.
76. Marino S, Pawar S, Fuller CL, Reinhart TA, Flynn JL, Kirschner DE: **Dendritic cell trafficking and antigen presentation in the human immune response to Mycobacterium tuberculosis**. *J Immunol* 2004, **173**:494-506.
77. Humphreys IR, Stewart GR, Turner DJ, Patel J, Karamanou D, Snelgrove RJ, Young DB: **A role for dendritic cells in the dissemination of mycobacterial infection**. *Microbes Infect* 2006, **8**:1339-1346.

78. Tascon RE, Soares CS, Ragno S, Stavropoulos E, Hirst EM, Colston MJ: **Mycobacterium tuberculosis-activated dendritic cells induce protective immunity in mice**. *Immunology* 2000, **99**:473-480.
79. Tian T, Woodworth J, Sköld M, Behar SM: **In vivo depletion of CD11c+ cells delays the CD4+ T cell response to Mycobacterium tuberculosis and exacerbates the outcome of infection**. *J Immunol* 2005, **175**:3268-3272.
80. Khader SA, Partida-Sanchez S, Bell G, Jelley-Gibbs DM, Swain S, Pearl JE, Ghilardi N, Desauvage FJ, Lund FE, Cooper AM: **Interleukin 12p40 is required for dendritic cell migration and T cell priming after Mycobacterium tuberculosis infection**. *J Exp Med* 2006, **203**:1805-1815.
81. Hanekom WA, Mendillo M, Manca C, Haslett PA, Siddiqui MR, Barry C, Kaplan G: **Mycobacterium tuberculosis inhibits maturation of human monocyte-derived dendritic cells in vitro**. *J Infect Dis* 2003, **188**:257-266.
82. Motta A, Schmitz C, Rodrigues L, Ribeiro F, Teixeira C, Detanico T, Bonan C, Zwickey H, Bonorino C: **Mycobacterium tuberculosis heat-shock protein 70 impairs maturation of dendritic cells from bone marrow precursors, induces interleukin-10 production and inhibits T-cell proliferation in vitro**. *Immunology* 2007, **121**:462-472.
83. Geijtenbeek TB, Van Vliet SJ, Koppel EA, Sanchez-Hernandez M, Vandenbroucke-Grauls CM, Appelmelk B, Van Kooyk Y: **Mycobacteria target DC-SIGN to suppress dendritic cell function**. *J Exp Med* 2003, **197**:7-17.
84. Nigou J, Zelle-Rieser C, Gilleron M, Thurnher M, Puzo G: **Mannosylated lipoarabinomannans inhibit IL-12 production by human dendritic cells: evidence for a negative signal delivered through the mannose receptor**. *J Immunol* 2001, **166**:7477-7485.
85. Chackerian AA, Alt JM, Perera TV, Dascher CC, Behar SM: **Dissemination of Mycobacterium tuberculosis is influenced by host factors and precedes the initiation of T-cell immunity**. *Infect Immun* 2002, **70**:4501-4509.
86. POULSEN A: **Some clinical features of tuberculosis. 1. Incubation period**. *Acta Tuberc Scand* 1950, **24**:311-346.
87. WALLGREN A: **The time-table of tuberculosis**. *Tubercle* 1948, **29**:245-251.
88. Urdahl KB, Shafiani S, Ernst JD: **Initiation and regulation of T-cell responses in tuberculosis**. *Mucosal Immunol* 2011, **4**:288-293.
89. Wolf AJ, Desvignes L, Linas B, Banaiee N, Tamura T, Takatsu K, Ernst JD: **Initiation of the adaptive immune response to Mycobacterium tuberculosis depends on antigen production in the local lymph node, not the lungs**. *J Exp Med* 2008, **205**:105-115.
90. Russell DG, Cardona PJ, Kim MJ, Allain S, Altare F: **Foamy macrophages and the progression of the human tuberculosis granuloma**. *Nat Immunol* 2009, **10**:943-948.
91. North RJ, Jung YJ: **Immunity to tuberculosis**. *Annu Rev Immunol* 2004, **22**:599-623.
92. Lyadova IV, Panteleev AV: **Th1 and Th17 Cells in Tuberculosis: Protection, Pathology, and Biomarkers**. *Mediators Inflamm* 2015, **2015**:854507.
93. Khader SA, Pearl JE, Sakamoto K, Gilmartin L, Bell GK, Jelley-Gibbs DM, Ghilardi N, deSauvage F, Cooper AM: **IL-23 compensates for the absence of IL-12p70 and is essential for the IL-17 response during tuberculosis but is dispensable for protection and antigen-specific IFN-gamma responses if IL-12p70 is available**. *J Immunol* 2005, **175**:788-795.
94. Peters W, Ernst JD: **Mechanisms of cell recruitment in the immune response to Mycobacterium tuberculosis**. *Microbes Infect* 2003, **5**:151-158.
95. Peyron P, Vaubourgeix J, Poquet Y, Levillain F, Botanch C, Bardou F, Daffé M, Emile JF, Marchou B, Cardona PJ, et al.: **Foamy macrophages from tuberculous patients' granulomas constitute a nutrient-rich reservoir for M. tuberculosis persistence**. *PLoS Pathog* 2008, **4**:e1000204.
96. Robertson HE: **The Persistence of Tuberculous Infections**. *Am J Pathol* 1933, **9**:711-718.711.
97. Mack U, Migliori GB, Sester M, Rieder HL, Ehlers S, Goletti D, Bossink A, Magdorf K, Hölscher C, Kampmann B, et al.: **LTBI: latent tuberculosis infection or lasting immune responses to M. tuberculosis? A TBNET consensus statement**. *Eur Respir J* 2009, **33**:956-973.

98. Kaplan G, Post FA, Moreira AL, Wainwright H, Kreiswirth BN, Tanverdi M, Mathema B, Ramaswamy SV, Walther G, Steyn LM, et al.: **Mycobacterium tuberculosis growth at the cavity surface: a microenvironment with failed immunity**. *Infect Immun* 2003, **71**:7099-7108.
99. Selwyn PA, Hartel D, Lewis VA, Schoenbaum EE, Vermund SH, Klein RS, Walker AT, Friedland GH: **A prospective study of the risk of tuberculosis among intravenous drug users with human immunodeficiency virus infection**. *N Engl J Med* 1989, **320**:545-550.
100. Keane J, Gershon S, Wise RP, Mirabile-Levens E, Kasznica J, Schwieterman WD, Siegel JN, Braun MM: **Tuberculosis associated with infliximab, a tumor necrosis factor alpha-neutralizing agent**. *N Engl J Med* 2001, **345**:1098-1104.
101. MEDLAR EM: **The pathogenesis of minimal pulmonary tuberculosis; a study of 1,225 necropsies in cases of sudden and unexpected death**. *Am Rev Tuberc* 1948, **58**:583-611.
102. Gordon S: **Alternative activation of macrophages**. *Nat Rev Immunol* 2003, **3**:23-35.
103. Guirado E, Schlesinger LS, Kaplan G: **Macrophages in tuberculosis: friend or foe**. *Semin Immunopathol* 2013, **35**:563-583.
104. Hussell T, Bell TJ: **Alveolar macrophages: plasticity in a tissue-specific context**. *Nat Rev Immunol* 2014, **14**:81-93.
105. Stout RD, Suttles J: **Functional plasticity of macrophages: reversible adaptation to changing microenvironments**. *J Leukoc Biol* 2004, **76**:509-513.
106. Hagemann T, Lawrence T, McNeish I, Charles KA, Kulbe H, Thompson RG, Robinson SC, Balkwill FR: **"Re-educating" tumor-associated macrophages by targeting NF-kappaB**. *J Exp Med* 2008, **205**:1261-1268.
107. Mosser DM, Edwards JP: **Exploring the full spectrum of macrophage activation**. *Nat Rev Immunol* 2008, **8**:958-969.
108. Stein M, Keshav S, Harris N, Gordon S: **Interleukin 4 potently enhances murine macrophage mannose receptor activity: a marker of alternative immunologic macrophage activation**. *J Exp Med* 1992, **176**:287-292.
109. Standiford TJ, Keshamouni VG, Reddy RC: **Peroxisome proliferator-activated receptor-{gamma} as a regulator of lung inflammation and repair**. *Proc Am Thorac Soc* 2005, **2**:226-231.
110. Bouhlel MA, Derudas B, Rigamonti E, Dièvart R, Brozek J, Haulon S, Zawadzki C, Jude B, Torpier G, Marx N, et al.: **PPARgamma activation primes human monocytes into alternative M2 macrophages with anti-inflammatory properties**. *Cell Metab* 2007, **6**:137-143.
111. Von Knethen A, Brüne B: **Activation of peroxisome proliferator-activated receptor gamma by nitric oxide in monocytes/macrophages down-regulates p47phox and attenuates the respiratory burst**. *J Immunol* 2002, **169**:2619-2626.
112. Jiang C, Ting AT, Seed B: **PPAR-gamma agonists inhibit production of monocyte inflammatory cytokines**. *Nature* 1998, **391**:82-86.
113. Lipscomb MF, Lyons CR, Nunez G, Ball EJ, Stastny P, Vial W, Lem V, Weissler J, Miller LM: **Human alveolar macrophages: HLA-DR-positive macrophages that are poor stimulators of a primary mixed leukocyte reaction**. *J Immunol* 1986, **136**:497-504.
114. Lyons CR, Ball EJ, Toews GB, Weissler JC, Stastny P, Lipscomb MF: **Inability of human alveolar macrophages to stimulate resting T cells correlates with decreased antigen-specific T cell-macrophage binding**. *J Immunol* 1986, **137**:1173-1180.
115. Coleman MM, Ruane D, Moran B, Dunne PJ, Keane J, Mills KH: **Alveolar macrophages contribute to respiratory tolerance by inducing FoxP3 expression in naive T cells**. *Am J Respir Cell Mol Biol* 2013, **48**:773-780.
116. Lugo-Villarino G, Vérollet C, Maridonneau-Parini I, Neyrolles O: **Macrophage polarization: convergence point targeted by mycobacterium tuberculosis and HIV**. *Front Immunol* 2011, **2**:43.

117. Kahnert A, Seiler P, Stein M, Bandermann S, Hahnke K, Mollenkopf H, Kaufmann SH: **Alternative activation deprives macrophages of a coordinated defense program to Mycobacterium tuberculosis**. *Eur J Immunol* 2006, **36**:631-647.
118. Marino S, Cilfone NA, Mattila JT, Linderman JJ, Flynn JL, Kirschner DE: **Macrophage polarization drives granuloma outcome during Mycobacterium tuberculosis infection**. *Infect Immun* 2015, **83**:324-338.
119. Krause P, Morris V, Greenbaum JA, Park Y, Bjoerheden U, Mikulski Z, Muffley T, Shui JW, Kim G, Cheroutre H, et al.: **IL-10-producing intestinal macrophages prevent excessive antibacterial innate immunity by limiting IL-23 synthesis**. *Nat Commun* 2015, **6**:7055.
120. Ehrt S, Schnappinger D, Bekiranov S, Drenkow J, Shi S, Gingeras TR, Gaasterland T, Schoolnik G, Nathan C: **Reprogramming of the macrophage transcriptome in response to interferon-gamma and Mycobacterium tuberculosis: signaling roles of nitric oxide synthase-2 and phagocyte oxidase**. *J Exp Med* 2001, **194**:1123-1140.
121. Redente EF, Higgins DM, Dwyer-Nield LD, Orme IM, Gonzalez-Juarrero M, Malkinson AM: **Differential polarization of alveolar macrophages and bone marrow-derived monocytes following chemically and pathogen-induced chronic lung inflammation**. *J Leukoc Biol* 2010, **88**:159-168.
122. Raju B, Hoshino Y, Belitskaya-Lévy I, Dawson R, Ress S, Gold JA, Condos R, Pine R, Brown S, Nolan A, et al.: **Gene expression profiles of bronchoalveolar cells in pulmonary TB**. *Tuberculosis (Edinb)* 2008, **88**:39-51.
123. Rajaram MV, Brooks MN, Morris JD, Torrelles JB, Azad AK, Schlesinger LS: **Mycobacterium tuberculosis activates human macrophage peroxisome proliferator-activated receptor gamma linking mannose receptor recognition to regulation of immune responses**. *J Immunol* 2010, **185**:929-942.
124. O'Leary S, O'Sullivan MP, Keane J: **IL-10 blocks phagosome maturation in mycobacterium tuberculosis-infected human macrophages**. *Am J Respir Cell Mol Biol* 2011, **45**:172-180.
125. Song CH, Lee JS, Lee SH, Lim K, Kim HJ, Park JK, Paik TH, Jo EK: **Role of mitogen-activated protein kinase pathways in the production of tumor necrosis factor-alpha, interleukin-10, and monocyte chemotactic protein-1 by Mycobacterium tuberculosis H37Rv-infected human monocytes**. *J Clin Immunol* 2003, **23**:194-201.
126. Schreiber T, Ehlers S, Heitmann L, Rausch A, Mages J, Murray PJ, Lang R, Hölscher C: **Autocrine IL-10 induces hallmarks of alternative activation in macrophages and suppresses antituberculosis effector mechanisms without compromising T cell immunity**. *J Immunol* 2009, **183**:1301-1312.
127. El Kasmi KC, Qualls JE, Pesce JT, Smith AM, Thompson RW, Henao-Tamayo M, Basaraba RJ, König T, Schleicher U, Koo MS, et al.: **Toll-like receptor-induced arginase 1 in macrophages thwarts effective immunity against intracellular pathogens**. *Nat Immunol* 2008, **9**:1399-1406.
128. Roach DR, Martin E, Bean AG, Rennick DM, Briscoe H, Britton WJ: **Endogenous inhibition of antimycobacterial immunity by IL-10 varies between mycobacterial species**. *Scand J Immunol* 2001, **54**:163-170.
129. Redford PS, Boonstra A, Read S, Pitt J, Graham C, Stavropoulos E, Bancroft GJ, O'Garra A: **Enhanced protection to Mycobacterium tuberculosis infection in IL-10-deficient mice is accompanied by early and enhanced Th1 responses in the lung**. *Eur J Immunol* 2010, **40**:2200-2210.
130. Harris J, De Haro SA, Master SS, Keane J, Roberts EA, Delgado M, Deretic V: **T helper 2 cytokines inhibit autophagic control of intracellular Mycobacterium tuberculosis**. *Immunity* 2007, **27**:505-517.
131. Kleinnijenhuis J, Joosten LA, van de Veerdonk FL, Savage N, van Crevel R, Kullberg BJ, van der Ven A, Ottenhoff TH, Dinarello CA, van der Meer JW, et al.: **Transcriptional and inflammasome-mediated pathways for the induction of IL-1beta production by Mycobacterium tuberculosis**. *Eur J Immunol* 2009, **39**:1914-1922.
132. Dinarello CA: **Biologic basis for interleukin-1 in disease**. *Blood* 1996, **87**:2095-2147.

133. Fremond CM, Togbe D, Doz E, Rose S, Vasseur V, Maillet I, Jacobs M, Ryffel B, Quesniaux VF: **IL-1 receptor-mediated signal is an essential component of MyD88-dependent innate response to Mycobacterium tuberculosis infection**. *J Immunol* 2007, **179**:1178-1189.
134. Mayer-Barber KD, Barber DL, Shenderov K, White SD, Wilson MS, Cheever A, Kugler D, Hieny S, Caspar P, Núñez G, et al.: **Caspase-1 independent IL-1beta production is critical for host resistance to mycobacterium tuberculosis and does not require TLR signaling in vivo**. *J Immunol* 2010, **184**:3326-3330.
135. Miller LS, Pietras EM, Uricchio LH, Hirano K, Rao S, Lin H, O'Connell RM, Iwakura Y, Cheung AL, Cheng G, et al.: **Inflammasome-mediated production of IL-1beta is required for neutrophil recruitment against Staphylococcus aureus in vivo**. *J Immunol* 2007, **179**:6933-6942.
136. Prantner D, Darville T, Sikes JD, Andrews CW, Brade H, Rank RG, Nagarajan UM: **Critical role for interleukin-1beta (IL-1beta) during Chlamydia muridarum genital infection and bacterial replication-independent secretion of IL-1beta in mouse macrophages**. *Infect Immun* 2009, **77**:5334-5346.
137. Ramos HJ, Lanteri MC, Blahnik G, Negash A, Suthar MS, Brassil MM, Sodhi K, Treuting PM, Busch MP, Norris PJ, et al.: **IL-1β signaling promotes CNS-intrinsic immune control of West Nile virus infection**. *PLoS Pathog* 2012, **8**:e1003039.
138. Netea MG, van de Veerdonk FL, van der Meer JW, Dinarello CA, Joosten LA: **Inflammasome-independent regulation of IL-1-family cytokines**. *Annu Rev Immunol* 2015, **33**:49-77.
139. Mayer-Barber KD, Andrade BB, Barber DL, Hieny S, Feng CG, Caspar P, Oland S, Gordon S, Sher A: **Innate and adaptive interferons suppress IL-1α and IL-1β production by distinct pulmonary myeloid subsets during Mycobacterium tuberculosis infection**. *Immunity* 2011, **35**:1023-1034.
140. Netea MG, Simon A, van de Veerdonk F, Kullberg BJ, Van der Meer JW, Joosten LA: **IL-1beta processing in host defense: beyond the inflammasomes**. *PLoS Pathog* 2010, **6**:e1000661.
141. Dinarello CA: **Interleukin-1 in the pathogenesis and treatment of inflammatory diseases**. *Blood* 2011, **117**:3720-3732.
142. O'Neill LA, Bowie AG: **The family of five: TIR-domain-containing adaptors in Toll-like receptor signalling**. *Nat Rev Immunol* 2007, **7**:353-364.
143. Juffermans NP, Florquin S, Camoglio L, Verbon A, Kolk AH, Speelman P, van Deventer SJ, van Der Poll T: **Interleukin-1 signaling is essential for host defense during murine pulmonary tuberculosis**. *J Infect Dis* 2000, **182**:902-908.
144. Yamada H, Mizumo S, Horai R, Iwakura Y, Sugawara I: **Protective role of interleukin-1 in mycobacterial infection in IL-1 alpha/beta double-knockout mice**. *Lab Invest* 2000, **80**:759-767.
145. Sugawara I, Yamada H, Hua S, Mizuno S: **Role of interleukin (IL)-1 type 1 receptor in mycobacterial infection**. *Microbiol Immunol* 2001, **45**:743-750.
146. Mayer-Barber KD, Andrade BB, Oland SD, Amaral EP, Barber DL, Gonzales J, Derrick SC, Shi R, Kumar NP, Wei W, et al.: **Host-directed therapy of tuberculosis based on interleukin-1 and type I interferon crosstalk**. *Nature* 2014, **511**:99-103.
147. Kafka D, Ling E, Feldman G, Benharroch D, Voronov E, Givon-Lavi N, Iwakura Y, Dagan R, Apte RN, Mizrachi-Nebenzahl Y: **Contribution of IL-1 to resistance to Streptococcus pneumoniae infection**. *Int Immunol* 2008, **20**:1139-1146.
148. Voronov E, Dotan S, Gayvoronsky L, White RM, Cohen I, Krelin Y, Benchetrit F, Elkabets M, Huszar M, El-On J, et al.: **IL-1-induced inflammation promotes development of leishmaniasis in susceptible BALB/c mice**. *Int Immunol* 2010, **22**:245-257.
149. Guler R, Parihar SP, Spohn G, Johansen P, Brombacher F, Bachmann MF: **Blocking IL-1α but not IL-1β increases susceptibility to chronic Mycobacterium tuberculosis infection in mice**. *Vaccine* 2011, **29**:1339-1346.
150. Di Paolo NC, Shafiani S, Day T, Papayannopoulou T, Papayannoupoulou T, Russell DW, Iwakura Y, Sherman D, Urdahl K, Shayakhmetov DM: **Interdependence between**

Interleukin-1 and Tumor Necrosis Factor Regulates TNF-Dependent Control of Mycobacterium tuberculosis Infection. *Immunity* 2015, **43**:1125-1136.
151. Kusuhara K, Yamamoto K, Okada K, Mizuno Y, Hara T: **Association of IL12RB1 polymorphisms with susceptibility to and severity of tuberculosis in Japanese: a gene-based association analysis of 21 candidate genes**. *Int J Immunogenet* 2007, **34**:35-44.
152. Naslednikova IO, Urazova OI, Voronkova OV, Strelis AK, Novitsky VV, Nikulina EL, Hasanova RR, Kononova TE, Serebryakova VA, Vasileva OA, et al.: **Allelic polymorphism of cytokine genes during pulmonary tuberculosis**. *Bull Exp Biol Med* 2009, **148**:175-180.
153. Sun H, Wang Y, Ma X, Pei F, Zhang Y, Yu B: **A method of oligochip for single nucleotide polymorphism genotyping in the promoter region of the interleukin-1 beta gene and its clinical application**. *Oligonucleotides* 2007, **17**:336-344.
154. Awomoyi AA, Charurat M, Marchant A, Miller EN, Blackwell JM, McAdam KP, Newport MJ: **Polymorphism in IL1B: IL1B-511 association with tuberculosis and decreased lipopolysaccharide-induced IL-1beta in IFN-gamma primed ex-vivo whole blood assay**. *J Endotoxin Res* 2005, **11**:281-286.
155. Zhang G, Zhou B, Li S, Yue J, Yang H, Wen Y, Zhan S, Wang W, Liao M, Zhang M, et al.: **Allele-specific induction of IL-1β expression by C/EBPβ and PU.1 contributes to increased tuberculosis susceptibility**. *PLoS Pathog* 2014, **10**:e1004426.
156. Mishra BB, Rathinam VA, Martens GW, Martinot AJ, Kornfeld H, Fitzgerald KA, Sassetti CM: **Nitric oxide controls the immunopathology of tuberculosis by inhibiting NLRP3 inflammasome-dependent processing of IL-1β**. *Nat Immunol* 2013, **14**:52-60.
157. O'Kane CM, Elkington PT, Jones MD, Caviedes L, Tovar M, Gilman RH, Stamp G, Friedland JS: **STAT3, p38 MAPK, and NF-kappaB drive unopposed monocyte-dependent fibroblast MMP-1 secretion in tuberculosis**. *Am J Respir Cell Mol Biol* 2010, **43**:465-474.
158. Carlsson F, Kim J, Dumitru C, Barck KH, Carano RA, Sun M, Diehl L, Brown EJ: **Host-detrimental role of Esx-1-mediated inflammasome activation in mycobacterial infection**. *PLoS Pathog* 2010, **6**:e1000895.
159. Gomez LM, Camargo JF, Castiblanco J, Ruiz-Narváez EA, Cadena J, Anaya JM: **Analysis of IL1B, TAP1, TAP2 and IKBL polymorphisms on susceptibility to tuberculosis**. *Tissue Antigens* 2006, **67**:290-296.
160. Wang Y, Hu C, Wang Z, Kong H, Xie W, Wang H: **Serum IL-1β and IL-18 correlate with ESR and CRP in multidrug-resistant tuberculosis patients**. *J Biomed Res* 2015, **29**:426-428.
161. Lopalco G, Rigante D, Giannini M, Galeazzi M, Lapadula G, Iannone F, Cantarini L: **Safety profile of anakinra in the management of rheumatologic, metabolic and autoinflammatory disorders**. *Clin Exp Rheumatol* 2016, **34**:531-538.
162. Singh JA, Wells GA, Christensen R, Tanjong Ghogomu E, Maxwell L, Macdonald JK, Filippini G, Skoetz N, Francis D, Lopes LC, et al.: **Adverse effects of biologics: a network meta-analysis and Cochrane overview**. *Cochrane Database Syst Rev* 2011:CD008794.
163. Settas LD, Tsimirikas G, Vosvotekas G, Triantafyllidou E, Nicolaides P: **Reactivation of pulmonary tuberculosis in a patient with rheumatoid arthritis during treatment with IL-1 receptor antagonists (anakinra)**. *J Clin Rheumatol* 2007, **13**:219-220.
164. Migkos MP, Somarakis GA, Markatseli TE, Matthaiou M, Kosta P, Voulgari PV, Drosos AA: **Tuberculous pyomyositis in a rheumatoid arthritis patient treated with anakinra**. *Clin Exp Rheumatol* 2015, **33**:734-736.
165. Lopez-Castejon G, Brough D: **Understanding the mechanism of IL-1β secretion**. *Cytokine Growth Factor Rev* 2011, **22**:189-195.
166. Hiscott J, Marois J, Garoufalis J, D'Addario M, Roulston A, Kwan I, Pepin N, Lacoste J, Nguyen H, Bensi G: **Characterization of a functional NF-kappa B site in the human interleukin 1 beta promoter: evidence for a positive autoregulatory loop**. *Mol Cell Biol* 1993, **13**:6231-6240.
167. Cogswell JP, Godlevski MM, Wisely GB, Clay WC, Leesnitzer LM, Ways JP, Gray JG: **NF-kappa B regulates IL-1 beta transcription through a consensus NF-kappa B binding site and a nonconsensus CRE-like site**. *J Immunol* 1994, **153**:712-723.

168. Ruse M, Knaus UG: **New players in TLR-mediated innate immunity: PI3K and small Rho GTPases**. *Immunol Res* 2006, **34**:33-48.
169. Abdel-Nour M, Tsalikis J, Kleinman D, Girardin SE: **The emerging role of mTOR signalling in antibacterial immunity**. *Immunol Cell Biol* 2014, **92**:346-353.
170. Ojaniemi M, Glumoff V, Harju K, Liljeroos M, Vuori K, Hallman M: **Phosphatidylinositol 3-kinase is involved in Toll-like receptor 4-mediated cytokine expression in mouse macrophages**. *Eur J Immunol* 2003, **33**:597-605.
171. Okugawa S, Ota Y, Kitazawa T, Nakayama K, Yanagimoto S, Tsukada K, Kawada M, Kimura S: **Janus kinase 2 is involved in lipopolysaccharide-induced activation of macrophages**. *Am J Physiol Cell Physiol* 2003, **285**:C399-408.
172. Fang HY, Hughes R, Murdoch C, Coffelt SB, Biswas SK, Harris AL, Johnson RS, Imityaz HZ, Simon MC, Fredlund E, et al.: **Hypoxia-inducible factors 1 and 2 are important transcriptional effectors in primary macrophages experiencing hypoxia**. *Blood* 2009, **114**:844-859.
173. Peyssonnaux C, Cejudo-Martin P, Doedens A, Zinkernagel AS, Johnson RS, Nizet V: **Cutting edge: Essential role of hypoxia inducible factor-1alpha in development of lipopolysaccharide-induced sepsis**. *J Immunol* 2007, **178**:7516-7519.
174. Tannahill GM, Curtis AM, Adamik J, Palsson-McDermott EM, McGettrick AF, Goel G, Frezza C, Bernard NJ, Kelly B, Foley NH, et al.: **Succinate is an inflammatory signal that induces IL-1β through HIF-1α**. *Nature* 2013, **496**:238-242.
175. Blanc L, Castanier R, Mishra AK, Ray A, Besra GS, Sutcliffe I, Vercellone A, Nigou J: **Gram-positive bacterial lipoglycans based on a glycosylated diacylglycerol lipid anchor are microbe-associated molecular patterns recognized by TLR2**. *PLoS One* 2013, **8**:e81593.
176. Takeda K, Takeuchi O, Akira S: **Recognition of lipopeptides by Toll-like receptors**. *J Endotoxin Res* 2002, **8**:459-463.
177. Farhat K, Riekenberg S, Heine H, Debarry J, Lang R, Mages J, Buwitt-Beckmann U, Röschmann K, Jung G, Wiesmüller KH, et al.: **Heterodimerization of TLR2 with TLR1 or TLR6 expands the ligand spectrum but does not lead to differential signaling**. *J Leukoc Biol* 2008, **83**:692-701.
178. Underhill DM, Ozinsky A, Smith KD, Aderem A: **Toll-like receptor-2 mediates mycobacteria-induced proinflammatory signaling in macrophages**. *Proc Natl Acad Sci U S A* 1999, **96**:14459-14463.
179. Reiling N, Hölscher C, Fehrenbach A, Kröger S, Kirschning CJ, Goyert S, Ehlers S: **Cutting edge: Toll-like receptor (TLR)2- and TLR4-mediated pathogen recognition in resistance to airborne infection with Mycobacterium tuberculosis**. *J Immunol* 2002, **169**:3480-3484.
180. Drennan MB, Nicolle D, Quesniaux VJ, Jacobs M, Allie N, Mpagi J, Frémond C, Wagner H, Kirschning C, Ryffel B: **Toll-like receptor 2-deficient mice succumb to Mycobacterium tuberculosis infection**. *Am J Pathol* 2004, **164**:49-57.
181. Schroder K, Tschopp J: **The inflammasomes**. *Cell* 2010, **140**:821-832.
182. Martinon F, Agostini L, Meylan E, Tschopp J: **Identification of bacterial muramyl dipeptide as activator of the NALP3/cryopyrin inflammasome**. *Curr Biol* 2004, **14**:1929-1934.
183. Zhou R, Tardivel A, Thorens B, Choi I, Tschopp J: **Thioredoxin-interacting protein links oxidative stress to inflammasome activation**. *Nat Immunol* 2010, **11**:136-140.
184. Sorbara MT, Girardin SE: **Mitochondrial ROS fuel the inflammasome**. *Cell Res* 2011, **21**:558-560.
185. Iyer SS, Pulskens WP, Sadler JJ, Butter LM, Teske GJ, Ulland TK, Eisenbarth SC, Florquin S, Flavell RA, Leemans JC, et al.: **Necrotic cells trigger a sterile inflammatory response through the Nlrp3 inflammasome**. *Proc Natl Acad Sci U S A* 2009, **106**:20388-20393.
186. Bours MJ, Dagnelie PC, Giuliani AL, Wesselius A, Di Virgilio F: **P2 receptors and extracellular ATP: a novel homeostatic pathway in inflammation**. *Front Biosci (Schol Ed)* 2011, **3**:1443-1456.

187. Elssner A, Duncan M, Gavrilin M, Wewers MD: **A novel P2X7 receptor activator, the human cathelicidin-derived peptide LL37, induces IL-1 beta processing and release**. *J Immunol* 2004, **172**:4987-4994.
188. Cooper AM, Magram J, Ferrante J, Orme IM: **Interleukin 12 (IL-12) is crucial to the development of protective immunity in mice intravenously infected with mycobacterium tuberculosis**. *J Exp Med* 1997, **186**:39-45.
189. Cooper AM, Dalton DK, Stewart TA, Griffin JP, Russell DG, Orme IM: **Disseminated tuberculosis in interferon gamma gene-disrupted mice**. *J Exp Med* 1993, **178**:2243-2247.
190. Flynn JL, Chan J, Triebold KJ, Dalton DK, Stewart TA, Bloom BR: **An essential role for interferon gamma in resistance to Mycobacterium tuberculosis infection**. *J Exp Med* 1993, **178**:2249-2254.
191. Altare F, Durandy A, Lammas D, Emile JF, Lamhamedi S, Le Deist F, Drysdale P, Jouanguy E, Döffinger R, Bernaudin F, et al.: **Impairment of mycobacterial immunity in human interleukin-12 receptor deficiency**. *Science* 1998, **280**:1432-1435.
192. Rider P, Kaplanov I, Romzova M, Bernardis L, Braiman A, Voronov E, Apte RN: **The transcription of the alarmin cytokine interleukin-1 alpha is controlled by hypoxia inducible factors 1 and 2 alpha in hypoxic cells**. *Front Immunol* 2012, **3**:290.
193. LeibundGut-Landmann S, Weidner K, Hilbi H, Oxenius A: **Nonhematopoietic cells are key players in innate control of bacterial airway infection**. *J Immunol* 2011, **186**:3130-3137.
194. Wang CH, Kuo HP: **Nitric oxide modulates interleukin-1beta and tumour necrosis factor-alpha synthesis, and disease regression by alveolar macrophages in pulmonary tuberculosis**. *Respirology* 2001, **6**:79-84.
195. Clay H, Volkman HE, Ramakrishnan L: **Tumor necrosis factor signaling mediates resistance to mycobacteria by inhibiting bacterial growth and macrophage death**. *Immunity* 2008, **29**:283-294.
196. Flynn JL, Goldstein MM, Chan J, Triebold KJ, Pfeffer K, Lowenstein CJ, Schreiber R, Mak TW, Bloom BR: **Tumor necrosis factor-alpha is required in the protective immune response against Mycobacterium tuberculosis in mice**. *Immunity* 1995, **2**:561-572.
197. Jayaraman P, Sada-Ovalle I, Nishimura T, Anderson AC, Kuchroo VK, Remold HG, Behar SM: **IL-1β promotes antimicrobial immunity in macrophages by regulating TNFR signaling and caspase-3 activation**. *J Immunol* 2013, **190**:4196-4204.
198. Serhan CN, Haeggström JZ, Leslie CC: **Lipid mediator networks in cell signaling: update and impact of cytokines**. *FASEB J* 1996, **10**:1147-1158.
199. Bafica A, Scanga CA, Serhan C, Machado F, White S, Sher A, Aliberti J: **Host control of Mycobacterium tuberculosis is regulated by 5-lipoxygenase-dependent lipoxin production**. *J Clin Invest* 2005, **115**:1601-1606.
200. Tobin DM, Vary JC, Ray JP, Walsh GS, Dunstan SJ, Bang ND, Hagge DA, Khadge S, King MC, Hawn TR, et al.: **The lta4h locus modulates susceptibility to mycobacterial infection in zebrafish and humans**. *Cell* 2010, **140**:717-730.
201. Tobin DM, Roca FJ, Oh SF, McFarland R, Vickery TW, Ray JP, Ko DC, Zou Y, Bang ND, Chau TT, et al.: **Host genotype-specific therapies can optimize the inflammatory response to mycobacterial infections**. *Cell* 2012, **148**:434-446.
202. Chen M, Divangahi M, Gan H, Shin DS, Hong S, Lee DM, Serhan CN, Behar SM, Remold HG: **Lipid mediators in innate immunity against tuberculosis: opposing roles of PGE2 and LXA4 in the induction of macrophage death**. *J Exp Med* 2008, **205**:2791-2801.
203. Divangahi M, Chen M, Gan H, Desjardins D, Hickman TT, Lee DM, Fortune S, Behar SM, Remold HG: **Mycobacterium tuberculosis evades macrophage defenses by inhibiting plasma membrane repair**. *Nat Immunol* 2009, **10**:899-906.
204. Kaul V, Bhattacharya D, Singh Y, Van Kaer L, Peters-Golden M, Bishai WR, Das G: **An important role of prostanoid receptor EP2 in host resistance to Mycobacterium tuberculosis infection in mice**. *J Infect Dis* 2012, **206**:1816-1825.

205. Divangahi M, Desjardins D, Nunes-Alves C, Remold HG, Behar SM: **Eicosanoid pathways regulate adaptive immunity to Mycobacterium tuberculosis**. *Nat Immunol* 2010, **11**:751-758.
206. Assis PA, Espíndola MS, Paula-Silva FW, Rios WM, Pereira PA, Leão SC, Silva CL, Faccioli LH: **Mycobacterium tuberculosis expressing phospholipase C subverts PGE2 synthesis and induces necrosis in alveolar macrophages**. *BMC Microbiol* 2014, **14**:128.
207. Rangel Moreno J, Estrada García I, De La Luz García Hernández M, Aguilar Leon D, Marquez R, Hernández Pando R: **The role of prostaglandin E2 in the immunopathogenesis of experimental pulmonary tuberculosis**. *Immunology* 2002, **106**:257-266.
208. Vilaplana C, Marzo E, Tapia G, Diaz J, Garcia V, Cardona PJ: **Ibuprofen therapy resulted in significantly decreased tissue bacillary loads and increased survival in a new murine experimental model of active tuberculosis**. *J Infect Dis* 2013, **208**:199-202.
209. Dutta NK, Kumar KA, Mazumdar K, Dastidar SG: **In vitro and in vivo antimycobacterial activity of antiinflammatory drug, diclofenac sodium**. *Indian J Exp Biol* 2004, **42**:922-927.
210. Dutta NK, Mazumdar K, Dastidar SG, Park JH: **Activity of diclofenac used alone and in combination with streptomycin against Mycobacterium tuberculosis in mice**. *Int J Antimicrob Agents* 2007, **30**:336-340.
211. Berry MP, Graham CM, McNab FW, Xu Z, Bloch SA, Oni T, Wilkinson KA, Banchereau R, Skinner J, Wilkinson RJ, et al.: **An interferon-inducible neutrophil-driven blood transcriptional signature in human tuberculosis**. *Nature* 2010, **466**:973-977.
212. Stanley SA, Johndrow JE, Manzanillo P, Cox JS: **The Type I IFN response to infection with Mycobacterium tuberculosis requires ESX-1-mediated secretion and contributes to pathogenesis**. *J Immunol* 2007, **178**:3143-3152.
213. Ottenhoff TH, Dass RH, Yang N, Zhang MM, Wong HE, Sahiratmadja E, Khor CC, Alisjahbana B, van Crevel R, Marzuki S, et al.: **Genome-wide expression profiling identifies type 1 interferon response pathways in active tuberculosis**. *PLoS One* 2012, **7**:e45839.
214. Redford PS, Mayer-Barber KD, McNab FW, Stavropoulos E, Wack A, Sher A, O'Garra A: **Influenza A virus impairs control of Mycobacterium tuberculosis coinfection through a type I interferon receptor-dependent pathway**. *J Infect Dis* 2014, **209**:270-274.
215. Manca C, Tsenova L, Bergtold A, Freeman S, Tovey M, Musser JM, Barry CE, Freedman VH, Kaplan G: **Virulence of a Mycobacterium tuberculosis clinical isolate in mice is determined by failure to induce Th1 type immunity and is associated with induction of IFN-alpha /beta**. *Proc Natl Acad Sci U S A* 2001, **98**:5752-5757.
216. Novikov A, Cardone M, Thompson R, Shenderov K, Kirschman KD, Mayer-Barber KD, Myers TG, Rabin RL, Trinchieri G, Sher A, et al.: **Mycobacterium tuberculosis triggers host type I IFN signaling to regulate IL-1β production in human macrophages**. *J Immunol* 2011, **187**:2540-2547.
217. Palsson-McDermott EM, O'Neill LA: **The Warburg effect then and now: from cancer to inflammatory diseases**. *Bioessays* 2013, **35**:965-973.
218. Berg J, Tymoczko J, Stryer L: **Biochemistry**. edn 5th. Edited by. New York: W.H. Freeman; 2002.
219. Cooper GM: **The Cell: A Molecular Approach**. edn 2nd. Edited by. Sunderland (MA): Sinauer Associates; 2000.
220. Pearce EL, Pearce EJ: **Metabolic pathways in immune cell activation and quiescence**. *Immunity* 2013, **38**:633-643.
221. O'Neill LA, Pearce EJ: **Immunometabolism governs dendritic cell and macrophage function**. *J Exp Med* 2016, **213**:15-23.
222. Warburg O: **Metabolism of tumours**. Edited by. Biochem Z; 1923:317 - 333. vol 142.]
223. EVANS WH, KARNOVSKY ML: **The biochemical basis of phagocytosis. IV. Some aspects of carbohydrate metabolism during phagocytosis**. *Biochemistry* 1962, **1**:159-166.
224. SBARRA AJ, KARNOVSKY ML: **The biochemical basis of phagocytosis. I. Metabolic changes during the ingestion of particles by polymorphonuclear leukocytes**. *J Biol Chem* 1959, **234**:1355-1362.

225. SBARRA AJ, KARNOVSKY ML: **The biochemical basis of phagocytosis. 2. Incorporation of C14-labeled building blocks into lipid, protein, and glycogen of leukocytes during phagocytosis**. *J Biol Chem* 1960, **235**:2224-2229.
226. OREN R, FARNHAM AE, SAITO K, MILOFSKY E, KARNOVSKY ML: **Metabolic patterns in three types of phagocytizing cells**. *J Cell Biol* 1963, **17**:487-501.
227. Newsholme P, Curi R, Gordon S, Newsholme EA: **Metabolism of glucose, glutamine, long-chain fatty acids and ketone bodies by murine macrophages**. *Biochem J* 1986, **239**:121-125.
228. Fukuzumi M, Shinomiya H, Shimizu Y, Ohishi K, Utsumi S: **Endotoxin-induced enhancement of glucose influx into murine peritoneal macrophages via GLUT1**. *Infect Immun* 1996, **64**:108-112.
229. Hard GC: **Some biochemical aspects of the immune macrophage**. *Br J Exp Pathol* 1970, **51**:97-105.
230. Newsholme P, Gordon S, Newsholme EA: **Rates of utilization and fates of glucose, glutamine, pyruvate, fatty acids and ketone bodies by mouse macrophages**. *Biochem J* 1987, **242**:631-636.
231. Bustos R, Sobrino F: **Stimulation of glycolysis as an activation signal in rat peritoneal macrophages. Effect of glucocorticoids on this process**. *Biochem J* 1992, **282 (Pt 1)**:299-303.
232. Wang T, Marquardt C, Foker J: **Aerobic glycolysis during lymphocyte proliferation**. *Nature* 1976, **261**:702-705.
233. Vander Heiden MG, Cantley LC, Thompson CB: **Understanding the Warburg effect: the metabolic requirements of cell proliferation**. *Science* 2009, **324**:1029-1033.
234. Jones RG, Thompson CB: **Revving the engine: signal transduction fuels T cell activation**. *Immunity* 2007, **27**:173-178.
235. Fox CJ, Hammerman PS, Thompson CB: **Fuel feeds function: energy metabolism and the T-cell response**. *Nat Rev Immunol* 2005, **5**:844-852.
236. Borregaard N, Herlin T: **Energy metabolism of human neutrophils during phagocytosis**. *J Clin Invest* 1982, **70**:550-557.
237. Guthrie LA, McPhail LC, Henson PM, Johnston RB: **Priming of neutrophils for enhanced release of oxygen metabolites by bacterial lipopolysaccharide. Evidence for increased activity of the superoxide-producing enzyme**. *J Exp Med* 1984, **160**:1656-1671.
238. Everts B, Amiel E, van der Windt GJ, Freitas TC, Chott R, Yarasheski KE, Pearce EL, Pearce EJ: **Commitment to glycolysis sustains survival of NO-producing inflammatory dendritic cells**. *Blood* 2012, **120**:1422-1431.
239. Everts B, Amiel E, Huang SC, Smith AM, Chang CH, Lam WY, Redmann V, Freitas TC, Blagih J, van der Windt GJ, et al.: **TLR-driven early glycolytic reprogramming via the kinases TBK1-IKKε supports the anabolic demands of dendritic cell activation**. *Nat Immunol* 2014, **15**:323-332.
240. Krawczyk CM, Holowka T, Sun J, Blagih J, Amiel E, DeBerardinis RJ, Cross JR, Jung E, Thompson CB, Jones RG, et al.: **Toll-like receptor-induced changes in glycolytic metabolism regulate dendritic cell activation**. *Blood* 2010, **115**:4742-4749.
241. Rodríguez-Prados JC, Través PG, Cuenca J, Rico D, Aragonés J, Martín-Sanz P, Cascante M, Boscá L: **Substrate fate in activated macrophages: a comparison between innate, classic, and alternative activation**. *J Immunol* 2010, **185**:605-614.
242. Galván-Peña S, O'Neill LA: **Metabolic reprograming in macrophage polarization**. *Front Immunol* 2014, **5**:420.
243. Lachmandas E, Boutens L, Ratter JM, Hijmans A, Hooiveld GJ, Joosten LA, Rodenburg RJ, Fransen JA, Houtkooper RH, van Crevel R, et al.: **Microbial stimulation of different Toll-like receptor signalling pathways induces diverse metabolic programmes in human monocytes**. *Nat Microbiol* 2016, **2**:16246.
244. Jha AK, Huang SC, Sergushichev A, Lampropoulou V, Ivanova Y, Loginicheva E, Chmielewski K, Stewart KM, Ashall J, Everts B, et al.: **Network integration of parallel metabolic and**

transcriptional data reveals metabolic modules that regulate macrophage polarization. *Immunity* 2015, **42**:419-430.
245. Vats D, Mukundan L, Odegaard JI, Zhang L, Smith KL, Morel CR, Wagner RA, Greaves DR, Murray PJ, Chawla A: **Oxidative metabolism and PGC-1beta attenuate macrophage-mediated inflammation**. *Cell Metab* 2006, **4**:13-24.
246. El Kasmi KC, Stenmark KR: **Contribution of metabolic reprogramming to macrophage plasticity and function**. *Semin Immunol* 2015, **27**:267-275.
247. Palsson-McDermott EM, Curtis AM, Goel G, Lauterbach MA, Sheedy FJ, Gleeson LE, van den Bosch MW, Quinn SR, Domingo-Fernandez R, Johnston DG, et al.: **Pyruvate kinase M2 regulates Hif-1α activity and IL-1β induction and is a critical determinant of the warburg effect in LPS-activated macrophages**. *Cell Metab* 2015, **21**:65-80.
248. Gleeson LE, Sheedy FJ, Palsson-McDermott EM, Triglia D, O'Leary SM, O'Sullivan MP, O'Neill LA, Keane J: **Cutting Edge: Mycobacterium tuberculosis Induces Aerobic Glycolysis in Human Alveolar Macrophages That Is Required for Control of Intracellular Bacillary Replication**. *J Immunol* 2016, **196**:2444-2449.
249. Deprez J, Vertommen D, Alessi DR, Hue L, Rider MH: **Phosphorylation and activation of heart 6-phosphofructo-2-kinase by protein kinase B and other protein kinases of the insulin signaling cascades**. *J Biol Chem* 1997, **272**:17269-17275.
250. Moon JS, Hisata S, Park MA, DeNicola GM, Ryter SW, Nakahira K, Choi AM: **mTORC1-Induced HK1-Dependent Glycolysis Regulates NLRP3 Inflammasome Activation**. *Cell Rep* 2015, **12**:102-115.
251. Düvel K, Yecies JL, Menon S, Raman P, Lipovsky AI, Souza AL, Triantafellow E, Ma Q, Gorski R, Cleaver S, et al.: **Activation of a metabolic gene regulatory network downstream of mTOR complex 1**. *Mol Cell* 2010, **39**:171-183.
252. Land SC, Tee AR: **Hypoxia-inducible factor 1alpha is regulated by the mammalian target of rapamycin (mTOR) via an mTOR signaling motif**. *J Biol Chem* 2007, **282**:20534-20543.
253. Harada H, Itasaka S, Kizaka-Kondoh S, Shibuya K, Morinibu A, Shinomiya K, Hiraoka M: **The Akt/mTOR pathway assures the synthesis of HIF-1alpha protein in a glucose- and reoxygenation-dependent manner in irradiated tumors**. *J Biol Chem* 2009, **284**:5332-5342.
254. Finlay DK, Rosenzweig E, Sinclair LV, Feijoo-Carnero C, Hukelmann JL, Rolf J, Panteleyev AA, Okkenhaug K, Cantrell DA: **PDK1 regulation of mTOR and hypoxia-inducible factor 1 integrate metabolism and migration of CD8+ T cells**. *J Exp Med* 2012, **209**:2441-2453.
255. Sumbayev VV: **LPS-induced Toll-like receptor 4 signalling triggers cross-talk of apoptosis signal-regulating kinase 1 (ASK1) and HIF-1alpha protein**. *FEBS Lett* 2008, **582**:319-326.
256. Papandreou I, Cairns RA, Fontana L, Lim AL, Denko NC: **HIF-1 mediates adaptation to hypoxia by actively downregulating mitochondrial oxygen consumption**. *Cell Metab* 2006, **3**:187-197.
257. Kim JW, Tchernyshyov I, Semenza GL, Dang CV: **HIF-1-mediated expression of pyruvate dehydrogenase kinase: a metabolic switch required for cellular adaptation to hypoxia**. *Cell Metab* 2006, **3**:177-185.
258. Semenza GL, Jiang BH, Leung SW, Passantino R, Concordet JP, Maire P, Giallongo A: **Hypoxia response elements in the aldolase A, enolase 1, and lactate dehydrogenase A gene promoters contain essential binding sites for hypoxia-inducible factor 1**. *J Biol Chem* 1996, **271**:32529-32537.
259. Wong N, De Melo J, Tang D: **PKM2, a Central Point of Regulation in Cancer Metabolism**. *Int J Cell Biol* 2013, **2013**:242513.
260. Yang W, Lu Z: **Nuclear PKM2 regulates the Warburg effect**. *Cell Cycle* 2013, **12**:3154-3158.
261. Chen M, David CJ, Manley JL: **Concentration-dependent control of pyruvate kinase M mutually exclusive splicing by hnRNP proteins**. *Nat Struct Mol Biol* 2012, **19**:346-354.
262. Infantino V, Convertini P, Cucci L, Panaro MA, Di Noia MA, Calvello R, Palmieri F, Iacobazzi V: **The mitochondrial citrate carrier: a new player in inflammation**. *Biochem J* 2011, **438**:433-436.

263. Qualls JE, Subramanian C, Rafi W, Smith AM, Balouzian L, DeFreitas AA, Shirey KA, Reutterer B, Kernbauer E, Stockinger S, et al.: **Sustained generation of nitric oxide and control of mycobacterial infection requires argininosuccinate synthase 1**. *Cell Host Microbe* 2012, **12**:313-323.
264. Haschemi A, Kosma P, Gille L, Evans CR, Burant CF, Starkl P, Knapp B, Haas R, Schmid JA, Jandl C, et al.: **The sedoheptulose kinase CARKL directs macrophage polarization through control of glucose metabolism**. *Cell Metab* 2012, **15**:813-826.
265. Brown GC: **Nitric oxide and mitochondrial respiration**. *Biochim Biophys Acta* 1999, **1411**:351-369.
266. Beltrán B, Mathur A, Duchen MR, Erusalimsky JD, Moncada S: **The effect of nitric oxide on cell respiration: A key to understanding its role in cell survival or death**. *Proc Natl Acad Sci U S A* 2000, **97**:14602-14607.
267. Garedew A, Henderson SO, Moncada S: **Activated macrophages utilize glycolytic ATP to maintain mitochondrial membrane potential and prevent apoptotic cell death**. *Cell Death Differ* 2012.
268. Garedew A, Henderson SO, Moncada S: **Activated macrophages utilize glycolytic ATP to maintain mitochondrial membrane potential and prevent apoptotic cell death**. *Cell Death Differ* 2010, **17**:1540-1550.
269. Mills EL, Kelly B, Logan A, Costa AS, Varma M, Bryant CE, Tourlomousis P, Däbritz JH, Gottlieb E, Latorre I, et al.: **Succinate Dehydrogenase Supports Metabolic Repurposing of Mitochondria to Drive Inflammatory Macrophages**. *Cell* 2016, **167**:457-470.e413.
270. Byles V, Covarrubias AJ, Ben-Sahra I, Lamming DW, Sabatini DM, Manning BD, Horng T: **The TSC-mTOR pathway regulates macrophage polarization**. *Nat Commun* 2013, **4**:2834.
271. Takeda N, O'Dea EL, Doedens A, Kim JW, Weidemann A, Stockmann C, Asagiri M, Simon MC, Hoffmann A, Johnson RS: **Differential activation and antagonistic function of HIF-{alpha} isoforms in macrophages are essential for NO homeostasis**. *Genes Dev* 2010, **24**:491-501.
272. Sag D, Carling D, Stout RD, Suttles J: **Adenosine 5'-monophosphate-activated protein kinase promotes macrophage polarization to an anti-inflammatory functional phenotype**. *J Immunol* 2008, **181**:8633-8641.
273. Winder WW, Holmes BF, Rubink DS, Jensen EB, Chen M, Holloszy JO: **Activation of AMP-activated protein kinase increases mitochondrial enzymes in skeletal muscle**. *J Appl Physiol (1985)* 2000, **88**:2219-2226.
274. Odegaard JI, Ricardo-Gonzalez RR, Goforth MH, Morel CR, Subramanian V, Mukundan L, Red Eagle A, Vats D, Brombacher F, Ferrante AW, et al.: **Macrophage-specific PPARgamma controls alternative activation and improves insulin resistance**. *Nature* 2007, **447**:1116-1120.
275. Szanto A, Balint BL, Nagy ZS, Barta E, Dezso B, Pap A, Szeles L, Poliska S, Oros M, Evans RM, et al.: **STAT6 transcription factor is a facilitator of the nuclear receptor PPARγ-regulated gene expression in macrophages and dendritic cells**. *Immunity* 2010, **33**:699-712.
276. Brunmair B, Staniek K, Dörig J, Szöcs Z, Stadlbauer K, Marian V, Gras F, Anderwald C, Nohl H, Waldhäusl W, et al.: **Activation of PPAR-delta in isolated rat skeletal muscle switches fuel preference from glucose to fatty acids**. *Diabetologia* 2006, **49**:2713-2722.
277. Lorsbach RB, Murphy WJ, Lowenstein CJ, Snyder SH, Russell SW: **Expression of the nitric oxide synthase gene in mouse macrophages activated for tumor cell killing. Molecular basis for the synergy between interferon-gamma and lipopolysaccharide**. *J Biol Chem* 1993, **268**:1908-1913.
278. Selak MA, Armour SM, MacKenzie ED, Boulahbel H, Watson DG, Mansfield KD, Pan Y, Simon MC, Thompson CB, Gottlieb E: **Succinate links TCA cycle dysfunction to oncogenesis by inhibiting HIF-alpha prolyl hydroxylase**. *Cancer Cell* 2005, **7**:77-85.
279. Koivunen P, Hirsilä M, Remes AM, Hassinen IE, Kivirikko KI, Myllyharju J: **Inhibition of hypoxia-inducible factor (HIF) hydroxylases by citric acid cycle intermediates: possible links between cell metabolism and stabilization of HIF**. *J Biol Chem* 2007, **282**:4524-4532.

280. Porporato PE, Dhup S, Dadhich RK, Copetti T, Sonveaux P: **Anticancer targets in the glycolytic metabolism of tumors: a comprehensive review**. *Front Pharmacol* 2011, **2**:49.
281. Lee JW, Bae SH, Jeong JW, Kim SH, Kim KW: **Hypoxia-inducible factor (HIF-1)alpha: its protein stability and biological functions**. *Exp Mol Med* 2004, **36**:1-12.
282. Blouin CC, Pagé EL, Soucy GM, Richard DE: **Hypoxic gene activation by lipopolysaccharide in macrophages: implication of hypoxia-inducible factor 1alpha**. *Blood* 2004, **103**:1124-1130.
283. Ramanathan M, Luo W, Csóka B, Haskó G, Lukashev D, Sitkovsky MV, Leibovich SJ: **Differential regulation of HIF-1alpha isoforms in murine macrophages by TLR4 and adenosine A(2A) receptor agonists**. *J Leukoc Biol* 2009, **86**:681-689.
284. Anand RJ, Gribar SC, Li J, Kohler JW, Branca MF, Dubowski T, Sodhi CP, Hackam DJ: **Hypoxia causes an increase in phagocytosis by macrophages in a HIF-1alpha-dependent manner**. *J Leukoc Biol* 2007, **82**:1257-1265.
285. Zhou J, Dehne N, Brüne B: **Nitric oxide causes macrophage migration via the HIF-1-stimulated small GTPases Cdc42 and Rac1**. *Free Radic Biol Med* 2009, **47**:741-749.
286. Kuhlicke J, Frick JS, Morote-Garcia JC, Rosenberger P, Eltzschig HK: **Hypoxia inducible factor (HIF)-1 coordinates induction of Toll-like receptors TLR2 and TLR6 during hypoxia**. *PLoS One* 2007, **2**:e1364.
287. Kim SY, Choi YJ, Joung SM, Lee BH, Jung YS, Lee JY: **Hypoxic stress up-regulates the expression of Toll-like receptor 4 in macrophages via hypoxia-inducible factor**. *Immunology* 2010, **129**:516-524.
288. Cramer T, Yamanishi Y, Clausen BE, Förster I, Pawlinski R, Mackman N, Haase VH, Jaenisch R, Corr M, Nizet V, et al.: **HIF-1alpha is essential for myeloid cell-mediated inflammation**. *Cell* 2003, **112**:645-657.
289. Cardoso MS, Silva TM, Resende M, Appelberg R, Borges M: **Lack of the Transcription Factor Hypoxia-Inducible Factor 1α (HIF-1α) in Macrophages Accelerates the Necrosis of Mycobacterium avium-Induced Granulomas**. *Infect Immun* 2015, **83**:3534-3544.
290. Elks PM, Brizee S, van der Vaart M, Walmsley SR, van Eeden FJ, Renshaw SA, Meijer AH: **Hypoxia inducible factor signaling modulates susceptibility to mycobacterial infection via a nitric oxide dependent mechanism**. *PLoS Pathog* 2013, **9**:e1003789.
291. Zhou R, Yazdi AS, Menu P, Tschopp J: **A role for mitochondria in NLRP3 inflammasome activation**. *Nature* 2011, **469**:221-225.
292. Nakahira K, Haspel JA, Rathinam VA, Lee SJ, Dolinay T, Lam HC, Englert JA, Rabinovitch M, Cernadas M, Kim HP, et al.: **Autophagy proteins regulate innate immune responses by inhibiting the release of mitochondrial DNA mediated by the NALP3 inflammasome**. *Nat Immunol* 2011, **12**:222-230.
293. Murphy MP: **How mitochondria produce reactive oxygen species**. *Biochem J* 2009, **417**:1-13.
294. Lambert AJ, Brand MD: **Superoxide production by NADH:ubiquinone oxidoreductase (complex I) depends on the pH gradient across the mitochondrial inner membrane**. *Biochem J* 2004, **382**:511-517.
295. Muller FL, Liu Y, Abdul-Ghani MA, Lustgarten MS, Bhattacharya A, Jang YC, Van Remmen H: **High rates of superoxide production in skeletal-muscle mitochondria respiring on both complex I- and complex II-linked substrates**. *Biochem J* 2008, **409**:491-499.
296. Chouchani ET, Pell VR, Gaude E, Aksentijević D, Sundier SY, Robb EL, Logan A, Nadtochiy SM, Ord EN, Smith AC, et al.: **Ischaemic accumulation of succinate controls reperfusion injury through mitochondrial ROS**. *Nature* 2014, **515**:431-435.
297. Kelly B, Tannahill GM, Murphy MP, O'Neill LA: **Metformin Inhibits the Production of Reactive Oxygen Species from NADH:Ubiquinone Oxidoreductase to Limit Induction of Interleukin-1β (IL-1β) and Boosts Interleukin-10 (IL-10) in Lipopolysaccharide (LPS)-activated Macrophages**. *J Biol Chem* 2015, **290**:20348-20359.
298. Chandel NS, McClintock DS, Feliciano CE, Wood TM, Melendez JA, Rodriguez AM, Schumacker PT: **Reactive oxygen species generated at mitochondrial complex III**

stabilize hypoxia-inducible factor-1alpha during hypoxia: a mechanism of O2 sensing. *J Biol Chem* 2000, **275**:25130-25138.
299. Bulua AC, Simon A, Maddipati R, Pelletier M, Park H, Kim KY, Sack MN, Kastner DL, Siegel RM: **Mitochondrial reactive oxygen species promote production of proinflammatory cytokines and are elevated in TNFR1-associated periodic syndrome (TRAPS)**. *J Exp Med* 2011, **208**:519-533.
300. West AP, Brodsky IE, Rahner C, Woo DK, Erdjument-Bromage H, Tempst P, Walsh MC, Choi Y, Shadel GS, Ghosh S: **TLR signalling augments macrophage bactericidal activity through mitochondrial ROS**. *Nature* 2011, **472**:476-480.
301. Dennis EA, Norris PC: **Eicosanoid storm in infection and inflammation**. *Nat Rev Immunol* 2015, **15**:511-523.
302. Segal BH, Grimm MJ, Khan AN, Han W, Blackwell TS: **Regulation of innate immunity by NADPH oxidase**. *Free Radic Biol Med* 2012, **53**:72-80.
303. O'Neill LA: **A critical role for citrate metabolism in LPS signalling**. *Biochem J* 2011, **438**:e5-6.
304. Michelucci A, Cordes T, Ghelfi J, Pailot A, Reiling N, Goldmann O, Binz T, Wegner A, Tallam A, Rausell A, et al.: **Immune-responsive gene 1 protein links metabolism to immunity by catalyzing itaconic acid production**. *Proc Natl Acad Sci U S A* 2013, **110**:7820-7825.
305. Strelko CL, Lu W, Dufort FJ, Seyfried TN, Chiles TC, Rabinowitz JD, Roberts MF: **Itaconic acid is a mammalian metabolite induced during macrophage activation**. *J Am Chem Soc* 2011, **133**:16386-16389.
306. Tangsudjai S, Pudla M, Limposuwan K, Woods DE, Sirisinha S, Utaisincharoen P: **Involvement of the MyD88-independent pathway in controlling the intracellular fate of Burkholderia pseudomallei infection in the mouse macrophage cell line RAW 264.7**. *Microbiol Immunol* 2010, **54**:282-290.
307. Degrandi D, Hoffmann R, Beuter-Gunia C, Pfeffer K: **The proinflammatory cytokine-induced IRG1 protein associates with mitochondria**. *J Interferon Cytokine Res* 2009, **29**:55-67.
308. Basler T, Jeckstadt S, Valentin-Weigand P, Goethe R: **Mycobacterium paratuberculosis, Mycobacterium smegmatis, and lipopolysaccharide induce different transcriptional and post-transcriptional regulation of the IRG1 gene in murine macrophages**. *J Leukoc Biol* 2006, **79**:628-638.
309. McFadden BA, Purohit S: **Itaconate, an isocitrate lyase-directed inhibitor in Pseudomonas indigofera**. *J Bacteriol* 1977, **131**:136-144.
310. Patel TR, McFadden BA: **Caenorhabditis elegans and Ascaris suum: inhibition of isocitrate lyase by itaconate**. *Exp Parasitol* 1978, **44**:262-268.
311. Carroll KC, Viollet B, Suttles J: **AMPKα1 deficiency amplifies proinflammatory myeloid APC activity and CD40 signaling**. *J Leukoc Biol* 2013, **94**:1113-1121.
312. Yang CS, Kim JJ, Lee HM, Jin HS, Lee SH, Park JH, Kim SJ, Kim JM, Han YM, Lee MS, et al.: **The AMPK-PPARGC1A pathway is required for antimicrobial host defense through activation of autophagy**. *Autophagy* 2014, **10**:785-802.
313. Eisele NA, Ruby T, Jacobson A, Manzanillo PS, Cox JS, Lam L, Mukundan L, Chawla A, Monack DM: **Salmonella require the fatty acid regulator PPARδ for the establishment of a metabolic environment essential for long-term persistence**. *Cell Host Microbe* 2013, **14**:171-182.
314. Deretic V, Levine B: **Autophagy, immunity, and microbial adaptations**. *Cell Host Microbe* 2009, **5**:527-549.
315. Kim J, Kundu M, Viollet B, Guan KL: **AMPK and mTOR regulate autophagy through direct phosphorylation of Ulk1**. *Nat Cell Biol* 2011, **13**:132-141.
316. Roberts DJ, Tan-Sah VP, Ding EY, Smith JM, Miyamoto S: **Hexokinase-II positively regulates glucose starvation-induced autophagy through TORC1 inhibition**. *Mol Cell* 2014, **53**:521-533.
317. Roberts DJ, Miyamoto S: **Hexokinase II integrates energy metabolism and cellular protection: Akting on mitochondria and TORCing to autophagy**. *Cell Death Differ* 2015, **22**:364.

318. Bellot G, Garcia-Medina R, Gounon P, Chiche J, Roux D, Pouysségur J, Mazure NM: **Hypoxia-induced autophagy is mediated through hypoxia-inducible factor induction of BNIP3 and BNIP3L via their BH3 domains**. *Mol Cell Biol* 2009, **29**:2570-2581.
319. Bohensky J, Shapiro IM, Leshinsky S, Terkhorn SP, Adams CS, Srinivas V: **HIF-1 regulation of chondrocyte apoptosis: induction of the autophagic pathway**. *Autophagy* 2007, **3**:207-214.
320. Zhou J, Zhang W, Liang B, Casimiro MC, Whitaker-Menezes D, Wang M, Lisanti MP, Lanza-Jacoby S, Pestell RG, Wang C: **PPARgamma activation induces autophagy in breast cancer cells**. *Int J Biochem Cell Biol* 2009, **41**:2334-2342.
321. Marsin AS, Bouzin C, Bertrand L, Hue L: **The stimulation of glycolysis by hypoxia in activated monocytes is mediated by AMP-activated protein kinase and inducible 6-phosphofructo-2-kinase**. *J Biol Chem* 2002, **277**:30778-30783.
322. Wu SB, Wei YH: **AMPK-mediated increase of glycolysis as an adaptive response to oxidative stress in human cells: implication of the cell survival in mitochondrial diseases**. *Biochim Biophys Acta* 2012, **1822**:233-247.
323. Hesse M, Modolell M, La Flamme AC, Schito M, Fuentes JM, Cheever AW, Pearce EJ, Wynn TA: **Differential regulation of nitric oxide synthase-2 and arginase-1 by type 1/type 2 cytokines in vivo: granulomatous pathology is shaped by the pattern of L-arginine metabolism**. *J Immunol* 2001, **167**:6533-6544.
324. Hesse M, Cheever AW, Jankovic D, Wynn TA: **NOS-2 mediates the protective anti-inflammatory and antifibrotic effects of the Th1-inducing adjuvant, IL-12, in a Th2 model of granulomatous disease**. *Am J Pathol* 2000, **157**:945-955.
325. Duque-Correa MA, Kühl AA, Rodriguez PC, Zedler U, Schommer-Leitner S, Rao M, Weiner J, Hurwitz R, Qualls JE, Kosmiadi GA, et al.: **Macrophage arginase-1 controls bacterial growth and pathology in hypoxic tuberculosis granulomas**. *Proc Natl Acad Sci U S A* 2014, **111**:E4024-4032.
326. Jantsch J, Chakravortty D, Turza N, Prechtel AT, Buchholz B, Gerlach RG, Volke M, Gläsner J, Warnecke C, Wiesener MS, et al.: **Hypoxia and hypoxia-inducible factor-1 alpha modulate lipopolysaccharide-induced dendritic cell activation and function**. *J Immunol* 2008, **180**:4697-4705.
327. Bhandari T, Olson J, Johnson RS, Nizet V: **HIF-1α influences myeloid cell antigen presentation and response to subcutaneous OVA vaccination**. *J Mol Med (Berl)* 2013, **91**:1199-1205.
328. Shin JH, Yang JY, Jeon BY, Yoon YJ, Cho SN, Kang YH, Ryu DH, Hwang GS: **(1)H NMR-based metabolomic profiling in mice infected with Mycobacterium tuberculosis**. *J Proteome Res* 2011, **10**:2238-2247.
329. Somashekar BS, Amin AG, Rithner CD, Troudt J, Basaraba R, Izzo A, Crick DC, Chatterjee D: **Metabolic profiling of lung granuloma in Mycobacterium tuberculosis infected guinea pigs: ex vivo 1H magic angle spinning NMR studies**. *J Proteome Res* 2011, **10**:4186-4195.
330. Somashekar BS, Amin AG, Tripathi P, MacKinnon N, Rithner CD, Shanley CA, Basaraba R, Henao-Tamayo M, Kato-Maeda M, Ramamoorthy A, et al.: **Metabolomic signatures in guinea pigs infected with epidemic-associated W-Beijing strains of Mycobacterium tuberculosis**. *J Proteome Res* 2012, **11**:4873-4884.
331. Chen Y, Wu J, Tu L, Xiong X, Hu X, Huang J, Xu Z, Zhang X, Hu C, Guo A, et al.: **(1)H-NMR spectroscopy revealed Mycobacterium tuberculosis caused abnormal serum metabolic profile of cattle**. *PLoS One* 2013, **8**:e74507.
332. Zhou A, Ni J, Xu Z, Wang Y, Lu S, Sha W, Karakousis PC, Yao YF: **Application of (1)h NMR spectroscopy-based metabolomics to sera of tuberculosis patients**. *J Proteome Res* 2013, **12**:4642-4649.
333. Zhou A, Ni J, Xu Z, Wang Y, Zhang H, Wu W, Lu S, Karakousis PC, Yao YF: **Metabolomics specificity of tuberculosis plasma revealed by (1)H NMR spectroscopy**. *Tuberculosis (Edinb)* 2015, **95**:294-302.

334. Shi L, Salamon H, Eugenin EA, Pine R, Cooper A, Gennaro ML: **Infection with Mycobacterium tuberculosis induces the Warburg effect in mouse lungs**. *Sci Rep* 2015, **5**:18176.
335. Lachmandas E, Beigier-Bompadre M, Cheng SC, Kumar V, van Laarhoven A, Wang X, Ammerdorffer A, Boutens L, de Jong D, Kanneganti TD, et al.: **Rewiring cellular metabolism via the AKT/mTOR pathway contributes to host defence against Mycobacterium tuberculosis in human and murine cells**. *Eur J Immunol* 2016, **46**:2574-2586.
336. Bhargava A, Khare NK, Bunkar N, Lenka RK, Mishra PK: **Role of mitochondrial oxidative stress on lymphocyte homeostasis in patients diagnosed with extra-pulmonary tuberculosis**. *Cell Biol Int* 2016, **40**:166-176.
337. Moreno-Altamirano MM, Paredes-González IS, Espitia C, Santiago-Maldonado M, Hernández-Pando R, Sánchez-García FJ: **Bioinformatic identification of Mycobacterium tuberculosis proteins likely to target host cell mitochondria: virulence factors?** *Microb Inform Exp* 2012, **2**:9.
338. Jamwal S, Midha MK, Verma HN, Basu A, Rao KV, Manivel V: **Characterizing virulence-specific perturbations in the mitochondrial function of macrophages infected with Mycobacterium tuberculosis**. *Sci Rep* 2013, **3**:1328.
339. Young F, Wotton CJ, Critchley JA, Unwin NC, Goldacre MJ: **Increased risk of tuberculosis disease in people with diabetes mellitus: record-linkage study in a UK population**. *J Epidemiol Community Health* 2012, **66**:519-523.
340. Pérez A, Brown HS, Restrepo BI: **Association between tuberculosis and diabetes in the Mexican border and non-border regions of Texas**. *Am J Trop Med Hyg* 2006, **74**:604-611.
341. Dobler CC, Flack JR, Marks GB: **Risk of tuberculosis among people with diabetes mellitus: an Australian nationwide cohort study**. *BMJ Open* 2012, **2**:e000666.
342. Leung CC, Lam TH, Chan WM, Yew WW, Ho KS, Leung GM, Law WS, Tam CM, Chan CK, Chang KC: **Diabetic control and risk of tuberculosis: a cohort study**. *Am J Epidemiol* 2008, **167**:1486-1494.
343. Restrepo BI, Camerlin AJ, Rahbar MH, Wang W, Restrepo MA, Zarate I, Mora-Guzmán F, Crespo-Solis JG, Briggs J, McCormick JB, et al.: **Cross-sectional assessment reveals high diabetes prevalence among newly-diagnosed tuberculosis cases**. *Bull World Health Organ* 2011, **89**:352-359.
344. Shen TC, Lin CL, Wei CC, Liao WC, Chen WC, Chen CH, Tu CY, Hsia TC, Shih CM, Hsu WH, et al.: **Increased risk of tuberculosis in patients with type 1 diabetes mellitus: results from a population-based cohort study in Taiwan**. *Medicine (Baltimore)* 2014, **93**:e96.
345. Liang CP, Han S, Senokuchi T, Tall AR: **The macrophage at the crossroads of insulin resistance and atherosclerosis**. *Circ Res* 2007, **100**:1546-1555.
346. DeFronzo RA, Ferrannini E, Simonson DC: **Fasting hyperglycemia in non-insulin-dependent diabetes mellitus: contributions of excessive hepatic glucose production and impaired tissue glucose uptake**. *Metabolism* 1989, **38**:387-395.
347. Rosa LF, Cury Y, Curi R: **Effects of insulin, glucocorticoids and thyroid hormones on the activities of key enzymes of glycolysis, glutaminolysis, the pentose-phosphate pathway and the Krebs cycle in rat macrophages**. *J Endocrinol* 1992, **135**:213-219.
348. Hodgson K, Morris J, Bridson T, Govan B, Rush C, Ketheesan N: **Immunological mechanisms contributing to the double burden of diabetes and intracellular bacterial infections**. *Immunology* 2015, **144**:171-185.
349. Vallerskog T, Martens GW, Kornfeld H: **Diabetic mice display a delayed adaptive immune response to Mycobacterium tuberculosis**. *J Immunol* 2010, **184**:6275-6282.
350. Liu HF, Zhang HJ, Hu QX, Liu XY, Wang ZQ, Fan JY, Zhan M, Chen FL: **Altered polarization, morphology, and impaired innate immunity germane to resident peritoneal macrophages in mice with long-term type 2 diabetes**. *J Biomed Biotechnol* 2012, **2012**:867023.

351. Yamasawa H, Nakayama M, Bando M, Sugiyama Y: **Impaired inflammatory responses to multiple toll-like receptor ligands in alveolar macrophages of streptozotocin-induced diabetic mice**. *Inflamm Res* 2012, **61**:417-426.
352. Sun C, Sun L, Ma H, Peng J, Zhen Y, Duan K, Liu G, Ding W, Zhao Y: **The phenotype and functional alterations of macrophages in mice with hyperglycemia for long term**. *J Cell Physiol* 2012, **227**:1670-1679.
353. Singhal A, Jie L, Kumar P, Hong GS, Leow MK, Paleja B, Tsenova L, Kurepina N, Chen J, Zolezzi F, et al.: **Metformin as adjunct antituberculosis therapy**. *Sci Transl Med* 2014, **6**:263ra159.
354. Ilyas R, Wallis R, Soilleux EJ, Townsend P, Zehnder D, Tan BK, Sim RB, Lehnert H, Randeva HS, Mitchell DA: **High glucose disrupts oligosaccharide recognition function via competitive inhibition: a potential mechanism for immune dysregulation in diabetes mellitus**. *Immunobiology* 2011, **216**:126-131.
355. Lachmandas E, Vrieling F, Wilson LG, Joosten SA, Netea MG, Ottenhoff TH, van Crevel R: **The effect of hyperglycaemia on in vitro cytokine production and macrophage infection with Mycobacterium tuberculosis**. *PLoS One* 2015, **10**:e0117941.
356. Mehrotra P, Jamwal SV, Saquib N, Sinha N, Siddiqui Z, Manivel V, Chatterjee S, Rao KV: **Pathogenicity of Mycobacterium tuberculosis is expressed by regulating metabolic thresholds of the host macrophage**. *PLoS Pathog* 2014, **10**:e1004265.
357. Eriksen M, Mackay J, Schluger N, Gomeshtapeh IF, Drope J: *The Tobacco Atlas, Fifth Edition* edn 5th Edition: American Cancer Society; 2015.
358. Pai M, Mohan A, Dheda K, Leung CC, Yew WW, Christopher DJ, Sharma SK: **Lethal interaction: the colliding epidemics of tobacco and tuberculosis**. *Expert Rev Anti Infect Ther* 2007, **5**:385-391.
359. van Zyl Smit RN, Pai M, Yew WW, Leung CC, Zumla A, Bateman ED, Dheda K: **Global lung health: the colliding epidemics of tuberculosis, tobacco smoking, HIV and COPD**. *Eur Respir J* 2010, **35**:27-33.
360. van Zyl-Smit RN, Brunet L, Pai M, Yew WW: **The convergence of the global smoking, COPD, tuberculosis, HIV, and respiratory infection epidemics**. *Infect Dis Clin North Am* 2010, **24**:693-703.
361. Slama K, Chiang CY, Enarson DA, Hassmiller K, Fanning A, Gupta P, Ray C: **Tobacco and tuberculosis: a qualitative systematic review and meta-analysis**. *Int J Tuberc Lung Dis* 2007, **11**:1049-1061.
362. Lin HH, Ezzati M, Murray M: **Tobacco smoke, indoor air pollution and tuberculosis: a systematic review and meta-analysis**. *PLoS Med* 2007, **4**:e20.
363. Bates MN, Khalakdina A, Pai M, Chang L, Lessa F, Smith KR: **Risk of tuberculosis from exposure to tobacco smoke: a systematic review and meta-analysis**. *Arch Intern Med* 2007, **167**:335-342.
364. Yen YF, Yen MY, Lin YS, Lin YP, Shih HC, Li LH, Chou P, Deng CY: **Smoking increases risk of recurrence after successful anti-tuberculosis treatment: a population-based study**. *Int J Tuberc Lung Dis* 2014, **18**:492-498.
365. d'Arc Lyra Batista J, de Fátima Pessoa Militão de Albuquerque M, de Alencar Ximenes RA, Rodrigues LC: **Smoking increases the risk of relapse after successful tuberculosis treatment**. *Int J Epidemiol* 2008, **37**:841-851.
366. Nijenbandring de Boer R, Oliveira e Souza Filho JB, Cobelens F, Ramalho DeP, Campino Miranda PF, Logo K, Oliveira H, Mesquita E, Oliveira MM, Kritski A: **Delayed culture conversion due to cigarette smoking in active pulmonary tuberculosis patients**. *Tuberculosis (Edinb)* 2014, **94**:87-91.
367. Siddiqui UA, O'Toole M, Kabir Z, Qureshi S, Gibbons N, Kane M, Keane J: **Smoking prolongs the infectivity of patients with tuberculosis**. *Ir Med J* 2010, **103**:278-280.
368. Jain K, Desai M, Solanki R, Dikshit RK: **Treatment outcome of standardized regimen in patients with multidrug resistant tuberculosis**. *J Pharmacol Pharmacother* 2014, **5**:145-149.

369. Smith CJ, Hansch C: **The relative toxicity of compounds in mainstream cigarette smoke condensate**. *Food Chem Toxicol* 2000, **38**:637-646.
370. Stämpfli MR, Anderson GP: **How cigarette smoke skews immune responses to promote infection, lung disease and cancer**. *Nat Rev Immunol* 2009, **9**:377-384.
371. Holt PG, Keast D: **Environmentally induced changes in immunological function: acute and chronic effects of inhalation of tobacco smoke and other atmospheric contaminants in man and experimental animals**. *Bacteriol Rev* 1977, **41**:205-216.
372. Holt PG: **Immune and inflammatory function in cigarette smokers**. *Thorax* 1987, **42**:241-249.
373. Sopori M: **Effects of cigarette smoke on the immune system**. *Nat Rev Immunol* 2002, **2**:372-377.
374. Mehta H, Nazzal K, Sadikot RT: **Cigarette smoking and innate immunity**. *Inflamm Res* 2008, **57**:497-503.
375. Rogers DF, Turner NC, Marriott C, Jeffery PK: **Cigarette smoke-induced 'chronic bronchitis': a study in situ of laryngo-tracheal hypersecretion in the rat**. *Clin Sci (Lond)* 1987, **72**:629-637.
376. Hümmer B, Purnama I, Hahn HL: **Stimulation of submucosal glands by nicotine applied locally to the airway mucosa**. *Klin Wochenschr* 1988, **66 Suppl 11**:161-169.
377. Hobson J, Wright J, Churg A: **Histochemical evidence for generation of active oxygen species on the apical surface of cigarette-smoke-exposed tracheal explants**. *Am J Pathol* 1991, **139**:573-580.
378. Elliott MK, Sisson JH, Wyatt TA: **Effects of cigarette smoke and alcohol on ciliated tracheal epithelium and inflammatory cell recruitment**. *Am J Respir Cell Mol Biol* 2007, **36**:452-459.
379. Sisson JH, Tuma DJ, Rennard SI: **Acetaldehyde-mediated cilia dysfunction in bovine bronchial epithelial cells**. *Am J Physiol* 1991, **260**:L29-36.
380. Agnew JE, Lopez-Vidriero MT, Pavia D, Clarke SW: **Functional small airways defence in symptomless cigarette smokers**. *Thorax* 1986, **41**:524-530.
381. Agnew JE, Pavia D, Clarke SW: **Mucus clearance from peripheral and central airways of asymptomatic cigarette smokers**. *Bull Eur Physiopathol Respir* 1986, **22**:263-267.
382. Mio T, Romberger DJ, Thompson AB, Robbins RA, Heires A, Rennard SI: **Cigarette smoke induces interleukin-8 release from human bronchial epithelial cells**. *Am J Respir Crit Care Med* 1997, **155**:1770-1776.
383. Barnes PJ: **Alveolar macrophages in chronic obstructive pulmonary disease (COPD)**. *Cell Mol Biol (Noisy-le-grand)* 2004, **50 Online Pub**:OL627-637.
384. Lee KM, Renne RA, Harbo SJ, Clark ML, Johnson RE, Gideon KM: **3-week inhalation exposure to cigarette smoke and/or lipopolysaccharide in AKR/J mice**. *Inhal Toxicol* 2007, **19**:23-35.
385. Martin RJ, Wexler RB, Day BJ, Harbeck RJ, Pinkerton KE, Chu HW: **Interaction between cigarette smoke and mycoplasma infection: a murine model**. *COPD* 2006, **3**:3-8.
386. Stringer KA, Tobias M, O'Neill HC, Franklin CC: **Cigarette smoke extract-induced suppression of caspase-3-like activity impairs human neutrophil phagocytosis**. *Am J Physiol Lung Cell Mol Physiol* 2007, **292**:L1572-1579.
387. Zappacosta B, Persichilli S, Minucci A, Stasio ED, Carlino P, Pagliari G, Giardina B, Sole PD: **Effect of aqueous cigarette smoke extract on the chemiluminescence kinetics of polymorphonuclear leukocytes and on their glycolytic and phagocytic activity**. *Luminescence* 2001, **16**:315-319.
388. Sköld CM, Forslid J, Eklund A, Hed J: **Metabolic activity in human alveolar macrophages increases after cessation of smoking**. *Inflammation* 1993, **17**:345-352.
389. Kirkham PA, Spooner G, Rahman I, Rossi AG: **Macrophage phagocytosis of apoptotic neutrophils is compromised by matrix proteins modified by cigarette smoke and lipid peroxidation products**. *Biochem Biophys Res Commun* 2004, **318**:32-37.

390. Hodge S, Hodge G, Scicchitano R, Reynolds PN, Holmes M: **Alveolar macrophages from subjects with chronic obstructive pulmonary disease are deficient in their ability to phagocytose apoptotic airway epithelial cells**. *Immunol Cell Biol* 2003, **81**:289-296.
391. Ortega E, Barriga C, Rodríguez AB: **Decline in the phagocytic function of alveolar macrophages from mice exposed to cigarette smoke**. *Comp Immunol Microbiol Infect Dis* 1994, **17**:77-84.
392. Harris JO, Gonzalez-Rothi RJ: **Abnormal phagolysosome fusion in pulmonary alveolar macrophages of rats exposed chronically to cigarette smoke**. *Am Rev Respir Dis* 1984, **130**:467-471.
393. Hodge S, Hodge G, Ahern J, Jersmann H, Holmes M, Reynolds PN: **Smoking alters alveolar macrophage recognition and phagocytic ability: implications in chronic obstructive pulmonary disease**. *Am J Respir Cell Mol Biol* 2007, **37**:748-755.
394. King TE, Savici D, Campbell PA: **Phagocytosis and killing of Listeria monocytogenes by alveolar macrophages: smokers versus nonsmokers**. *J Infect Dis* 1988, **158**:1309-1316.
395. Aoshiba K, Tamaoki J, Nagai A: **Acute cigarette smoke exposure induces apoptosis of alveolar macrophages**. *Am J Physiol Lung Cell Mol Physiol* 2001, **281**:L1392-1401.
396. Droemann D, Goldmann T, Tiedje T, Zabel P, Dalhoff K, Schaaf B: **Toll-like receptor 2 expression is decreased on alveolar macrophages in cigarette smokers and COPD patients**. *Respir Res* 2005, **6**:68.
397. Gaschler GJ, Zavitz CC, Bauer CM, Skrtic M, Lindahl M, Robbins CS, Chen B, Stämpfli MR: **Cigarette smoke exposure attenuates cytokine production by mouse alveolar macrophages**. *Am J Respir Cell Mol Biol* 2008, **38**:218-226.
398. Noda N, Matsumoto K, Fukuyama S, Asai Y, Kitajima H, Seki N, Matsunaga Y, Kan-O K, Moriwaki A, Morimoto K, et al.: **Cigarette smoke impairs phagocytosis of apoptotic neutrophils by alveolar macrophages via inhibition of the histone deacetylase/Rac/CD9 pathways**. *Int Immunol* 2013, **25**:643-650.
399. Bratke K, Klug M, Bier A, Julius P, Kuepper M, Virchow JC, Lommatzsch M: **Function-associated surface molecules on airway dendritic cells in cigarette smokers**. *Am J Respir Cell Mol Biol* 2008, **38**:655-660.
400. Yanagita M, Kobayashi R, Kojima Y, Mori K, Murakami S: **Nicotine modulates the immunological function of dendritic cells through peroxisome proliferator-activated receptor-γ upregulation**. *Cell Immunol* 2012, **274**:26-33.
401. Vassallo R, Tamada K, Lau JS, Kroening PR, Chen L: **Cigarette smoke extract suppresses human dendritic cell function leading to preferential induction of Th-2 priming**. *J Immunol* 2005, **175**:2684-2691.
402. Ekberg-Jansson A, Andersson B, Avrå E, Nilsson O, Löfdahl CG: **The expression of lymphocyte surface antigens in bronchial biopsies, bronchoalveolar lavage cells and blood cells in healthy smoking and never-smoking men, 60 years old**. *Respir Med* 2000, **94**:264-272.
403. O'Shaughnessy TC, Ansari TW, Barnes NC, Jeffery PK: **Inflammation in bronchial biopsies of subjects with chronic bronchitis: inverse relationship of CD8+ T lymphocytes with FEV1**. *Am J Respir Crit Care Med* 1997, **155**:852-857.
404. Saetta M, Di Stefano A, Turato G, Facchini FM, Corbino L, Mapp CE, Maestrelli P, Ciaccia A, Fabbri LM: **CD8+ T-lymphocytes in peripheral airways of smokers with chronic obstructive pulmonary disease**. *Am J Respir Crit Care Med* 1998, **157**:822-826.
405. Geng Y, Savage SM, Johnson LJ, Seagrave J, Sopori ML: **Effects of nicotine on the immune response. I. Chronic exposure to nicotine impairs antigen receptor-mediated signal transduction in lymphocytes**. *Toxicol Appl Pharmacol* 1995, **135**:268-278.
406. Geng Y, Savage SM, Razani-Boroujerdi S, Sopori ML: **Effects of nicotine on the immune response. II. Chronic nicotine treatment induces T cell anergy**. *J Immunol* 1996, **156**:2384-2390.
407. McCue JM, Link KL, Eaton SS, Freed BM: **Exposure to cigarette tar inhibits ribonucleotide reductase and blocks lymphocyte proliferation**. *J Immunol* 2000, **165**:6771-6775.

408. Feldman C, Anderson R: **Cigarette smoking and mechanisms of susceptibility to infections of the respiratory tract and other organ systems**. *J Infect* 2013, **67**:169-184.
409. Feng Y, Kong Y, Barnes PF, Huang FF, Klucar P, Wang X, Samten B, Sengupta M, Machona B, Donis R, et al.: **Exposure to cigarette smoke inhibits the pulmonary T-cell response to influenza virus and Mycobacterium tuberculosis**. *Infect Immun* 2011, **79**:229-237.
410. Shang S, Ordway D, Henao-Tamayo M, Bai X, Oberley-Deegan R, Shanley C, Orme IM, Case S, Minor M, Ackart D, et al.: **Cigarette smoke increases susceptibility to tuberculosis--evidence from in vivo and in vitro models**. *J Infect Dis* 2011, **203**:1240-1248.
411. O'Leary SM, Coleman MM, Chew WM, Morrow C, McLaughlin AM, Gleeson LE, O'Sullivan MP, Keane J: **Cigarette smoking impairs human pulmonary immunity to Mycobacterium tuberculosis**. *Am J Respir Crit Care Med* 2014, **190**:1430-1436.
412. van Zyl-Smit RN, Binder A, Meldau R, Semple PL, Evans A, Smith P, Bateman ED, Dheda K: **Cigarette smoke impairs cytokine responses and BCG containment in alveolar macrophages**. *Thorax* 2014, **69**:363-370.
413. Hunninghake GM, Cho MH, Tesfaigzi Y, Soto-Quiros ME, Avila L, Lasky-Su J, Stidley C, Melén E, Söderhäll C, Hallberg J, et al.: **MMP12, lung function, and COPD in high-risk populations**. *N Engl J Med* 2009, **361**:2599-2608.
414. Hautamaki RD, Kobayashi DK, Senior RM, Shapiro SD: **Requirement for macrophage elastase for cigarette smoke-induced emphysema in mice**. *Science* 1997, **277**:2002-2004.
415. Graff JW, Powers LS, Dickson AM, Kim J, Reisetter AC, Hassan IH, Kremens K, Gross TJ, Wilson ME, Monick MM: **Cigarette smoking decreases global microRNA expression in human alveolar macrophages**. *PLoS One* 2012, **7**:e44066.
416. Wallace WA, Gillooly M, Lamb D: **Intra-alveolar macrophage numbers in current smokers and non-smokers: a morphometric study of tissue sections**. *Thorax* 1992, **47**:437-440.
417. Richens TR, Linderman DJ, Horstmann SA, Lambert C, Xiao YQ, Keith RL, Boé DM, Morimoto K, Bowler RP, Day BJ, et al.: **Cigarette smoke impairs clearance of apoptotic cells through oxidant-dependent activation of RhoA**. *Am J Respir Crit Care Med* 2009, **179**:1011-1021.
418. Berg RD, Levitte S, O'Sullivan MP, O'Leary SM, Cambier CJ, Cameron J, Takaki KK, Moens CB, Tobin DM, Keane J, et al.: **Lysosomal Disorders Drive Susceptibility to Tuberculosis by Compromising Macrophage Migration**. *Cell* 2016, **165**:139-152.
419. Monick MM, Powers LS, Walters K, Lovan N, Zhang M, Gerke A, Hansdottir S, Hunninghake GW: **Identification of an autophagy defect in smokers' alveolar macrophages**. *J Immunol* 2010, **185**:5425-5435.
420. Thomas WR, Holt PG, Keast D: **Cigarette smoke and phagocyte function: effect of chronic exposure in vivo and acute exposure in vitro**. *Infect Immun* 1978, **20**:468-475.
421. Fisher GL, McNeill KL, Finch GL, Wilson FD, Golde DW: **Functional evaluation of lung macrophages from cigarette smokers and nonsmokers**. *J Reticuloendothel Soc* 1982, **32**:311-321.
422. Berenson CS, Wrona CT, Grove LJ, Maloney J, Garlipp MA, Wallace PK, Stewart CC, Sethi S: **Impaired alveolar macrophage response to Haemophilus antigens in chronic obstructive lung disease**. *Am J Respir Crit Care Med* 2006, **174**:31-40.
423. Martí-Lliteras P, Regueiro V, Morey P, Hood DW, Saus C, Sauleda J, Agustí AG, Bengoechea JA, Garmendia J: **Nontypeable Haemophilus influenzae clearance by alveolar macrophages is impaired by exposure to cigarette smoke**. *Infect Immun* 2009, **77**:4232-4242.
424. Phipps JC, Aronoff DM, Curtis JL, Goel D, O'Brien E, Mancuso P: **Cigarette smoke exposure impairs pulmonary bacterial clearance and alveolar macrophage complement-mediated phagocytosis of Streptococcus pneumoniae**. *Infect Immun* 2010, **78**:1214-1220.
425. Tomita K, Caramori G, Lim S, Ito K, Hanazawa T, Oates T, Chiselita I, Jazrawi E, Chung KF, Barnes PJ, et al.: **Increased p21(CIP1/WAF1) and B cell lymphoma leukemia-x(L) expression and reduced apoptosis in alveolar macrophages from smokers**. *Am J Respir Crit Care Med* 2002, **166**:724-731.

426. Vayssier M, Banzet N, François D, Bellmann K, Polla BS: **Tobacco smoke induces both apoptosis and necrosis in mammalian cells: differential effects of HSP70**. *Am J Physiol* 1998, **275**:L771-779.
427. Kojima J, Araya J, Hara H, Ito S, Takasaka N, Kobayashi K, Fujii S, Tsurushige C, Numata T, Ishikawa T, et al.: **Apoptosis inhibitor of macrophage (AIM) expression in alveolar macrophages in COPD**. *Respir Res* 2013, **14**:30.
428. D'Agostini F, Balansky RM, Izzotti A, Lubet RA, Kelloff GJ, De Flora S: **Modulation of apoptosis by cigarette smoke and cancer chemopreventive agents in the respiratory tract of rats**. *Carcinogenesis* 2001, **22**:375-380.
429. Kim HP, Wang X, Chen ZH, Lee SJ, Huang MH, Wang Y, Ryter SW, Choi AM: **Autophagic proteins regulate cigarette smoke-induced apoptosis: protective role of heme oxygenase-1**. *Autophagy* 2008, **4**:887-895.
430. Shaykhiev R, Krause A, Salit J, Strulovici-Barel Y, Harvey BG, O'Connor TP, Crystal RG: **Smoking-dependent reprogramming of alveolar macrophage polarization: implication for pathogenesis of chronic obstructive pulmonary disease**. *J Immunol* 2009, **183**:2867-2883.
431. Yuan F, Fu X, Shi H, Chen G, Dong P, Zhang W: **Induction of murine macrophage M2 polarization by cigarette smoke extract via the JAK2/STAT3 pathway**. *PLoS One* 2014, **9**:e107063.
432. Fu X, Shi H, Qi Y, Zhang W, Dong P: **M2 polarized macrophages induced by CSE promote proliferation, migration, and invasion of alveolar basal epithelial cells**. *Int Immunopharmacol* 2015, **28**:666-674.
433. Birrell MA, Wong S, Catley MC, Belvisi MG: **Impact of tobacco-smoke on key signaling pathways in the innate immune response in lung macrophages**. *J Cell Physiol* 2008, **214**:27-37.
434. Bozinovski S, Vlahos R, Zhang Y, Lah LC, Seow HJ, Mansell A, Anderson GP: **Carbonylation caused by cigarette smoke extract is associated with defective macrophage immunity**. *Am J Respir Cell Mol Biol* 2011, **45**:229-236.
435. Hristova M, Spiess PC, Kasahara DI, Randall MJ, Deng B, van der Vliet A: **The tobacco smoke component, acrolein, suppresses innate macrophage responses by direct alkylation of c-Jun N-terminal kinase**. *Am J Respir Cell Mol Biol* 2012, **46**:23-33.
436. Chen H, Cowan MJ, Hasday JD, Vogel SN, Medvedev AE: **Tobacco smoking inhibits expression of proinflammatory cytokines and activation of IL-1R-associated kinase, p38, and NF-kappaB in alveolar macrophages stimulated with TLR2 and TLR4 agonists**. *J Immunol* 2007, **179**:6097-6106.
437. Brown GP, Iwamoto GK, Monick MM, Hunninghake GW: **Cigarette smoking decreases interleukin 1 release by human alveolar macrophages**. *Am J Physiol* 1989, **256**:C260-264.
438. Soliman DM, Twigg HL: **Cigarette smoking decreases bioactive interleukin-6 secretion by alveolar macrophages**. *Am J Physiol* 1992, **263**:L471-478.
439. Thomassen MJ, Barna BP, Wiedemann HP, Farmer M, Ahmad M: **Human alveolar macrophage function: differences between smokers and nonsmokers**. *J Leukoc Biol* 1988, **44**:313-318.
440. Metcalfe HJ, Lea S, Hughes D, Khalaf R, Abbott-Banner K, Singh D: **Effects of cigarette smoke on Toll-like receptor (TLR) activation of chronic obstructive pulmonary disease (COPD) macrophages**. *Clin Exp Immunol* 2014, **176**:461-472.
441. Ouyang Y, Virasch N, Hao P, Aubrey MT, Mukerjee N, Bierer BE, Freed BM: **Suppression of human IL-1beta, IL-2, IFN-gamma, and TNF-alpha production by cigarette smoke extracts**. *J Allergy Clin Immunol* 2000, **106**:280-287.
442. Hagiwara E, Takahashi KI, Okubo T, Ohno S, Ueda A, Aoki A, Odagiri S, Ishigatsubo Y: **Cigarette smoking depletes cells spontaneously secreting Th(1) cytokines in the human airway**. *Cytokine* 2001, **14**:121-126.

443. Sköld CM, Lundahl J, Halldén G, Hallgren M, Eklund A: **Chronic smoke exposure alters the phenotype pattern and the metabolic response in human alveolar macrophages**. *Clin Exp Immunol* 1996, **106**:108-113.
444. Matsunaga K, Klein TW, Friedman H, Yamamoto Y: **Involvement of nicotinic acetylcholine receptors in suppression of antimicrobial activity and cytokine responses of alveolar macrophages to Legionella pneumophila infection by nicotine**. *J Immunol* 2001, **167**:6518-6524.
445. Gaschler GJ, Skrtic M, Zavitz CC, Lindahl M, Onnervik PO, Murphy TF, Sethi S, Stämpfli MR: **Bacteria challenge in smoke-exposed mice exacerbates inflammation and skews the inflammatory profile**. *Am J Respir Crit Care Med* 2009, **179**:666-675.
446. Gairola C, Aleem MI: **Cigarette smoke: effect of aqueous and nonaqueous fractions on mitochondrial function**. *Nature* 1973, **241**:287-288.
447. Kennedy JR, Elliott AM: **Cigarette smoke: the effect of residue on mitochondrial structure**. *Science* 1970, **168**:1097-1098.
448. Miró O, Alonso JR, Jarreta D, Casademont J, Urbano-Márquez A, Cardellach F: **Smoking disturbs mitochondrial respiratory chain function and enhances lipid peroxidation on human circulating lymphocytes**. *Carcinogenesis* 1999, **20**:1331-1336.
449. van der Toorn M, Slebos DJ, de Bruin HG, Leuvenink HG, Bakker SJ, Gans RO, Koëter GH, van Oosterhout AJ, Kauffman HF: **Cigarette smoke-induced blockade of the mitochondrial respiratory chain switches lung epithelial cell apoptosis into necrosis**. *Am J Physiol Lung Cell Mol Physiol* 2007, **292**:L1211-1218.
450. Aravamudan B, Kiel A, Freeman M, Delmotte P, Thompson M, Vassallo R, Sieck GC, Pabelick CM, Prakash YS: **Cigarette smoke-induced mitochondrial fragmentation and dysfunction in human airway smooth muscle**. *Am J Physiol Lung Cell Mol Physiol* 2014, **306**:L840-854.
451. Bagchi M, Bagchi D, Stohs SJ: **In vitro effects of a smokeless tobacco extract on the production of reactive oxygen species by human oral epidermal cells and rat hepatic mitochondria and microsomes, and peritoneal macrophages**. *Arch Environ Contam Toxicol* 1996, **30**:418-422.
452. Kim J, Sharma RP: **Calcium-mediated activation of c-Jun NH2-terminal kinase (JNK) and apoptosis in response to cadmium in murine macrophages**. *Toxicol Sci* 2004, **81**:518-527.
453. Yang BC, Pan XJ, Yang ZH, Xiao FJ, Liu XY, Zhu MX, Xie JP: **Crotonaldehyde induces apoptosis in alveolar macrophages through intracellular calcium, mitochondria and p53 signaling pathways**. *J Toxicol Sci* 2013, **38**:225-235.
454. Bagchi M, Bagchi D, Hassoun EA, Stohs SJ: **Subchronic effects of smokeless tobacco extract (STE) on hepatic lipid peroxidation, DNA damage and excretion of urinary metabolites in rats**. *Toxicology* 1998, **127**:29-38.
455. Myrvik QN, Evans DG: **Metabolic and immunologic activities of alveolar macrophages**. *Arch Environ Health* 1967, **14**:92-96.
456. Harris JO, Swenson EW, Johnson JE: **Human alveolar macrophages: comparison of phagocytic ability, glucose utilization, and ultrastructure in smokers and nonsmokers**. *J Clin Invest* 1970, **49**:2086-2096.
457. Hoidal JR, Fox RB, LeMarbre PA, Takiff HE, Repine JE: **Oxidative metabolism of alveolar macrophages from young asymptomatic cigarette smokers. Increased superoxide anion release and its potential consequences**. *Chest* 1980, **77**:270-271.
458. Agarwal AR, Yin F, Cadenas E: **Metabolic shift in lung alveolar cell mitochondria following acrolein exposure**. *Am J Physiol Lung Cell Mol Physiol* 2013, **305**:L764-773.
459. Agarwal AR, Yin F, Cadenas E: **Short-term cigarette smoke exposure leads to metabolic alterations in lung alveolar cells**. *Am J Respir Cell Mol Biol* 2014, **51**:284-293.
460. Vulimiri SV, Misra M, Hamm JT, Mitchell M, Berger A: **Effects of mainstream cigarette smoke on the global metabolome of human lung epithelial cells**. *Chem Res Toxicol* 2009, **22**:492-503.

461. Sun W, Chang SS, Fu Y, Liu Y, Califano JA: **Chronic CSE treatment induces the growth of normal oral keratinocytes via PDK2 upregulation, increased glycolysis and HIF1α stabilization**. *PLoS One* 2011, **6**:e16207.
462. Ba Q, Huang C, Fu Y, Li J, Li J, Chu R, Jia X, Wang H: **Cumulative metabolic effects of low-dose benzo(a)pyrene exposure on human cells**. Edited by; 2016:107 - 115. vol 5.]
463. Van den Bossche J, Baardman J, de Winther MP: **Metabolic Characterization of Polarized M1 and M2 Bone Marrow-derived Macrophages Using Real-time Extracellular Flux Analysis**. *J Vis Exp* 2015.
464. Gohil VM, Sheth SA, Nilsson R, Wojtovich AP, Lee JH, Perocchi F, Chen W, Clish CB, Ayata C, Brookes PS, et al.: **Nutrient-sensitized screening for drugs that shift energy metabolism from mitochondrial respiration to glycolysis**. *Nat Biotechnol* 2010, **28**:249-255.
465. Chang CH, Curtis JD, Maggi LB, Faubert B, Villarino AV, O'Sullivan D, Huang SC, van der Windt GJ, Blagih J, Qiu J, et al.: **Posttranscriptional control of T cell effector function by aerobic glycolysis**. *Cell* 2013, **153**:1239-1251.
466. Anastasiou D, Yu Y, Israelsen WJ, Jiang JK, Boxer MB, Hong BS, Tempel W, Dimov S, Shen M, Jha A, et al.: **Pyruvate kinase M2 activators promote tetramer formation and suppress tumorigenesis**. *Nat Chem Biol* 2012, **8**:839-847.
467. Jiang JK, Boxer MB, Vander Heiden MG, Shen M, Skoumbourdis AP, Southall N, Veith H, Leister W, Austin CP, Park HW, et al.: **Evaluation of thieno[3,2-b]pyrrole[3,2-d]pyridazinones as activators of the tumor cell specific M2 isoform of pyruvate kinase**. *Bioorg Med Chem Lett* 2010, **20**:3387-3393.
468. Gohil VM, Zhu L, Baker CD, Cracan V, Yaseen A, Jain M, Clish CB, Brookes PS, Bakovic M, Mootha VK: **Meclizine inhibits mitochondrial respiration through direct targeting of cytosolic phosphoethanolamine metabolism**. *J Biol Chem* 2013, **288**:35387-35395.
469. Bernhard D, Huck CW, Jakschitz T, Pfister G, Henderson B, Bonn GK, Wick G: **Development and evaluation of an in vitro model for the analysis of cigarette smoke effects on cultured cells and tissues**. *J Pharmacol Toxicol Methods* 2004, **50**:45-51.
470. Garaude J, Acín-Pérez R, Martínez-Cano S, Enamorado M, Ugolini M, Nistal-Villán E, Hervás-Stubbs S, Pelegrín P, Sander LE, Enríquez JA, et al.: **Mitochondrial respiratory-chain adaptations in macrophages contribute to antibacterial host defense**. *Nat Immunol* 2016.
471. Kelly B, O'Neill LA: **Metabolic reprogramming in macrophages and dendritic cells in innate immunity**. *Cell Res* 2015, **25**:771-784.
472. Izquierdo E, Cuevas VD, Fernández-Arroyo S, Riera-Borrull M, Orta-Zavalza E, Joven J, Rial E, Corbi AL, Escribese MM: **Reshaping of Human Macrophage Polarization through Modulation of Glucose Catabolic Pathways**. *J Immunol* 2015, **195**:2442-2451.
473. Datta G, Kramer PA, Johnson MS, Sawada H, Smythies LE, Crossman DK, Chacko B, Ballinger SW, Westbrook DG, Mayakonda P, et al.: **Bioenergetic programming of macrophages by the apolipoprotein A-I mimetic peptide 4F**. *Biochem J* 2015, **467**:517-527.
474. Pararasa C, Ikwuobe J, Shigdar S, Boukouvalas A, Nabney IT, Brown JE, Devitt A, Bailey CJ, Bennett SJ, Griffiths HR: **Age-associated changes in long-chain fatty acid profile during healthy aging promote pro-inflammatory monocyte polarization via PPARγ**. *Aging Cell* 2016, **15**:128-139.
475. Huang Z, Luo Q, Guo Y, Chen J, Xiong G, Peng Y, Ye J, Li J: **Mycobacterium tuberculosis-Induced Polarization of Human Macrophage Orchestrates the Formation and Development of Tuberculous Granulomas In Vitro**. *PLoS One* 2015, **10**:e0129744.
476. Ives A, Nomura J, Martinon F, Roger T, LeRoy D, Miner JN, Simon G, Busso N, So A: **Xanthine oxidoreductase regulates macrophage IL1β secretion upon NLRP3 inflammasome activation**. *Nat Commun* 2015, **6**:6555.
477. Liu W, Peng Y, Yin Y, Zhou Z, Zhou W, Dai Y: **The involvement of NADPH oxidase-mediated ROS in cytokine secretion from macrophages induced by Mycobacterium tuberculosis ESAT-6**. *Inflammation* 2014, **37**:880-892.

478. Sugawara I, Yamada H, Kaneko H, Mizuno S, Takeda K, Akira S: **Role of interleukin-18 (IL-18) in mycobacterial infection in IL-18-gene-disrupted mice**. *Infect Immun* 1999, **67**:2585-2589.
479. Placido R, Auricchio G, Falzoni S, Battistini L, Colizzi V, Brunetti E, Di Virgilio F, Mancino G: **P2X(7) purinergic receptors and extracellular ATP mediate apoptosis of human monocytes/macrophages infected with Mycobacterium tuberculosis reducing the intracellular bacterial viability**. *Cell Immunol* 2006, **244**:10-18.
480. Cheng SC, Quintin J, Cramer RA, Shepardson KM, Saeed S, Kumar V, Giamarellos-Bourboulis EJ, Martens JH, Rao NA, Aghajanirefah A, et al.: **mTOR- and HIF-1α-mediated aerobic glycolysis as metabolic basis for trained immunity**. *Science* 2014, **345**:1250684.
481. Liu TF, Vachharajani VT, Yoza BK, McCall CE: **NAD+-dependent sirtuin 1 and 6 proteins coordinate a switch from glucose to fatty acid oxidation during the acute inflammatory response**. *J Biol Chem* 2012, **287**:25758-25769.
482. Netea MG, Joosten LA, Latz E, Mills KH, Natoli G, Stunnenberg HG, O'Neill LA, Xavier RJ: **Trained immunity: A program of innate immune memory in health and disease**. *Science* 2016, **352**:aaf1098.
483. Cheng SC, Scicluna BP, Arts RJ, Gresnigt MS, Lachmandas E, Giamarellos-Bourboulis EJ, Kox M, Manjeri GR, Wagenaars JA, Cremer OL, et al.: **Broad defects in the energy metabolism of leukocytes underlie immunoparalysis in sepsis**. *Nat Immunol* 2016, **17**:406-413.